ABSTRACT

Title: NEUROMORPHIC VLSI REALIZATION OF THE HIPPOCAMPAL FORMATION AND THE LATERAL SUPERIOR OLIVE

Anu Aggarwal, Doctor of Philosophy, 2015

Directed by: Prof Robert W. Newcomb
Department of Electrical and Computer Engineering

In this work, the focus is on realizing the function of the hippocampal formation (HF) and the lateral superior olive (LSO) in electronic circuits.

The first major contribution of this dissertation is to realize the function of the HF in silicon. This was based on the GRIDSmap model and the Bayesian integration. For this, two novel circuits were designed and integrated with others. The first circuit was that of a Bayesian integration synapse which can perform Bayesian integration at the single neuron level. The second circuit was that of a velocity integrator which is so compact that it can enable integration of the entire system on a single chip compared to its predecessors which would have needed 27 chips!

However, since the computational neuroscience models of the hippocampal place cells do not explain all the characteristics observed empirically, a novel model for the place cells, based on the sensori-motor integration of inputs is proposed. This is the second major contribution of this thesis.

The third major contribution is to demonstrate a VLSI system which can perform azimuthal localization based on population response of the LSO. This system was based on the Reed and Blum's model of the LSO. For this, a novel circuit of a second order synapse and that of a conductance neuron was designed and integrated with other circuits. This synapse circuit can produce an output current whose peak is delayed and is proportional to the number of inputs it receives.

The HF is thought to aid in spatial navigation and the LSO is thought to be involved in azimuthal localization of sounds both of which are useful for autonomous robotic spatial navigation. Hence, silicon realization of these two will be useful in robotics which is an area of interest for the neuromorphic engineers.

NEUROMORPHIC VLSI REALIZATION OF THE HIPPOCAMPAL FORMATION AND THE LATERAL SUPERIOR OLIVE

By

Anu Aggarwal

Dissertation submitted to the Faculty of the Graduate School of the
University of Maryland, College Park, in partial fulfilment
of the requirements for the degree of
Doctor of Philosophy
2015

Advisory committee:
Professor Robert W Newcomb, Chair
Professor Neil Goldsman
Professor Jens Herberholz
Professor Agis Iliadis
Professor Martin Peckerar

DEDICATION

To my parents, teachers and my late grandfather.

ACKNOWLEDGEMENTS

I would like to extend gratitude to my advisor, Prof Robert W Newcomb without whose support I would not have been able to come this far. I would also like to thank my thesis committee members for their time and valuable feedback on my work.

I would like to thank the department chair, Prof Rama Chellappa and the associate chair for graduate studies, Prof Ankur Srivastava, for the financial support when my research funding stopped midway through my work. Without this support, I would not have been able to complete my work with the required mental peace.

I would also like to extend gratitude to Mr. Brian Quinn, Director technical operations and Mr. Shyam Mehrotra, lab manager in the department for lab support for my work.

I also thank my colleague, Mr. Bathiya Senvirathna for the beginner's tutorials on the Spartan 3E FPGA board and cadence software.

.

TABLE OF CONTENTS

Table of figures

Table of Abbreviations

AER	Address event representation
AVCN	Antero Ventral Cochlear Nucleus
BVC	Boundary Vector Cell
CA	Cornu Ammonis
DG	Dentate Gyrus
DNLL	Dorsal Nucleus of Lateral Lemniscus
ERC or EC	Entorhinal Cortex
FPGA	Field Programmable Gate Arrays
FSM	Finite state machine
GRIDS	Grid Regularity from Integrated Distance through Self-organizing
HD	Head Direction
HF	Hippocampal Formation
IC	Inferior Colliculus
ICA	Independent Component Analysis
IE	Inhibitory-Excitatory
IFN	Integrate and Fire Neuron
ILD	Interaural Level Difference
ILDci	Interaural Level Difference of complete inhibition
IPD	Interaural Phase Difference
ITD	Interaural Time Difference
lEC	Lateral entorhinal cortex
LSO	Lateral Superior Olive

MEC	Medial entorhinal cortex
MNTB	Medial Nucleus of Trapezoid Body
MPO	Membrane Potential Oscillation
MSO	Medial Superior Olive
OI	Oscillatory Interference
VCO	Velocity Controlled Oscillator
WTA	Winner Take All

1. INTRODUCTION

It has been the endeavour of neuromorphic engineers to emulate the working of the brain in silicon because the brain is energetically efficient, robust and can perform varied mathematical computations. One important characteristic of the brain is that it can learn from its surroundings, store the learned information in memory and respond accordingly. This is especially useful in spatial navigation which is quintessential to the survival of a species.

For successful spatial navigation, information about direction and distance of the target w.r.t. current position of the animal is needed. In conventional navigation, e.g., that with a GPS, a fixed map of the environment and a compass is used to achieve this. In contrast, the autonomous robotic spatial navigation requires exploration of a new or a changing environment. It needs constant integration of information from the environment to update existing maps of the environment and store them in memory to calculate the new optimal path to a goal. Another important clue for spatial navigation is the ability to localize the direction from which sound is coming. These sounds could be of the predators, mating calls or of such similar survival value to the animal.

The hippocampal formation (HF) of the brain is thought to be involved in spatial navigation and encoding a spatiotemporal stamp on episodic memories. The lateral superior olive (LSO) of the brain is involved in azimuthal localization. Their realization in silicon can be useful tools for robotic spatial navigation. As such, this work presents a silicon realization of the hippocampal formation and of the LSO. These were designed using the currently accepted computational

neuroscience models- the GRIDSmap model (Mhatre et. al., 2012) and the Bayesian integration (Madl et. al., 2014) for the HF, and the Reed and Blum's model (Reed and Blum, 1990) for the LSO. On further study of the HF and its implementation in silicon, it was realized that the current computational neuroscience models for it do not explain the hippocampal place cell firing well. Hence, further study of the empirical observations was done and, a novel model for the place cells is proposed. This model not only describes the mechanism for place cell firing but also a mechanism for encoding new trajectories in space as the animal moves around in its environment. It also suggests how the brain could possibly be calculating the optimal trajectories from several of those stored in memory.

A. Contributions of this dissertation

1. A novel, first as far as our knowledge of literature goes, **VLSI design and testing of the hippocampal formation** based on the neurophysiological models as a part of which
    a) A very compact stripe cell ring circuit based on biological and computational model (GRIDSmap model) of the grid cells was developed.
    b) Circuit of a Bayesian integration synapse was designed and tested.
    c) The head direction cell system was implemented in a very compact form.
2. A novel, first as far as our knowledge of literature goes, **sensori-motor model** of the hippocampal place cells.

3. VLSI implementation of the **central pattern generator** in a very compact manner**.**
4. **VLSI design and testing** of the population response of **the LSO** for azimuthal localization of sound based on the neurophysiological model of Reed and Blum as part of which
    a) An update on the second order synapse circuit (previously realized in conjunction with Prof Horiuchi) – used on both the LSO and the grid chip was done.
    b) Conductance neuron circuit (modified from the version which was designed with Prof Horiuchi) was developed.

These circuits can also be used in analog VLSI realization of other neural systems which perform similar computations.

Briefly, the flow chart in Fig. 1 presents an overview of the system design in this dissertation including how the chips and the circuits on them fit together in realizing the working of the hippocampal formation, the central pattern generator and the lateral superior olive in brain.

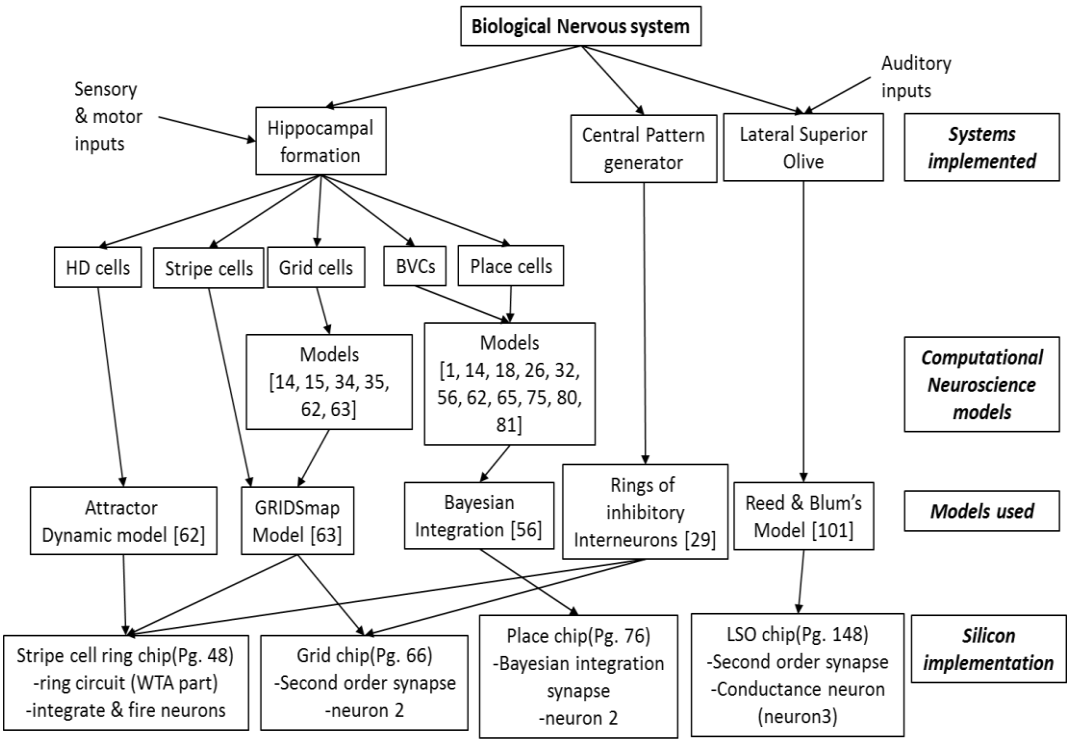

Fig. 1 Flowchart showing the various systems that were realized in silicon in this dissertation. It shows that the hippocampal formation, the central pattern generator and the lateral superior olive (LSO) of the biological nervous system were implemented using four different silicon chips-the stripe cell ring chip, the grid chip, the place chip and the LSO chip. The circuits on these chips were inspired by the various computational neuroscience models viz., the attractor dynamic model of the head direction cells (HD), the GRIDSmap model of the grid cells and the Bayesian integration for the place cells. The LSO chip and the circuits on it were designed based on the Reed and Blum's model of the LSO. The central pattern generator system was implemented based on the neural demonstration of the presence of actual rings of inhibitory interneurons in the biological nervous system. All these systems have potential applications in designing robotic systems, details on which can be seen in section 9 on Open questions & future work. BVCs - the boundary vector cells.

2. HIPPOCAMPAL FORMATION: BACKGROUND

The Hippocampal formation (HF) is a part of the nervous system which is thought to be involved in spatial navigation (Purves et. al., 2012). The neurons of the HF are capable of sensing the direction of motion of the animal, integrating motor information to form a matrix which spans the environment and then use this matrix and incoming sensory information to build a map of the environment. They are also involved in storing these maps in memory, updating them based on new information and retrieving them during homing. The behavioural evidence for the role of the hippocampus in this crucial task comes from rodent experiments in which the mean latency on maze tasks and radial arm maze does not decrease with training in animals with hippocampal lesions as compared to that in healthy animals and from the clinical case of patient Henry G. Molaison (Scoville, 1957) who experienced difficulty in encoding new episodic memories when his temporal lobe was removed for epilepsy treatment.

A. Anatomy

Anatomically, the HF is a C-shaped structure (Nieuwenhuys et. al., 1988, Fig. 2, Fig. 3) which is located on the medial[1] side of the cerebral hemispheres. Relative to the corpus callosum, it can be divided into pre-, supra- and retro- commissural parts. The former two are small and rudimentary and the retro commissural part is the main one. The pre-commissural part is a thin strip which connects the retro and the supra commissural parts. The supra-commissural part contains two fibre

[1] Medial means the position closer to the midline of the body as opposed to something located more laterally.

bundles, the medial and the lateral longitudinal striae, which carry connections of the hippocampus to other parts of the brain. Near the splenium of the corpus callosum, the supra-commissural part of the hippocampus is continuous with the retro commissural part which is the expanded, most caudal[2] part of the HF. During development, this part rolls in on itself and protrudes into the inferior horn of the lateral ventricle. The most rostral part of this recurves dorsally and forms a rounded swelling called the uncus, on the medial surface of the cerebral hemisphere.

Developmentally, the HF belongs to the archipallium, i.e., the most primitive part of the cerebral hemisphere and histologically[3], it is made of three layers throughout. Morphologically, this part of the HF contains three longitudinally arranged structures- the dentate gyrus (DG), the cornu ammonis (CA) and the subiculum. Due to the infolding, the DG lies above and the CA lies below the hippocampal sulcus. DG contains small neurons called the granule cells and the CA and the subiculum contain large pyramidal cells predominantly. CA is well developed in primates. CA3 lies near the DG and the CA1 lies near the subiculum. The subiculum is separated by 2 strips of the mesocortex into the pre and para subiculum, from the entorhinal cortex (area 28 of Broadman[4]) and occupies a

[2] Caudal means towards the tail of the animal as opposed to cranial/rostral which means more towards the head of the animal.

[3] Histology is the study of the microscopic structure of cells and tissues of plants and animals.

[4] Brodmann areas were originally defined and numbered by the German anatomist Korbinian Brodmann based on the cytoarchitectural organization of neurons he observed in the cerebral cortex using the Nissl method of cell staining. Brodmann published his maps of cortical areas in humans, monkeys, and other species in 1909, along with many other findings and observations regarding the general cell types and laminar organization of the mammalian cortex. (source: Wikipedia)

large part of the para hippocampal gyrus. Ventral to the entorhinal cortex is the peri rhinal cortex, which includes areas 35 and 36 of Broadman.

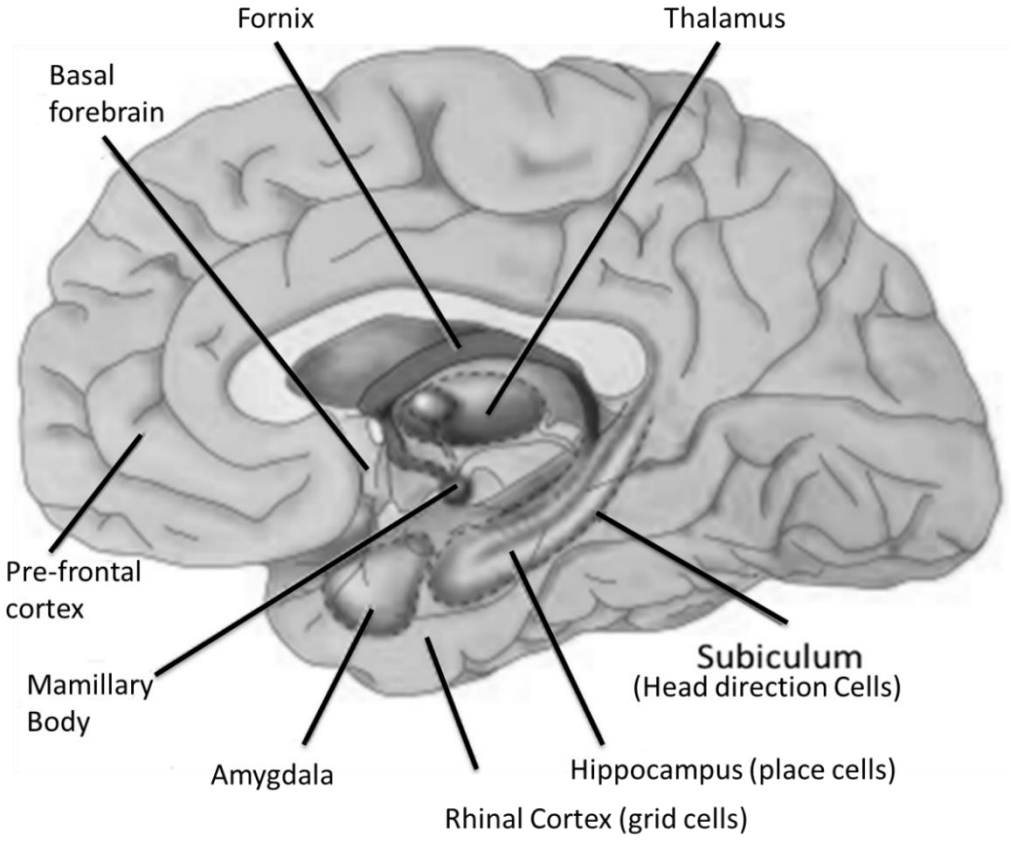

Fig. 2 Sagittal section of the brain showing the hippocampal formation on the medial aspect of the cerebral hemispheres [72]. Among other areas, the hioppocampal formation includes the hippocampus which contains the place cells, the subiculum which contains the head direction cells and the rhinal cortex which contains the grid cells, primarily. The unique firing patterns of the grid, place and the head direction cells were implemented in silicon as part of this dissertation work because these cells are thought to be important in spatial navigation and updating episodic memories.

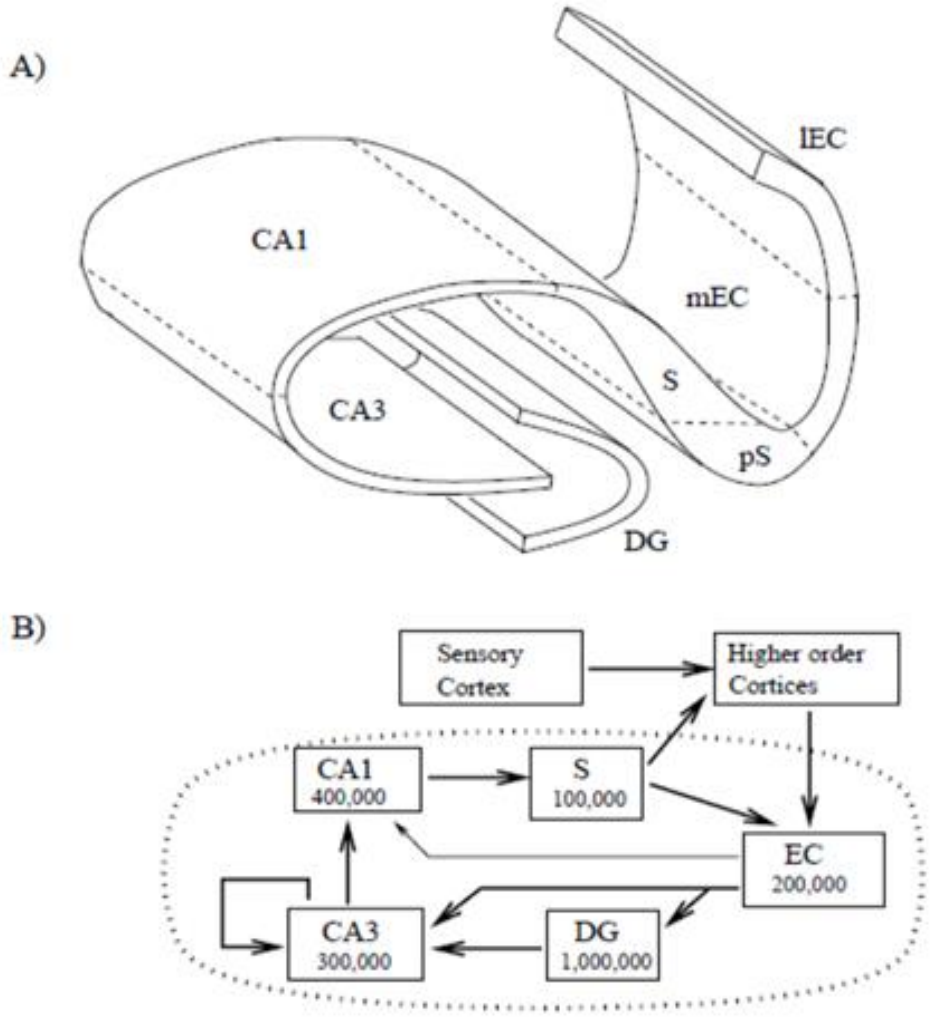

Fig. 3 Anatomy of the hippocampal formation – arrangement of its components and their connections [13]. Several loops of connections are formed within various regions of the hippocampal formation and with outside regions of the brain. One such loop is formed between entorhinal cortex→ cornu ammonis 1, subiculum, dentate gyrus → entorhinal cortex. The main inputs to the hippocampal formation arrive at the entorhinal cortex and leave from the subiculum and the cornu ammonis 1. Main inputs (afferents) to the hippocampal formation are highly processed sensory inputs from various association cortices, inputs from thalamus including the head direction signal and the theta oscillations from the medial septum. The outputs (efferents) from the hippocampal formation project to the ventral pallidum which controls the motor activity, to areas which control secretions of the anterior pituatory, the master gland of the body and to the lateral septal nucleus on to control the theta rhythm. (CA-cornu ammonis, DG-dentate gyrus, mEC-medial entorhinal cortex, lEC-lateral entorhinal cortex, S-subiculum, EC-entorhinal cortex)

i) Internal connections of the HF

The perforant pathway contains efferents from the entorhinal cortex (ERC or EC) to the DG primarily and some connections to the subiculum, CA1 and CA3. Mossy fibres arising from the DG end in CA3 which in turn send projections, called schaffer collaterals to the CA1. The CA1 in turn projects back to the ERC, thus, completing the loop. These projections are both direct and indirect through the subiculum.

ii) Afferents to the HF

The HF receives inputs from various cortical areas, the amygdaloid complex, the medial septal-diagonal band complex, the thalamus, the supra-mamillary nucleus, the mesencephalic nuclei and the locus coeruleus.

Most of the inputs from different areas of the cortex end in the entorhinal cortex (ERC or EC). Others end in the peri rhinal area and still others in the subicular cortex. Substantial contributions of these afferents arise from the posterior orbitofrontal, infra-limbic, insular, cingulate and temporal polar cortices. Several of these areas are the sites of convergence of multimodal sensory information. Pathways leading out of the primary visual, auditory and somesthetic areas converge on these areas eventually. Association areas converge directly on the parahippocampal cortices. Thus, the visual and the auditory association areas project to the peri and the ento-rhinal areas and fibres originating from the multimodal association areas situated in the prefrontal cortex, the inferior parietal lobule and the inferior temporal lobe end in the pre-subiculum. The entorhinal

area also receives inputs from the olfactory bulb. Thus, the region gets inputs from widespread sensory areas directly and after processing in the association areas.

The lateral part of the entorhinal cortex receives information from the cortical pathways which in turn receive it from different sensory modalities. In contrast, the medial part receives information from the sub cortical centres such as the septum, the thalamic midline nuclei and the amygdala. The connections from the entorhinal cortex to the hippocampus have distinct topographic organization. Those from the lateral entorhinal cortex project to the more splenial portion of the hippocampus while those from the medial entorhinal cortex project to the more temporal portion of the hippocampus. Thus, the splenial[5] portion of the hippocampus receives more exteroceptive sensory information and the temporal portion receives information from the limbic related subcortical centres, reflecting the internal status of the organism. Other afferents to the HF arrive from the amygdaloid complex, medial septal nucleus and the nucleus of the diagonal band, dorsal thalamus, anterior nuclei, the midline complex, the supra-mammillary nucleus, the locus coeruleus and the mesencephalic raphe nuclei.

iii) Efferents from the HF

Fibres from the CA project to the lateral septal nuclei, which project back to the HF through the medial septal-diagonal band complex. Subiculum projects to the lateral septal nucleus, the nucleus accumbens, the anterior olfactory nucleus, the pre-commissural hippocampus, the medial part of the frontal cortex and the gyrus

[5] Splenial region means more towards the tongue as opposed to that towards the temporal region of the brain. Thus, splenial will be more ventral than the temporal which is more dorsal.

rectus. Nucleus accumbens in turn projects massively to the ventral pallidum, and the fibres from the ventral pallidum terminate in and around the tegmental pedunculo-pontine nucleus, which is thought to be associated with the mesencephalic[6] locomotor region, thus, it is important in mediating locomotor responses associated with the exploratory behaviour. The post commissural fornix contains only fibres originating from the subicular complex, most of which terminate in the mammillary body, in the anterior thalamic nucleus, the bed nucleus of the stria terminalis and the cell free capsular zone surrounding the ventromedial hypothalamic nucleus, via which the hippocampus might influence the secretions of the anterior pituitary hormones.

Thus, the hippocampus has reciprocal connections with the associational cortical areas and with the subcortical structures due to which it receives a variety of highly processed sensory inputs, and the head direction signal. It also receives the theta frequency (4-7Hz) oscillatory inputs from the medial diagonal band of broca, which could provide a timestamp to the information processed in the hippocampal formation. Thus, it could integrate both head direction and sensory inputs. Outputs from the hippocampal formation regulate the voluntary motor movements through the ventral pallidum and the function of the internal body organs by control over secretions of the anterior pituitary.

[6] Mesencephalic means midbrain.

B. HF, spatial navigation and memory

The clinico-pathological evidence strongly suggests that the hippocampal-parahippocampal complex and its bi-directional relationships with the associational cortical areas are prominent in learning and memory processes. The hippocampus is thought to be involved primarily in encoding of new episodic memories. This is evident from the case of patient Henry G. Molaison (Scoville, 1957) who underwent bilateral removal of temporal lobes to cure his temporal lobe epilepsy. As a result, however, he developed anterograde amnesia. His past memories remained intact but there was impairment of capacity to form new memories. He also had intact procedural memories but had problems only in building new episodic memories. Studies in rodents also indicate a role for the hippocampus in spatial navigation and encoding of new memories. Fig. 4 and Fig. 5 show that the mean latency on maze tasks does not decrease with training in animals with hippocampal lesions as compared to their normal counterparts. It also shows that the animal is unable to correctly locate a platform even after training over several trials if it has a lesion in the hippocampus.

One noteworthy thing here is that in case of lesions of the HF in animals spatial navigation is affected more as compared to humans in whom memory is affected more (as observed empirically, Purves et. al., 2012).

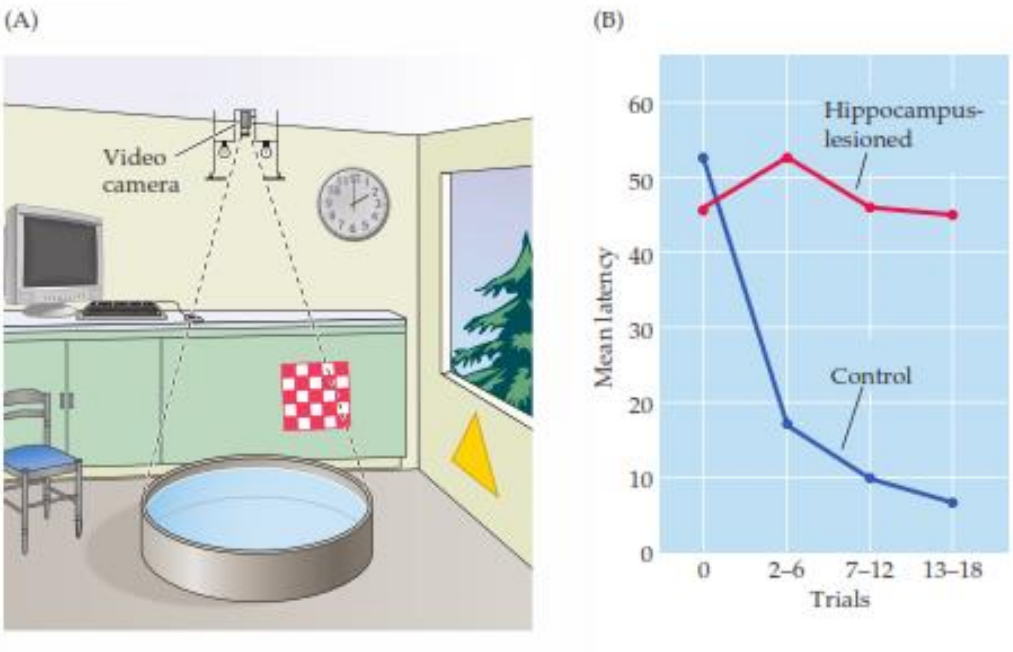

Fig. 4 [72] Performance of normal Vs subjects with lesions of the hippocampus on a new memory formation task. In this experiment, animals with and without hippocampal lesions were trained to perform maze tasks. It was observed that the mean latency on learning new maze tasks does not reduce in animals with hippocampal lesions even after several trials.

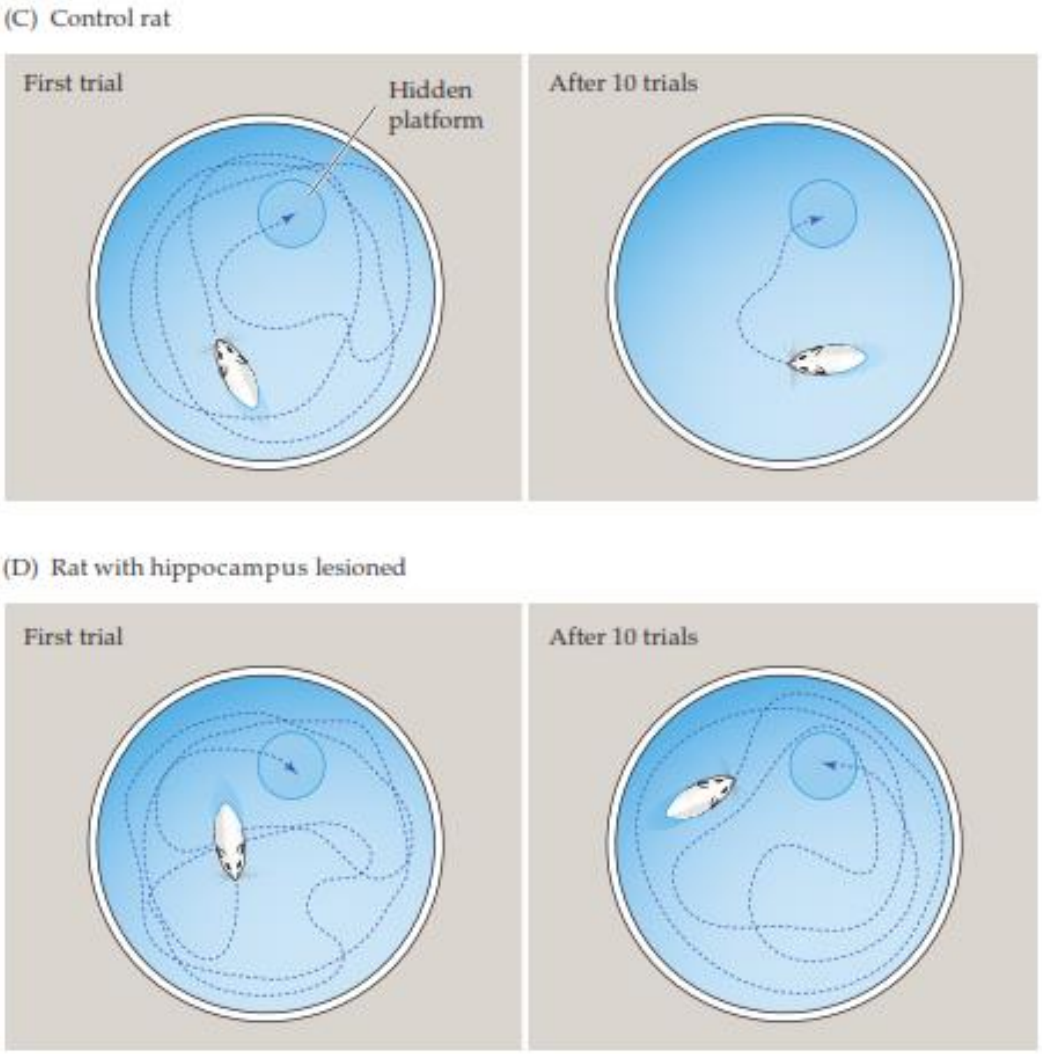

Fig. 5 [72] Failure of a rat with lesions of the hippocampus to be trained in spatial navigation tasks. In this figure, we can see that after 10 trials, the rat without any hippocampal lesions (figures at the top) is able to follow a much shorter path to the goal as compared to when it was untrained. However, in the animals with lesions (figures at the bottom), the path followed to reach the goal even after 10 trials is not any shorter than that followed in the untrained state.

C. Cells of the HF

The different areas of the HF contain different cells with a predominant functional characteristic. Primarily, the subiculum contains the **head direction** (HD) cells (Fig. 6), the ERC contains the **grid cells** (Fig. 6) and the hippocampus proper the

place cells (Fig. 7**)**. These are the cells whose unique firing patterns were implemented in silicon in this dissertation work. The entorhinal cortex is also thought to contain the stripe cells and the subiculum to contain the boundary vector cells. The rings of stripe cells are thought to integrate motion of the animal in space (GRIDSmap model, Mhatre et. al., 2012) and send inputs to the grid cells. The boundary vector cells (BVC model, Barry et. al., 2006) are thought to fire when the animal is located near the boundaries of the environment. Before demonstration of the grid cell firing patterns, the BVCs were thought to control firing of the place cells.

Ranck, 1984 and Taube et al, 1990 performed single cell recording by placing electrodes near the head direction cells in the subiculum. As the animal moved around the environment freely, the firing patterns of these cells were observed. They observed that each head direction cell fired when the head of the animal was pointing in a particular direction w.r.t. the cues in the environment called the polarising cues (not known how these are identified by the animal in natural settings but in experiments, this is generally a cue card provided in the enclosure by the researchers) or within 45 degrees thereof. Whenever, the position of this polarising cue was rotated, the preferred firing direction of the head direction cell also changed. However, the relative preferred firing directions of the head direction cells w.r.t. each other remained the same. This preferred orientation is maintained even in the absence of visual inputs, for instance, when the animal is moving around in the environment in dark. Their firing is seen to be blocked by lesions of the vestibular input and to depend upon voluntary movement. The

signals from these cells could provide a self-motion signal based on motor input which can update spatial representation in the hippocampus and the medial ERC. To explain this maintenance of head direction specific firing patterns even in the absence of visual inputs and w.r.t. each other even when the orienting cues are rotated, the attractor dynamic model (McNaughton et.al., 2006) was proposed. This is explained later in this dissertation in section 2. E. i) a).

Hafting et. al., 2005 performed single cell recordings (intracranial electrodes) from the medial entorhinal cells as the animal foraged for food inside a closed enclosure. They showed that there are cells in the medial ERC which fire at regular intervals at the corners of a regular hexagon as the animal moved freely in the enclosure. They coined the term grid cells for these. The spatial frequency of the hexagonal firing pattern of the grid cells increases along the ventro-dorsal axis of the medial entorhinal cortex, i.e., the cells located more ventrally have more widely distributed fields. The neighbouring grid cells show similar spacing, field size and orientation but differ in phase. Their phase and orientation shift if visual cues are changed. However, the hexagonal firing pattern is visible even in the dark. Thus, the grid cells form a matrix spanning the environment which exists irrespective of external inputs but whose orientation is set by the visual cues. This matrix is similar to the grid on a map.

Similarly, using single cell recordings from animals (primarily rats) foraging freely in the enclosure, O'Keefe, Dostrovsky, 1971, demonstrated the presence of hippocampal cells (CA and DG) which fire when the animal is at a particular place in space. These cells are called 'place cells'. Each place cell can encode

different locations in more than one environment, but might not have obvious topographic relationship between the place fields in two different environments. Adjacent place cells may or may not have adjacent place fields. The shape of the enclosure is a major determinant of the way in which the place fields are distributed. The place cell firing is thought to be the result of integration of motor inputs from the grid cells and sensory inputs. Their firing is thought to provide a spatial map of the environment. They are also involved in encoding a 'space and time stamp' on newly created episodic memories. Their firing field sizes scale along the dorso-ventral axis as do the spatial firing frequencies of the grid cells. Moreover, as the size of the environment increases, their field size also increases. The same place cells can fire at different locations in different environments. The firing is seen even in the dark which indicates a role for path integration mechanisms. Changes in size, shape or colour of the enclosure lead to changes in firing rate but not firing pattern which indicates a role for environmental cues. An important empirical observation (Hafting et. al, 2008) is that the place cell and the grid cell firing (of the corresponding scaling) is coincident as indicated by similar phase precession observed in both place cells and grid cells.

In short, based on our current understanding, the head direction cells provide information about the direction in which the animal is moving. This is integrated by the grid cells to provide a matrix spanning the entire environment. Using this matrix and sensory inputs (possibly), the place cells identify locations of significance in the environment and encode their spatiotemporal information to episodic memories. This information is constantly learned, unlearned and updated

based on fresh inputs from the environment. Thus, the hippocampal formation of the brain is thought to function as a self-learning internal GPS with memory and plasticity. In a later section, we present the prevalent models of the hippocampal formation as these models were used in implementation of our system.

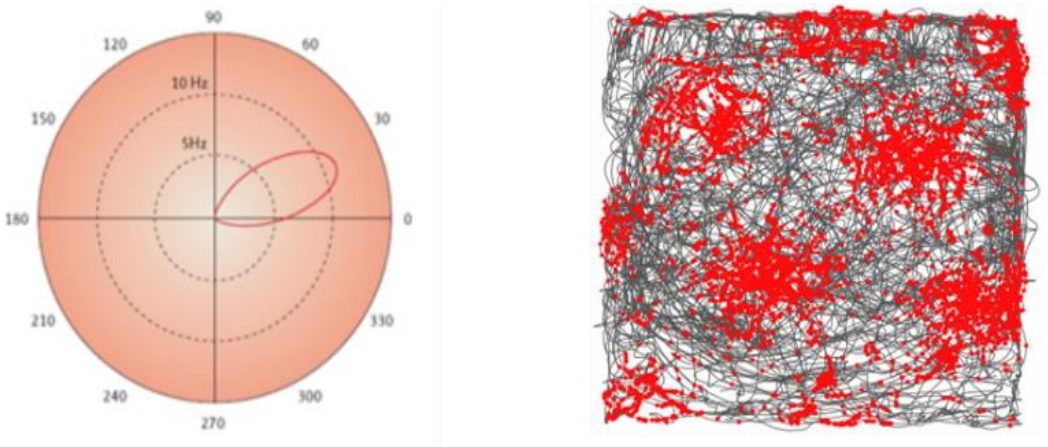

Fig. 6 [13] (left) A head direction cell fires as the animal's head points in its preferred firing direction or 45 degrees thereof. The graph shows that the firing rate (in Hz) of a single head direction cell, with preferred firing direction at ~20 degrees along the azimuth, increases from 0 to 12 Hz and back to 0 as the animal's head moves from -10 to 50 degrees along the azimuth. (right) A grid cell fires [31] as the animal is present at different positions in space which are located at the corners of an equilateral triangle or at the corners of intercalated hexagons forming a pattern like the grid on a map. The results shown here are from animal experiments in an enclosure of size 1m X 1m. The recordings are from electrodes placed near a single grid cell in the medial entorhinal cortex while the animal was moving along a trajectory in the enclosure which is denoted by the grey lines. The red regions indicate the points in space at which the grid cell's firing is triggered.

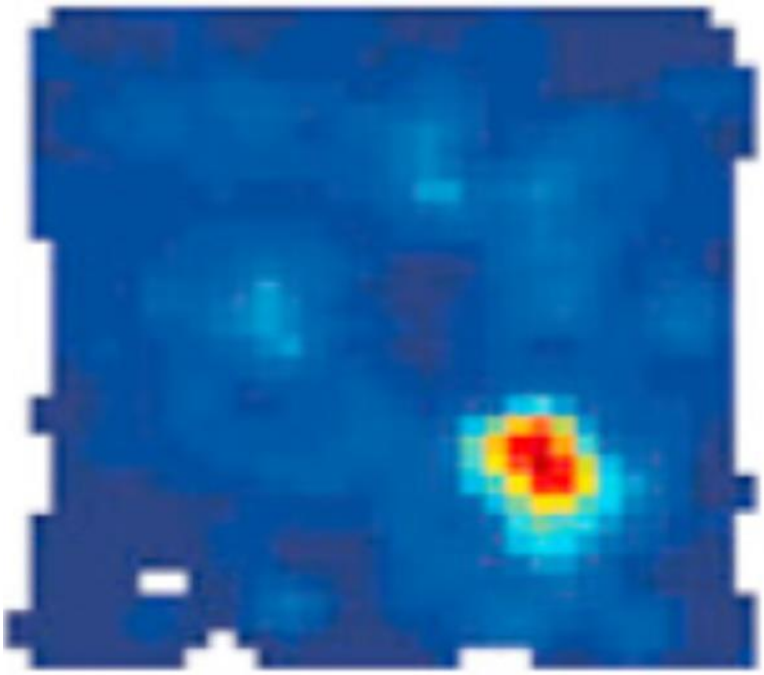

Fig. 7 A single hippocampal place cell firing pattern [34] seen on the heat plot of the firing rates from it when the animal moved freely in the enclosure (represented by the blue square). The red color means the firing rate at that position was higher than that at places with blue color. In this experiment, the animal with an intracranial electrode positioned near a hippocampal place cell was left to forage for food particles spread in the enclosure. The place cell under observation had the maximum firing rate only when the animal reached the place shown in red color. This pattern was constant over repeated trials which implies that one place cell fires when the animal is stationed at a particular position in an environment and hence, it encodes for that place in space. Similarly, ensembles of place cells (not shown here) together can form a map of the enclosure by encoding for different places in it.

D. Further empirical observations

There are some more empirical observations on the cells of the hippocampal formation which are mentioned here because they are the basis for our novel sensori-motor model of the place cells. The hippocampal place cells (O'Keefe & Dostrovsky, 1971, O'Keefe & Conway, 1976, 1978, O'Keefe, 1976, O'Keefe & Nadel, 1977) were demonstrated to form a spatial map of the environment and

provide a spatiotemporal stamp on the newly formed episodic memories. Several experiments have been performed since their first demonstration to investigate the relative importance of sensory and motor inputs (processed by head direction and grid cells) in determining place cell firing. Some of the noteworthy ones are mentioned below. The causal link between sensory cues and place cell firing was shown in Muller & Kubie, 1987, where rotation of a single visual cue in the environment caused rotation of the place cell firing pattern associated with it. However, in their paper, the orientation of grid cell firing pattern also changed with change in position of visual cues. Thus, this could have been processed by place cells either through grid cell inputs or directly. Further, in O'Keefe & Conway, 1978 place cell firing ceased in the absence of external cues, reward or a 'significance' attached to a place. This means that 'something else' is also needed for place cell firing in addition to sensory inputs. Also, in Best & Thompson, 1987, place cell firing was shown in the presence of sensory cues like visual, olfactory, auditory and tactile, and in O'Keefe & Conway, 1978, Save et. al., 2000, and Nakazawa et. al., 2002, it was demonstrated that in the absence of one of the sensory cues, the cells fire in response to another. This observation does not exclude dependence of place cell firing on motor integration though. The firing is seen even in the dark (Quirk, et. al., 1990) which indicates a role for path integration mechanisms. However, in this case, the role of sensory inputs cannot be excluded because the rats can see in UV range as well.

Some other studies (Barry et. al, 2006 and Etienne, 1996) demonstrate homing by path integration by grid cells in the absence of sensory cues. In Mittelstaedt, 1980,

and Etienne, 1992 also, gerbils missed a target by an amount that they were rotated without triggering path integration by grid cells, indicating a prime role of grid cells in place cell firing. However, these experiments did not include recordings from the place cells, thus, these are only behavioural and, hence, less conclusive. Moreover, they also show that in the absence of visual cues, the estimates are only approximate and prone to drift due to error accumulation which can be corrected by sensory inputs. In Jeffery & O'Keefe, 1999, actual place cell recordings were performed which show that the place cell firing is associated with visual cues which are stationary or are perceived to be stationary. If there are no visual cues which polarize the environment, then the place cell firing is mainly dependent upon motor inputs.

Changing the shape and size of an environment or insertion of a barrier (Muller & Kubie, 1987, O'Keefe & Burgess, 1996, Fenton et. al., 2008, Monaco & Abbott, 2011) can trigger changes in both motor and sensory inputs. Empirically, change in size of an environment has been shown to commensurately change the number of nodes of grid firing and the size of firing fields of the place cells. Change in shape of an environment has been shown to change orientation of the grid firing fields (Hafting et. al., 2005) and the firing frequency of the place cells. Observations in O'Keefe & Conway, 1978 and Poucet, 2014 point to a role for both grid cell path integration and sensory cues in place cell firing. The above observations indicate that the place cell firing is influenced by both sensory and motor inputs and needs both for higher accuracy. In a more recent study (Brandon, 2014), the theta oscillations from the medial septum were suppressed to suppress

grid firing. This did not suppress place cell firing even though the firing frequency reduced. This indicates that the place cell firing is not based on grid cell firing solely but needs grid firing and sensory information for optimal performance. The empirical observations point to a role for both motor and sensory inputs in grid and place cell firing. These form the basis for the various computational neuroscience models of the HF which are explained in the next section.

E. Current models of the HF

Neuroscientists have been trying to solve the mystery behind the firing patterns seen in the HF and of the function performed by it. They have postulated several models for the same of which the important ones are presented below. Of these, the attractor dynamic model for the head direction cell system, the GRIDSmap model for the grid cells and the Bayesian integration for the place cells were used for our silicon implementation of the HF. The rest of the models are described here because their critical analysis was needed to come up with our novel sensori-motor model for the place cells.

i) Grid cell & HD cell Models

a) Attractor dynamic model

This is a computational neuroscience model describing the firing patterns of different cells (HD, grid and place cells) of the hippocampal formation. Presence of such a network has not been demonstrated in the brain. An attractor is a network of neurons that can settle into a stable pattern of firing (Amit, 1989). 'Continuous attractor' neural networks can maintain a localised packet of neuronal

activity (Fig. 8(a)) representing the current state in a continuous space without external sensory input. Activity shifts from one attractor state to another based on external inputs. The stable states in case of neural networks are formed and maintained by the pattern of excitatory and inhibitory connections between neurons.

According to this model (McNaughton, et. al., 2006), the head direction cell system consists of 3 rings of neurons (Fig. 8). One of these is the main ring and the other two integrate motion in clockwise and anticlockwise direction. The main ring has several neurons, each of which is connected to its neighbors through excitatory connections whose strength reduces as the distance between the neurons increases. All the neurons also get inhibitory input from a global inhibitory neuron. This connectivity pattern leads to a stable bump of activity being formed at a location along the ring which corresponds to the current head direction of the animal. As the head of the animal moves around in (say) the clockwise direction, the vestibular apparatus in the inner ear provides information to another ring of neurons in the head direction cell system which integrates the estimate of position based on this information and prior information and updates the estimate of head direction. The neurons in this ring are connected to that of the main ring such that they cause movement of the bump of activity around in the clockwise direction to a position which corresponds to the current head direction of the animal. The anti-clockwise motion is integrated by another ring of neurons which is similar to that responsible for updating motion along the clockwise direction but whose connections to the main ring are in opposite direction. Thus,

the head direction cell system can estimate the current head direction of the animal with respect to the polarising cues (used by the animal to define head direction of 0 degrees – not known how these are identified by the animal), hold it at a place for the duration while the head is held stationary and can update it to a new position by integrating information about the head direction as the animal's head is moved around in clockwise or anti-clockwise directions. This model has been used to implement the head direction cell system in silicon (Massoud and Horiuchi, 2012, Corradi et. al., 2014) earlier also using 3 rings as described by this model, with one ring on a chip. For these systems, the chips communicated with each other through software interfaces which were also used to provide varying strengths of excitatory and inhibitory connections. In this dissertation work, we abstract out the function of the system from the rather complicated model and then implement it. This reduced the hardware and software dimensions of the system to 1 ring circuit (Fig. 20) which was designed on $1/12^{th}$ of the area of a single tiny chip unit (1275mm X 1275mm). This ring circuit performs all the functions of the head direction cell system, viz., holding the activity of a neuron at a place for a duration of choice, moving it around the ring in either clockwise or anti-clockwise direction on application of external inputs but in a very compact form.

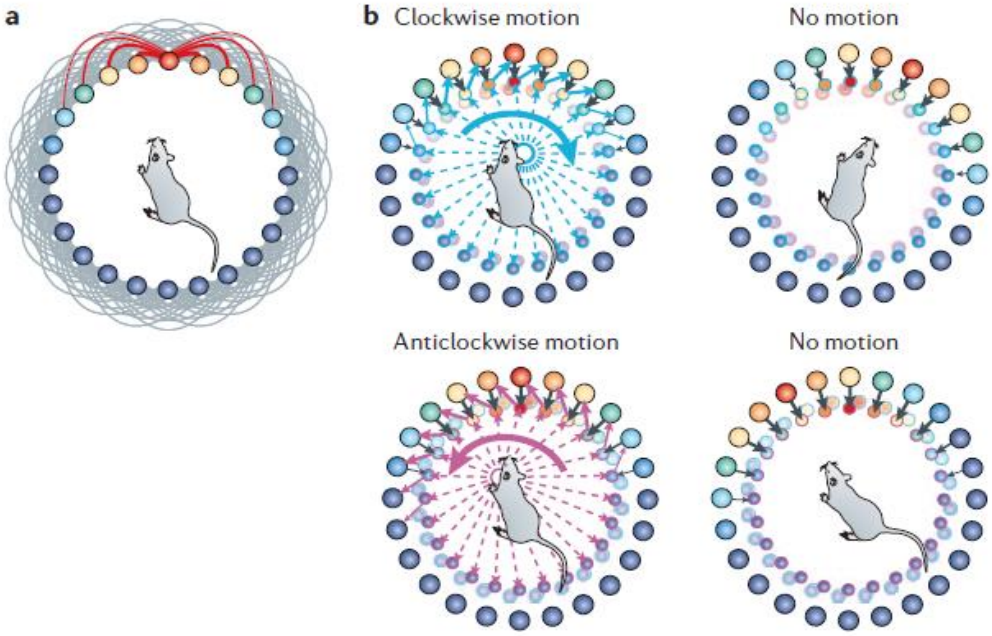

Fig. 8 Attractor dynamic model [62] for the HD cells showing (a) the head direction cell system arranged in a ring of neurons (say, the main ring). Each neuron in the main ring is connected to its neighbors with excitatory connections which decrease in strength as the distance to it increases. All the neurons also receive an input from a global inhibitory neuron (not shown here). This balance between the excitatory and the inhibitory inputs leads to formation of a stable bump of activity which corresponds to the current head direction of the animal. (b) As the head of the animal is moved around in the clockwise direction, this movement is sensed by the vestibular apparatus in the inner ear which sends inputs to another ring of neurons. This ring of neurons, say ring 2, integrates the motion information. Each neuron on this ring is connected to that on the main ring such that it moves the bump of activity on the main ring in clockwise direction to a position which corresponds to the new head direction of the animal. Similar information processing also occurs for movement in the anti-clockwise direction when the motion is integrated by another ring of neurons (say ring 3) which shifts the bump of activity on the main ring in anti-clockwise direction.

In the same vein, the grid pattern is formed due to the arrangement of neurons in two dimensional sheets (Fig. 9), the adjacent ones of which are connected through excitatory connections, whose strength reduces gradually as their distance from the neuron increases. This results in neuronal firing at regular intervals in a

hexagonal spatial pattern as the animal moves around in space. This model also explains how grid cell firing of different spatial frequency could be obtained due to different gain with speed (Fig. 10). However, this model was not used in silicon implementation of the grid cell firing patterns because it requires a lot of software interfaces and hardware and hence, will not be very energy efficient.

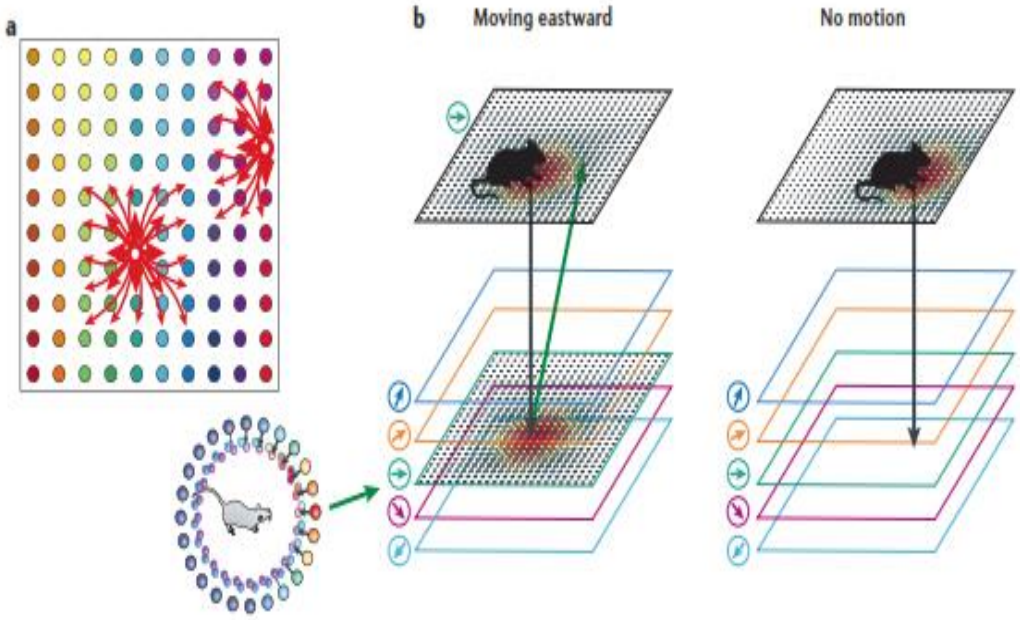

Fig. 9 [62] According to the attractor dynamic model, the grid cell spatial firing pattern is produced due to two dimensional arrangements of the cells in (a) a plane (say main plane). In this plane, each neuron is connected to its neighbours by excitatory connections whose strengths change with distance from the neuron. All the neurons in this plane also receive common inhibitory inputs. Resultant of excitatory and inhibitory activity produces a bump of activity at a place in the head direction cell system. To move this bump around, motion inputs are integrated by different planes which project on to the main plane in such a manner that they move the bump of activity along the direction of motion (as described for the head direction cell system). In earlier attempts at silicon implementations of this model, inability to move the bump around has been seen as a major limitation. Hence, this model was not used in this dissertation work to implement the grid cell firing patterns.

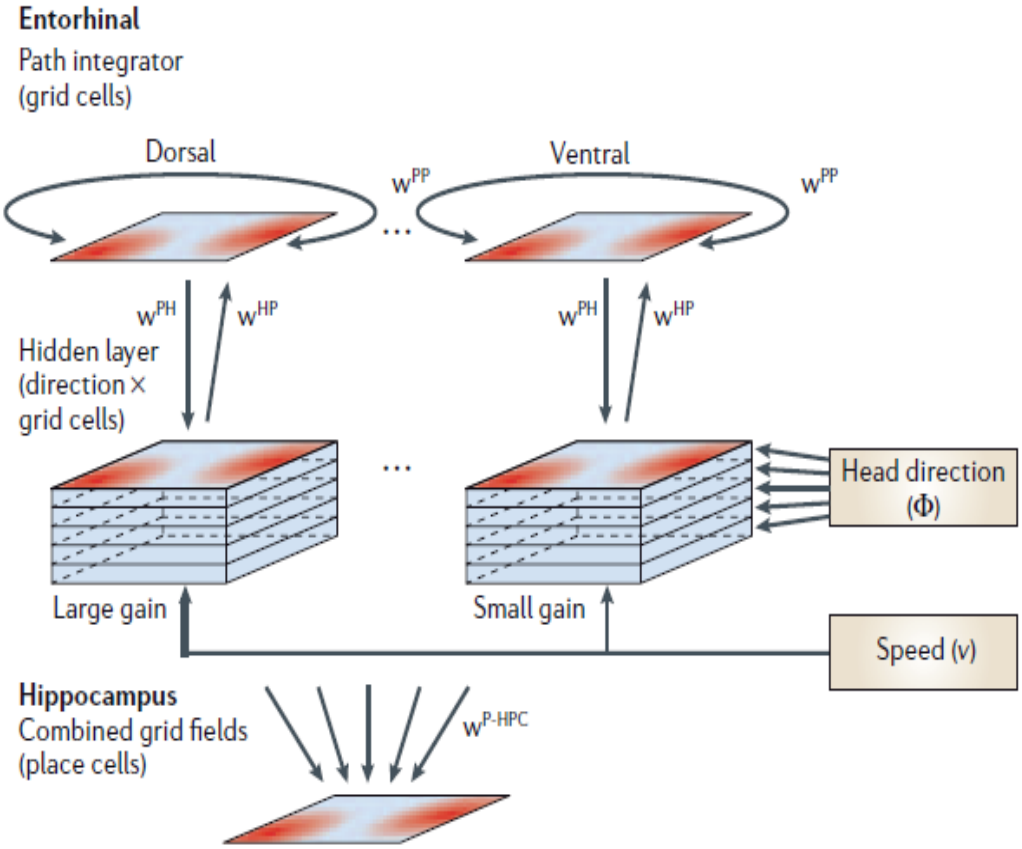

Fig. 10 [62] Shows the path integration by a grid cell and differential gain of frequency with speed producing different spatial firing frequency for the grid cell based on the attractor dynamic model.

Another class of models (Burak, Fiete, 2006, 2009, Fuhs, Touretsky, 2006) proposes path integration by grid cells, i.e., grid firing in space moves as the animal moves around.

b) The GRIDSmap model

The GRIDSmap (Grid Regularity from Integrated Distance through Self-organizing map) model (Mhatre et. al., 2012, Fig. 11) was used to implement our silicon realization of the grid cell system because it describes the grid cell spatial

firing pattern based on trigonometric principles which maps the entire space on to 3 rings of stripe cells.

According to this model, the stripe cell rings are present in layer III of the entorhinal cortex and provide input to the grid cells located in layer II of the entorhinal cortex. Each grid cell receives inputs from at least 3 stripe cells – one on each of the 3 rings. The rings have a preferred firing direction, i.e., the neurons on a ring will have a higher firing rate when the animal's head is pointing towards their preferred firing direction and less otherwise. The 3 rings which provide inputs to a grid cell are arranged at 120 degrees to each other in space. These rings of stripe cells perform velocity integration along their preferred direction. As the animal moves around in the environment, the distance covered by it is projected onto these stripe cells using the trigonometric principles as shown in Fig. 11(a). This distance wraps around as the number of stripe cells is limited. The grid cell fires only when all the inputs to it are coincident. Thus, the grid cell fires at regular intervals as shown in Fig.12, forming a hexagonal spatial firing pattern. For instance, if the motion along the neurons on the ring wraps around in 1m, then the grid cell attached to it will fire at intervals of 1m (called its spatial firing frequency). If, instead of being connected to a single neuron on each of the 3 rings, a grid cell is attached to two equidistant neurons on each of the 3 rings, its firing frequency shall be reduced to half a meter and if it is connected to 4 equidistant neurons on each of the 3 rings, then the spatial firing frequency of the grid cell shall be a quarter of a meter. In the model, it is described how this pattern can be learned by using self-organizing maps.

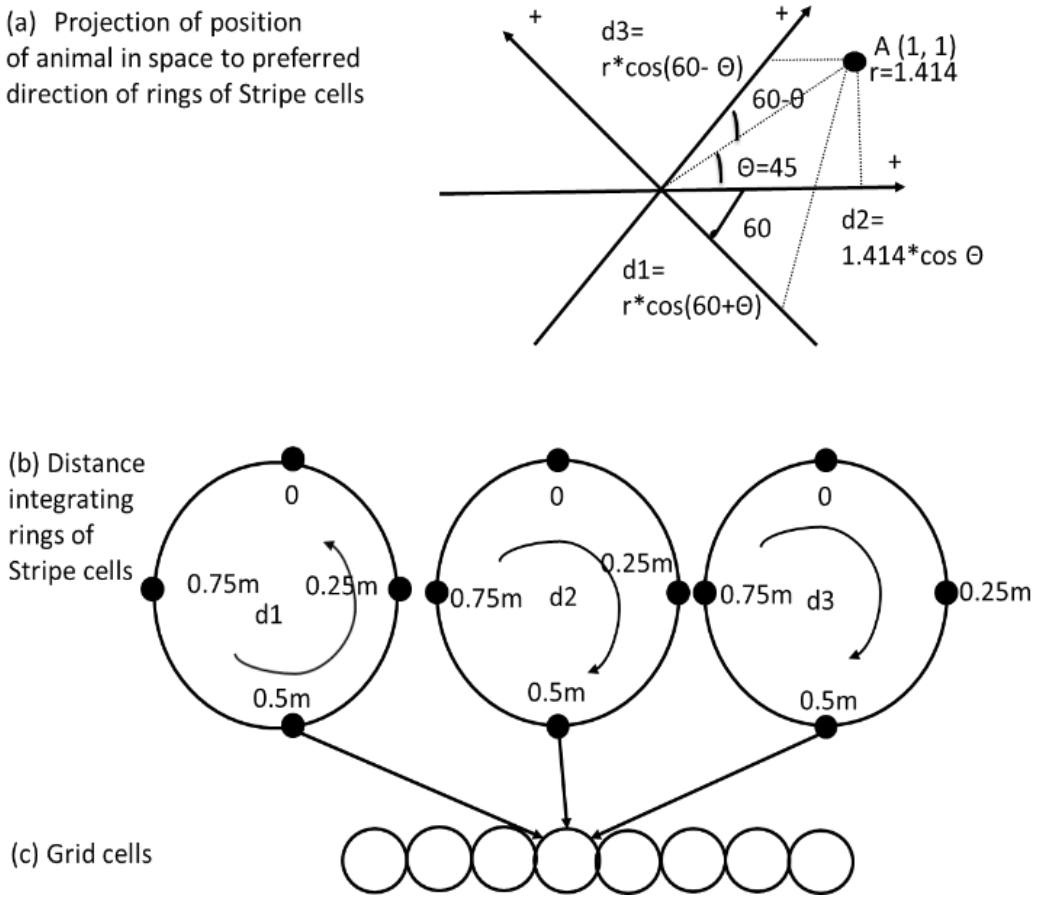

Fig. 11(a) Position of the animal is projected onto the stripe cells ring's orientation according to the trigonometric principles. The position of the aixs corresponds to the preferred firing direction of the stripe cells in the stripe cell rings shown in (b). (b) Integration of distance travelled in space on to the three rings of stripe cells, one of the stripe cells from each ring is connected to a (c) grid cell which fires only when it gets inputs from the neurons on the 3 rings attached to it. Other cells on the ring are connected to other grid cells which fire at different times. For instance, if the animal is located at position A (1m, 1m) in the x-y plane, then its position can be projected to all the three axis using trigonometric principles to find out the distance covered along each axis. Here, the distance d1=1m, d2= -0.37m and d3=1.37m. Thus, the neuron number on ring 1 corresponding to 1m shall fire, on ring 2 that corresponding to 0.37 m in anticlockwise direction (from the neuron representing 0m) and on ring 3, the neuron number corresponsding to 0.37m in the clockwise direction (from neuron number representing resting position of 0m). Similarly, when the animal moves around in space, each point will be mapped on to a neuron position on the ring of stripe cells. Whenever the place happens to map onto the 3 neuron numbers connected to the grid cell, the grid cell shall fire. Due to the alignment of rings at 120 degrees to each other, this coincidence shall happen at regular intervals in space which correspond to the corners of a regular hexagon.

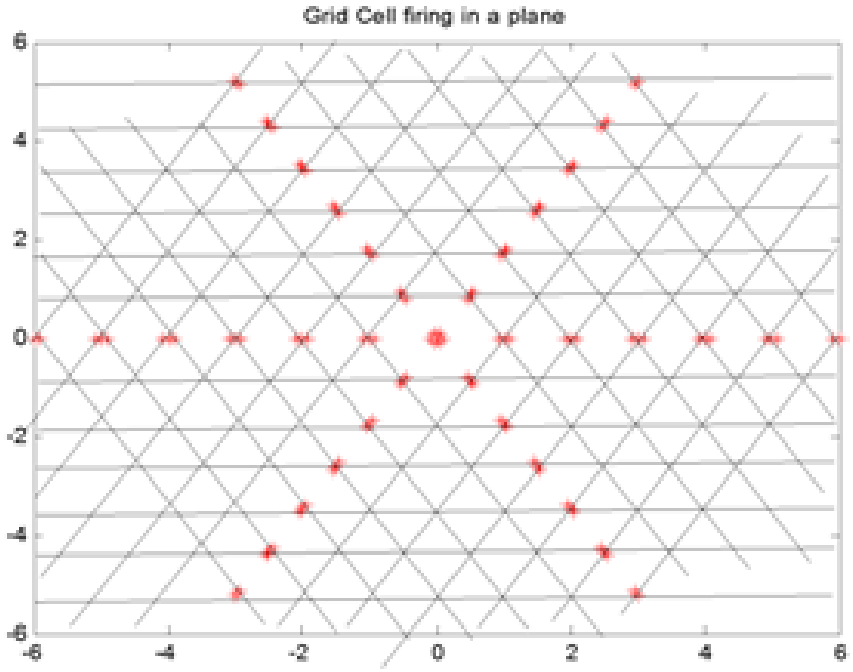

Fig.12 Formation of the hexagonal firing pattern of the grid cell attached to 1 of the stripe cells on each of the 3 stripe cell rings occurs when all the inputs to it are received at the same time (from the 3 rings with preferred orientations at 120 degrees to each other and hence the three directions of the lines/stripes). This pattern repeats as the distance travelled along each direction wraps around the ring. If the rings are moved around a full circle in 1m and only one neuron on each ring is connected to the grid cell, the spatial firing frequency of the grid cell shall be 1m. However, if two equidistant neurons on each ring are connected to the grid cell, then the grid cell spatial firing frequency shall be reduced to 0.5m and if 4 equidistant neurons on all the rings are attached to the grid cell, then the spatial firing frequency of the grid cell shall be reduced to 0.25 m. This was used in the silicon implementation of grid cells in this dissertation to achieve different spatial firing frequencies.

Once this pattern is learnt, we assume it shall be more or less stable and hence, we built three rings of stripe cells with preferred orientations aligned at 120 degrees to each other. These three rings perform velocity integration based on the trigonometric principles described in this model. One of the stripe cells from each of the three rings provides inputs to the grid cells which fire when they get inputs

from all the three stripe cells at the same time. Thus, the hexagonal spatial firing pattern of the grid cells as observed empirically, is realized.

c) Oscillatory interference model (OI)

As the animal moves around through the place cell field, it was observed that the phase of firing of the place cell precessed w.r.t. theta[7] and its firing rate changed from peak in the centre to a minimum at the edges of the place field. This could theoretically be obtained when oscillations of different frequencies are added. However, contrary to single place fields observed in an environment, this predicts multiple fields. The grid cell firing pattern was observed by Hafting et. al. in 2005 and was found to have multiple firing foci or fields as predicted by this model. Thus, interference of membrane potential oscillations of different frequencies at the grid cells was proposed as the basis for their firing, according to this model, (Burgess, Barry, O'Keefe, 2007, O'Keefe, Burgess, 2005) which was named the oscillatory interference model. Each grid cell (Fig. 13, Fig. 14) in this model is thought to be associated with 1 somatic and 3 dendritic membrane potential oscillations (MPOs). The frequency of the grid cell somatic MPO is fixed in the theta frequency range (4-7 Hz) while that of the dendritic is variable and slightly higher (7-11 Hz). When the animal moves around in space, the frequency of the dendritic MPOs increases while that of the somatic remains constant. This gain in frequency is proportional to speed (Fig. 15). Dendritic and somatic MPOs summate at the grid cell, producing a regular interference pattern, (Fig. 13) whose

[7] Theta oscillations are regular, 4-12 Hz waves seen on the electrical recordings of impulses (EEG) from the brain of several animals including humans and rats (Burgess and O'Keefe, 2007).

magnitude and phase vary over time. The gain in frequency varies along the dorso-ventral axis of the ERC producing grid cells of varying frequencies. Outputs from grid cells with varying spatial frequencies are thought to feed into a place cell. However, since the grid cells do not get direct external sensory inputs while the place cells do, the latter are thought to control the initial phase of the interference pattern by a reset mechanism. This in turn resets the alignment and orientation of the grid cells and hence, enables the place cell to fire at the place. In an extension of the oscillatory interference model (Bush, Burgess, 2014), grid cell inputs were thought to be derived from 6 velocity controlled oscillators (VCOs), assumed to be arranged in ring attractor circuits, whose preferred orientation is similar but whose phases are offset by 60 degrees to each other (as the interference pattern is hexagonal). Each grid cell is connected to each of the 6 VCOs with a different synaptic strength (Gaussian distribution of weights). Each VCO has an initial phase, which changes in proportion to the distance moved. Whenever inputs to a grid cell exceed its firing threshold, it fires. This model was not used for our system implementation as it uses velocity and not distance integration and, it explains motion only along the three axis of preference of the three oscillators and not for those in between these spaces.

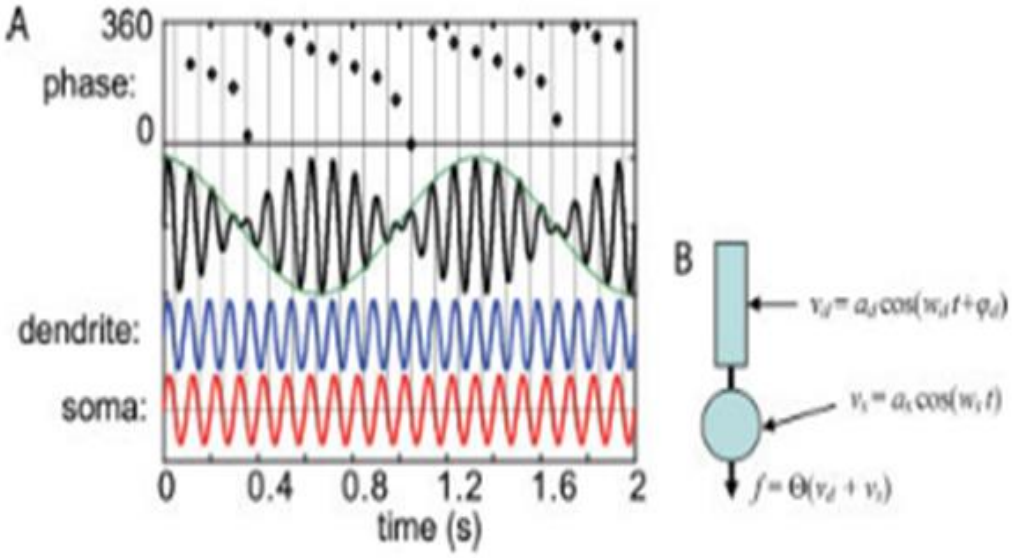

Fig. 13 [45] On empirical observations in animal experiments, it was observed that the place cell firing occurred at successively earlier phases of theta (top graph in (a)) oscillations as the animal moved around in the environment. To explain this observation, it was hypothesised that the firing of place cells was due to interference of the somatic and the dendritic membrane potential oscillations (MPOs) of different frequencies which produces peaks of interference at regular intervals and phase precession throughout the cycle. However, if this were true then the place cell pattern should have been regular but it is not regular. Instead, the grid cell pattern was observed to be regular and hence, this model was used to explain grid cell spatial firing patterns.

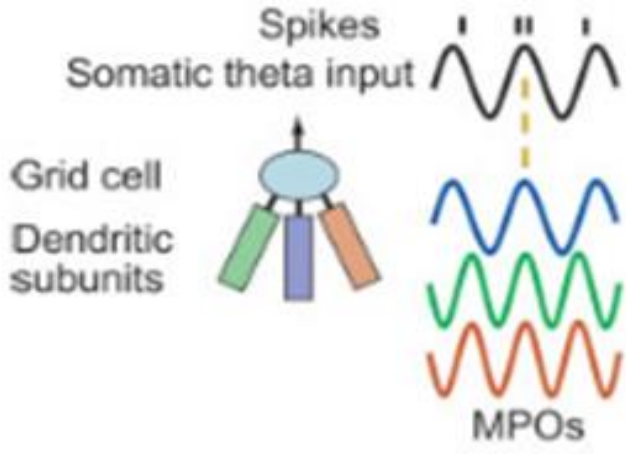

Fig. 14 [45] Since the grid cell spatial firing pattern is hexagonal, the oscillatory interference model postulated it to be the result of interference of 3 dendritic MPOs aligned at 120 degrees to each other with the somatic MPO which has a constant frequency. According to this model, the grid cell fires when all the inputs to it are coincident and their sum exceeds the firing threshold of the grid cell. Also, the oscillation frequency of the somatic MPO is assumed to be constant while that of dendritic is assumed to change in proportion to the velocity of the animal along its direction of orientation. Thus, as the animal moves around in space, the grid cell getting inputs from these dendritic and somatic MPOs will fire at regular intervals located at the corners of a regular hexagon in space.

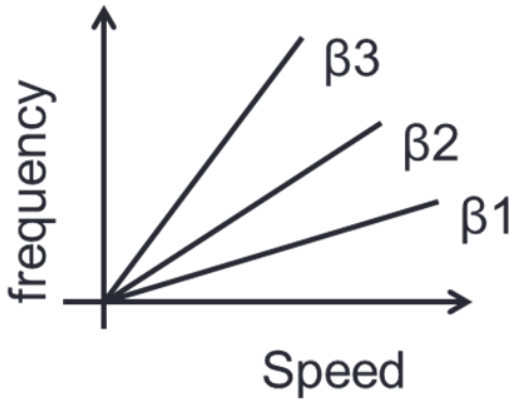

Fig. 15 According to the oscillatory interference model of grid cells, the frequency of the dendritic MPOs changes in proportion to the speed of movement of the animal along its direction of orientation in space. Different grid cells are attached to different MPOs which have different slopes for this frequency Vs speed plot. Thus, different grid cells will integrate the same animal motion with different gains and elicit firing patterns with different spatial firing frequencies.

d) Persistent spiking model

This model was postulated by Hasselmo, 2012, based on the persistent spiking properties of the entorhinal grid cells and inspired by the oscillatory interference model. In this model, it is assumed that there is a systemic theta oscillation which provides the base oscillation. In addition, there are velocity controlled oscillators which also produce oscillations whose frequency changes with movement of the animal in the environment along their preferred firing direction. As the oscillation frequency of these oscillators increases, their firing goes out of phase with that of the baseline theta oscillation. This phase difference between the two determines the distance travelled by the animal in space. 3 such oscillators aligned at 120 degrees to each other have been proposed in this model. As the animal moves in any direction in space, the firing frequency of each of these oscillators' advances as a function of the distance travelled along the preferred direction of the oscillator as determined by trigonometric principles (as cosine of the angle formed by the direction of preference of the oscillator and direction of motion of the animal). All the 4 (baseline and the three aligned at 120 degrees to each other) oscillators feed into a grid cell which fires only when the phases of all these oscillators are synchronous (same at the same time). Since the three oscillators are aligned at 120 degrees to each other, their phases synchronise at the corners of an equilateral triangle which implies that their firing pattern is hexagonal (intercalated hexagons). This model also suggests that since head direction cells in the subiculum have similar response to head direction, they could work as velocity controlled oscillators providing inputs to grid cells. This suggestion could be valid

as the subiculum provides inputs to the medial ERC. However, the persistent spiking has been observed in cells of the entorhinal cortex and not of the subiculum. Hence, the very basis of this model is subject to question. Thus, we did not use this model for our system implementation.

e) A model combining oscillations and attractor dynamics

This model has been proposed in Hasselmo and Brandon, 2012 in an endeavour to overcome the shortcomings of both the oscillatory interference and the attractor dynamic models by combining the two. According to this model, the grid cells are connected to an array of head direction cells (rather than just 3 or 6 as in the OI model described in section 2. E. i) c)) with different phases and preferred firing directions. When an animal is moving along the preferred firing direction of a HD cell, the grid cell connected to it shall fire. This explains a mechanism of movement of the grid cell firing across space. This also tries to connect the phase precession and theta rhythm seen empirically but not explained by the attractor dynamic model. It also tries to explain the effect of cellular properties on grid cell firing based on the OI model. But it hypothesizes the presence of too many connections which makes it difficult to implement in hardware.

ii) Place cell Models

Several models were proposed in the pre grid cell era which considered place cell firing to depend upon sensory inputs alone. These manifested as the relative distance of the animal from a landmark, or as fixed distance from the boundary vector cells which fire when the animal is either along the boundaries of the enclosure or along a partition in the enclosure. The boundary vector cell (BVC)

model (Hartley et. al., 2000), (a pre-grid cell era model) suggests that the place cells fire based on fixed distance from firing of the BVCs and BVCs are thought to fire either when the animal moves along the boundaries of the enclosure or along a partition inside the enclosure. According to this model, the place cell fires optimally when a barrier is at a given distance and in a particular direction from the animal. This response was postulated to be Gaussian tuned in response to the presence of a barrier, peaked at a preferred distance and direction/orientation. It was also observed that on insertion of a barrier in the room, the place cell firing shifted in proportion to distance from the newly formed boundary. Thus, this model attaches importance to environmental boundaries and distance as a determinant of place cell firing. Now this could be because a boundary acts as a reference from which distance of the place of significance can be calculated. Looking at this model in the post grid era, the sensory cues could provide a landmark and the grid firing pattern a matrix for calculation of distance of this landmark from the boundary in an environment. However, this model holds little appeal in explaining place cell firing in the post grid cell era because it does not take motion integration by the animal into account.

After the demonstration of regular spatial firing patterns of the grid cells, many other models were proposed based on integration of grid cell firing patterns (integrated motor inputs) of varying spatial frequencies. Of this, the attractor dynamic model (McNaughton et. al., 2006) attributes place cell firing to summation and thresholding of inputs from several grid cells with varying spatial frequencies.

The grid cells in turn are thought to integrate the distance moved along a direction at a particular speed to produce hexagonal spatial firing patterns. The coincidence of inputs from grid cells with different spatial frequencies produces place cell firing. However, this model suggests that the place cell fields should be multiple and regular as are grid cell fields which is not seen empirically.

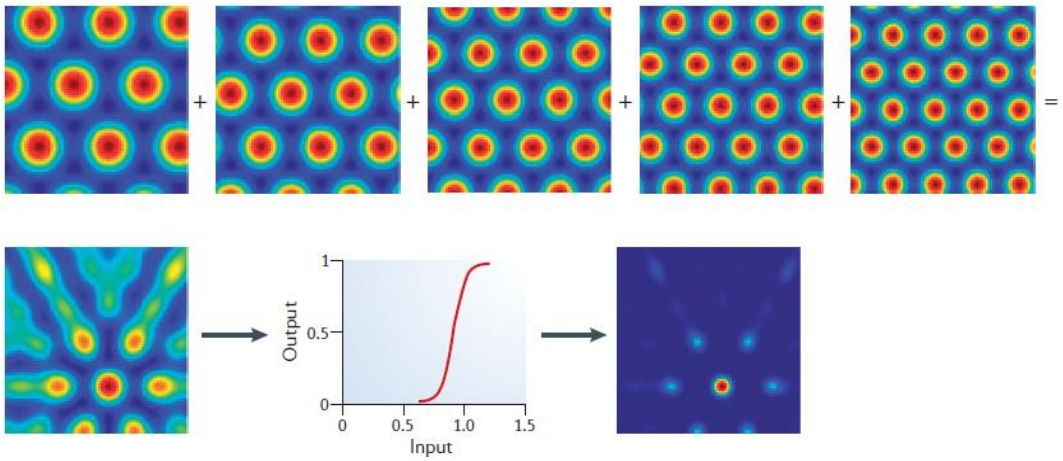

Fig. 16 [62] According to the attractor dynamic model of the place cells, each place cell fires (bottom right) due to summation and thresholding of inputs from grid cells with different spatial firing frequencies (top). In the top row are shown firing patterns of grid cells of different spatial frequencies whose summation produces a firing pattern shown on bottom right. The place cell fires (bottom right) only when the sum of all these inputs exceeds the threshold (bottom middle) of firing of the neuron.

The oscillatory interference model also considers place cells to be connected through synapses of varying strengths to the grid cells with varying spatial firing frequencies. However, the place where they fire is controlled by phase resetting of theta as explained earlier (Section 2. E. i) c) Oscillatory interference model (OI)). When an external cue is encountered by the animal, the place cells fire and reset the phase of theta so that the grid cell inputs sum at that place.

Another category of models is based on networks of synapses with different weights connecting grid to place cells and generating place cell firing patterns based on learning rules like Hebbian learning, independent component analysis (ICA) or other competitive learning mechanisms. Some of the notable ones are briefly described here.

In Solstad et. al., 2006, the authors looked at the possible phase, spacing and orientation of the grid cells which can combine to produce biologically plausible place cell firing. They also propose a gaussian profile of synaptic weights connecting grid cells to place cells. They propose that each place cell receives inputs from 100-1000 grid cells of varying spacing but similar phase and orientation.

In Rolls, Stringer and Elliot, 2006, Si & Treves, 2009, the authors wanted to show how place cell firing patterns could be generated by a self-organizing process from the grid cells. For this, they used a network of 100 grid cells and 100 place cells. The activity from the grid cells was propagated through the feedforward connections to activate a winning set of cells in the place cell layer. Within the place cell layer, there was feedback inhibition. The grid cells had 10 different spatial frequencies with each frequency exhibiting 10 different phases. The initial synaptic weights between the grid and the place cells were set to random values. The synaptic weights between the two were strengthened based on activity of the network according to the Hebbian learning rule. This produced single but narrow place fields. Thus, modified associative learning rule which incorporates a short term memory trace of previous firing was used – called the trace rule. This rule

produced wider place fields which are more akin to those observed empirically. They also simulated 2D place field formation using the same methods. They observed that multiple peaks were evident in the place cell firing. They also observed that the time taken for learning is commensurate to the time available for the place fields to appear in the first instance as observed empirically.

In Franzius, Vollgraf and Wiskott, 2007, authors have proposed the grid to place transformation to be achieved by simply increasing the sparsification by using ICA. They used 100 input grid cells and 100 output place cells. The output units showed a localized place field. They also refuted the slow feature analysis, principal component analysis and random mixtures as the possible mechanism for such outcome.

In Molter & Yamaguchi, 2008, authors have shown (through Matlab simulations) how the place cell firing depends upon grid cell firing and theta phase precession which provides a precise timing for the place cell firing.

In DeAlmeida et.al, 2009, Savelli & Kneirim, 2010, the authors have refuted hebbian learning or plasticity to be the mechanism of transformation from grids to place fields but have suggested the connectivity patterns between the two to be responsible for the same. They suggested that each place cell receives 1200 grid cell inputs and that the synaptic strengths are variable. The grid cells are of varying spatial frequencies and the ones connected to the grid cell are randomly selected. Moreover, they have suggested the role of gamma frequency inhibition in delineating the place fields.

In Cheng & Frenk, 2011, the authors derive a family of feedforward networks that generate the grids to places transformations. These networks have an inverse relationship between the synaptic weights and the grid normalized offset (as defined in the paper). With this map, they try to construct explicit solutions for the grids to places transformation with multiple spatial maps, i.e., with arbitrary locations either within the same or in different enclosures. These maps are possible because the weights are learned or assigned in such a way that a group of weights contributes to spatial specificity in one context but remains spatially unstructured in another context. Next they also show global remapping solutions which are useful in synaptic learning by spiking neurons. But all these models do not explain why multiple place fields which are formed from the grid cells do not have regular spacing like the grid cells and why place fields are seen in the absence of grid firing as in pre-weanling rats.

Though different in their approach, all models suggest place cell firing due to integration of motor or sensory inputs. In a recent study Madl et. al. 2014, it has been contended that this integration could possibly occur in a Bayes' optimal manner. We also agree with the proposal of Madl et. al. 2014, that Bayesian integration of inputs at the place cells is more plausible than that by summation and thresholding.

F. Bayesian integration of inputs at the place cell

Bayesian integration (as used by computational neuroscientists) of inputs means that the information from different sources is combined by weighting information

from each source according to its accuracy, i.e. more precise information receives a higher weight. Mathematically, it can be represented as

$$p(x \mid O) \propto p(x) * p(O \mid x) \qquad (1)$$

Where x is the animal's location in space and O= $\{o_1, \ldots o_N\}$ represents a set of firings of a place cell. Assuming that the p(O) is the same for all locations, from equation (1), we can infer that the probability of being at a location given observation of the place cell firing (p(x|O)) is proportional to the probability of being at the place (p(x)) weighted by the observed firing of place cell given the place (p(O|x)). Thus, realising this function needs a multiplication of different probability distributions. Though evidence of information integration in brain based on Bayesian statistics has been postulated for neuronal ensembles Knill & Pouget, 2004, Colombo & Series, 2012, Ernst & Banks, 2002, Kording & Wolpert, 2004, Ma, et. al., 2008, Zemel, et. al., 1998, Pfuhl, et. al., 2011 and MacNeilage et. al., 2008, for the first time, Madl et. al., 2014 have demonstrated its existence at the single cell level. Here, it is contended that as seen in neuronal ensembles elsewhere in the brain, Bayesian integration could also be the mechanism for integration of inputs from many sources inside single place cells. Madl et. al., 2014, have contended that though the results do not fit the data exactly, the model is simple and fits the data reasonably well. They have used simulations to explain integration of external cues as per the boundary vector cell (BVC) model. In this dissertation, we extend this concept to the GRIDSmap model. For testing it, we did MATLAB simulations of the animal motion in free

space based on the GRIDSmap model. Simulating the motion of an animal in free space, we obtained the grid cell firing pattern in space. The firing pattern had the Gaussian shape of a probability distribution suitable for implementing equation (1). We used another similar Gaussian distribution to represent the probability of sensory inputs received by the place cell. Thereafter, we performed integration of these probability distributions in Bayes' optimal manner in MATLAB (code provided in Appendix IV). Results in Fig. 17(b) show that the integration of grid cell inputs in a Bayes' optimal manner can produce a localized field which becomes sharper when sensory inputs are integrated (Fig. 17(c)) on to it- as observed empirically. We also simulated (Fig. 17(a)) place cell firing due to summation and thresholding of inputs from these grid cells with varying spatial frequencies in MATLAB. This produces multiple foci of firing for a place cell within an environment. The multiple foci of firing are not observed empirically.

Hence, we also agree with the proposal of Madl et. al., 2014 that the integration of inputs to place cells in a Bayes' optimal manner is more plausible than summation and thresholding as proposed in the original GRIDSmap and other models mentioned above and thus, it is applicable to the GRIDSmap model. Thus, to implement the function of place cells in silicon based on the GRIDSmap model and integration of sensory and motor information in a Bayes' optimal manner, we modified the GRIDSmap model and designed and fabricated a synapse circuit (described in detail in section 4.B. iii) - the Bayesian integration synapse). In conjunction with a conductance neuron, we realized the function of the place cells in silicon using this Bayesian integration synapse circuit.

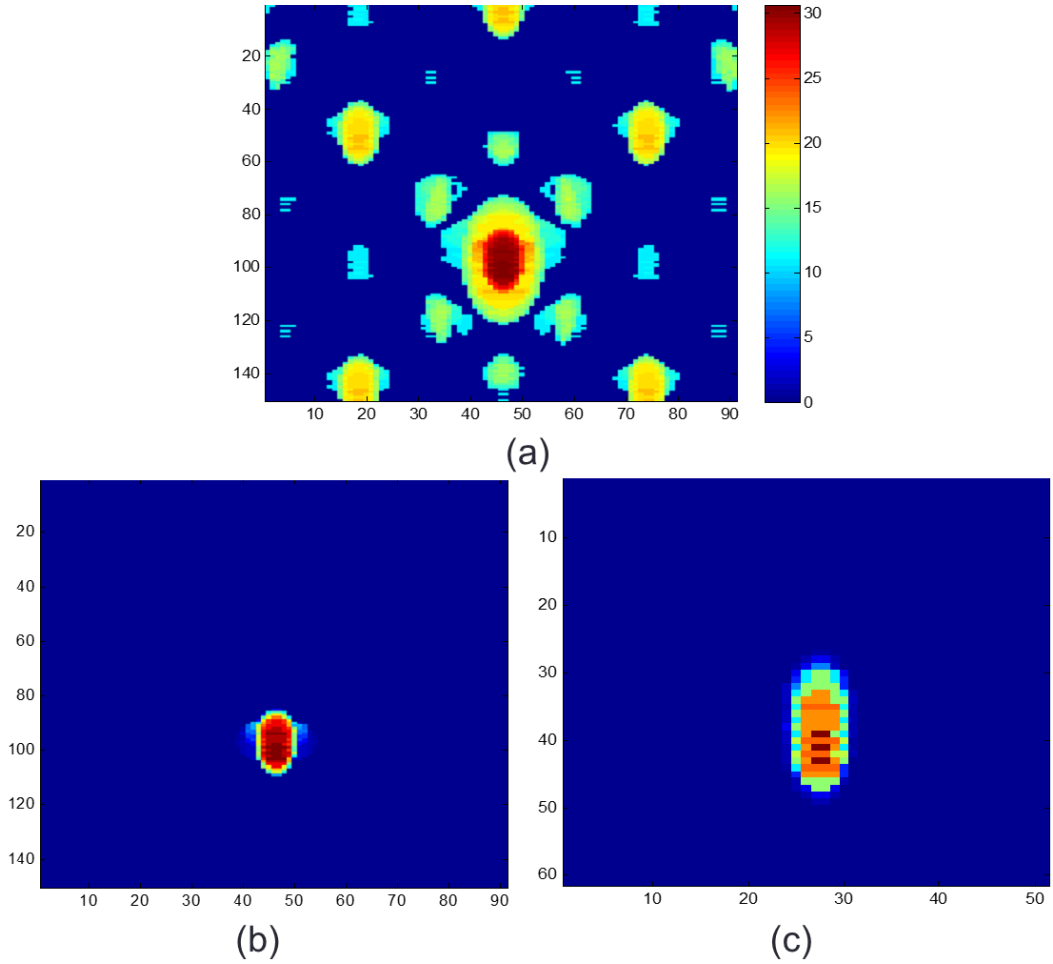

Fig. 17 MATLAB simulation of place cell firing (a) by summation and thresholding of inputs from grid cells with different spatial frequencies (b) by integration of grid cell inputs in a Bayes' optimal manner (c) sensory inputs being integrated on to those in (b). Most well defined fields, as observed empirically, are formed by integration of sensory and grid cell inputs in a Bayes' optimal manner.

G. Conclusion

This section provides a brief background on anatomy, empirical observations and computational neuroscience models of the cells of the HF – the HD, the grid and the place cells. In the following sections, the silicon realization of these shall be described.

3. HEAD DIRECTION CELL SYSTEM: SILICON IMPLEMENTATION

The head direction cell system (Taube et. al., 1990 a, b and Zhang, 1996) is a collection of head direction cells, of which one of the cells fires when the head is pointing in its preferred firing direction (or 45 degrees thereof) which is defined w.r.t. sensory cues in the environment called the polarizing cues. Different head direction cells have different preferred firing direction. With movement of the polarizing cues, the preferred firing directions of all the cells moves in unison. This has lead the computational neuroscientists to propose that the head direction cell system works as an attractor dynamic network with a single bump of activity focused on the preferred firing direction of a head direction cell. As the animal moves its head around along the horizon, its vestibular system (McNaughton, et. al., 1991) gets activated and provides motion information to the head direction cell system. The latter integrates this motion information to update the current estimate of the head direction. This involves movement of this bump of activity to the right or to the left. To update the estimate of head direction from information on the current position and motion integration, the input signals need to come from the vestibular apparatus in the inner ear (primarily). This pathway from the vestibular apparatus to the subiculum is shown in fig. 2 in Taube, 2007 which indicates that to reach the post subiculum, where the head direction cells are present from the vestibular apparatus, the signal has to pass through at least 6 different nuclei. In this paper, it has also been mentioned that a visual cue could reset a cell's preferred firing direction within 80ms when restoring light to the room after an

animal had spent a period of time moving in darkness based on a study by Zugaro et. al., 2003.

As per Massoud and Horiuchi, 2012, and Corradi et. al., 2014, the head direction cell system has been implemented as three rings of neurons, as described in the attractor dynamic model (described in section 2. E. i) a)) of the head direction cell system, with interconnections coded in software. However, implementations of both these systems required 3 silicon chips, interconnected through software interfaces. Hence, it was expensive in terms of hardware, in addition to requiring software interfaces. Here, instead, we describe and present results from a silicon chip which implements an abstracted version of the attractor dynamic model for the head direction cell system, i.e., a single ring circuit, fabricated on $1/12^{th}$ of the area of a tiny chip unit (1275mmX1275mm), can maintain the bump of activity at a place, and move it in a controlled fashion in either the clockwise or the anti-clockwise direction. Moreover, if this system is integrated with other chips to implement the entire hippocampal formation in silicon, it can be done very efficiently. At least 3 different ring circuits (aligned at 120 degrees to each other) are needed to demonstrate the firing pattern of the grid cells. If each ring needs 3 chips as presented in Massoud and Horiuchi, 2011, and Corradi et. al., 2014, then a total of 9 chips are needed. Whereas, with the system that we have designed, only 3 ring circuits are needed to implement the grid cell firing pattern, all of which can be fabricated on small portion of a single chip. To realize the firing of a place cell, we need inputs from grid cells of at least 3 different spatial frequencies. This means, 9 rings are needed, all of which can be integrated on a single chip

with the circuit that we have designed as opposed to the previous systems which needed at least 27 chips!

A. System design

To implement the head direction cell system (Fig. 18) in silicon, we designed a new ring circuit which has 24 nodes. Each node on the ring represents a direction along the azimuth from 0-360 degrees. With 24 nodes on the ring, the resolution is 15 degrees (360/24). The ring circuit can maintain the firing neuron position at a node, representing the current head direction of the animal. It can also move the firing neuron position around in a clockwise direction or anti-clockwise direction when *RS* (right shift) or *LS* (left shift) pulse signals are applied as inputs. The outputs are neuron numbers each of which encodes for a head direction. For instance, firing of neuron number 1 corresponds to 0 or 360 degrees and that of neuron number 12 to 180 degrees.

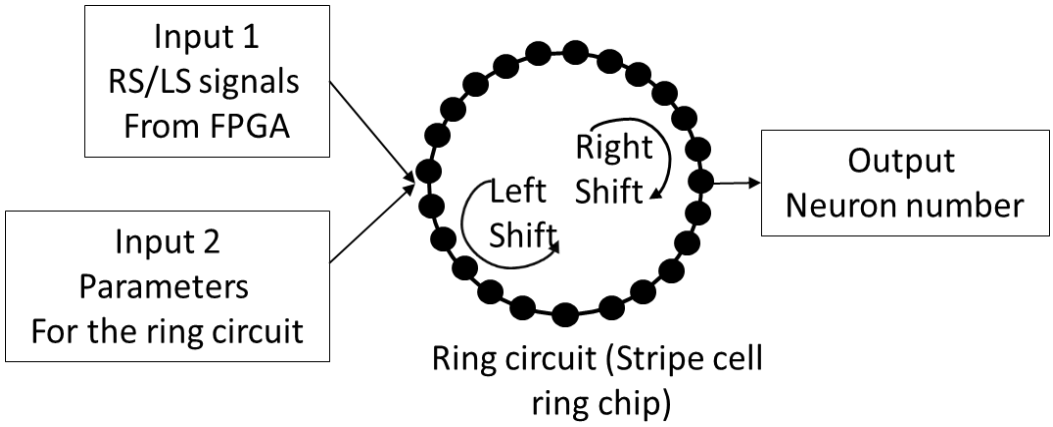

Fig. 18 Showing design of the head direction cell system in silicon. The entire system was designed using one ring circuit (Fig. 20) on the stripe cell ring chip (Fig. 19). Inputs to the chip were provided through the FPGA (as *RS* or *LS* signals) or the PCB (voltage parameters) and outputs from the chip were read out using the mixed signal oscilloscope.

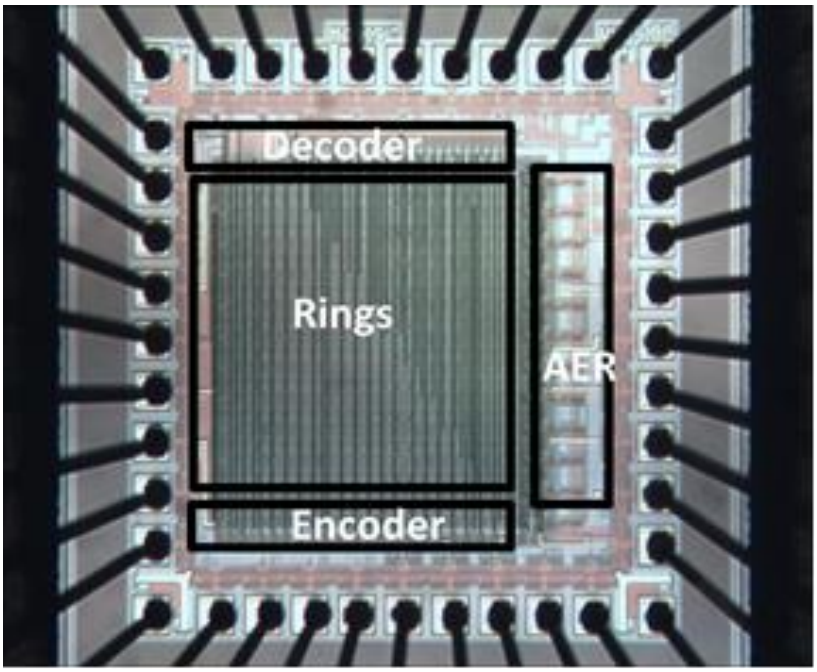

(a)

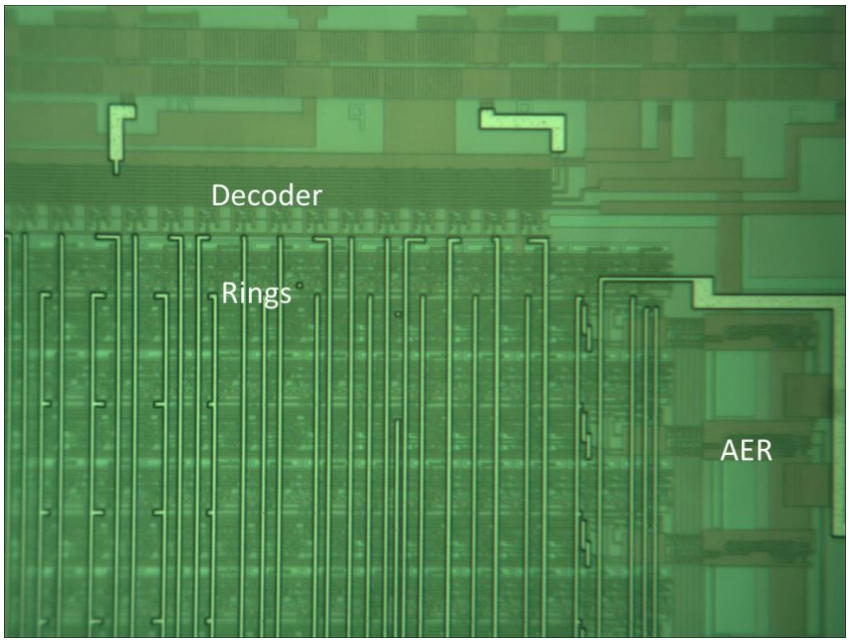

(b)

Fig. 19 Micrographs of the stripe cells ring chip (a) showing the 12 rings, the 5 bit to 24 line decoder, the 32 to 5 bit encoder and the address event representation (AER) circuits. (b) Zoomed in version of the same chip showing the rings in more detail. Also seen are portions of the AER and the decoder.

B. Circuits

The function of the HD cell system was realized with a ring shaped circuit (Fig. 20, Fig. 21) on a chip, called the stripe cell ring chip (Fig. 19).

i) The stripe cell ring chip

This chip has 12 rings which are provided *RS* or *LS* signals from an FPGA through an on chip decoder circuit (Fig. 79). The outputs from the chip are neuron numbers and the ring numbers of the neurons which fire simultaneously. These are read using a 24 to 5 bit encoder circuit and another 12 to 4 bit AER encoder circuit respectively.

The ring circuit has two parts – one is the winner take all (WTA) (Lazzaro et. al., 1989) circuit with 24 nodes (Fig. 20) and the other is 24 integrate and fire neurons (IFN, Fig. 21). The WTA circuit has 24 nodes, arranged in a ring, only two of which are shown in Fig. 20. The rest of the nodes are similar to node 2. The first node is designed differently to provide two different voltages by using the reset signal. As per the WTA circuit, only one node wins at a time which shall correspond to a bump of activity at the node. The reset signal helps node 1 to be the initial winning node (by applying voltage V1, which is less than V2, to the gate of transistor M3) whenever the ring is reset. Once this node wins, it stays as the winner as long as the parameters *RS* (right shift) and *LS* (left shift) are held at 0V. During this time, the M5-M6 current mirror (Fig. 20) copies the current from the winning node to the connected capacitor C1 which charges up to Vdd. This current is controlled by the cCon parameter on M13. The capacitors of the non-

winning nodes cannot charge up due to the leak nfet (M9). The current is also copied to the IFN whose address is read by the two encoders. [8]

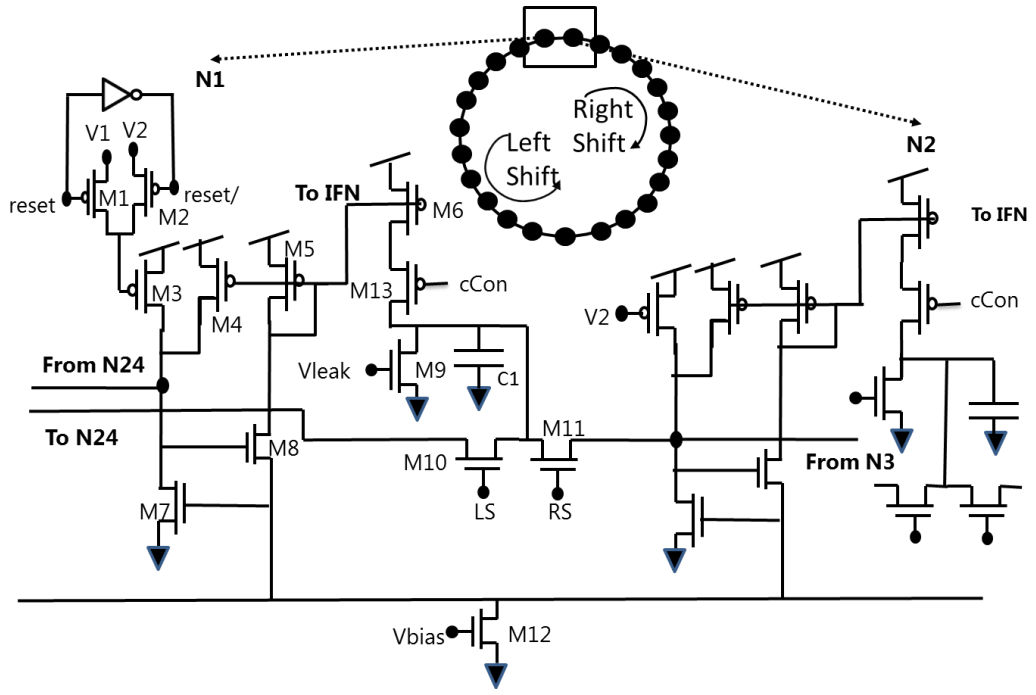

Fig. 20 Showing the circuit schematic of part of a ring on the stripe cell ring chip. Each ring circuit has 24 nodes of which two-N1 and N2 are shown here for clarity, the rest of the nodes were similar to node N2. As per the working of the WTA circuit, only one node wins at a time depending on the value of the parameter applied to the gate of M3 (given all the nodes are otherwise similar). Node N1 has provision for resetting the winning position of the ring circuit to N1 by application of voltage V1 to the gate of transistor M3. V1 is less than V2 so it makes this node the winning node whenever the circuit is reset. Once the winning position is set to N1, the current is copied on to the attached capacitor, C1 and to the integrate and fire neuron through the current mirrors. The capacitors attached to the non-winning nodes are prevented from charging up due to the leak nfet M9. To move the position of the winning node around the ring, the *RS* or the *LS* signals are applied to the gate of M11 or M10. W/L for M4 =2.4 µm/12 µm, and for the rest, it was 2.4 µm/2.4 µm. C1=75 fF. Capacitors were designed using poly-poly1. IFN here means an Integrate and Fire neuron the circuit for which is shown in Fig. 21.

[8]The earlier version of this circuit was developed by me in the Horiuchi lab. That version did not have the transistor M13 and had a different W/L for M6. M13 was introduced to enable control over the current used to charge up the capacitor node.

Table 1 Showing the function of various transistors in the stripe cell ring circuit

Transistor	Function
M1, M2	Reset the position of the winning node to first node N1, by applying V1 to it instead of V2 (V1 is less than V2).
M3	Current source
M7, M8	WTA circuit
M4, M5, M6	2 current mirrors
M13	Controls current copied on to the capacitor.
M9	Leak transistor- prevents the non-winning nodes from charging up.
M10-M11	Pass nfets to work as switches to allow the position of the winning node to be shifted to the right or the left in a controlled manner.
M12	Current for biasing
C1	Capacitor which stores charge from the winning node and acts as a charge pump to shift winning position to the next node

When the *RS* pulse is applied to the gate of M11, the charge stored in the capacitor C1 is transferred to the second node, N2, which starts winning and when the *LS* signal is applied to the gate of M12, node 24 becomes the winning node. Thus, the bump of activity in this ring can be reset to the first node, N1, held at a particular value for a duration of choice and moved around as is required to implement the head direction cell system based on the attractor dynamic network. The decoder was designed using 24 five input (5 bit address) NAND gates whose output and req/ signal were inputs to the 24 NOR gates whose outputs drive the *RS* and *LS* signals of the 12 rings. Details on the decoder are provided in Appendix V (Fig. 81). For instance, to provide an *LS* signal to ring 1, the address bits were set to 5 bit binary 00000 and a *req/* signal (active low) was applied and to apply *RS* to ring 1, the address was set to 5 bit binary 00001 and *req/* signal was pulled active low. These generated active high *LS* and *RS* signals respectively, which were applied to the gates of M10 and M11 in Fig. 20.

Since the WTA circuits are prone to mismatch, current mirror M4-M5 (of each node on the ring circuit in Fig. 20) was used to copy the current back to the winning node (positive feedback) and help it stay winning. In this circuit, the W/L of M4 was kept at 1/5 so that the positive feedback is not too strong to hinder movement to the next node but is strong enough to overcome potential mismatch. Another aspect of the circuit design was that when the *RS* or the *LS* signal is pulled high, a lot of charge is transferred in a very short time (1 µs). This could cause charging of all the capacitors and uncontrolled movement of the winning node if M6 is wide enough. To avoid this, M13 was introduced and current through it was controlled by using a gate voltage parameter, *cCon* so that the capacitor charges up slowly (over 1 ms as the ring will not be moved around at a frequency greater than 1 kHz). The capacitor value was chosen to be 75fF so that it could store enough charge to overcome capacitance at the drain of M3, M4, M7 and the gate of M8, which had to be raised above 2V to make the next node winning. The capacitor value could not be too high as this would have fabrication constraints (12 rings with 24 nodes and 24 neurons each were to be designed on one tiny chip unit). The *reset* signal was used to apply *V1* to the gate of M3 through M1 and to reset the position of the winning node to the first node.

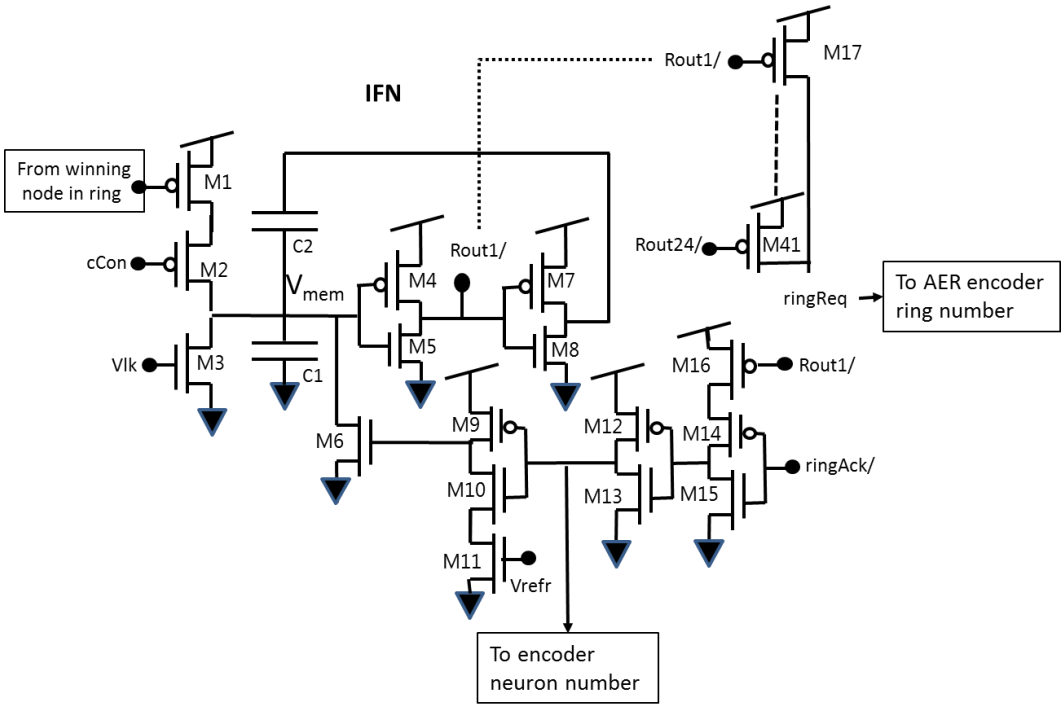

Fig. 21 Circuit schematic of the integrate and fire neuron, used to read the output current from each of the 24 nodes on the ring circuit. The copied current is multiplied 5 times (W/L of M1) and controlled by M2. The neuron sends an output (*Rout/*) when the V_{mem} rises and exceeds the threshold voltage determined by the size of M4 and M5. *Rout/* signal from all the 24 neurons in the ring is 'OR'ed by using a chain of pfets (M17-M41) to produce the *ringReq* signal which is processed by the AER encoder to read the ring number. The AER sends back an acknowledge (*ringAck/*) signal which enables the neuron number to be read by the encoder for the neuron number and also allows the neuron to be reset after a refractory period determined by the parameter V_{refr} applied to the gate of M11. C1=60fF, C2=30fF, W/L of M1=6µm/1.2µm, M11=2.4µm/2.4µm, and for the rest=1.5 µm/1.5 µm. Capacitors were designed using poly-poly1.

Table 2 Showing the function of various transistors in the integrate and fire neuron circuit.

Transistor	Function
M1	Part of the current mirror (the other transistor is M5 on the ring circuit- Fig. 8) which copies current from the ring circuit on to the IFN and multiplies it by a factor of 5 (its W/L ratio).
M2	Controls the amount of current copied
M3	Leak transistor- prevents firing of neurons of the non-winning nodes
M4, M5, M7, M8	Inverters to amplify the output spike amplitude.
M6	To reset the neuron.
M9, M10, M12-M14	Buffers to produce a correct logic level pulse at the required point.
M16	To route the rout/ such that the neuron number is read out only after the ring number has been read.
M11	To set the refractory period.
M17-M41	To logically 'OR' inputs from all 24 neurons in a ring and generate a ring req if any of them is firing.
C1, C2	Capacitors which hold the membrane potential of the neuron for a while to enable its persistent firing.

Current from the winning node was copied on to its corresponding integrate and fire neuron (IFN, shown in Fig. 21) through the current mirror formed by M5-M6. It multiplies this copied current 5 times (W/L ratio of the input transistor). To control neuronal firing, the current integrating on to the two capacitors, C1 and C2 was controlled by *cCon* applied as a gate voltage to the gate of transistor M2 (IFN circuit). When the capacitor voltage reaches the threshold defined by the size of the transistors of the inverter, the neuron fires a spike, which is amplified by the gain of the two inverters (M4-M5, M7-M8). The feedback capacitor, C2 maintains the membrane potential (V_{mem}) for a while to enable persistent spiking. The spikes so generated from all 24 neurons on a ring were processed using a chain of pfets (M17-M41 in Fig. 21) whose drains were connected to the address event representation (AER) circuit (details in Appendix V-Fig. 80). The AER circuit

reads the ring number using a 16 to 4 encoder. Once the ring to be read is chosen, the *ackRing/* signal is sent back and the neuron number is read using an orthogonally placed 32 to 5 encoder. Once the ring and neuron numbers have been read, the neuron is reset after a refractory period determined by V_{refr}.

C. Measurement Results

The chips were fabricated using 0.5 µm ON semiconductor process from MOSIS and tested using a PCB designed for each chip. The results were read using an Agilent MSO 6014A mixed signal oscilloscope and processed using MATLAB.

Several measurements were performed on one of the rings on the chip to demonstrate its function as the head direction cell system and a central pattern generator. These include applying the *reset* signal to shift the winning node position to the first node (N1), applying a train of *LS* signals to demonstrate movement of the node of activity from the first node to the 24th node and so on, followed by application of *RS* signal to demonstrate movement of bump of activity from node 1 to 2 and so on. Parameters used for the tests to demonstrate the function as a head direction system were V_{lk} (neuron)=0.52V, *cCon*=4.17V, V_{refr}=0.50V, V_{leak} (ring)=0.404V, *V1*=3.89V, *V2*=4.15V, V_{bias}=1.457V. Firstly, the ring was reset (N1 is the winning node) by providing a *rese*t signal which resulted in applying V1 to the gate of transistor M3 in the WTA ring circuit. This corresponds to head direction of 0 degrees along the azimuth. If now the head moves by 15 degrees and then by another 15 degrees to the right, this shall be represented by nodes 2 and 3 of the ring respectively. Thus, the *RS* signal (5V logic high pulse of 5 µs duration) was applied twice at an interval of 3ms to move

the winning node position. As seen in Fig. 22, the activity of the ring is concentrated on N1 (0 degrees) after the reset (not shown in the figure) and shifts to N2 (15 degrees) and then to N3 (30 degrees) on application of the *RS* signal.

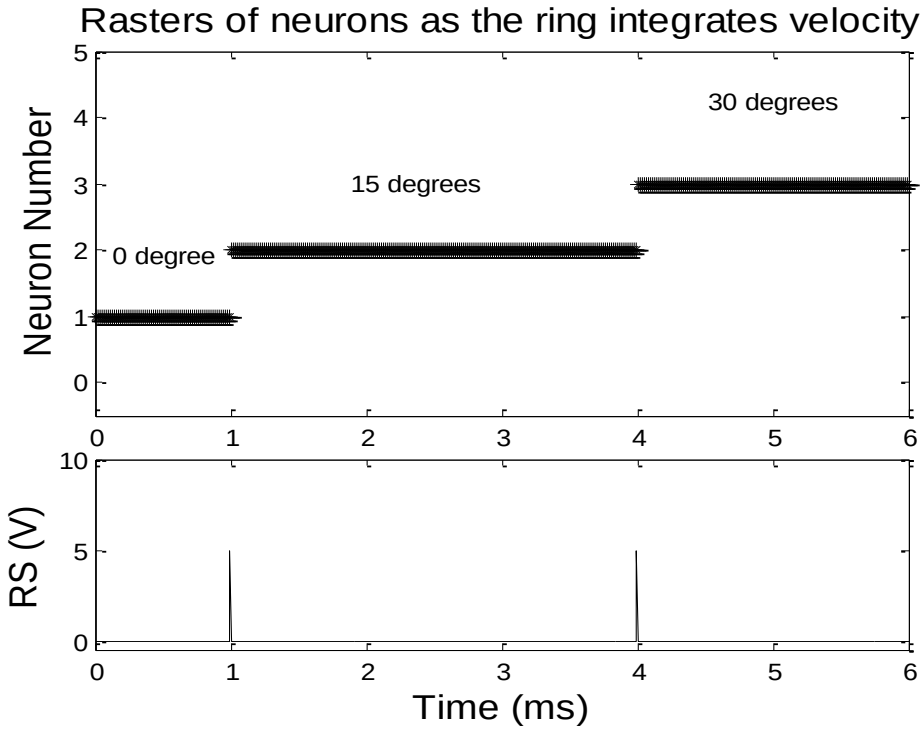

Fig. 22 Chip measurement results showing neuronal firing and holding of bump of activity at node 1 and its shift to the right to nodes 1, 2 in a controlled manner when a *RS* pulse signal is applied. Each neuron on the ring corresponds to a head direction in degrees. Neuron 1 corresponds to 0 or 360 degrees and neuron numbers 2 and 3 to 15 and 30 degrees respectively. Thus, the ring circuit can perform all the functions required of a head direction cell system, viz., holding the bump of activity at a neuron while the head is stationary and then moving the bump around to correspond to the new head direction as the head moves around the horizon.

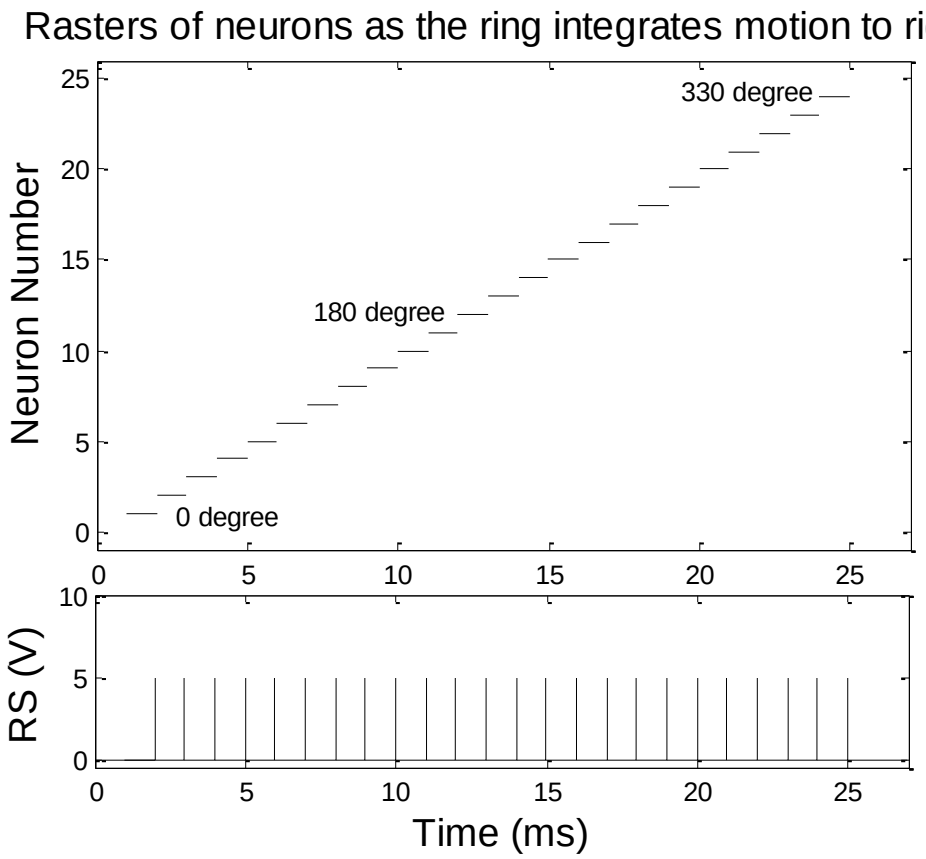

Fig. 23 Showing movement of the neuron numbers on the ring circuit on the stripe cell ring chip around in clockwise direction as a train of *RS* signals is applied to it. Each neuron number corresponds to a head direction (in degrees) along the azimuth. Thus, these results demonstrate movement of the head from 0 degrees to 180 to 330 and back to 0 degrees as a train of *RS* signals is applied.

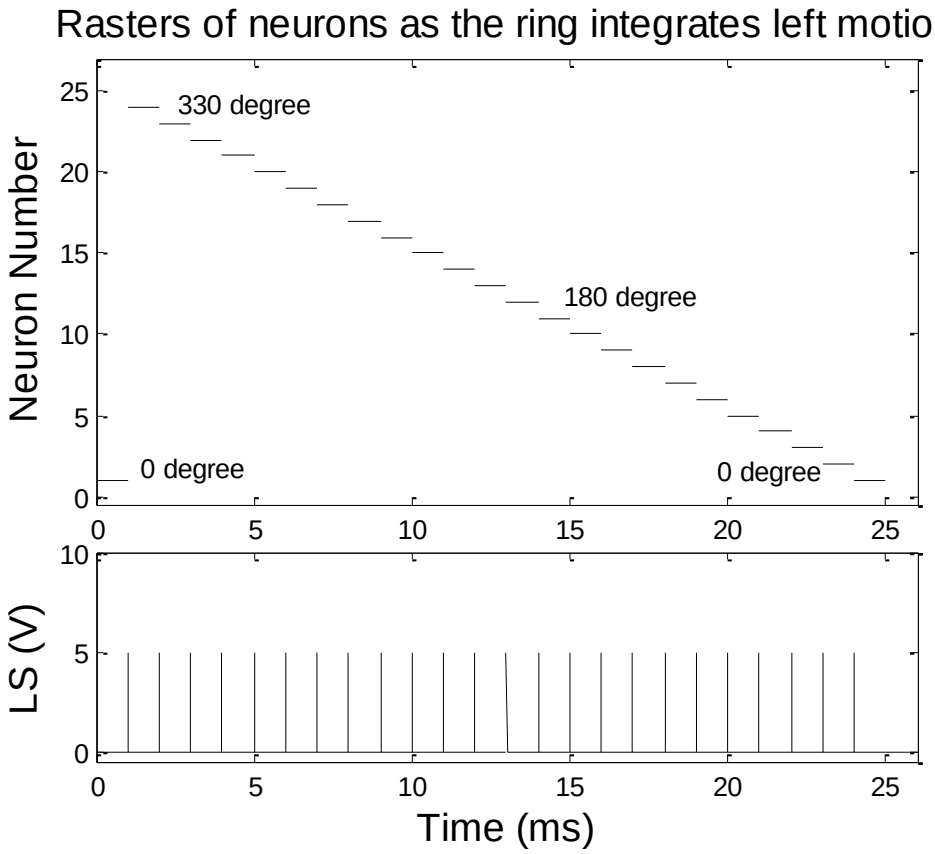

Fig. 24 Showing movement of the neuron numbers, on the ring circuit on the stripe cell ring chip, around in anti-clockwise direction as a train of *LS* signals is applied to it. Each neuron number corresponds to a head direction (in degrees) along the azimuth. Thus, this figure demonstrates movement of head from 0 to 330 back to 0 through 180 degrees.

Now if the head moves through a complete rotation in the clockwise or anticlockwise direction, the estimates on the ring circuit can be correspondingly updated by applying a train of *RS* or *LS* signals. The results, from an application of a train of *RS* signals shown in Fig. 23, demonstrate that the activity bump shifts smoothly from one node to the next from N1→N2…→N24→N1 and so on. This corresponds to movement of the head direction from 0 to 330 degrees through 180 degrees. The experimental results in Fig. 24 demonstrate that the activity bump shifts smoothly from one node to the next from N1→N24…→N1→N24 and so on

at each application of the *LS* signal. This corresponds to movement of the head direction from 0 to 360 degrees through 330 and 180 degrees in the anti-clockwise direction. The maximum frequency of the *RS* or the *LS* signal at which this ring can move from one node to another was observed to be 4 kHz. This was designed such because, as far as we understand, the biological neural systems do not require a frequency faster than this. The results shown in the figures demonstrate that the ring can maintain a stable state or bump of activity which can shift from one position to the next in a controlled manner as required for successful working as a head direction cell system.

D. Conclusion

This section presents a novel VLSI circuit which can implement the head direction cell system, a type of attractor dynamic network on $1/12^{th}$ of a single chip as compared to earlier implementations of the system which required at least 3 chips and a lot of software interfaces.

The maximum speed at which unmyelinated axons (Purves, 2012) can conduct signals is ~ 0.5 to 10 m/s, while myelinated axons can conduct at velocities of up to 150 m/s. At each synapse, there is an additional delay of about 2-3 ms. Thus, the biological head direction cell system which receives inputs from structures, 5-6 nuclei away from it, (assuming only 1 synapse in each of these nuclei, the length of the axons to be around 10 cm and that these are unmyelinated) will be able to receive input only after 10-18 ms (synaptic delay, 2X5 to 3X6) plus 10-20ms (conduction time along the unmyelinated axons), i.e., around 20-38 ms. The time required for updating of preferred firing direction (80 ms) as observed in Zugaro

et. al., 2003 is also an indication. As compared to the biological system, our system is capable of updating the estimates much faster – up to 0.25 ms (1/4 ms) as the maximum operating frequency for the ring circuit is 4 kHz. The system can also be operated at much lower frequencies (in the biological range ~ 50-100 Hz), if needed.

The circuit has potential applications in compactly implementing spatial navigation and memory in robotics. Performing spatial navigation using this system shall allow updating the head direction based on environmental signals which shall make the robot learn from the environment and navigate in space autonomously. The ring circuit can also be used for other system implementations where we need a circuit with an activity node which can be moved around in a controlled manner. The fact that the position of the winning node can be read using an AER circuit provides an easy mechanism for reading the output from the chip which can be useful in non-neural electronic circuits as well.

4. THE GRID AND THE PLACE CELLS: SILICON IMPLEMENTATION

Silicon implementation of the hippocampal formation could provide a mechanism for autonomous robotic spatial navigation as it performs similar function in biology. In biology, the hippocampal formation maintains the maps of the environment and estimates of the head direction, which are updated regularly. Thus, the spatial navigation based on the principles of the hippocampal formation enables autonomous updating. There have been prior attempts (Massoud & Horiuchi, 2011, 2012) at building parts of the system in silicon but none of them have been able to achieve the functionality fully. Therefore, in this work we propose silicon circuits which successfully realize the function of the HF.[9]

A. System description

The schematic of the system is shown in Fig. 25. To implement the hexagonal firing pattern of the grid cells in silicon based on the GRIDSmap model described in Mhatre et. al., 2012, and the place cells based on the Bayesian integration, we designed and fabricated neuromorphic VLSI circuits on 3 chips, viz., the stripe cell ring chip, the grid chip and the place chip. Only a few circuits on each chip were used, therefore, in future implementations of the system, all these circuits can be integrated on a small area of a single tiny chip unit. Communication interfaces between these chips were built using encoder, decoder and AER circuits

[9] Initially, when I was working in the Horiuchi lab, we were thinking of implementing the function of the grid cells using a model developed by him [90] and using 12 ring circuits. But I used the GRIDSmap model instead to implement the functioning of the grid cells in silicon. The GRIDSmap model also implements the grid cell firing pattern but using an entirely different model which was implemented with 3 ring circuits.

which were connected either directly or through an FPGA. (Note: The ring circuits used here are the same as those used for realization of the head direction cell system. However, in that system, each node on the ring circuit represented a direction along the azimuth while in this application, each node of the ring represents distance travelled in space – with all the nodes on the ring circuit representing 1m in the experiments performed in this dissertation work.)

Three rings of stripe cells were aligned at 120 degrees to each other to enable mapping of the animal motion in space on to the three rings (as per the GRIDSmap model of Mhatre et. al., 2012). Mapping included calculating the number of the winning node on all the three rings when animal motion in space was being simulated. Once mapped, the neuron numbers on the three rings were moved to the required positions using Verilog code (for details, see Appendix II) implemented on the FPGA board. The resulting neuron numbers which fired on the ring circuit were read using the same FPGA board.

Whenever neuron numbers 24 on all the three rings fired simultaneously, the FPGA sent an input pulse to a neuron-synapse circuit (grid cell 1) on the grid chip. Since the neuron numbers on the ring wrapped around after 1m, this resulted in the spatial firing frequency of 1m for the grid cell. Another neuron-synapse circuit (grid cell 2) on the grid chip was sent an input pulse from the FPGA when either neuron numbers 12 or 24 simultaneously fired on all the 3 rings. Thus, grid cell 2 had a spatial firing frequency of 0.5m. Similarly, to obtain a spatial firing frequency of 0.25m, the grid cell 3 was connected to neuron numbers 6, 12, 18, and 24 on all the 3 rings. The output from all the 3 grid cells was connected

directly to the three inputs to the Bayesian integration synapse, the neuron attached to which produced output firing pattern like that of a place cell (based on the Bayesian integration model of the place cells).

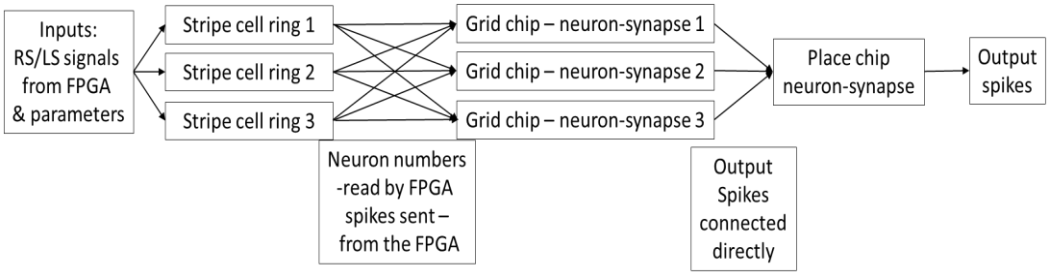

Fig. 25 System organization of the electronic hippocampal formation. To implement the firing patterns of the grid cells based on the GRIDSmap model and the place cells based on the Bayesian integration in silicon, circuits on 3 different chips were used, viz., 3 ring circuits on the stripe cell ring chip, 3 neuron-synapse circuits on the grid chip and 1 synapse-neuron circuit from the place chip. The preferred direction of motion integration of the 3 ring circuits was placed at 120 degrees to each other. As the animal motion in space is simulated, each position visited by the animal is projected on to the three axis representing the orientation of the ring circuits in space using trigonometric principles. This distance was converted to the neuron number (all 24 nodes were taken as representing 1 m movement in space) representing the distance travelled along the rings. To move the position of the winning node on each ring to that calculated, the rings were sent *RS* and *LS* signals from the FPGA, routed through the on chip decoder. The corresponding neuron numbers which fire on the ring circuits were read using the FPGA board. Whenever neuron number 24 on all the three rings fired, the neuron-synapse circuit on the grid chip was sent an input pulse. This resulted in spatial firing frequency of grid cell to be 1m. To obtain grid cell spatial firing frequency of 0.5m, another neuron-synapse circuit on the grid chip was sent inputs from the FPGA whenever neuron numbers 12 or 24 on all the rings fired at the same time. To obtain a spatial firing frequency of 0.25m, the third synapse-neuron circuit was sent an input pulse whenever neuron numbers 6, 12, 18 or 24 on all the 3 ring circuits fired simultaneously. Output firing patterns of these grid cells were connected as inputs to the Bayesian integration synapse on the place chip and corresponding firing pattern of the neuron attached to the synapse was noted using mixed signal oscilloscope.

B. Circuits

All three silicon chips were designed using the ON semiconductor process on a tiny chip unit (1275mmX1275mm) and named to reflect the function that they perform– the stripe cell ring chip (Fig. 19), the grid chip (Fig. 26) and the place chip (Fig. 30), connected through software interfaces designed in Verilog and implemented on a Spartan 3E digilent FPGA board.

i) The stripe cell ring chip

The circuits on this chip have already been described in section 3 on the head direction cell system. The same chip was used to implement the stripe cell ring function of the hippocampal formation. Note that even though the same chip was used to perform the function of the ring of stripe cells, the function performed by the circuit as part of the system in section 3 is entirely different from that being performed here.

ii) The grid chip

The grid chip (Fig. 26, Fig. 82) has 25 synapse-neuron circuits on it. The pulse inputs to the synapse circuits are routed through a 5 bit to 24 line decoder and the outputs from the neuron circuit are read using an AER encoder. Each synapse circuit provides input to a neuron circuit. The synapse circuit is a second order, current mode, log domain circuit. The neuron circuit is that of a conductance neuron simplified to function as a read out neuron.

Based on the GRIDSmap model, the grid pattern can be demonstrated with a single grid neuron-synapse circuit where the synapse can sum the 3 inputs and present it to the neuron whose threshold can be set such that it fires only when it

receives inputs from 3 stripe cells simultaneously. Here, the grid chip was used to demonstrate the hexagonal spatial firing pattern of the medial entorhinal grid cells. This second order synapse circuit was used here so that output to each of the 3 consecutive pulse inputs could be coincident with magnitude proportional to the number of input pulses. This synapse circuit provided an excitatory input to the neuron circuit whose threshold could be set such that it fired only when the circuit received at least 3 inputs as is required to implement the GRIDSmap model of the grid cells. Hence, these circuits were used to implement the grid cell function. However, in the final implementation of the system, the coincidence detection of inputs (neuron numbers from the 3 ring circuits) was done using the Spartan 3E digilent FPGA board which sent a single input pulse to the grid cell synapse only if outputs from the required nodes on the three rings were coincident.

The AER processing of outputs from different synapse-neuron circuits interfered with each other, which was not desirable for our system, thus, we could not use all the circuits on one chip. In the final system, we used the test circuit and one other synapse-neuron circuit on one chip and the test circuit on a second chip. Instead, if we had the provision for reading the neuron outputs without routing through the AER circuit, we could have used 3 synapse-neuron circuits from the same grid chip. This can be done in future implementations of the system to save chip area.

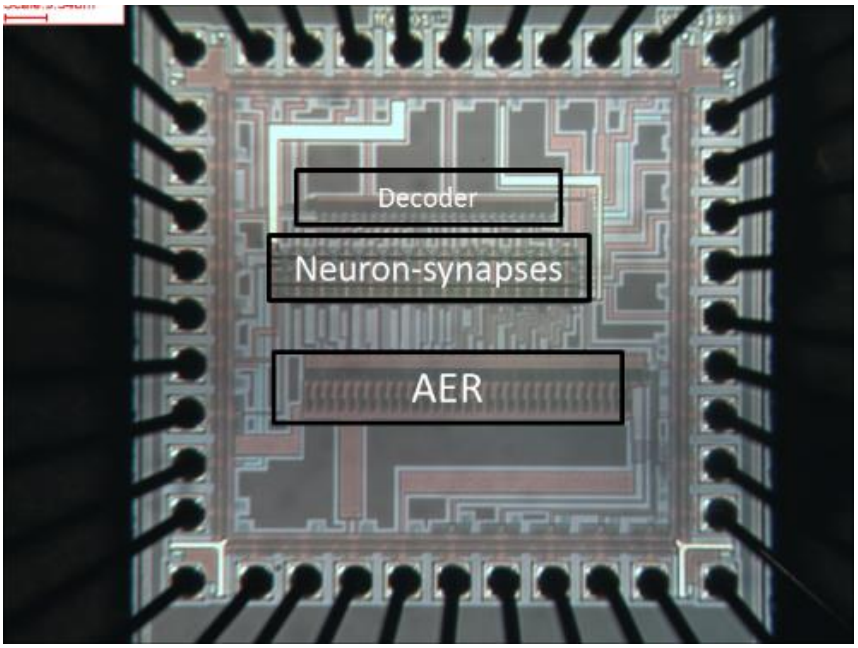

(a)

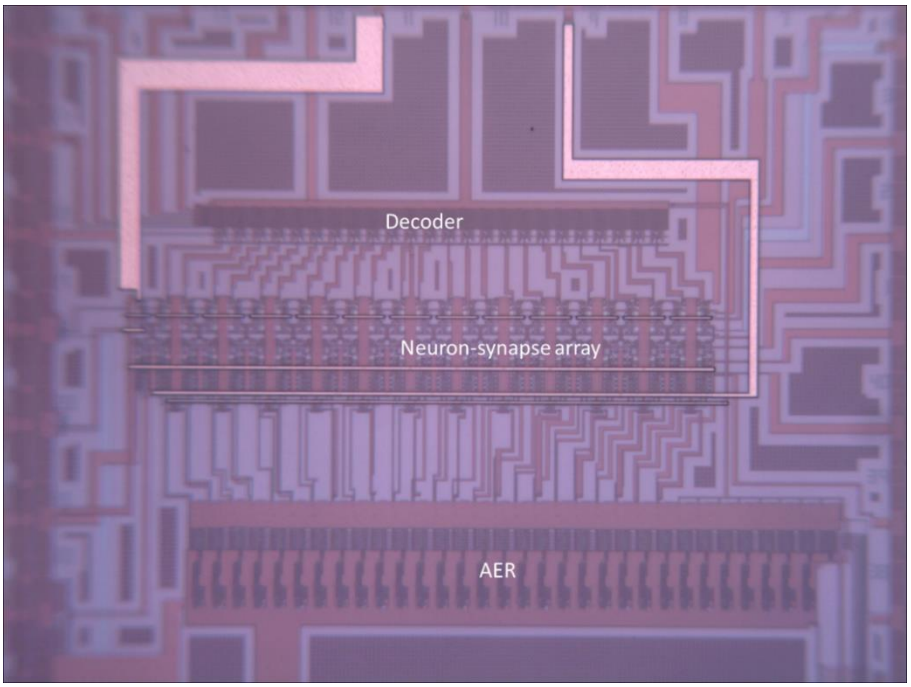

(b)

Fig. 26 (a) Micrograph of the grid chip showing the decoder circuit routing inputs to the synapse circuits and the AER circuit reading neuron numbers from the neurons in the array of circuits integrated on the chip. (b) Zoomed in version of the same chip showing the circuits in more detail.

In the following section, the synapse and the neuron circuits are described and discussed.

a) The Synapse circuit

To achieve the delayed peak and long-lasting response (as seen in biology) that can vary in magnitude with the number of input pulses, the synapse circuit was implemented using a cascade of two first-order, low pass filters. The synapse circuit (Fig. 78) was intended to take inputs from the address-event representation (AER) system which utilizes very short pulses (< 1 μsec) to transmit spikes between systems. Synapse circuits like those in Boahen, 1997, Chicca, Indiveri, 2003 and Shi, Horiuchi, 2004 have shown either summation or extension of pulse input timing or both but not a second order shaped function response. Even though this synapse circuit combines control over both time and magnitude of the output current, there are two problems in the output being perfectly proportional to the inputs in this version of the second order synapse circuit- first, the currents I_{m1} and I_{m2} depend upon V_x and V_e respectively and second, the current is related to the exponent of the gate voltage in the subthreshold region of circuit operation and not the gate voltage directly. Therefore, we came up with another circuit (Fig. 27) which does not suffer from the first problem. If this circuit is operated using small currents with each input pulse, so that linear approximation to the exponential can be used, then the second problem could also be taken care of.

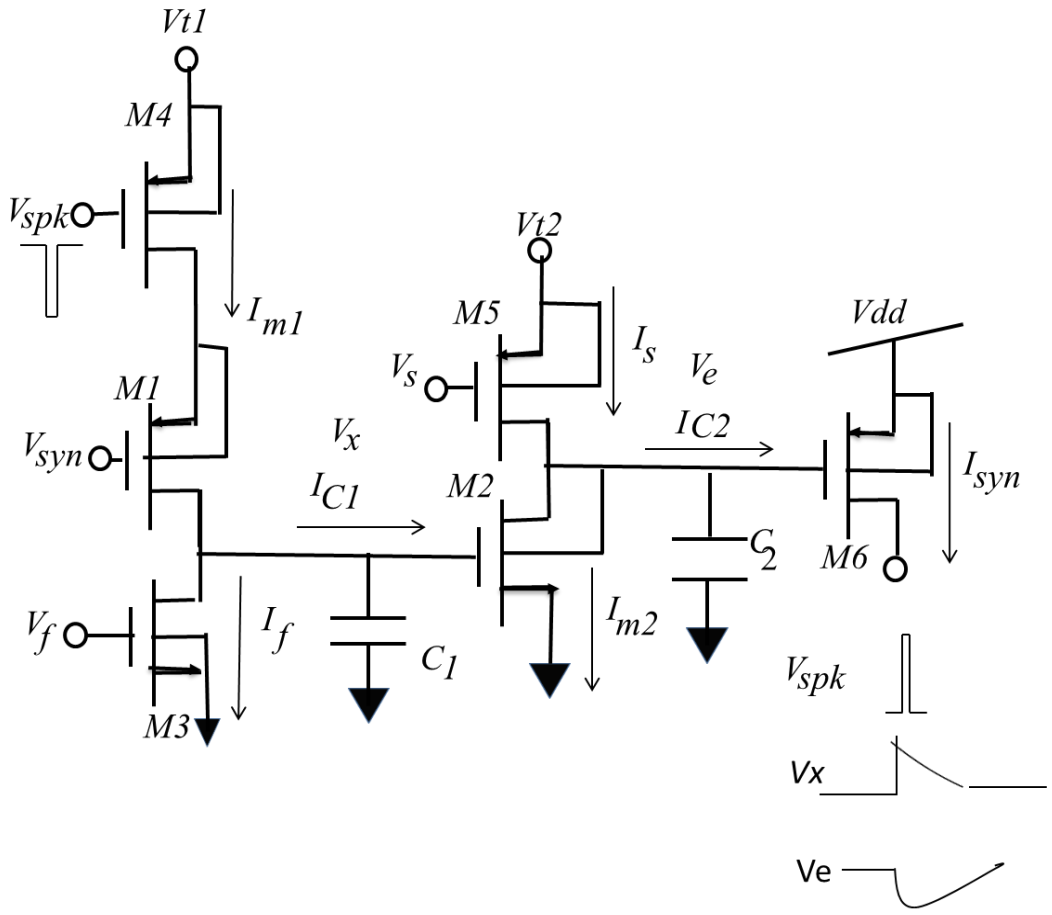

Fig. 27 New refined circuit for the second order synapse based on that in Fig. 78. This does not suffer from problems of the original circuit like dependence of input on V_x and hence, will be able to integrate more inputs while still producing output currents proportional to the number of input pulses. The voltages V_f and V_s are used to vary the time constants and V_{syn} is used to vary the magnitude of the output current. The sources of M4 and M5 are tied to voltages other than Vdd because for this circuit to work, the output current with each input pulse cannot be too large. The body terminals of all the pfets are tied to their source terminals by providing separate wells.

Table 3 Showing the function of various transistors in the second order synapse circuit

Transistor	Function
M1, M3, C1	First low pass filter, M1 also changes the strength of the synapse circuit and M3 controls the fast time constant.
M2, M5, C2	Second low pass filter, M5 also controls the slow time constant.
M3	Leak transistor- prevents firing of neurons of the non-winning nodes.
M6	To convert the voltage at node V_e to current of a similar shape.

The synapse circuit is a second order, log domain, current mode circuit whose output is a second order function when it is presented with an input spike. As is expected for the second order function, the output from this circuit continues to rise long after the actual input has ceased. When this circuit is presented with multiple input spikes separated by short intervals, the peak of the output current is proportional to the number of input spikes received. This circuit is designed to operate in the weak inversion region. It is triggered by a digital pulse (logic low) at the gate of M4, and produces an output current, I_{syn} at the drain of M6 which is connected to the neuron circuit (at the drain of M1) shown in Fig. 29. The first low pass filter (M1, M3, and C1) operates by producing an exponential current as the output which is processed by the second order filter (M2, M5, and C2) to produce a second order function shaped output current, I_{syn}.

Qualitatively, in the absence of input (V_{spk}), voltage V_x has the quiescent value approximately 0V. As one pulse input (V_{spk}) is applied, it pulls V_x up to $V_{t1.}$ After a time determined by the value of parameter V_f, the value of V_x returns to baseline (0V) in an exponential manner due to the capacitor C1. Since this V_x is the gate voltage for transistor M2, the current I_{m2} changes correspondingly. This current

pulls the V_e down exponentially and this change is integrated by the capacitor C2 so that the V_e changes as a second order function. Since the output current I_{syn} depends on the voltage V_e, it also changes correspondingly. Since this circuit does not produce output current without application of input pulses (V_{syn}) to it, we do not consider the first case (as mentioned in Appendix III for the previous second order synapse circuit). At rest, V_x =0, V_e =*Vdd*, I_{m1}, I_{m2}, I_{syn} and I_f are zero and the value of I_s depends on the value of V_s.

$$I_S = I_o e^{\frac{\kappa(Vdd - V_S)}{V_T}} \tag{2}$$

When an input pulse (0V) is applied to the gate of transistor M4,

$$I_{m1} = I_o e^{\frac{\kappa\left(Vdd - V_{syn}\right)}{V_T}} \tag{3}$$

The change in I_{syn} with each input pulse (using small signal approximation for the exponential)

$$\delta I_{syn} = I_o e^{-\frac{\kappa(\delta Ve)}{V_T}} \approx -I_o \frac{\kappa \delta V_e}{V_T} \tag{4}$$

Where, δV_e is given by (using small signal approximation for the exponential)

$$\delta V_e = -\frac{\delta I_{m2}}{C_2}\delta t \tag{5}$$

$$\delta I_{m2} = I_o e^{\frac{\kappa\left(\delta Vx\right)}{V_T}} \approx I_o \frac{\kappa \delta V_x}{V_T} \tag{6}$$

$$\delta V_x = \frac{I_{m1}}{C_1}\delta t \qquad (7)$$

Substituting from (5)-(7) into (4) gives

$$\delta I_{syn} = \left(I_o \frac{\kappa\delta t}{V_T}\right)^2 e^{\frac{\kappa Vdd}{V_T}} \frac{I_{m1}}{C_1 C_2} = \frac{\left(I_o\right)^3 e^{\frac{\kappa\left(2Vdd - V_{syn}\right)}{V_T}}}{C_1 C_2}\left(\frac{\kappa\delta t}{V_T}\right)^2 \qquad (8)$$

Since the output current for each input pulse is given by equation (8) that due to multiple such pulses will be a sum of each one of them. (Note: Even though large signals are used here, small signal approximation to the exponential was used to solve equations (4) and (6) to simplify the otherwise complex calculations. This gives appropriate results as with each input applied to the circuit, only a small amount of charge is integrated on to capacitor C1 as the duration for which the pulse is applied is very short.)

Results from the PSPICE simulation of this circuit are shown in Fig. 28. The parameters used for the test were: V_{t1}=3.5V, V_{t2}=4.5V, Vdd=5V, V_s=3.83V, V_f=0.72V, V_{syn}=2.6V.

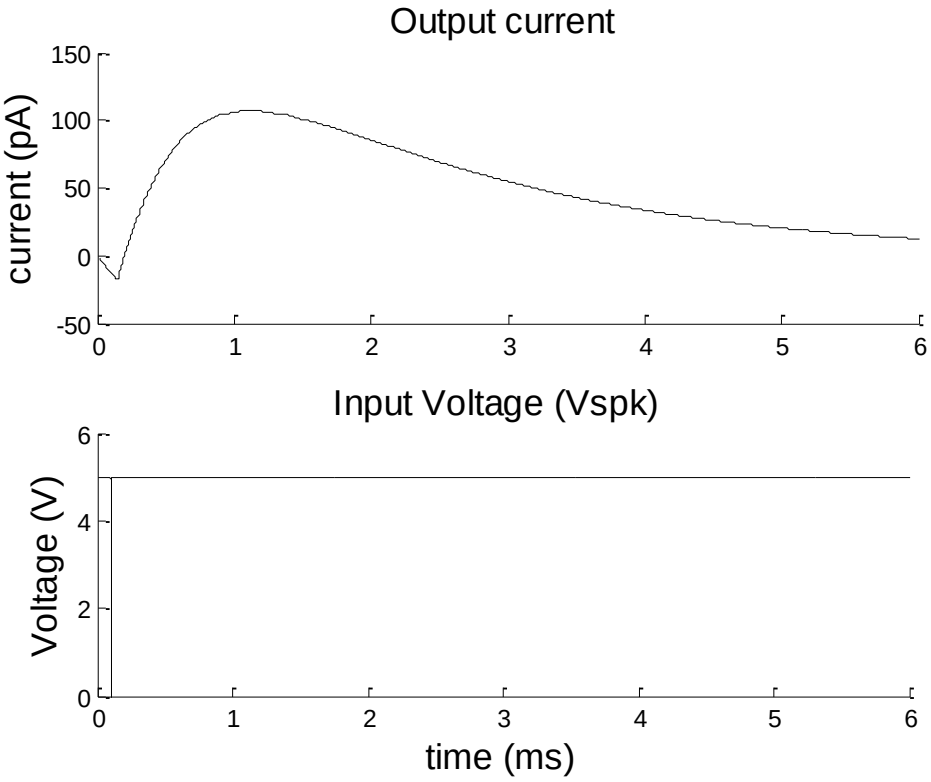

Fig. 28 Current output from the synapse circuit (PSPICE simulation) shown in Fig. 27 when it is excited by an input pulse (V_{spk}). The results show that the circuit is capable of transforming a sub microsecond duration input into a long duration output current with the shape of a second order function. The output continues to rise long after the input is applied to the circuit. This is very similar to the kind of neural processing of input pulses which is seen in the biological nervous system at the level of synapses. Hence, an earlier version of the circuit (Fig. 78) was used on the grid chip and the LSO chip to perform as a synapse circuit.

b) The Neuron Circuit

The circuit for the neuron (Fig. 29) gets the excitatory input from the synapse, which gets integrated on C_{mem} to V_x. The excitatory input pulls the V_x down to V_{we}. The resulting V_x is compared to V_{thr} and if it is comparable to V_{thr} then the neuron fires. V_{lk} is provided to prevent the neuron from firing in the quiescent state. R_{out} is the spike generated which is the request sent to the Address Event Representation (AER) (Boahen, 1989) and acknowledge (*ack*) is the signal coming back from the

AER which resets the neuron and prepares it to fire again. The time for resetting is adjusted by V_{refr}.[10]

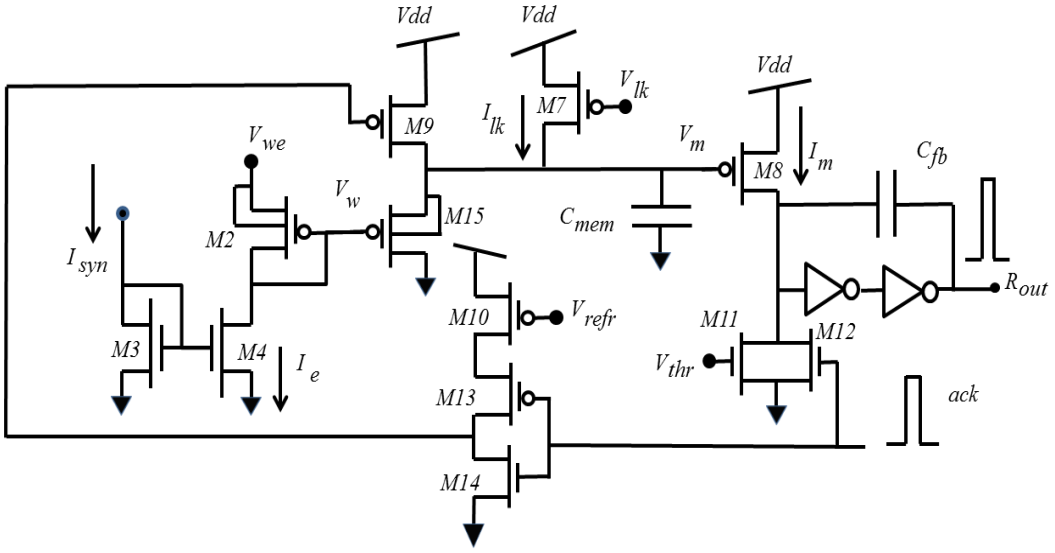

Fig. 29 Schematic of the neuron used to read out the response of the synapse circuit. The I_{syn} from the second order synapse circuit shown in Fig. 78 was connected to the drain of M3. It pulls the membrane potential of this silicon neuron, V_m down to V_{we}. If the V_m is comparable to V_{thr}, then the neuron fires a spike, R_{out}, which is sent out to the AER circuit which sends back the *ack* signal which resets the neuron after a refractory period determined by the value of the parameter, V_{refr}. The neuron is prevented from firing in the quiescent state by providing a small leak conductance through transistor M7. With no design constraints on transistor sizing, all transistors had W/L=2.4µm/2.4µm and C_{mem}=0.1pF. Capacitors were designed using poly-poly1. Transistors M2 and M15 were provided with separate wells. Body terminals of all pfets were tied to their source.

[10] The earlier version of this circuit (developed jointly with Prof Horiuchi) had two extra transistors and performed a weighted average of the two inputs. In contrast, this circuit does not perform weighted average of inputs but acts as a read out neuron.

Table 4 Showing the function of various transistors in the neuron 2 circuit

Transistor	Function
M2-M4, M15	To copy and scale the current received from the synapse circuit
M7	Leak transistor to prevent neuronal firing in the quiescent state
M8	To convert membrane potential V_m to output current
C_{fb} and 2 invertors	To amplify the output spike amplitude and to hold membrane potential at a value for a while.
M9, M12	To reset the neuron.
M13-M14	Buffers to produce a correct logic level pulse at the required point.
M10	To set the refractory period
M11	To set threshold voltage value for the neuron

Starting from the drain equations for M7, M4, and M8,

$$I_{lk} = I_0 e^{\frac{\kappa(V_m - V_w)}{V_T}} \quad (9)$$

$$I_e = I_0 e^{\frac{\kappa(V_{we} - V_w)}{V_T}} \quad (10)$$

$$I_m = I_0 e^{\frac{\kappa(Vdd - V_m)}{V_T}} \quad (11)$$

The value of the "membrane potential" current (I_m), when the excitatory input and input current through leak transistor are constant, can be described by the following equation, (obtained by solving equations (9)-(11))

$$I_m = I_o e^{\frac{\kappa(V_{dd} - V_{we})}{V_T}} \left(\frac{I_e}{I_{lk}} \right) \quad (12)$$

In the case where I_e is much larger than I_{lk}, I_m becomes large (near the excitatory synaptic reversal potential defined by V_{we}) and when I_{lk} is much larger than I_e, the membrane current will be near zero. The excitatory input pulls I_m towards a

maximum level defined by V_{we}. The I_m in steady-state becomes a function of the ratio of the two conductances. When the membrane potential exceeds a threshold level, the neuron generates a logic level pulse. The interface circuits for the neuron to communicate with the address-event arbiter are shown along with circuits for the control of a refractory period (V_{refr}) in Fig. 29. Here, the capacitor is not acting as an integrator but just delays the response to subsequent inputs so that response to them is not affected by that to previous inputs.

iii) The place chip

The place chip (Fig. 30, Fig. 83) has an array of 8 synapse-neuron circuits and a test synapse-neuron circuit. Each synapse circuit is that of a Bayesian integration synapse (Fig. 31) and each neuron circuit that of a simplified conductance neuron (Fig. 29). The inputs to the array of 8 synapse circuits are routed through a 5 bit to 24 line decoder circuit (each synapse circuit needs 3 inputs) and outputs from the neuron circuits are read using the on chip AER circuit. The neuron firing is read from the on chip AER circuit using a mixed signal oscilloscope.

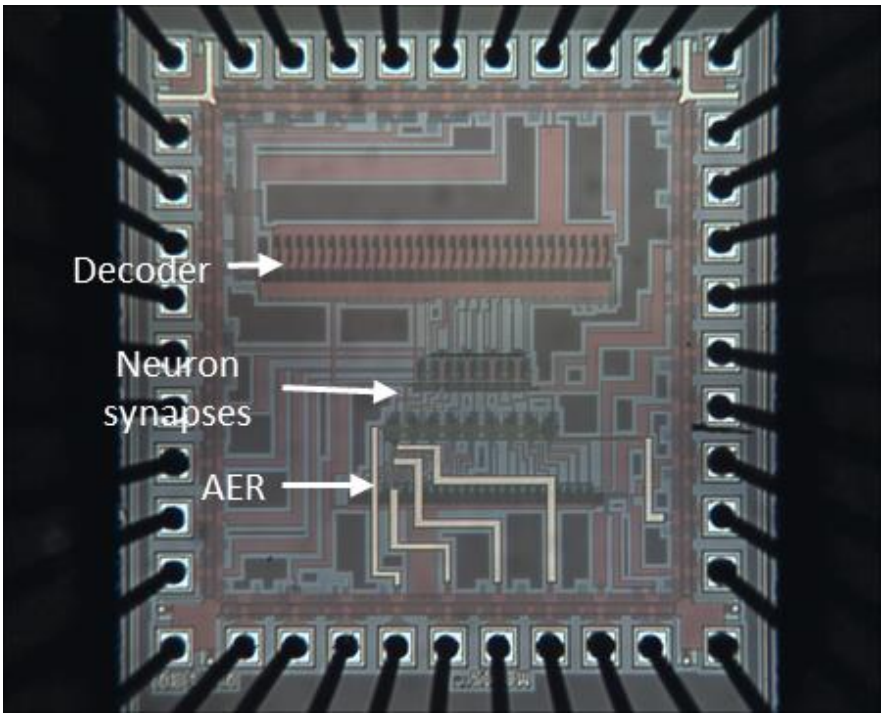

(a)

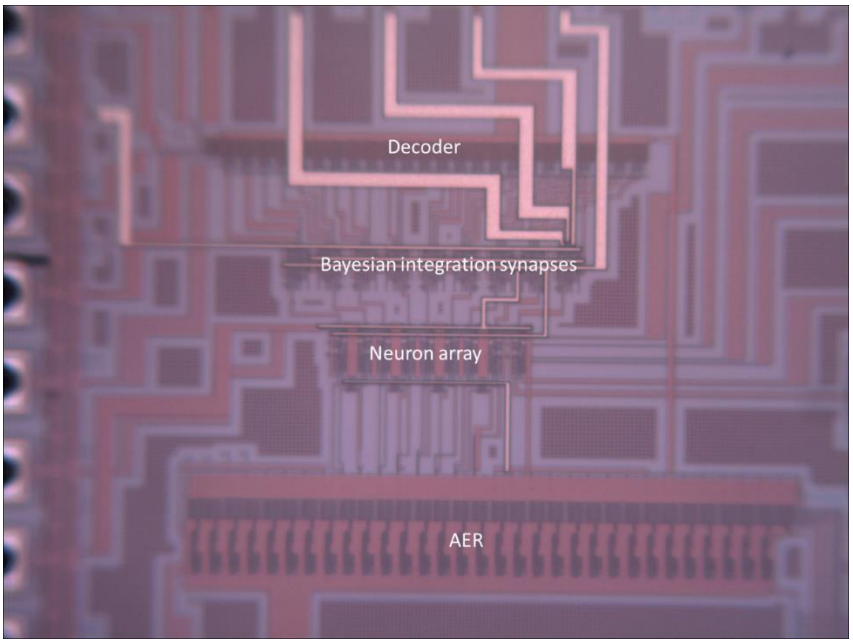

(b)

Fig. 30 (a) Micrograph of the place chip showing an array of synapse neuron circuits, inputs to which are routed through an on chip decoder circuit and outputs are read out using the AER circuit. (b) Zoomed in version of the same chip showing these circuits more closely.

a) The Bayesian integration synapse

The Bayesian integration (as seen in section 2. F), when implemented in software, involves weighting by inverse of standard deviation and then multiplication of probability distributions of the different inputs. Because in a hardware implementation, we have actual firing rates of neurons (proportional to the probabilities) and not the probabilities, we need to look at how we can perform Bayesian integration on inputs in terms of the firing rates. Assuming the neuron to be Poisson (Dayan & Abbott, 2000), the probability of firing (p) of a neuron in terms of its firing rate (r) and time (t) (δt is a very small interval of time)

$$p = r.\delta t \qquad (13)$$

Since, the rates are proportional to probabilities of firing, the multiplication of firing rates of different neurons is equivalent to the Bayesian integration of their probability distributions.

To implement the Bayesian integration of inputs at the place cells in hardware, a circuit for the Bayesian integration synapse was designed and fabricated on the place chip (Fig. 31, Fig. 30, Fig. 83). The outputs from this synapse were processed using a conductance neuron (Fig. 29) fabricated on the same chip. In total, this chip had 9 such synapse-neuron circuits including a test circuit. The circuit proposed to perform Bayesian integration (coincidence detection or multiplication) of inputs was a current mode, sub threshold synapse circuit, based on the bump and the correlator circuits (Liu et. al., 2002). Thus, with the synapse and neuron circuits, the chip could perform Bayesian integration of inputs and

produce neuronal firing as output which was read using the AER circuits. This was used to implement the place cell firing.

The Bayesian integration synapse circuit (Fig. 31) can perform multiplication on 3 inputs, V1, V2 and V3 and hence, detect coincidence of inputs. If different inputs are provided to the gates of M10 and M11, the circuit can perform Bayesian integration on 4 inputs. M1 and M2 form the core of a correlator circuit and the rest form 2 bump circuits. Each bump circuit receives two inputs and if they are equal, current flows through all three limbs of the circuit. If one of the inputs to M9 and M10 or to M11 and M12 is greater than the other, the common mode voltage (at the drain of M17 and M18) rises and shuts off the I_{mid}. When the two input voltages (V1=V2 or V2=V3) are equal, the I_{mid} is given by equation (14), where S is the ratio between the W/L of M13 to M9, M14 to M10, M15 to M11, and M16 to M12. Thus, the bump circuit shall have finite I_{mid} only if inputs to it are coincident and equal. For the correlator circuit (M1 and M2), equation (15) describes the function. Where *I (M1)* and *I (M2)* are the currents mirrored on from M3 and M4. Thus, the correlator circuit works only if both bump circuits have finite I_{mid}. The transistor sizing for the circuit was done such that $I_{mid} = I_b/2$ and currents through M1 and M2 are I_b. Thus, the $I_{syn} = I_b/2$. Therefore, using this synapse circuit, we can perform multiplication or Bayesian integration on V1, V2 and V3.

$$\mathrm{I}_{mid} = \frac{I_b}{1+\frac{4}{S}} \qquad (14)$$

$$I_{syn} = \frac{I_g(\mathrm{M1}) * I_g(M2)}{I_g(\mathrm{M1}) + I_g(M2)} \qquad (15)$$

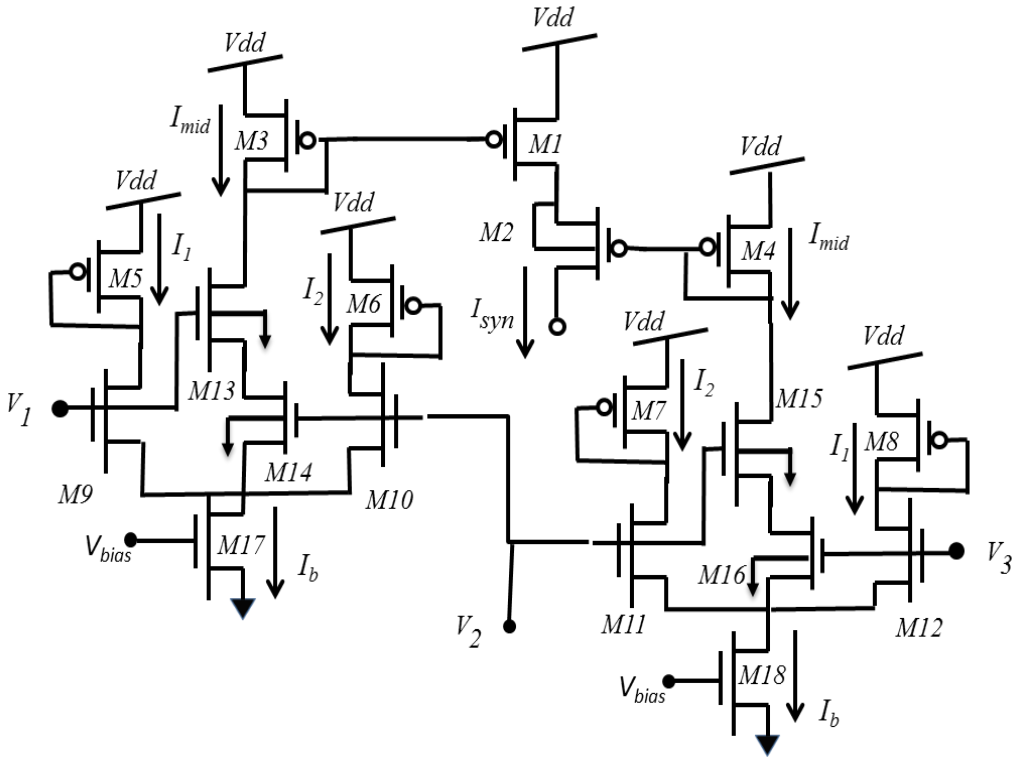

Fig. 31 Circuit schematic for the Bayesian integration synapse based on the bump and the correlator circuits. The transistors M1 and M2 form the core of the correlator circuit which produces an output current which is proportional to the product of the two input currents copied to the circuit using current mirrors formed by M3-M1 and M4-M2. The currents I_{mid} in the two bump circuits are proportional to the inputs V1-V3 applied to the two circuits which in this case were firing rates from the grid cells. W/L=9.6 µm /2.4 µm for M3, M4, M13-M16; W/L=4.8 µm /2.4 µm for M1 and M2 and W/L=2.4 µm/2.4 µm for the rest. Separate well was used for transistor M2 on the core correlator circuit.

Table 5 Showing the function of various transistors in the Bayesian integration synapse circuit.

Transistor	Function
M1, M2	Correlator circuit
M3-M1, M2-M4	Current mirrors
M5, M6, M9, M10, M13, M14, M17	First bump circuit
M7, M8, M11, M12, M15, M16, M18	Second bump circuit

The neuron circuit (Fig. 29) used here was the same as that used on the grid chip as described above. With these two circuits, we could perform Bayesian integration of inputs and obtain output as neuronal firing which could be read out using the AER circuits. This was used to implement the place cell firing in this work. It could also be used for any other single neurons performing Bayesian integration.

C. Testing & results

i) Testing the ring of stripe cells

The test results from this chip are shown in section 3 on the head direction cell system. Therefore, these are not repeated here.

ii) Testing the Grid chip

a) The Synapse Circuit

It should be noted that the synaptic current was not directly measured due to the lack of test equipment for high-bandwidth current measurements. Instead, the gate voltage (V_e) of the output pFET (M6 of Fig. 78) was recorded and mathematically converted to current using I_{0p} (6E-20A) and K_p (0.72) extracted from PSPICE simulations with models from the same run by MOSIS. An array of measurements was performed on the circuit in Fig. 78 to demonstrate the basic

operation of the circuit to generate the second order function shaped output current with control over the time constants and, to show the linearity of response to a burst of input spikes. For all these tests, a single input spike, V_{spk} was 4V, 0.5 µs, $V_{\tau 1}$ was 3.5V, and $V_{\tau 2}$ was 4.5V. The amplitude of V_{spk} was kept at 4V as that of $V_{\tau 1}$ was only 3.5V. Other parameters are mentioned in appropriate sections. In the following sections: the basic second order function shaped response, different time constant tunings, and linear response to a burst of tightly-spaced spikes is demonstrated. Other tests for the circuit will be presented in section 8 on the lateral superior olive.

1) Varying the time constants

In this set of measurements, the bias voltages V_{syn}, V_s and V_f (Fig. 78) were varied to obtain three different time constants for the second order function shaped output current. Voltage parameters used in these measurements are shown in Table 8 in Appendix I under '*Varying time constants'*. The results shown in Fig. 32 indicate that the time constant of the circuit can be varied from as low as 0.5 to as long as 50 ms. This could be further increased but is not relevant to the biological systems hence, was not done. This is important for our system implementation as this time constant is in the biologically observed range which can make the emulation of the biological system more appropriate. The computational neuroscience models also consider the synaptic output to be in the form of a second order response. Thus, the shape and time constant of the output both match the biological ones very closely.

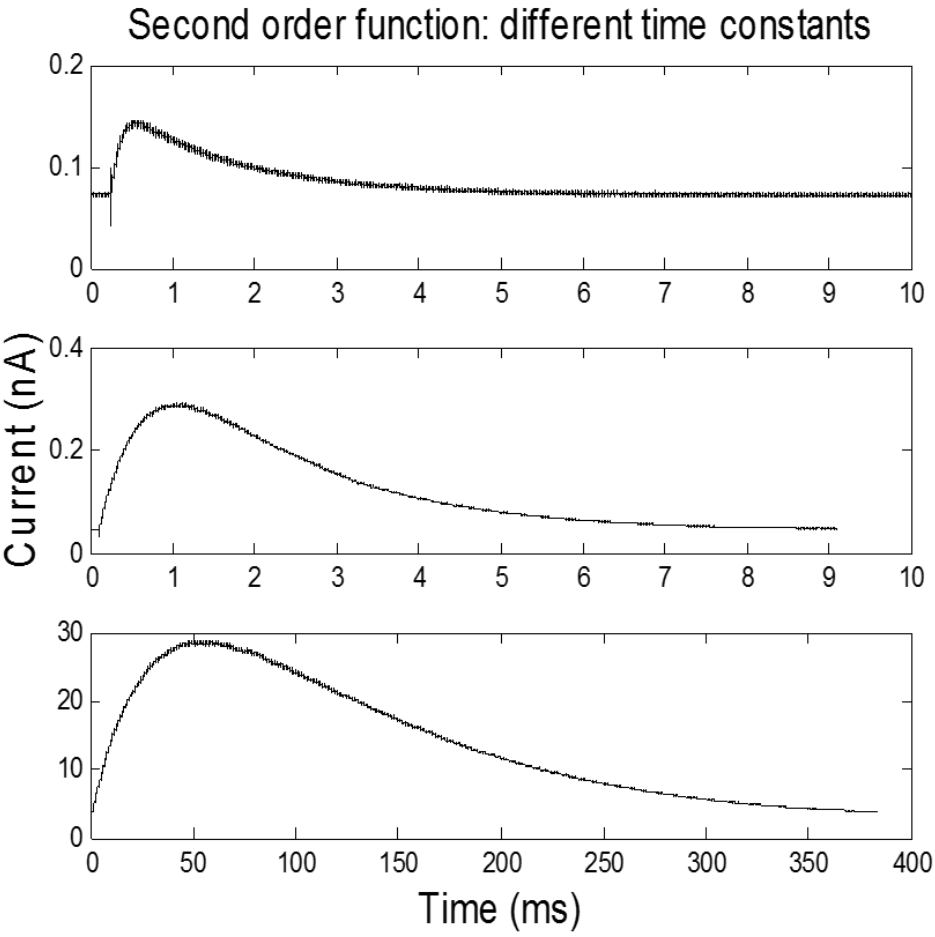

Fig. 32. These are the measurements results from chip testing for the second order synapse circuit which show that with a single circuit, the time constant of the output current can be changed to 0.5 ms, 1ms, and 50 ms (note time scale for the bottom graph). This was achieved by changing the circuit parameters V_{syn}, V_f and V_s.

2) Summating multiple input spikes

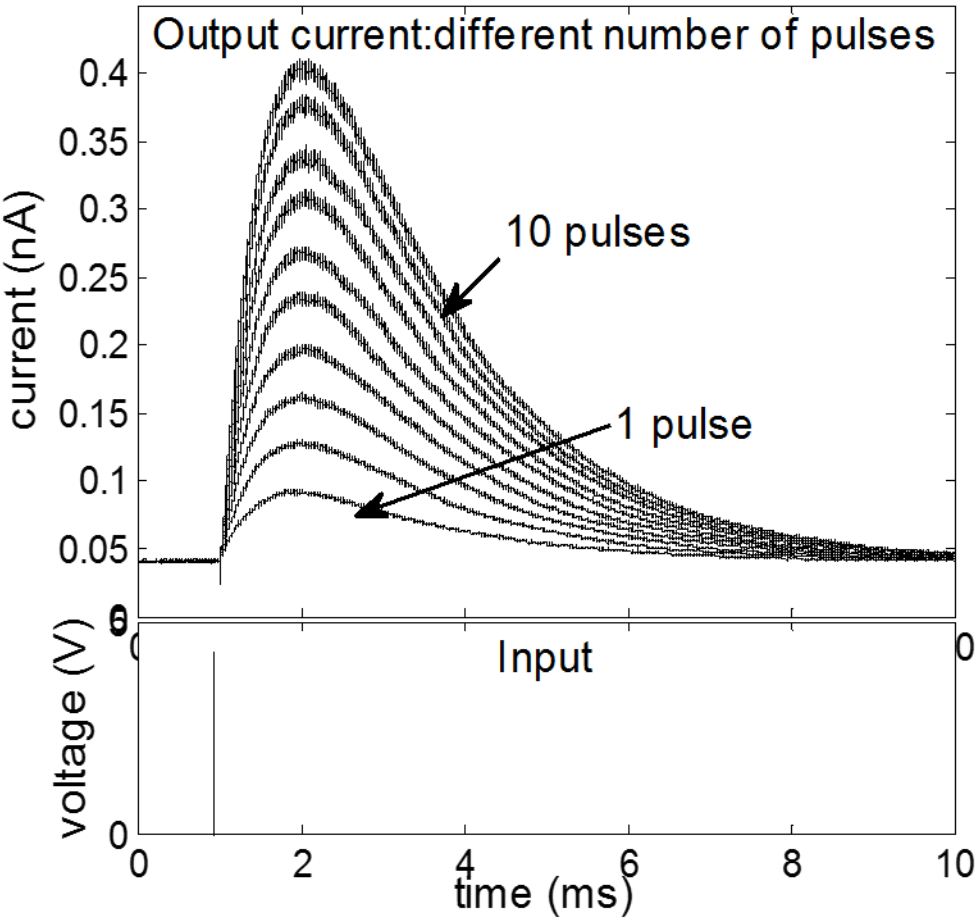

Fig. 33. Showing results from chip measurements of the second order synapse circuit when different number (1-10) of input pulses were applied to it at 1 µs intervals. Each pulse (shown in bottom graph) was a narrow sub-microsecond digital 4V magnitude pulse. The output currents from the second order synapse circuit with different number of spikes in an input burst are shown here. Note that the peaks of all the output currents increase in proportion to the number of input pulses applied and occur at the same time. (Baseline current has not been subtracted)

As a linear filter, the response to a burst of input spikes is expected to be the summation of these output currents. Voltage parameters used for this test are shown in Table 8 in Appendix I under '*Summating spikes*' and the circuit was

stimulated with different numbers of pulses in a given burst. Pulses were separated by 1µs. The currents for pulses 1-10 have the shape of a second order function as shown in Fig. 33, their peak occurs at the same time and the amplitude rises as a function of the number of input pulses until the current saturates.

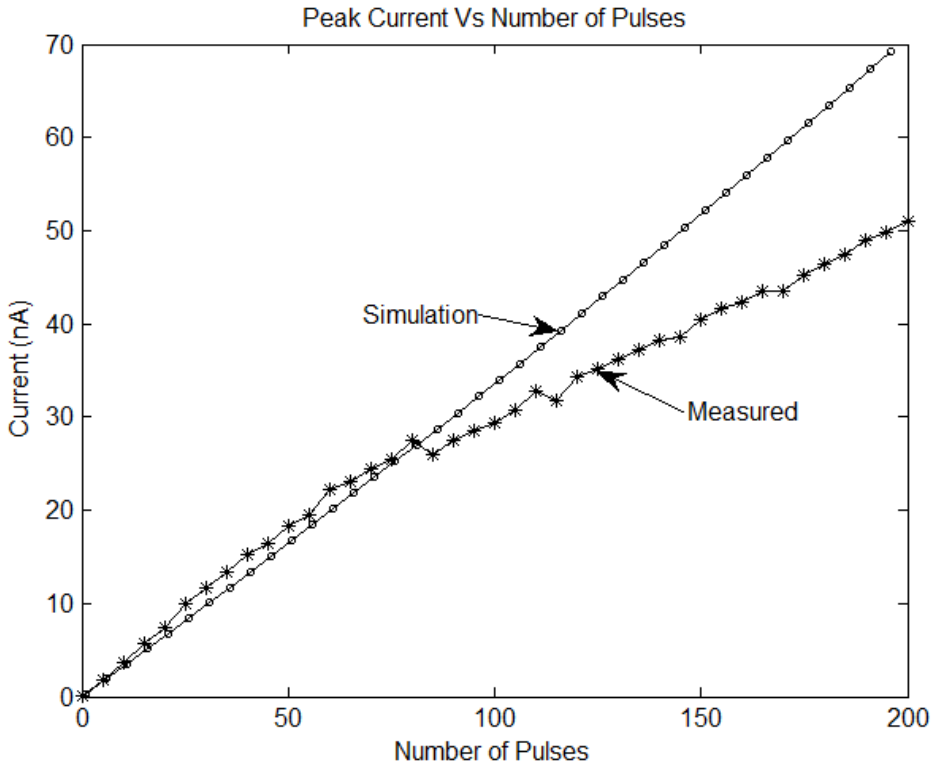

Fig.34 The results shown are from the chip measurements of the second order synapse circuit when it was provided different number of input (1-200) pulses. The peak output current increases in proportion to the number of spiking inputs in the burst. A comparison with the simulation shows a trend towards saturation as the circuit moves out of the subthreshold region of operation. (Note: the baseline current was subtracted from all datapoints.)

The graph in Fig.34 shows the peak current for each run (1-200 in increments of five for each subsequent measurement) as this is expected to rise in proportion to the number of pulses. Note that the baseline current of ~40 pA was subtracted from all currents in plotting the graph. In addition to the currents measured from

the circuit, Fig.34 also shows the expected peak currents for different number of inputs from simulations using equation (39). For the simulation, the peak current increases in proportion to the number of input spikes as expected. However, the measured values show a weakly sub-linear rise with saturating behaviour because with increasing number of inputs, the V_e decreases to an extent that the circuit leaves the subthreshold region.

b) The Neuron Circuit

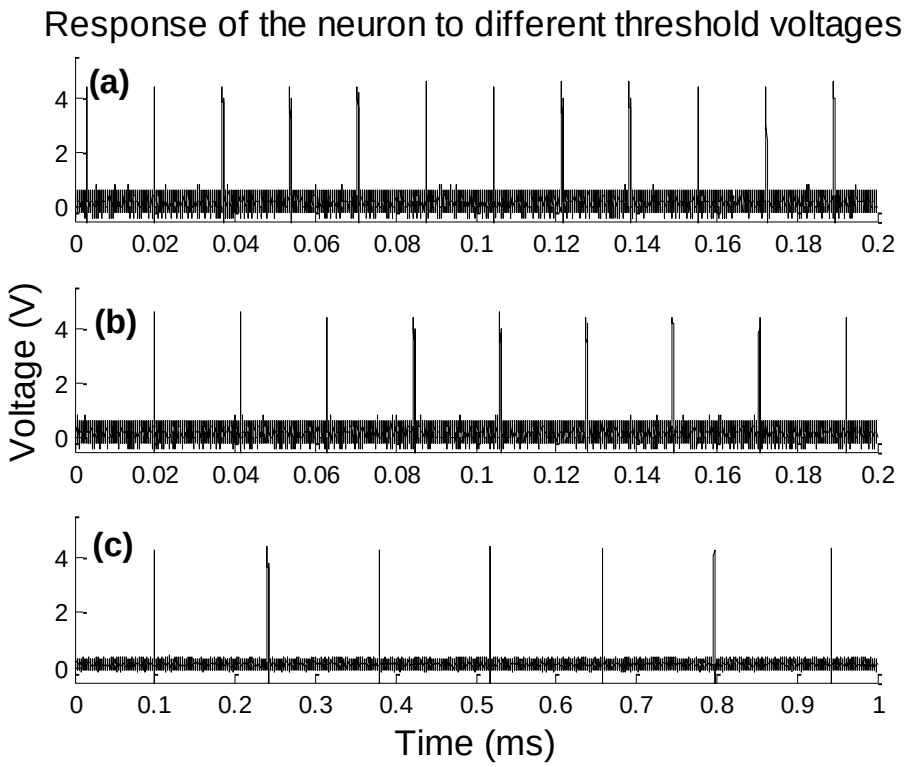

Fig. 35 These are chip measurement results from testing of neuron 2 circuit when different inputs were applied to it directly (without routing them through the synapse circuit). Results are spiking outputs from the neuron circuit which shows that as the threshold voltage rises, the inter-spike interval also rises. (a) V_{thr}=0.55V, (b) V_{thr} =0.60V, (c) V_{thr}=0.64V.

This section describes testing of the standalone test neuron circuit (Fig. 29) on the chip, with provision to apply direct voltage inputs for its proper function. Here,

R_{out} was recorded at different values of threshold voltage, V_{thr}=0.55, 0.60, 0.64V using the oscilloscope. Other parameters were set to values shown in Table 9 in Appendix I row labelled '*Initial measurements'*. The results shown in Fig. 35 indicate that the neuron is working properly and that the spike frequency is inversely proportional to the threshold voltage.

iii) Testing the place chip: the Bayesian integration synapse

The place chip was fabricated using 0.5 µm ON semiconductor technology and tested using a test PCB customized for the chip. The results were measured using the Agilent MSO 6014A mixed signal oscilloscope. The following parameters were used for the neuron circuit (Fig. 29): V_{we}=4.1V, V_{refr}=4.1V, V_{thr}=0.50V, V_{leak}=4.41V, and for the Bayesian integration synapse circuit (Fig. 31): V_{bias}=1.5V, *V1*, *V2* and *V3* were varied depending on the test. The resultant output of the neuron in each case was recorded using the oscilloscope. Firstly, the correct operation of the circuit was demonstrated by providing only one, two or all three (*V1*, *V2* and *V3)* inputs (1 µs, 5V pulse input at 1 kHz) to the circuit while holding the others at ground. Results shown in Fig. 36 indicate that the neuron fires only when all the inputs are coincident on it and for a duration thereafter determined by the parameter V_{refr}. Secondly, all the 3 inputs were provided simultaneously but their pattern was changed from square to ramp and sinusoidal (5V peak to peak and 1 kHz).

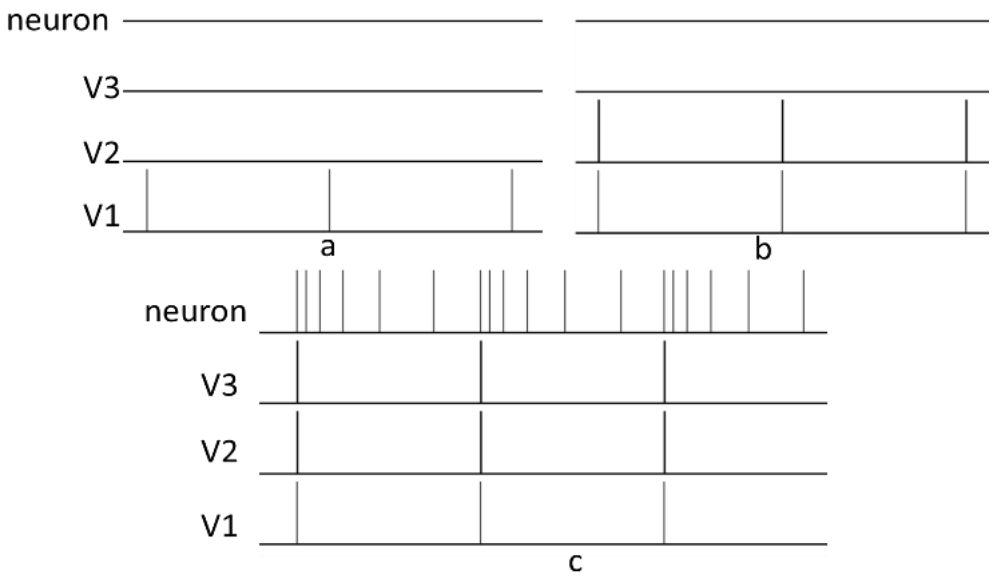

Fig. 36 Shows the results from chip measurements of the Bayesian integration synapse when it is provided with three inputs. (a) and (b) Showing that neuronal firing is absent when all the three inputs *(V1, V2 & V3*) are not coincident (c) but appears as soon they are. In (c), the firing of the neuron is persistent because of the feedback capacitor but it can be reduced to the time of inputs precisely by changing the value of the parameter V_{refr}.

The results shown in Fig. 37 indicate that the synapse circuit can perform Bayesian integration for a variety of inputs and not just pulses because the neuron output is present only when all the three inputs are applied to the circuit but is zero otherwise. Thirdly, three inputs of different frequencies viz., 1 kHz, 500 and 250 Hz, and 5V peak to peak, were applied to the synapse circuit and the corresponding neuronal output was recorded. Similar tests were done using square, sine and ramp inputs (with no offset). Results shown in Fig. 38 show that the circuit responds only when all the three inputs to it are coincident and not otherwise and hence, it can perform multiplication of the inputs.

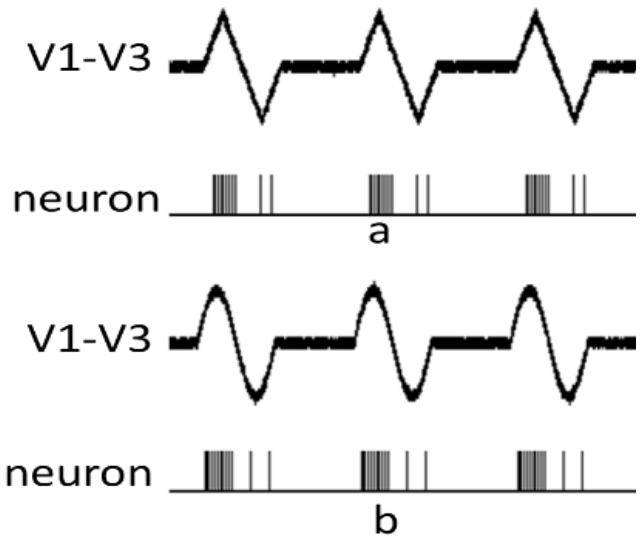

Fig. 37 Results from the chip measurements on the Bayesian integration synapse showing that the ramp and the sinusoidal inputs (no offset) produce the same results as those for the square pulses as long as all the inputs to the synapse are coincident. The firing of the neuron is persistent because of the feedback capacitor but it can be reduced to the time of inputs precisely by changing the parameter V_{refr}.

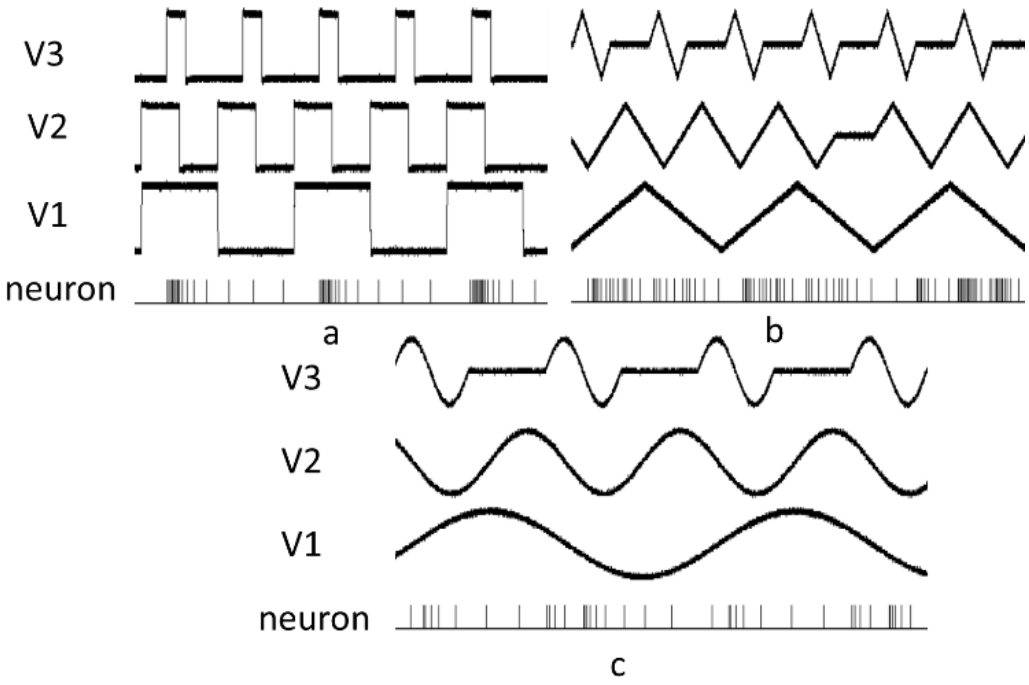

Fig. 38 Chip measurement results from application of three different inputs (no offset) of three different frequencies to the Bayesian integration synapse circuit show that the circuit can produce output which is proportional to the product of the inputs as required for Bayesian integration of the inputs. The firing of the neuron is persistent because of the feedback capacitor but it can be reduced to the time of inputs precisely by changing the parameter V_{refr}.

iv) Testing the system

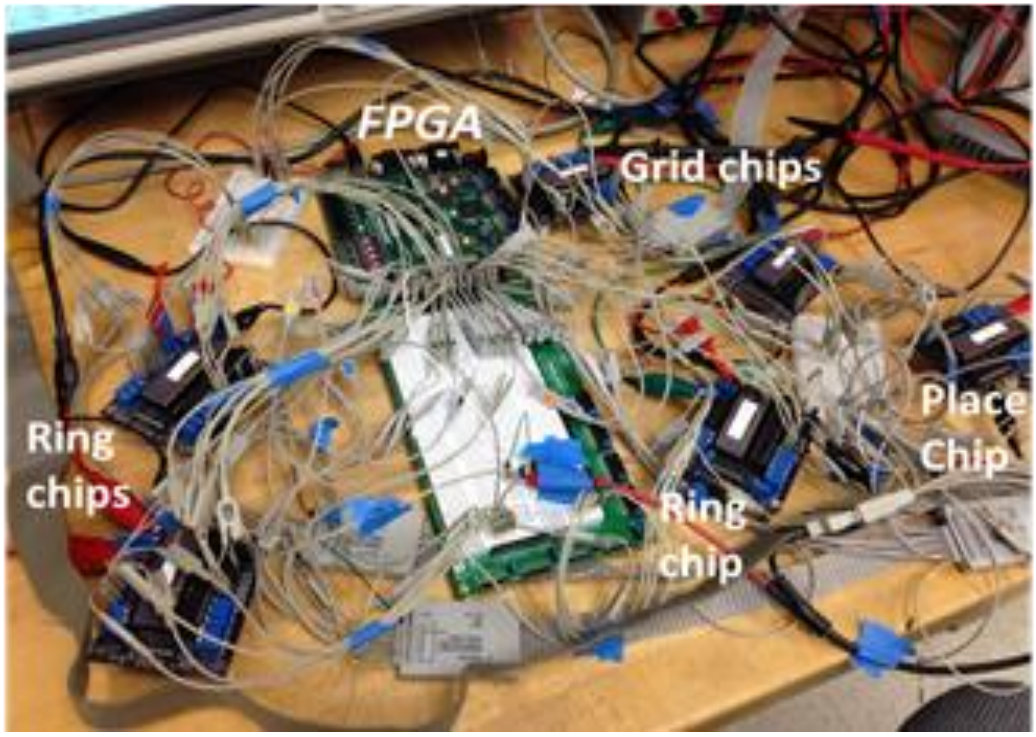

Fig. 39 Showing the complete system for the silicon implementation of firing patterns of the grid and the place cells which was tested with 6 chips (3 stripe cell ring chips, 2 grid chips and one place chip) and an FPGA board connecting the chips through software interfaces. However, only a few circuits on each chip were used for the silicon implementation of the system. Thus, in future implementations of the same, all the circuits can be integrated on a single chip.

To demonstrate the function of the hippocampal formation in silicon based on the GRIDSmap model of the grid cells (section 2.E. i) b)) and the Bayesian integration (section 2. F), we used the chips described above, connected in the system described above (section 4. A)). Custom test PCBs (Fig. 39) were designed to test these chips, and software interfaces for communication between the chips were designed using Verilog, implemented on a Spartan 3E digilent FPGA board. The output was recorded using Agilent MSO 6014A mixed signal oscilloscope and then processed in MATLAB. Firstly, the animal's motion in straight line

along the preferred direction of a ring of stripe cells, secondly that along a circle and finally that in open space was coded in Verilog to provide inputs to the 3 stripe cell rings. Parameters used for these tests are shown in Table10 in Appendix I.

a) Motion in straight line

When an animal moves in a straight line along the preferred direction of one of the rings of stripe cells (ring1), then according to the GRIDSmap model, the position of the winning node will change only on ring1 while that on other two will remain stationary. Thus, to observe the grid and the place cell firing in response to movement along a straight line, a right shift (*RS*) signal was provided to one of the rings while the winning nodes of the other two were held at node 24 (Verilog code can be seen in Appendix II). The neuron numbers on the three rings were read using the FPGA board. Whenever neuron numbers 24 on all the three rings fired simultaneously, grid cell 1 was sent an input pulse by the FPGA. Similarly, when neuron numbers 12 and 24 fired on all the three ring circuits simultaneously, grid cell 2 was sent an input pulse and whenever neuron numbers 6, 12, 18 or 24 on all the three rings fired simultaneously, grid cell 3 was sent an input pulse from the FPGA. Since, all 24 neurons on the ring represent 1 m movement in space (along their preferred firing direction), the spatial firing frequency of grid cell 1 was 1m, that of grid cell 2 was 0.5m and that of grid cell 3 was 0.25m. Output from these three grid cells was connected directly to the inputs of the Bayesian integration synapse circuit and the corresponding firing of the neuron (neuron 2) connected to it was recorded. This represents the place cell

firing. Chip measurement results read using the mixed signal oscilloscope and processed in MATLAB, are shown in Fig. 40.

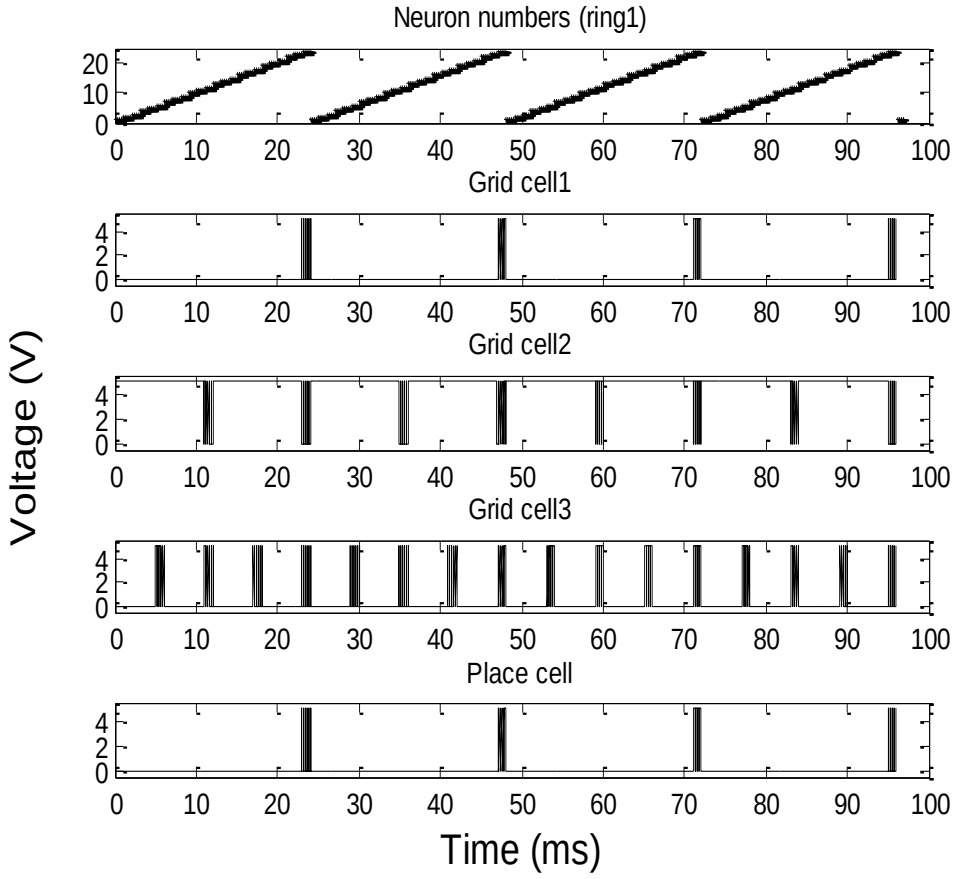

Fig. 40 Chip measurement results from the silicon implementation of the grid and the place cell as the animal motion along the preferred firing direction of one of the ring of stripe cells was simulated. In this case, a train of *RS* signals was applied to one of the rings while the winning neuron position on the other two was held at neuron number 24. As shown in the top graph, the position of the winning node on ring 1 moved around from 1 to 24 and back to 1 over and over again. The numbers of neurons which fired on all the 3 rings were read using the FPGA board. Whenever neuron numbers 24 on all the rings fired, an input pulse was sent to grid cell 1 which fired as shown in the second graph from top. Similarly, whenever neuron numbers 12 and 24 on all the rings fired, an input pulse was sent to the grid cell 2 which fired as shown in the third graph from top and whenever neuron numbers 6, 12, 18 or 24 on all the rings fired, an input pulse was sent to the grid cell 3 which fired as shown in the fourth graph from top. The place cell (bottom graph) fired only when all inputs to it were coincident. Note that the firing of two of the grid cells is from 0 to 5V while that of Gridcell2 is from 5-0V because it was being read through the AER while the rest were being read directly.

The top subplot in the figure shows the movement of ring number 1 from one node to the next and its wrapping around, to repeat the pattern over and over. The neuron numbers of only ring1 (which is being moved around) are shown. This number is moving from 1→2→….. →23→24→1→ and so on. The results shown in subplots 2-4 are the neuronal outputs from the three grid neurons which have different spatial firing frequencies as required by the GRIDSmap model. These in turn form inputs to a place neuron, routed through the Bayesian integration synapse. The bottom subplot shows that the place cell fires only when inputs to it are coincident from all the three grid cells, else it does not. Based on the chip results, projections were made for motion over longer distances in the x-y plane and plotted in MATLAB (Fig. 41). Results shown indicate that the system implementation in silicon can correctly track the position and motion of the animal along a straight line.

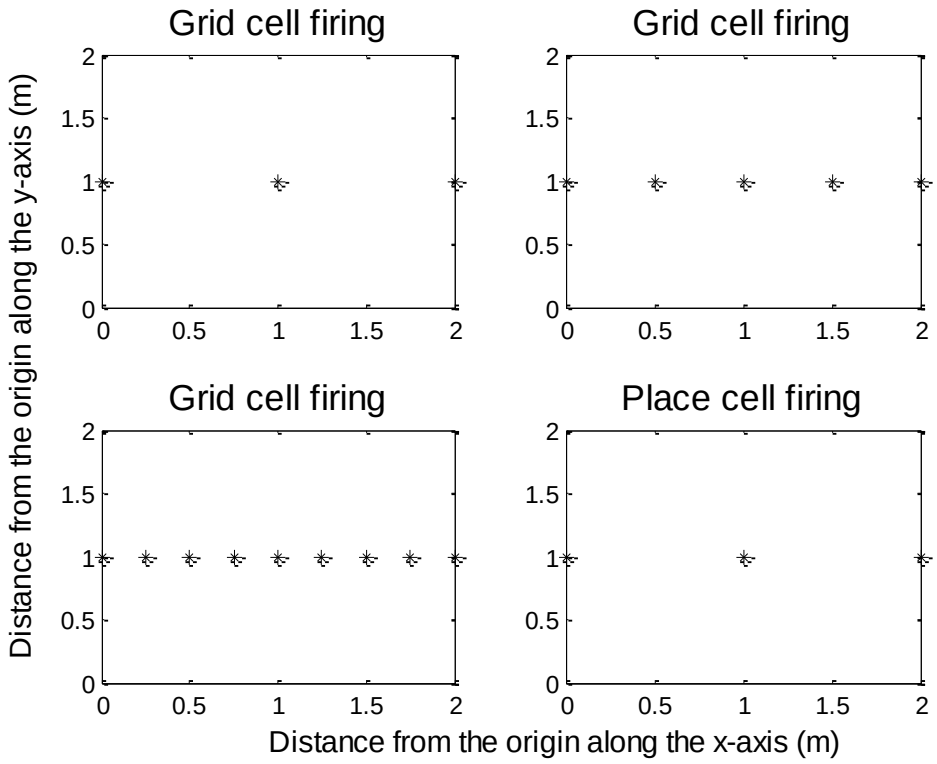

Fig. 41 Showing extrapolation of the grid and the place cell firing (*) patterns and their MATLAB plot as the animal motion along the preferred firing direction of a ring is simulated. This indicates that we could successfully implement the firing patterns of both the grid and the place cells in silicon using our system as predicted by the computational models used here. Actual measurements from the chip are shown in Fig. 40.

b) Motion in a circle

To measure the place cell firing as the animal motion in a circle is simulated, node position on rings of stripe cells for 12 points in space was calculated. The points used are shown in Fig. 42 – 6 points were located on the axes (aligned along the preferred firing directions of the rings) and 6 half way between these but on the circle. Using the GRIDSmap model, the corresponding position of the winning nodes along the three rings was calculated. These node numbers were [24, 24, 24] for the six points shown in the figure and [22, 22, 24], [24, 22, 22] or [22, 24, 22] for the other 6 positions on the circle which were exactly half way between these

points. Based on these calculations, the position of winning nodes on the three rings was shifted by providing *LS* or *RS* signals to the ring from the FPGA (details of the Verilog code can be seen in Appendix II). As the rings were moved, the neuron numbers of the winning nodes were recorded. If the neuron numbers of all the rings were 24, then the synapse of grid cell1 was sent a spike as a result of which it fired. Similarly, spike inputs were sent to grid cell2 if either of the neuron numbers 12 or 24 and to grid cell3 if either of the neuron numbers 6, 12, 18 or 24 from all the rings fired simultaneously. Since, the neuron numbers 6, 12 or 18 on the rings did not fire in this case, all the three grid cells as well as the place cell firing had similar spatial scaling (as shown in Fig. 43). Measurement results in Fig. 43 show (a)-(c) the neuron numbers corresponding to each time step when they were read by the FPGA. The system produced grid cell firing patterns of same frequency (d)-(f). Different spatial frequencies will be seen if the radius of the circle was changed from 1m to 0.5m or 0.25m. The place cells fired only when all the grid cell inputs to them were coincident. Hence, this system can correctly track the motion of the animal using place and grid cell firing patterns. The results obtained from chip measurements were plotted in MATLAB as shown in Fig. 42 which shows that the system can correctly code and decode information and hence, can perform spatial navigation in artificial autonomous robotic systems.

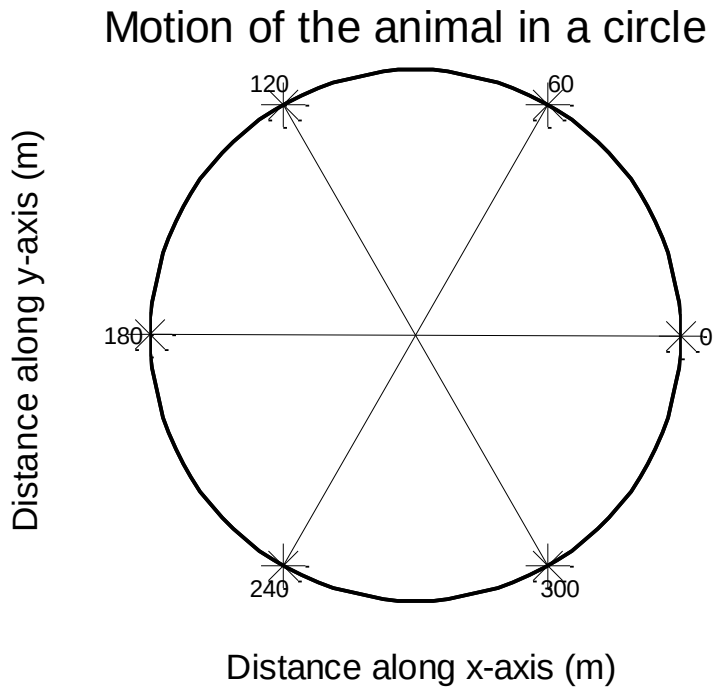

Fig. 42 Showing decoding of place information from the measured firing patterns of the place cell and grid cell firing (*) when animal motion along a circle of radius 1 m is simulated. This is a plot in Matlab based on the data obtained from the chips (Fig. 43). This is plotted in the x-y plane and shows that our system is capable of correctly decoding position information from spatial firing patterns of the grid and the place cells.

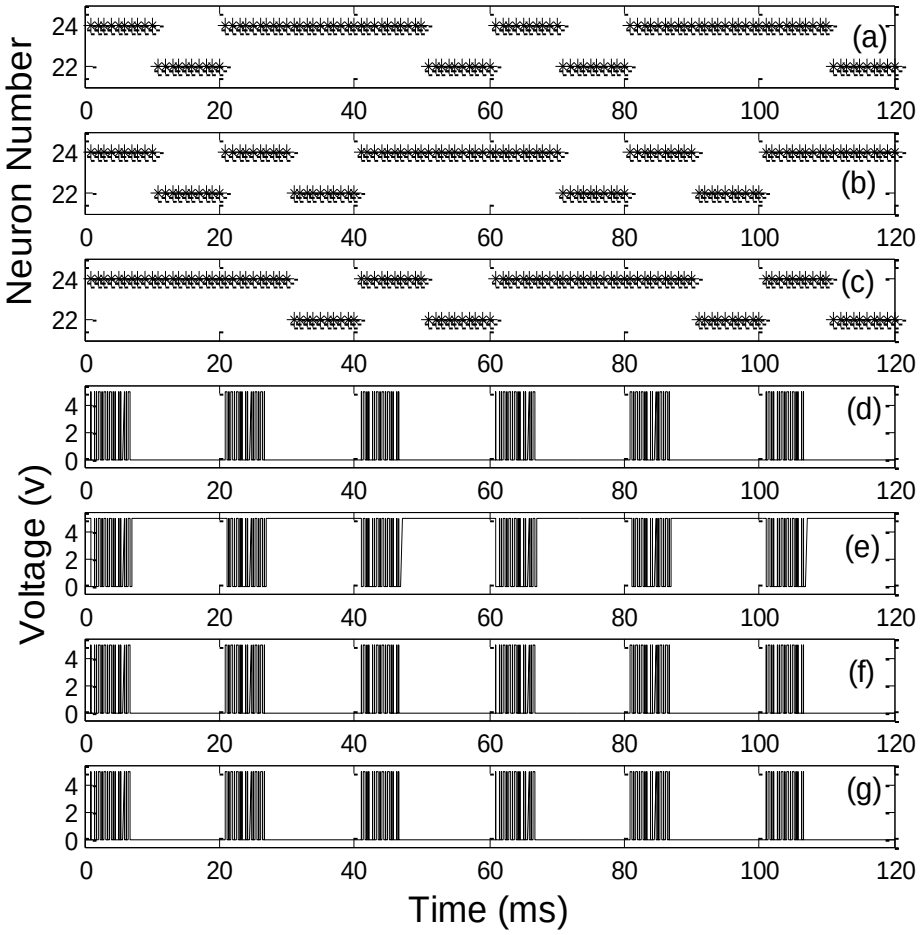

Fig. 43 Shows chip measurement results from the system implementation of the grid and the place cell firing patterns in silicon. In this case, animal motion along a circle of radius 1 m was simulated. The corresponding neuron positions on the three rings were calculated and obtained by providing inputs through the FPGA. (a)-(c) Movement of winning node along the 3 stripe cell rings as the animal moves along a circle (neuron numbers of the 3 rings are shown). Also seen are (d)-(f) the corresponding firing patterns of 3 grid cells and that of a (g) place cell, recorded using a mixed signal oscilloscope. Note that the firing of two of the grid cells is from 0 to 5V while that of one of them (e) goes from 5-0V because that was being read through the AER while the rest were being read directly. This also shows that our system is capable of producing the grid and the place cell firing patterns as observed empirically.

c) Motion in open space

To cover the entire space with animal motion, we simulated motion of the animal along one axis for 1/4 m, then along an axis perpendicular to this one for 1/2 m, and repeated this pattern over and over. So the animal's position at representative points for all places in space was mapped on to the 3 stripe cell rings. For this, firstly ring 1 was moved 6 positions to the right, then its position was held there while that of rings 2 and 3 was shifted 6 positions to the right. This pattern of movement along the rings was repeated over and over. Thereafter, using the software interface in FPGA (Verilog code is provided in Appendix II), the first grid cell was connected to neuron numbers 2, 8, 14 and 20 of each ring, second grid cell to neuron numbers 2 and 14 and the third grid cell to neuron number 2 of each of the rings. The place cell fired only when it received inputs from all the three grid cells. Detailed grid firing pattern of different spatial frequencies and that of the place cell was projected to the entire space and plotted in MATLAB. This is shown in Fig. 44. One snippet of the recordings from the 3 chips, as seen on the oscilloscope and later processed in MATLAB, is shown in Fig. 45. This shows the movement of neuron numbers on the three rings around repeatedly. (a)-(c) Firstly, the neuron numbers on all the rings were shifted to neuron number 2, then those on ring 1 were shifted 6 positions to the right, followed by movement of neuron numbers on rings 2 and 3, by 6 positions to the right. (d)-(f) show that due to the connectivity pattern built using software interfaces designed on the FPGA board, three different spatial firing frequencies for the three grid cells were obtained, which were connected to the place cell through the Bayesian integration

synapse to provide (f) place cell firing pattern. These results demonstrate that we could successfully achieve the function of the hippocampal formation based on the models with these 3 chips/circuits in silicon.

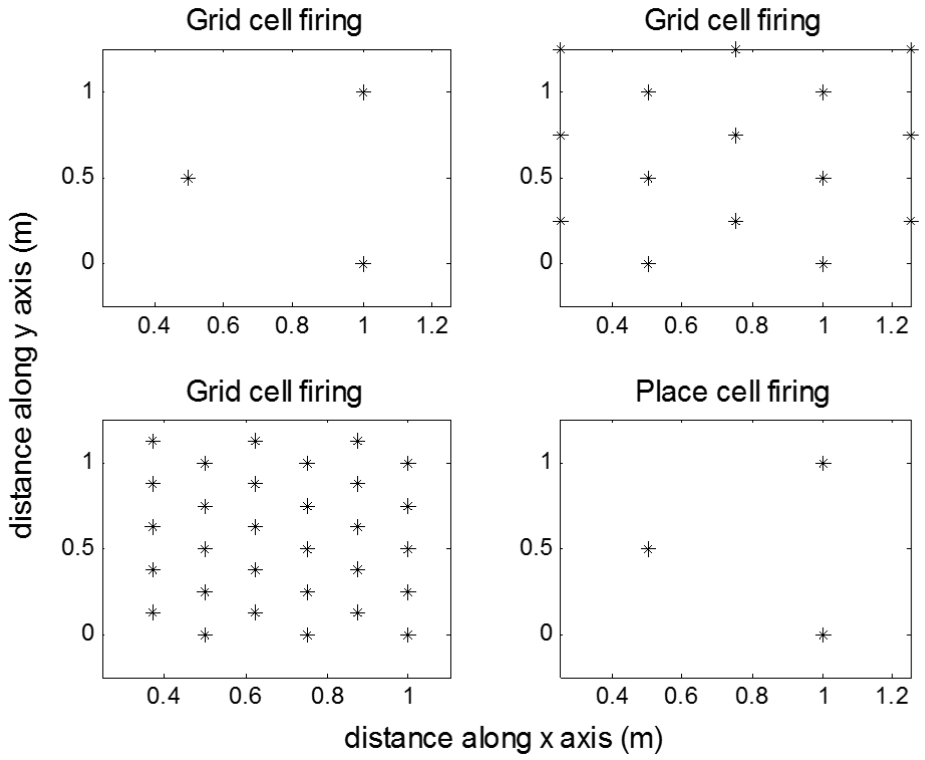

Fig. 44 MATLAB plots showing the grid and the place cell firing (*) extrapolated in the x-y plane from that recorded from the chips (Fig. 45) as the animal motion in open space is simulated. These results show that the grid cell firing patterns of different spatial frequencies could be achieved and that the place cells fire only when inputs from all the grid cells are coincident on it. This implies that our system is correctly implementing the grid and the place cell firing patterns.

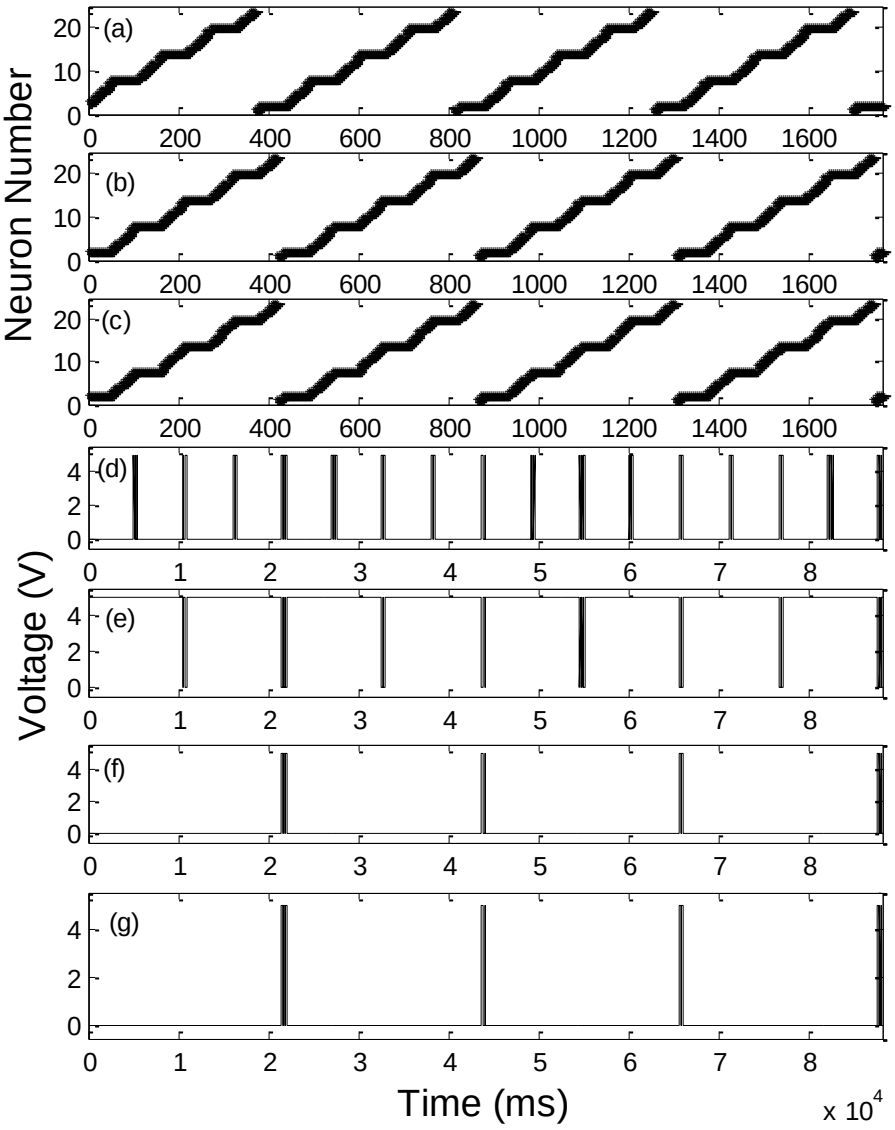

Fig. 45 Measurement results from 3 stripe cell rings, 3 grid cells and one place cell when animal motion in open space is simulated. (a)-(c) Neuron numbers of the 3 stripe cell rings change repeatedly as the animal moves around in space. (d)-(f) The results show firing of grid cells at regular intervals with different scaling. Note that the firing of two of the grid cells is from 0 to 5V while that of one of them (e) goes from 5-0V because that was being read through the AER while the rest were being read directly. (g) The place cell fires when it gets inputs from all the grid cells simultaneously. Thus, our system can produce the grid and the place cell firing patterns as expected from the computational models.

D. Conclusion

In this section, integration of 3 silicon chips, fabricated using 0.5 μm ON semiconductor technology, into a system which mimics the spatial navigation function of the hippocampal formation based on the GRIDSmap model and the Bayesian integration was demonstrated. With the circuits on the chips, we could realize the function of the stripe cells ring which could perform motion integration. Three stripe cells from these rings were connected to a grid neuron through a second order synapse circuit to demonstrate firing patterns with a spatial frequency of 1m.

Multiples of this frequency were obtained by connecting more stripe cells with 2 other grid cells. Thus, we could demonstrate the hexagonal firing patterns of the entorhinal cortex grid cells with different spatial frequencies as per the GRIDSmap model. As far as our knowledge of the literature, this is the first such demonstration of grid cell firing in silicon. Further, we extended the idea of the Bayesian integration as a possible mechanism for input integration at a place cell (based on the GRIDSmap model). To implement it in silicon, we designed and fabricated a circuit which can perform Bayesian integration and demonstrated results from chip measurements. Hence, in this work, we could demonstrate the working of the entire hippocampal formation from the perspective of the GRIDSmap model and the Bayesian integration in silicon. This system is capable of learning new paths (by changing connections between stripe cells and grid cells) and encoding for the animal's position in space by storing firing patterns of ensembles of place cells.

However, this implementation is only as close to empirical observations as the models on which it is based. Since the models have been able to describe grid cell spatial firing pattern (as observed empirically) reasonably well, our system could effectively produce grid spatial firing pattern based on motion integration. The models and, more so, the empirical data has not provided enough insights into a valid model for place cell firing which can explain all the empirical observations regarding place cell firing. Moreover, there has been debate on whether place cells integrate only the motor or both motor and sensory inputs. As such, this implementation includes integration of motor inputs (through grid cells) to current estimate of position of the animal in space to update the estimate. As such, the mapping of place in the environment and that of place cell firing is not strictly one to one. It will be possible only if we have a more robust model of the place cells. As such in this dissertation work, section 6, we propose a novel sensori-motor model of the hippocampal place cells which describes their firing patterns more closely to those observed empirically.

Moreover, the system, like any other prior implementation or like those in biology, suffered from drift due to noise, mismatch, etc. We devised a simple system (described in detail in section 5) for repeatedly resetting the rings to node 1 to take care of that issue. Thus, our system could perform path integration and spatial mapping accurately over extended periods of time and space.

Here, we had to use several chips because the system was designed based on the PSPICE simulations which have their limitations. However, chip measurement results brought forth limitations in operation of the circuits due to problems in

reading addresses in the correct order through the AER. In future versions, the entire system can be built on a single chip as only 1 or 2 circuits from each of the chips were being used. This could save chip area. The software interfaces can also be replaced by hardware connections which can speed up implementation and reduce the footprint but this will not allow the system to be flexible.

The system has potential applications in implementing autonomous robotic spatial navigation and memory compactly.

5. ERROR CORRECTION IN THE SYSTEM

As is true of the biological systems and for the artificial systems inspired by the biological systems, our system is also prone to drift over time due to mismatch and noise. This drift in the system is a problem because the errors accumulate over time and eventually, the system cannot perform as expected. Biological systems have their own mechanisms to correct for it and maintain correct estimate of the position while performing under such noisy conditions. However, the systems engineered based on the biological systems need to be especially provided with such mechanisms. One such system which depended upon memory of space and matching it to current arrangement was designed and described in Massoud & Horiuchi, 2011. This required storing past estimates of the position in memory, implementing which has a software and possibly, hardware overhead. In this work, we describe a novel mechanism to perform error correction over time which utilises in built hardware rather than hardware-software interface. To achieve this, we introduced a mechanism to reset the system. By periodically resetting the system, the problem of drift could be taken care of and the system continued to perform correctly over a longer duration of time. This reset could be effected using the same software interface that we built to demonstrate the function of rest of the system, i.e., in Verilog on Spartan 3E FPGA board. Thus, this system provides the same function, does not need stored memory for estimates of positions in space or specialized software for implementation.

A. System description

Each stripe ring circuit (Fig. 20) was based on the winner take all (WTA) circuit, with 24 nodes in each ring. As per the principles of the WTA circuits, only one node wins at a given time and this was used to represent the projection of the animal's position in space along the ring's preferred direction. The rings of stripe cells receive information (through software interface built on FPGA) about position of the animal in the environment projected on to their preferred direction using the trigonometric principles mentioned in Mhatre et. al., 2012. At the time of starting the circuit operation, the position of the winning node was reset to node 1 by pulling the *reset* parameter on the circuit to 0V. Thereafter, the position of the winning node was moved around the ring to register the animal's position in space by using short pulses as *RS/LS* signals to transistors M10 and M11 in the schematic shown in the figure. The current from the winning node was copied to an integrate and fire neuron (Fig. 21) through a current mirror. The address of this neuron was read using the AER circuits.

One node on each ring was connected to a grid cell represented by synapse-neuron circuits. Thus, the grid cell so connected fires spikes only when the neurons on the nodes connected to it, fire simultaneously which according to the GRIDSmap model occurs at regular intervals in space. These regular intervals occur at the corners of an equilateral triangle. 3 different spatial firing patterns on 3 different grid cells were demonstrated by connecting 2 or 3 or 4 nodes of the rings to each grid cell. Connections between rings of stripe cells and grid cells were also implemented in Verilog on FPGA. Outputs from these 3 grid cells were integrated

on to a place cell through a Bayesian integration synapse. Thus, the place cell fired only when all the grid cells fired simultaneously. The connections from grid chip to place chip were routed through wires connecting one chip to the next. We demonstrated the working of this system when the animal is moving along a straight line, in a circle or in open space. This was done by calculating the projection of the animal position in environment on to the 3 rings and then moving the winning node of the ring around in a controlled manner using software interfaces built in Verilog and implemented on the FPGA board. For instance, to simulate the animal movement in a circle, we calculated the projection of 12 points on the circle in space, onto the three rings as node positions. To implement this, all the rings' winning nodes were reset to node 1. Then, the position of the winning node was moved to 24 for all the rings. After this initial setting, the position of nodes was shifted repeatedly through the node numbers mentioned in the given order. During movement of the rings in a controlled manner, right shift or left shift signals and *req/* signals were provided through the decoder to the rings. These were very narrow pulses (0.5 μs long) at 1 ms intervals. As the nodes fired, their numbers were read using the FPGA board and when node numbers of all the rings were 24, the grid cells received a spike input. As a result, all the grid cells fired and resulted in firing of the connected place cells. These allowed the system to correctly integrate motion to update position estimates over a period but not forever due to mismatch and noise. Without using the error correction mechanism, after a period of successful estimation of the current position and

movement of the animal in space, the estimates drifted. Over a time, the drift became so severe that the system could not work as desired.

B. Results

For demonstrating the error correction over a period, the animal motion along a circle was simulated on the system and measurements from the chips were obtained using the Agilent MSO 6014A mixed signal oscilloscope. The measurement results were processed in MATLAB and are presented here. Fig. 43 shows the correct estimate of position as indicated by the correct spatial firing frequency of the grid and the place cells when the animal motion along a circle was being simulated as described above. This was observed both before the system suffered from drift and after the system was corrected for drift using the reset mechanism.

After a few minutes of correct path integration, the system estimate of the animal's position in space as depicted by position of the winning node on the 3 rings, drifted. One such instance of the drift is shown in Fig. 46. Here, instead of moving between neuron numbers 24 and 22 (as calculated), the winning node moves between 7 and 8 or 15 and 16 or 24 and 0. And as expected, this leads to loss of firing of the grid and the place cells. To overcome this problem, the rings were provided with a mechanism to reset the winning node back to the first node as was at the beginning of the path integration. This was done in anticipation of this problem and was implemented by providing a mechanism for the same as shown in Fig. 20.

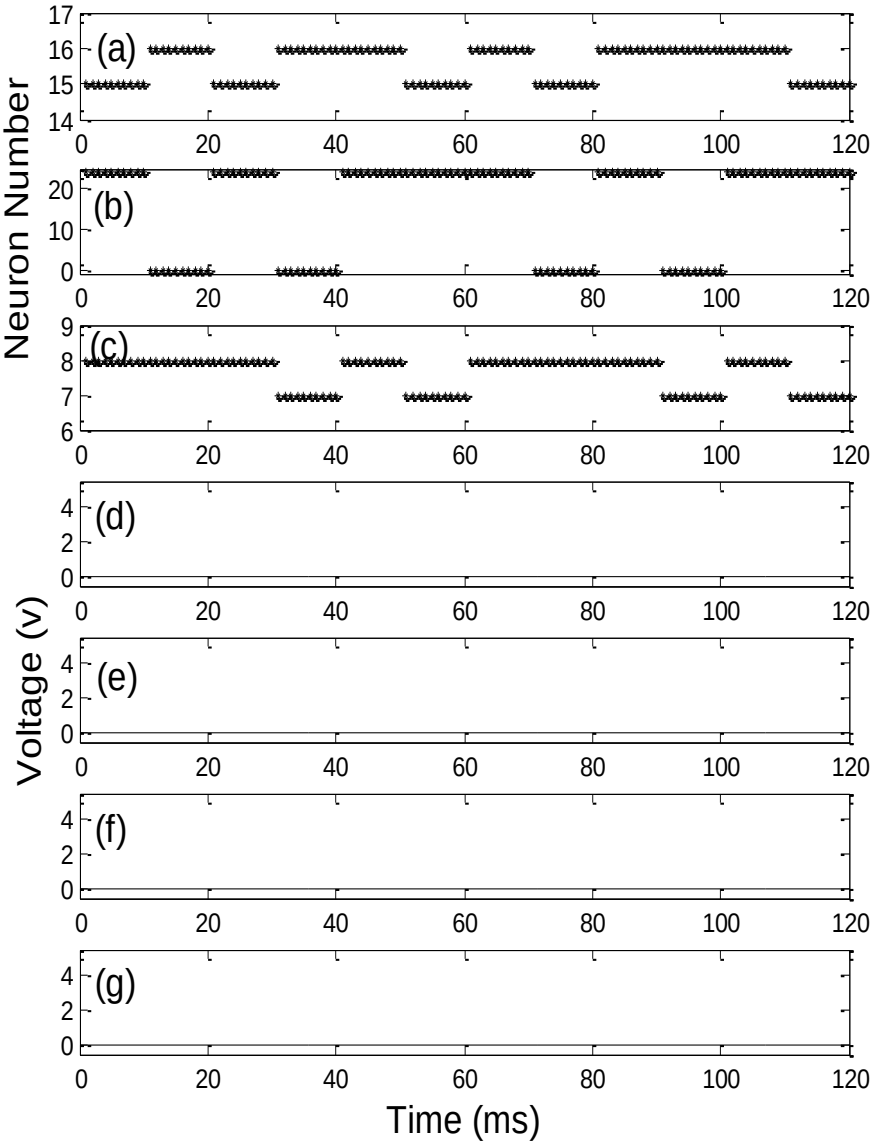

Fig. 46 Shows the results from chip measurements of the silicon implementation of the grid and the place cell firing patterns when animal motion in a circle was simulated over a period of time. After integrating motion information correctly (as shown in Fig. 43) for around 60 s, the system accumulates error and stops functioning. (a)-(c) Neuron number positions after the system has accumulated error for long enough (in the absence of reset) move between (a) 16 and 15, (b) 20 and 0 and (c) 8 and 7 instead of between 22 and 24 as seen in Fig. 43. As a result of this, the grid (e)-(g) and the place cell firing (d) stops as they do not receive inputs from the cells to which they are connected. This was fixed by resetting the ring circuit to neuron number 1 at regular intervals.

It was implemented using software code in Verilog, implemented on the FPGA board. As the system was integrating motion of the animal in space and updating the estimate of its current position, the system provided reset signal to the chip at intervals of 50 s. As a result, the system was restored to its correct orientation and started integrated movement to update current position estimates as shown in Fig. 43. Thus, with a simple reset mechanism repeated at regular intervals, the system could perform path integration correctly and over extended periods of time as is desirable for autonomous robotic spatial navigation. This also did not require additional software implementation overhead.

C. Conclusion

The problem of error accumulation and drift due to noise or mismatch is common in biological systems and engineering systems inspired by biological systems. This section demonstrates one such error correction scheme for a bio-inspired system, the hippocampal formation. This scheme is based on resetting the system at regular time intervals so that error does not accumulate further and whatever has accumulated is corrected for. As seen in the results section, if the system was not reset, it accumulated so many errors that it stopped working in the desired manner. However, as soon as it was reset, it started working as desired and could perform path integration and update the current estimate of position of the animal in space correctly. Advantages of this correction mechanism are that it does not need additional sensory or motor inputs from the environment or any recourse to information stored in memory, and that it can be implemented using the same hardware and software resources as are required for implementation of the system.

However, it could potentially cause delay in processing information due to the time spent on periodic resetting of the system. In short, the system has an ability to implement an important error correction scheme using a simple in built mechanism which can also be used in designing similar systems.

6. THE SENSORI-MOTOR MODEL OF PLACE CELLS

As was observed in section 2 on the Hippocampal formation, the place cell firing, as described theoretically by the GRIDSmap model and the Bayesian integration does not produce firing patters as observed empirically. Thus, a further study of the literature and currently prevalent models was done and based on these, a new sensori-motor model of the place cell firing is proposed and presented here.

A. Problems with the current models of the place cells

There is dissonance between the models and empirical observations.

Firstly, if the place cell firing was due to summation and thresholding of inputs from the grid cells with different spatial frequencies, then all the place cells should exhibit multiple regular firing fields, however, only multiple but not regular fields have been observed for the place cells.

Secondly, Witter et. al., 1984, 1989 demonstrate connections of dorsal entorrhinal cortex (ERC) to dorsal hippocampus and the temporal ERC to the temporal hippocampus which means that place cells cannot get inputs from grid cells with different spatial firing frequencies as required for these models.

Thirdly, some of the post-grid cell era models suggest place cell activity based only on the grid cell inputs while empirically, the place cell firing has been seen in the absence of the grid cell activity in early development (Langston et. al., 2010, Wills et. al., 2010) or when the medial septum is inactivated (Brandon et. al., 2011, 2014, Koenig et. al., 2011), meaning that grid cell inputs are not vital to firing of the place cells (Bush, Barry, Burgess, 2014).

Fourthly, the pre grid era models emphasize a lot on sensory inputs alone as the possible reason for place cell firing which is defied by empirical observations.

Fifthly, the episodic memories have been documented to have a context, i.e., they vary depending upon the place of prior events (Hasselmo, 2012). For instance, if an animal enters an environment from a particular direction, the spatial location will be encoded in memory differently from when it enters the same environment from a different direction. Moreover, the events are remembered in a sequential manner while none of these models takes context into account.

Therefore, in this section we wish to present the sensori-motor model explaining place cell firing based on optimal integration of both sensory (visual, auditory, olfactory, etc.) and motor inputs (processed through the head direction and the grid cells) and only none or suboptimal firing otherwise.

B. Evolutionary differences

In the animals without binocular vision, the position of an object could not be identified by visual inputs alone. Hence, this could be done by spatial mapping of the entire environment by the medial entorhinal cortex grid cells as the animal moves around in space. The grid cells update the estimate of animal position in space by integrating the motor inputs to update the estimate of current position of the animal. Information about the heading direction is provided to the grid cells by the head direction cells. And that of distance by motion integration along the rings of the head direction cell system. Thus, the grid cells provide a matrix spanning the entire environment which is used by the place cells to ‘hang’ the image of

objects visible to the eyes. Thus, the place cells integrate the processed motor and sensory information.

In animals with binocular vision, even though the estimate of position could primarily be performed by visual inputs, place cells could still perform the function of encoding it in memory. Moreover, the processed motor information from the grid cells could also be integrated with the sensory inputs at the place cells to reduce error in estimation of a place. Evidence in support of the above could be the poorer visual abilities of the rats and that phylogenetically, hippocampus is a more primitive part of the brain. It is less developed relative to other brain areas (cortex) in animals with binocular vision because its function of spatial estimation is almost 'overtaken' by the visual information processing centres (occipital, parietal etc.). This could also explain why humans have little problems in spatial navigation but significant problems in formation of new episodic memories while rodents have more problems in spatial navigation when the hippocampus is malfunctioning or removed.

C. The sensori-motor model

i) Place cell firing

We propose that each place cell fires based on Bayesian integration (Madl et. al., 2014) of both sensory inputs (from vision, auditory, olfaction etc.) and processed motor inputs from a single grid cell (Fig. 47). Based on the connectivity pattern of the medial ERC and the hippocampus (Witter, et. al., 1984, 1989) we propose that each place cell gets processed motor inputs only from one grid cell located at a

corresponding position along the dorso-ventral axis. We also propose that the place cell does not receive direct input from this grid cell but through a ring of intermediate neurons. This ring is similar to the HD cell system, in which neurons are connected in rings, which perform path integration (because on movement of the orienting visual cue, the orientation of all the grid cells changes in the same direction). The grid cell outputs are also processed by this ring of intermediate neurons. Thus, as the grid cell attached to the ring fires, the neuron position along this ring moves. This converts 2D firing of the grid cell into a 1D motion along the ring which helps keep track of how many grid cell firings have occurred along the path followed by the animal (Fig. 47 (a)). According to our model, when the animal first enters a new environment, the place cell is reset and is not connected to any of the neurons in this ring. However, the place cell can fire due to the sensory inputs incident on it. Thus, by hebbian learning, it forms synaptic connections to the intermediate neuron in the ring which is firing at the same time. Thus, when the animal visits the same environment, this place cell fires again due to either one or a combination of motor and sensory inputs. Since this integration at the place cell occurs in a Bayes' optimal manner the place cell firing is stable and optimal when it receives both sensory and motor inputs and suboptimal otherwise. This can also explain empirical evidence from studies where the place cell firing has been observed in the absence of the grid cell firing or the sensory inputs alone as described in the section on empirical evidence.

Since the grid cell firing wraps around along the ring of intermediate neurons, the place cell can fire again provided it receives another sensory input at the same

time as the neuron in the ring of intermediate neurons which it gets connected to. Thus, the place cells can produce repeated firing in the same environment (as observed empirically) and this firing need not have a regular pattern, as that of the attached grid cell, as in the optimal case, it depends on both the grid and the sensory inputs and not on the grid firing alone.

Since the ring of intermediate neurons will advance in position based on number of firings and not the direction of grid cells, the place cell firings could be multiple but not necessarily at regular intervals. This shall also provide context. For instance, if the animal traverses a different route to reach the same place, the place shall be identified as different even in the presence of visual inputs because the number of firings between entering a new environment and reaching the point of significance changes (Fig. 47 (a)).

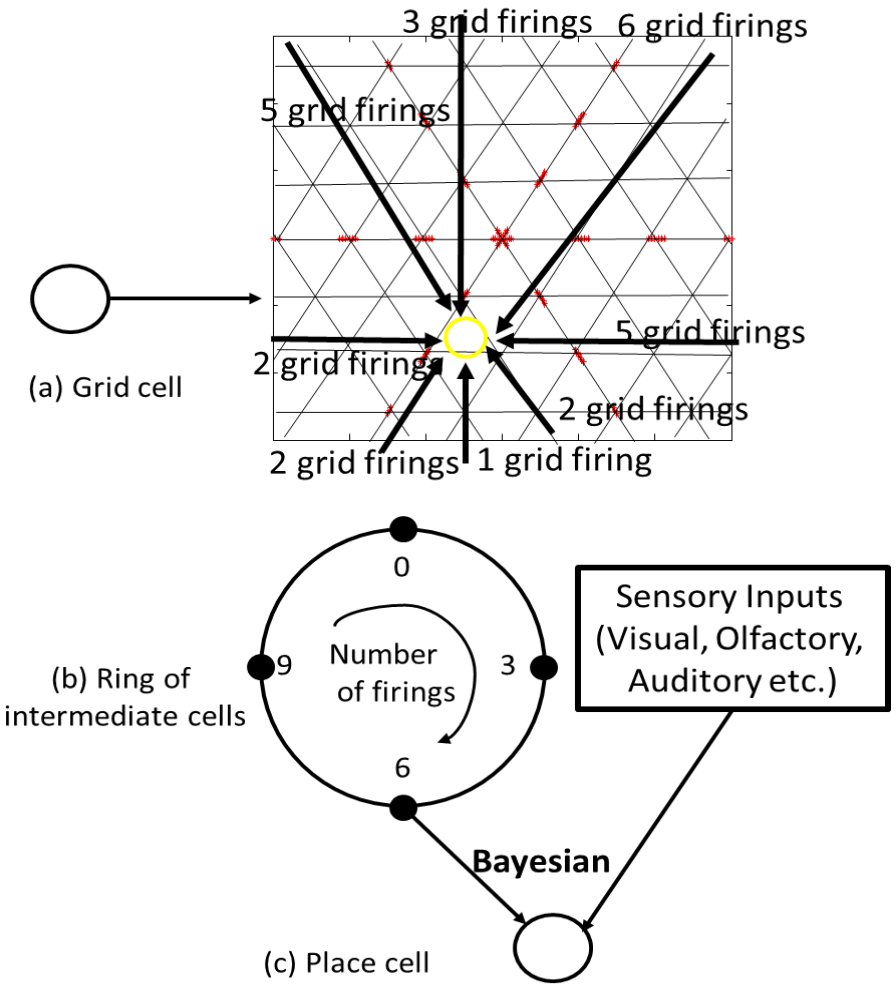

Fig. 47 Schematic representation of the sensori-motor model of the hippocampal place cells. According to this model, each place cell is connected to (a) only one grid cell with a particular spatial firing frequency. As the animal moves around in space, the grid cell fires as described by the GRIDSmap model. (b) The number of firings of the grid cell are integrated by a ring of intermediate cells. The place cell receives inputs from the grid cell after they have been integrated by a ring of intermediate cells. (c) Also, the place cell combines the sensory inputs with motor inputs from the connected grid cell. Whenever the animal enters an environment, the place cell and the position of the ring of intermediate neurons reset. As the animal gets sensory inputs which define the place to be signficant enough to merit place cell firing, the place cell fires. Through hebbian learning, connections develop between the place cell and the simultaneously firing neuron on the ring of intermediate cells. Whenever the animal enters the environment again, even in the absence of sensory inputs, it can fire sub optimally because of its connections to the neuron in the ring of intermediate neurons. This provides context and continuity in the firing pattern.

Another important question is why do we need several grid cells if only one was enough to provide a matrix for the entire space? All the grid cells get similar motion information from the environment with a phase shift w.r.t. each other. Thus, inputs from multiple grid cells could be used for calculating time between two events and storing it in memory. Moreover, by having different spatial firing frequencies, they could help in localizing objects of different sizes in the same environment.

Empirical observations in rats also show that place cell firing fields become bigger in bigger environments while grid fields become more numerous. This may or may not be true in animals with binocular vision though. Our model could explain this also because if the place cells were to fire based on a combination of the visual and the motor inputs, and the visual inputs are to be from a rat eye, then the bigger the environment, the rat eye could make image of each object bigger. This is contrary to what we would expect based on our own visual experience but it could be true if that is how the rat eye responded to changes in its environment. For instance, if a rat could detect the distance of the corner of the enclosure by motion parallax, then it could perhaps adjust the focal length of its lens commensurate to this distance – could be a behavioural adaptation of a rat to its environment (we are unable to explain why). But if this occurred, then the place fields which are based on the Bayesian integration of both visual and sensory inputs will become bigger as the animal is placed in a bigger environment while the number of the grid fields (and not their size) increases as observed empirically.

ii) Path Retrieval

According to our model, the place cell firing encodes a path in memory as the animal moves through its environment (Fig. 48). When the animal follows different paths in the environment, correspondingly different trajectories get encoded in memory. During path planning, the animal thinks through all these available trajectories in memory simultaneously and the one with least number of place cell inputs is chosen as the shortest path and followed by the animal. Here we have used the assumption that given the required inputs, the place cell shall be able to fire at similar intervals in space along all different trajectories and hence, distance between the two place cell firings is indicative of the distance traversed in space.

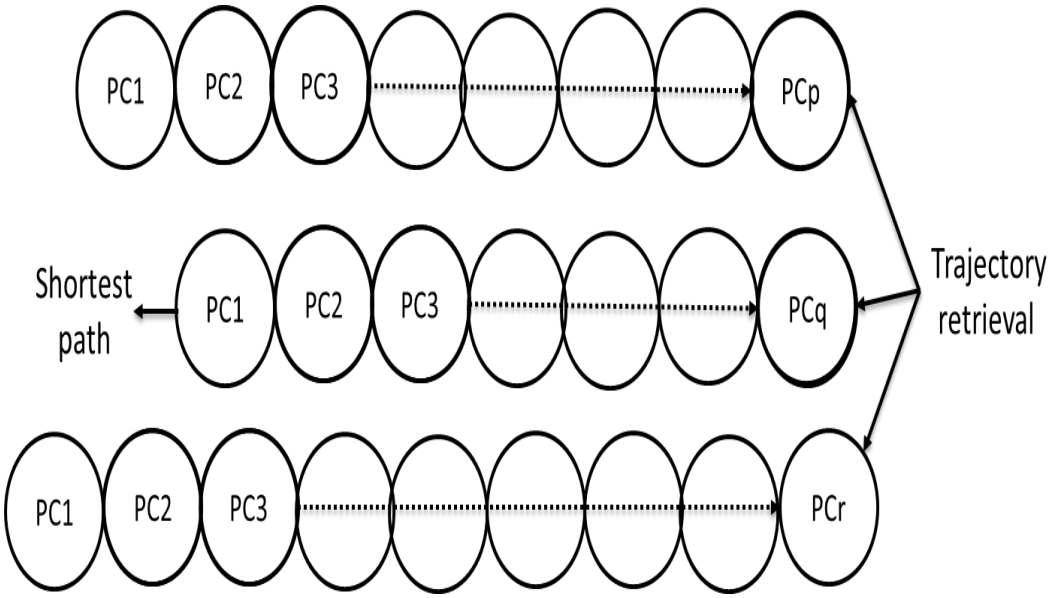

Fig. 48 According to our sensorimotor model of the place cells, different trajectories are encoded in memory as the animal moves around in the environment. During retrieval, all of them are scanned simultaneously to find out which one is the shortest – as judged by the time taken to traverse it. Thus, the animal decides on the shortest path to be followed by it to reach the goal.

D. Conclusion

Here, we describe a model to explain place specific firing patterns of the pyramidal neurons in the hippocampus. This model derives inspiration from differences in binocular and non-binocular vision. It explains how both sensory and motor inputs could be integrated in a Bayes' optimal manner on the place cell. It is more plausible based on anatomical connections between the hippocampus and the entorhinal cortex and empirical observations. This model can be utilised in future silicon implementations of the place cell firing patterns.

7. THE CENTRAL PATTERN GENERATOR

The central pattern generators (Goldman et. al., 2001, Golowasch et. al., 2002) are rings of inhibitory interneurons connected to each other through inhibitory synapses. In contrast to the attractor dynamic networks, which are purely neuro-computational models, the presence of these rings of inhibitory interneurons has actually been demonstrated in the spinal cord and the brain. The central pattern generators are responsible for driving rhythmic activities like breathing, walking, heartbeat, peristalsis etc. These systems are of interest to engineers as they describe a mechanism for controlling gait in robotic systems (Lewis et. al., 2000, Arena et. al., 2005, Still et. al., 2006, Luo et. al., 2004).

A. System implementation

To demonstrate the working of the ring circuit (Fig. 20) as a central pattern generator (Fig. 49), the output from the ring circuit was provided a train of inputs at a particular frequency (say, 1 kHz). This causes one of the nodes on the ring to be excited at $1/25^{th}$ of the frequency, i.e., at 40 Hz. If this node is connected to a synapse- neuron circuit on the grid chip (Fig. 26), then this neuron will produce a regular firing pattern which can be varied with the frequency of the *RS* or *LS* signals applied or with multiple nodes being considered and hence, it can function as a central pattern generator and can possibly be used to provide motor inputs to robotic systems.

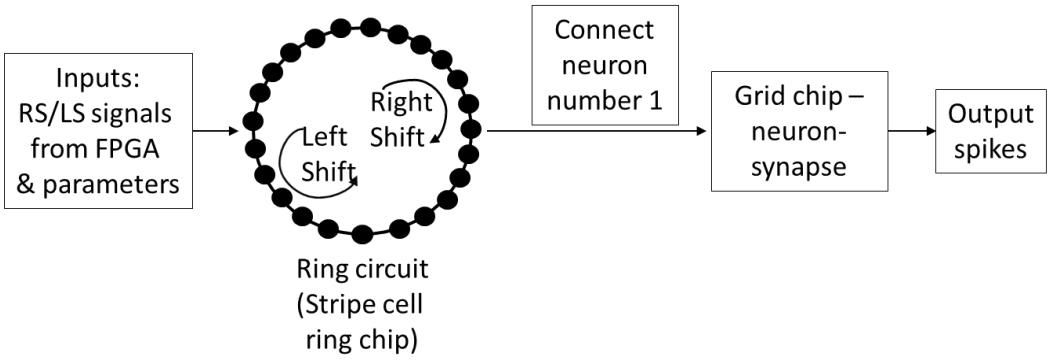

Fig. 49 Schematic of the connections to perform as a central pattern generator in silicon. One ring circuit from the stripe cell ring chip and one synapse-neuron circuit from the grid chip was used to demonstrate the working of the system. When the ring circuit was provided a train of *RS* or *LS* signals as inputs, for instance at 1kHz, then each neuron on the ring circuit, is excited at 40 Hz. The neuron number 1 was read using the FPGA. Whenever it fired, the FPGA sent an input pulse to the neuron-synapse circuit on the grid chip whose output was read using mixed signal oscilloscope. This output can function as a central pattern generator. Different firing patterns can be generated by moving the ring around at different frequencies and by connecting multiple neurons on the ring to the neuron-synapse circuit on the grid chip. If two equidistant neurons on the ring are connected to two different neuron-synapse circuits, each can work as a central pattern generator to provide inputs to muscles which have antagonist functions – for instance, one could provide input to the leg extensors and the other to leg flexors, to control robotic walking.

B. Circuits

To realize the function of the central pattern generator, two chips were used, viz., the stripe cell ring chip (Fig. 19) and the grid chip (Fig. 26). The details on these have been presented in sections on the head direction cell system and the grid and the place cells – silicon implementation. Thus, these are not presented again. Here, only the testing of the two chips as a system is presented.

C. Testing and results

In this experiment, the output from node N1 of the ring circuit on the stripe cell ring chip was provided as an input to the second order synapse circuit on the grid chip and the subsequent firing of the conductance neuron connected to the synapse circuit was recorded using a mixed signal oscilloscope (Fig. 49). Since, the *RS* and the *LS* signals to the ring circuit were provided at 1 kHz, the node N1 was activated at (1000/25=) 40 Hz. Thus, the second order synapse was provided an input pulse at 40 Hz through the FPGA to mimic the output from N1. The parameters used for the second order synapse and the conductance neuron were $V_{\tau 1}$=3.5V, $V_{\tau 2}$=4.5V, V_s=3.79V, V_f=2.88V, V_{syn}=2.60V, V_{thr}=0.77V, V_{leak}=4.31V, V_{we} =4.10V, V_{refr} =4.20V. Now, if the pulse frequency of the *RS* or the *LS* is reduced to one half or a quarter of 1 kHz, then the N1 will get activated at a frequency of 20 and 10 Hz respectively and the resultant firing of the conductance neuron was recorded using the mixed signal oscilloscope. The results shown in Fig. 50 demonstrate that the neuron connected to one of the nodes of this ring can produce different patterns as the *RS* or *LS* signals are provided at different frequencies. Hence, this ring circuit along with the synapse-neuron circuit can be used as a pattern generator.

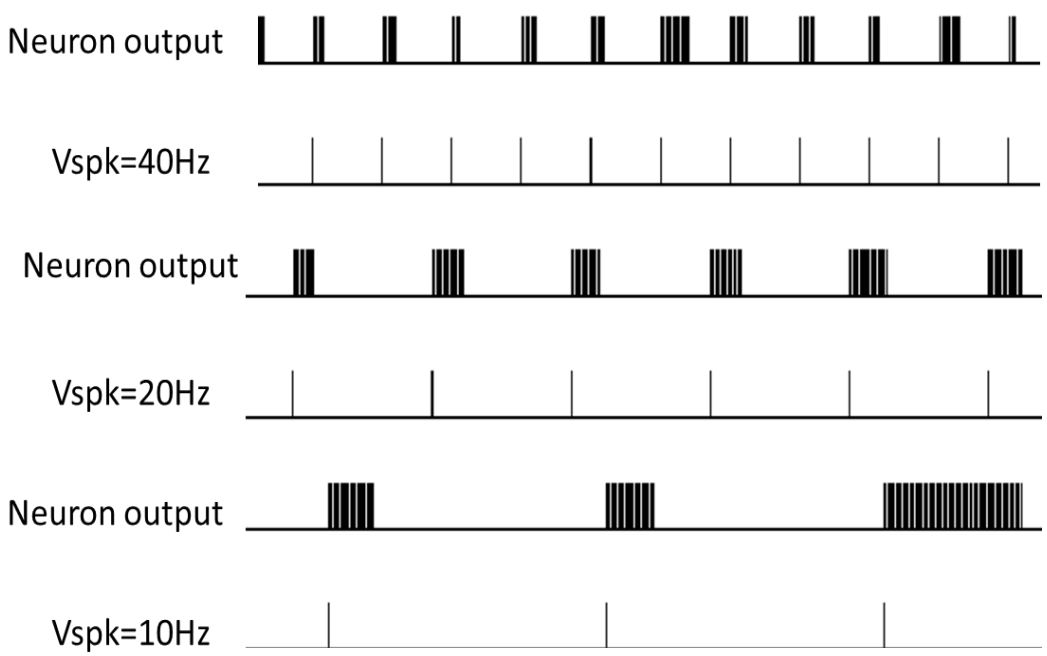

Fig. 50 Results from chip measurements showing the output of the central pattern generator. For these measurements, the ring circuit on the stripe cell ring chip was moved at 1 kHz, 500 Hz and 250 Hz by applying a train of *RS* signals. As such, one of the neurons on the ring circuit fired at 40, 20 and 10 Hz. The firing of this neuron was detected using the FPGA. Whenever this neuron on the ring circuit fired, an input pulse was sent to the neuron-synapse circuit on the grid chip. The corresponding firing from the neuron was recorded as is shown here. These can be used as central pattern generator for controlling muscle movements in robotics.

D. Conclusion

Here, the silicon implementation of a central pattern generator was successfully demonstrated using very compact circuitry. These circuits are of use in robotic gait control. Walking around in an environment needs coordination of muscle movements. For instance, the leg flexors and extensors cannot be active at the same time but should be activated alternately. Thus, the central pattern generators provide them regular alternating inputs and hence, provide stable gait. In the

above presented silicon implementation of the central pattern generator, only three different frequencies of output signals are shown, each of which is independent of the other. However, in the same system if we connect N1 and N12 on the ring circuit to two different neurons, then these shall produce regular patterns of same frequency which shall alternate and hence, can provide inputs to the flexors and the extensors to control robotic gait.

8. THE LATERAL SUPERIOR OLIVE

Azimuthal localization (Purves, et. al., 2012) of sounds means detecting the direction along the azimuth from which the sound is incident. It is of survival value to a species as it helps the animal in spatial navigation, localizing the prey, defence against predators, etc. It depends upon a combination of cues - detection of interaural time difference, interaural level difference and direction dependent spectral filtering. The relative importance of each of these depends upon the species of the animal. In animals with smaller head sizes and high frequency sound perception, the azimuthal localization is primarily performed by detecting the interaural intensity or level difference (IID or ILD) at the lateral superior olive (LSO). This is because the head size is very small and the sound frequency is too high to provide a detectable time difference. The LSO receives excitatory inputs from sounds of a narrow range of frequencies from the ipsilateral ear and inhibitory inputs from sounds of the same narrow range of frequencies from the contralateral ear. The distance from which the sound is coming changes the intensity of the sound received at both ears which only changes the response latency of the LSO neurons. On the other hand, the azimuthal direction (Fig. 51) of sound changes the ILD which changes the response of the LSO neuron which helps localize the sounds. Thus, an electronic LSO can provide a mechanism for sound localization in autonomous robotic spatial navigation.[11]

[11] Initially, when I was in the Horiuchi lab, the plan was to implement the population response of the LSO based on the transistor mismatch. But when I moved out of his lab, I conceived of using the Reed and Blum's model of LSO to base the silicon implementation on. Thus, in this work, we present the electronic LSO based on the Reed and Blum's model.

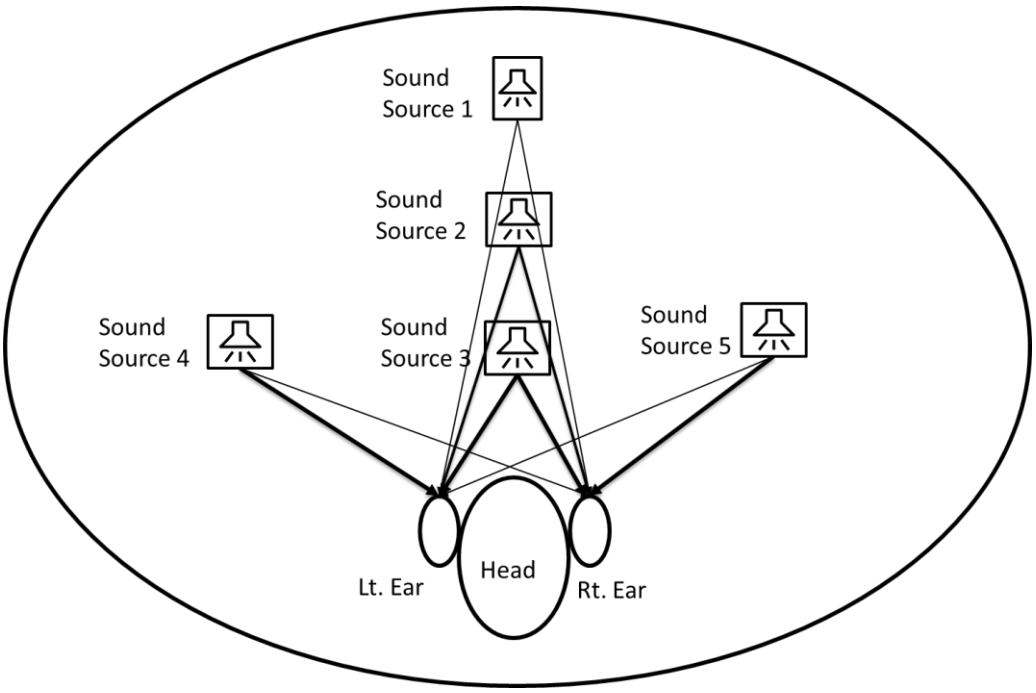

Fig. 51 Showing the different ranges and azimuthal angles for a sound source and its impact on intensity of sound received at both ears. In case of sound source 1, 2 and 3, the interaural level difference (ILD) is expected to be the same because the intensity of sound received at both ears reduces as the source moves from position 3 to 2 to 1. As the sound source moves from position 3 to 4 to 5, the intensity of sound received at one ear is different from that received at the other thus, the ILD is different at different positions. For source 3, the ILD is expected to be 1, and for source 4 and 5 it will be greater than one for the left and the right ear respectively. This information is used by the lateral superior olive in calculating the direction along the azimuth from which the sound is coming.

A. Anatomy

The ears (Purves et. al., 2012) receive sounds of several frequencies which are segregated by the inner ear cochlea. The cochlear nerve carries these frequency segregated sounds in separate nerve fibres to higher centres in the auditory pathway.

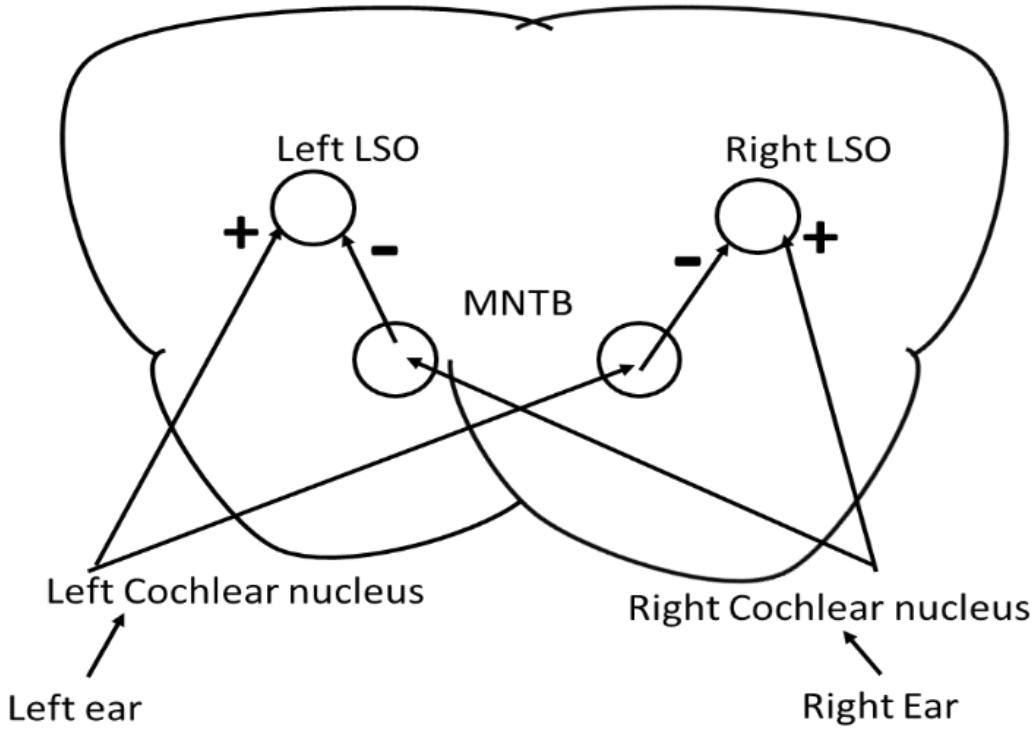

Fig. 52 Schematic of connections of the LSO showing direct excitatory inputs from the ipsilateral ear through the ipsilateral antero-ventral cochlear nucleus (AVCN) and indirect inhibitory connections from the contralateral ear through the contralateral AVCN and the ipsilateral medial nucleus of the trapezoid body (MNTB). Since the LSO receives inputs from both the ears, it is in a position to calculate the ILD and hence, determine the azimuthal direction from which sound is coming.

The fibres (Fig. 52) from each ear relay in the ipsilateral cochlear nucleus (AVCN) and the contralateral medial nucleus of the trapezoid body (MNTB). Outputs from these nuclei relay in the superior olivary complex which is a collection of nuclei (medial and lateral superior olive (MSO & LSO)) in the auditory pathway. These are the first nuclei in the pathway which receive auditory inputs from both the ears. Thus, they are in a unique position to compare the time and the intensity differences of sounds incident on the two ears. The

corresponding LSO neurons on the two sides provide inhibitory inputs to the ipsilateral and excitatory inputs to the contralateral dorsal nucleus of the lateral leminiscus (DNLL) and the DNLL provides inhibitory inputs to the ipsilateral and excitatory inputs to the contralateral IC as shown in Fig. 55.

The LSO receives excitatory inputs from sounds of a narrow range of frequencies from the ipsilateral ear through the ipsilateral anteroventral cochlear nucleus (AVCN) and inhibitory inputs from sounds of the same frequencies from the contralateral ear through the contralateral AVCN and the ipsilateral medial nucleus of trapezoid body (MNTB). The LSO is made up of columns of neurons. The LSO neurons are arranged with best frequencies (frequencies for which the neuron responds maximally), increasing from the lateral to the dorso-medial region. Each iso-frequency slab of the LSO is 10-30 cells thick and gets inputs from several AVCN and MNTB neurons. Each AVCN and MNTB neuron also projects to several LSO neurons. Bilateral inputs (Fig. 53) to the LSO column are arranged such that strength of the excitatory inputs increases and that of the inhibitory inputs decreases as we move from the top to the bottom of the column.

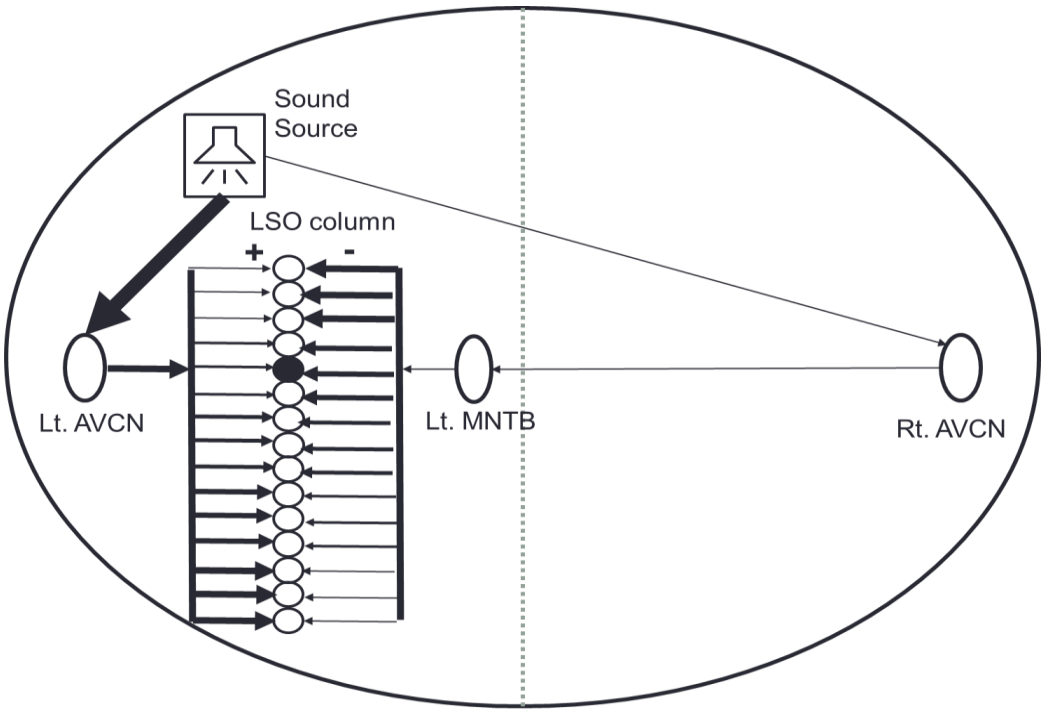

Fig. 53 Schematic representation of the azimuthal encoding by the LSO. The LSO column receives inputs from both sides. The strength (represented by thickness of the arrows) of the excitatory inputs increases and that of the inhibitory decreases as we move from top to bottom along the length of the column. The example shown in this case is of a sound source located near the left ear as a result of which the intensity of sound (represented by thickness of the arrows) received by the left ear is much greater than that by the right ear. This information reaches the left LSO through the left AVCN and right AVCN and left MNTB. The former increases and the latter reduces the conductance of the LSO neurons but in a weighted manner. The neuron in the LSO column (here neuron number 5 from the top) which receives equal change in conductance from the two sides, stops firing (because the ILD received is equal to its ILDci or interaural level difference of complete inhibition). This value of ILDci is different for each neuron. Thus, the neuron whose ILDci matches the ILD of incoming sound, given the azimuthal direction, encodes for the azimuthal direction of sound.

B. Azimuthal localization

i) Azimuthal encoding and ILD ci

Interaural level difference (ILD) is the difference between power levels or square of intensity of sound pressure inputs received from the two ears (Purves et. al.,

2012). It is defined as a difference or a log of the ratio of the two inputs, i.e., if $h_R(\theta)$ is the intensity of sound pressure from the right ear and $h_L(\theta)$ is the intensity of sound pressure from the left ear, (where, θ is the direction along the azimuth from which sound is incident) then ILD in dB is defined as

$$ILD = 20.\log(\frac{h_R(\theta)}{h_L(\theta)}) \qquad (16)$$

Thus, the ILD is a function of the direction along the azimuth from which the sound is received. The ILD has been empirically observed to affect the output of the LSO neurons (Purves et. al., 2012) producing a characteristic response curve. Fig. 54 shows that the firing rate of the neuron is dependent on the ILD (hence, on the azimuthal direction) and that there is an ILD for which the neuron does not fire (ILD of complete inhibition, ILDci). At this ILD, weighted inputs from the left and the right ear reaching the LSO are observed to be equal. Thus, each LSO neuron responds based on the direction from which sound is received. For each azimuthal direction, the intensity of inputs to the two ears will vary. Thus, the net conductance change produced by the weighted inputs received at each LSO neuron also changes. This changes the output of the neuron. For each azimuthal direction, a different neuron number along the LSO column gets no net conductance change, i.e., the ILD received matches its ILDci and hence it does not fire. Thus, the LSO neuron which stops firing first along its column, encodes for the azimuthal direction. The left and the right LSO together span the entire azimuth, each one separately covering 180 degrees on its side.

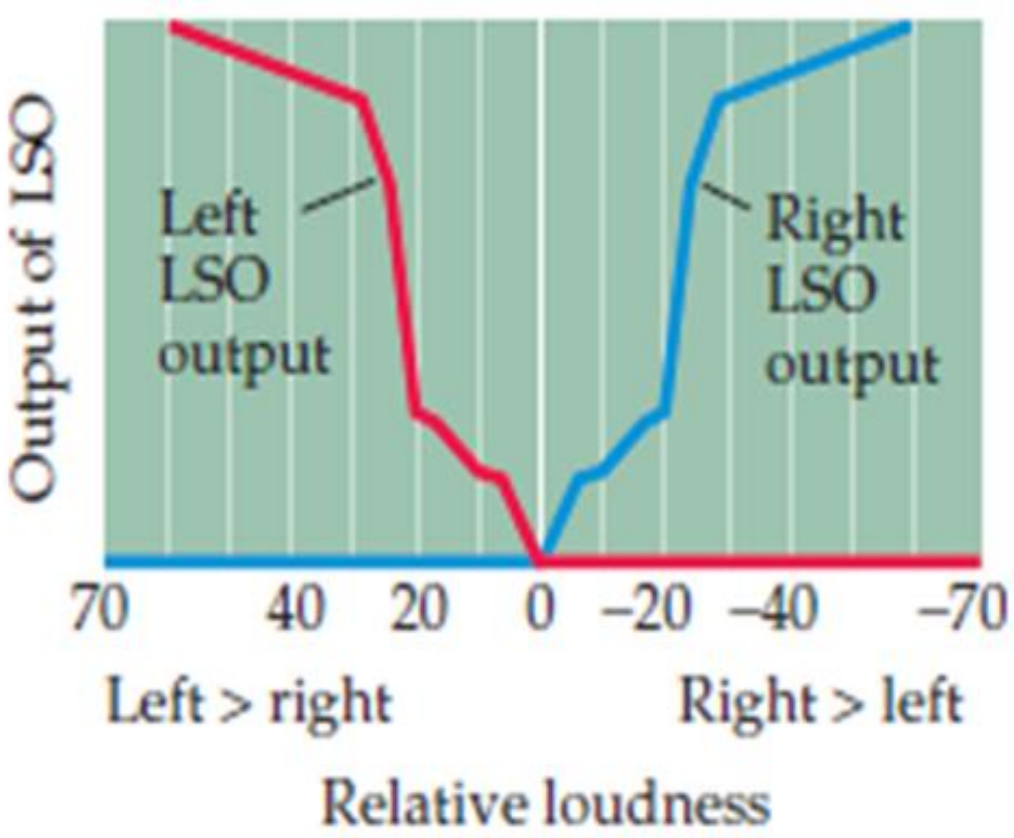

Fig. 54 Graph showing response of the left and the right LSO to varying ILD – response is higher on the side which receives higher intensity of incoming sound with eventual saturation of response. For each LSO neuron, there is a value of ILD at which it stops firing, this is called its ILD of complete inhibition or ILDci [102].

ii) Directional selectivity at the inferior colliculus

As seen above, each LSO neuron in the LSO column on either side produces a response curve as shown in Fig. 54. The corresponding LSO neurons on the two sides provide inhibitory inputs to the ipsilateral and excitatory inputs to the contralateral DNLL and the DNLL provides inhibitory inputs to the ipsilateral and excitatory inputs to the contralateral inferior colliculus (IC) as shown in Fig. 55. Thus, the sigmoid shape of the response curve at the LSO changes to a tuning

curve at the IC. This tuning curve has a preference for a particular azimuthal direction. Thus, each IC neuron can encode for the azimuthal direction from which the sound is incident on it.

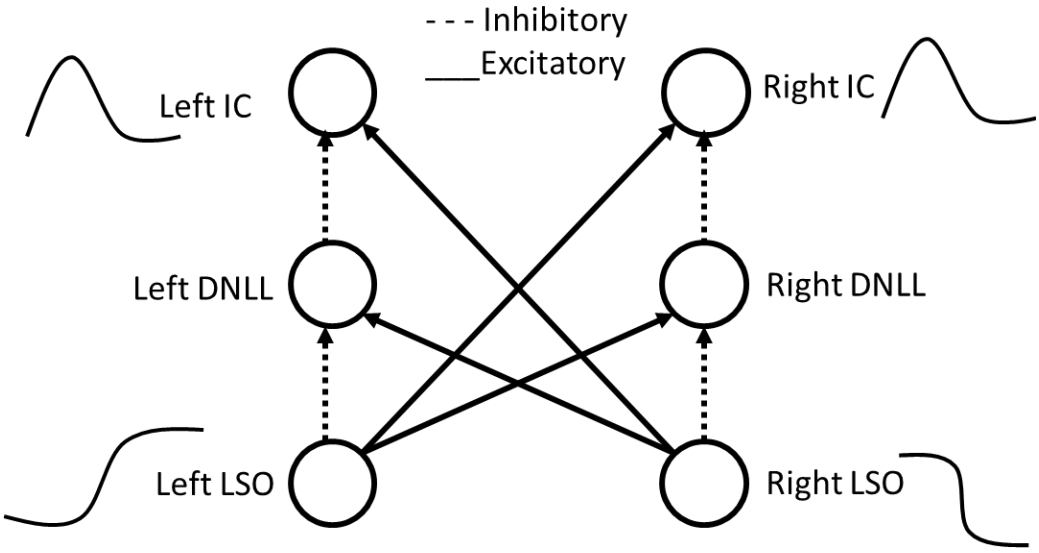

Fig. 55 Schematic of the connections between the LSO, the DNLL and the IC which help in processing the sigmoid shaped ILD response curves at the LSO to bell shaped curves at the IC. Thus, inferior colliculus neurons will have a preferential ILD for which they fire.

C. Species differences in azimuthal localization

The relative importance of interaural time difference, interaural level difference and direction dependent spectral filtering in echolocation depends upon the species of the animal. For sounds of frequencies lower than 3 kHz, the temporal differences (Schnupp & Carr, 2009) can provide adequate information for azimuthal localization in humans. The neural circuits providing azimuthal localization based on interaural time differences are located in the medial superior olive (MSO). However, for sound frequencies above 3 kHz, the human head provides an acoustic shadow as the wavelengths of the sounds are too short to

bend around at these frequencies. This leads to intensity differences in sounds reaching the two ears. These intensity differences provide an additional cue for azimuthal localization which is processed by the LSO.

In animals with smaller head sizes and high frequency sound perception, the azimuthal localization is primarily performed by detecting the interaural intensity or level differences (IID or ILD) at the LSO. This is because the head size is very small and the sound frequency is very high to provide a detectable time difference. In Park et. al., 1996, it was demonstrated that the ITD enhances or reinforces the effect of ILD as the more intense input produces a shorter latency and longer duration so that the more intense sound dominates the LSO response. Also where the head is bigger, the ITD is significant so it can contribute to the azimuthal localization in addition to the ILD.

In Schnupp & Carr, 2009, it was observed that since the contralateral inhibitory input has a longer path length to traverse to reach the LSO, it leads the ipsilateral excitation or in other words, it has higher intensity than the excitation.

D. LSO models

The circuit design of the LSO is inspired by the mathematical models proposed for the system (the Reed and Blum's model) and that for the individual neuron (the conductance model) and the synapses (the second order function). The latter two are more general models for the synapse and neuron which are valid across almost all systems while the former is specific to the LSO. Therefore, in this section, we briefly describe these models.

i) The Reed and Blum's model of the LSO

According to this model (Reed and Blum, 1990), inputs to the LSO column are arranged (Fig. 56) such that their strength varies along the length of the column. The strength of excitatory inputs increases and that of inhibitory inputs decreases as we move from top to bottom of the column. Wherever the two inputs are equal, ILDci is achieved and hence, the LSO neuron does not exhibit any response. As mentioned earlier, ILD depends on the azimuthal direction from which the sound is incident (primarily). While ILDci depends on the neuron number along the LSO column according to this model.

Azimuthal direction → ILD = ILDci← neuron number ← arrangement of inputs along the LSO column

Thus, the ILD=ILD ci for a unique combination of azimuthal direction and neuron number. Thus, the neuron number which stops firing first encodes for the direction along the azimuth from which the sound is incident. Results from simulation of this model described in the same paper are shown in Fig. 57. It is clear that as the ILD changes with change in direction along the azimuth from which the sound is coming, the neuron number experiencing ILDci also changes along the LSO column. Thus, determining the neuron number which experiences ILDci can help in azimuthal localization of sound by the animal.

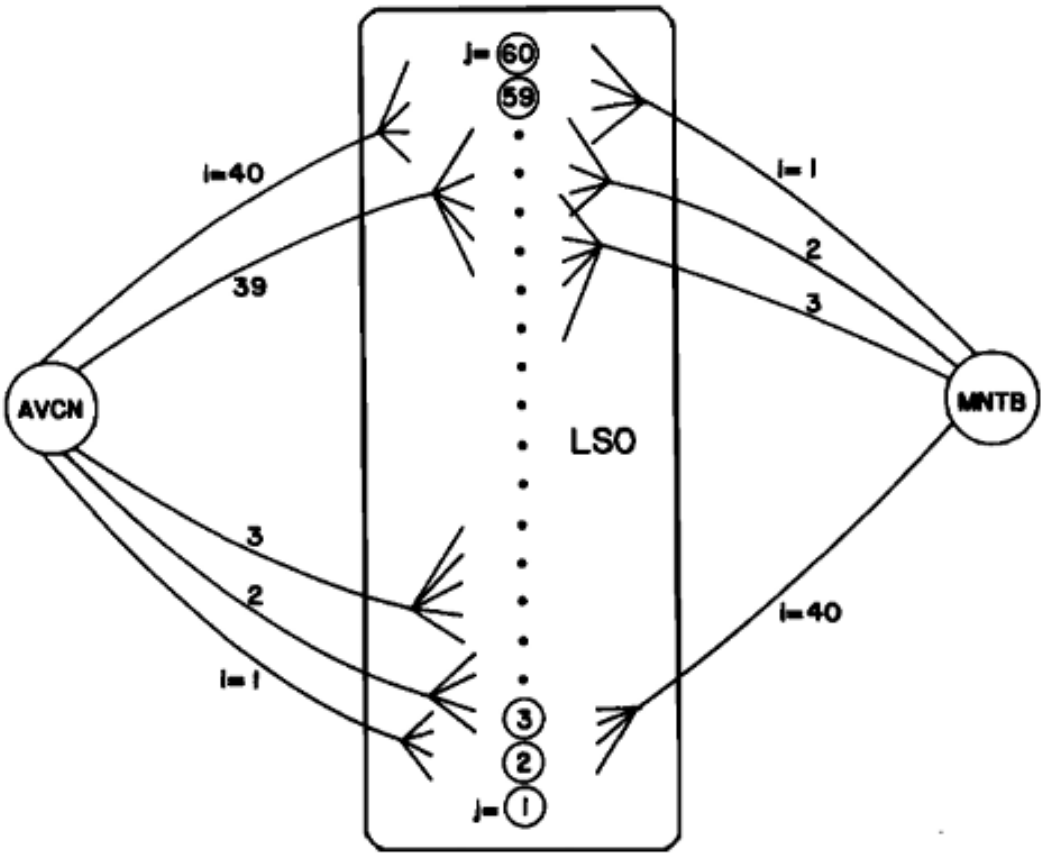

Fig. 56 The Reed and Blum model of [103] the lateral superior olive for azimuthal localization of sound based on the ILDci. As shown here, the strength of inhibitory (MNTB) and excitatory inputs (AVCN) to the LSO column varies from above to below in opposite direction on the two sides, leading to varying ILDci for neurons along the column. Since the ILD is a function of the direction from which the sound is incident, the neuron number which attains ILD ci at the received ILD, encodes the azimuthal direction of incoming sound.

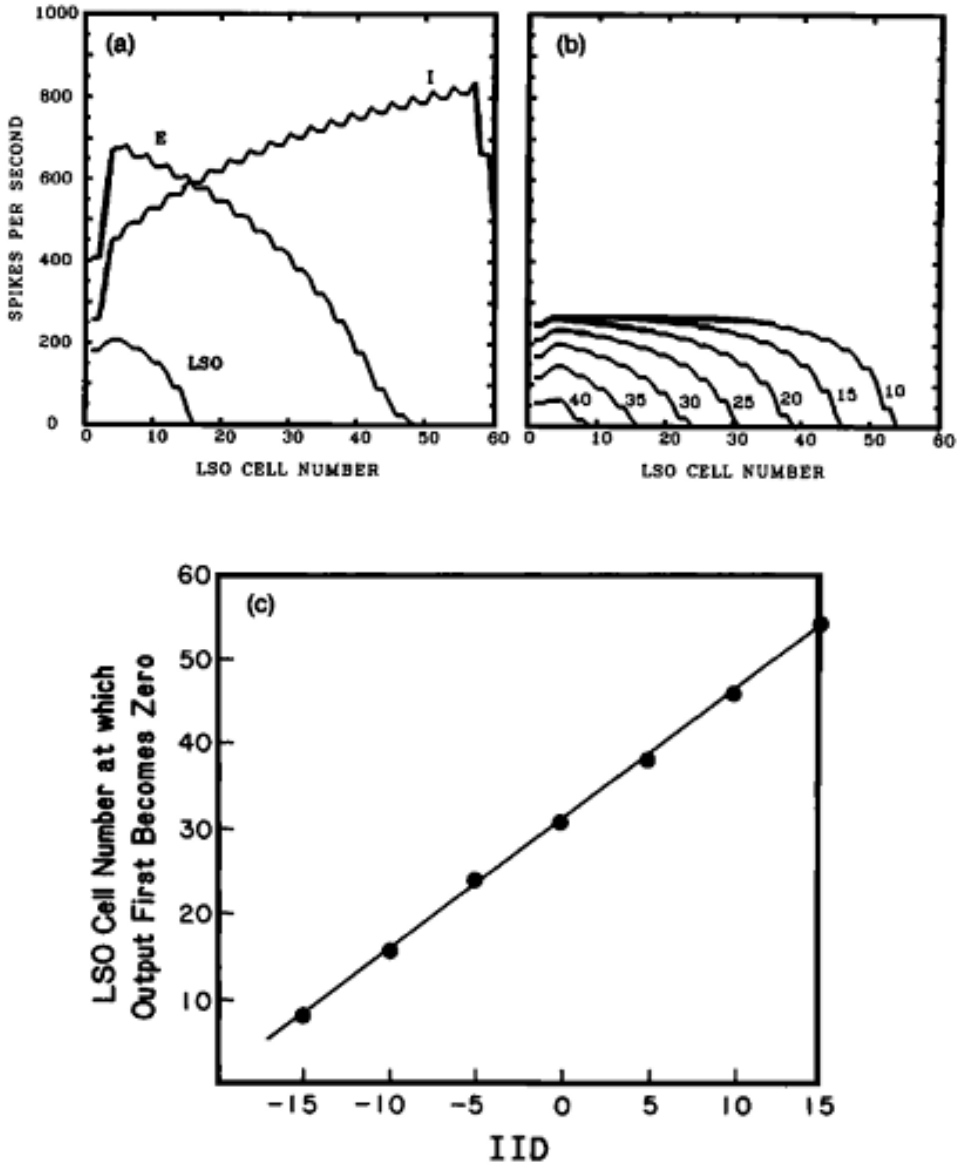

Fig. 57 [103] Test results from the Reed and Blum's simulation of their model are presented here which show the (a) response curve of a single LSO neuron to varying excitatory (E) and inhibitory (I) inputs from the two ears. (b) ILDci for the neurons in the LSO column with varying strengths of inputs. (c) As the ILD or IID (same meaning) changes, the LSO cell number whose output becomes zero also changes. This encodes the azimuthal direction of incoming sound.

ii) Conductance model of the neuron

The way the LSO has been modelled in circuits has been to assume a difference computation (M. Zacksenhouse, et. al., 1998) of the inhibitory-excitatory (IE) input to the LSO. If the intensities incident from both sides were log encoded then their difference will produce a response that is unique to the ILD.

$$L = h_{L}(\theta) \quad (17)$$

$$R = h_{R}(\theta) \quad (18)$$

$$G_L = \log(L) - \log(\mathrm{R}) = \log(\frac{h_{L}(\theta)}{h_{R}(\theta)}) \quad (19)$$

Where,

$$g_L = k_L.h_L(\theta) \quad (20)$$

$$g_R = k_R.h_R(\theta) \quad (21)$$

$$ILD = 20.\log(\frac{h_R(\theta)}{h_L(\theta)}) \quad (22)$$

Here, *g* is the conductance on the left or the right side, *h* is the intensity of inputs on either side, *k* is the scaling of inputs on either side. However, the biological synapses do not perform subtraction or log encoding but are time dependent changes in conductance. Thus, in this work, the time dependent conductance change model of the neuron, was designed and fabricated in silicon to represent each LSO neuron.

According to this model (Horiuchi et. al., 2009), the excitatory and the inhibitory conductances are modelled as time varying conductances which compete to determine the membrane potential of the neuron. The neuron's membrane

capacitance merely slows down the response of the cell as a result of which response to the current input does not depend on that to the past inputs. The time constant in this model is inversely proportional to the intensity of sound so that the sounds with higher intensity shall have shorter latency as compared to those with lower intensity but the same ILD.

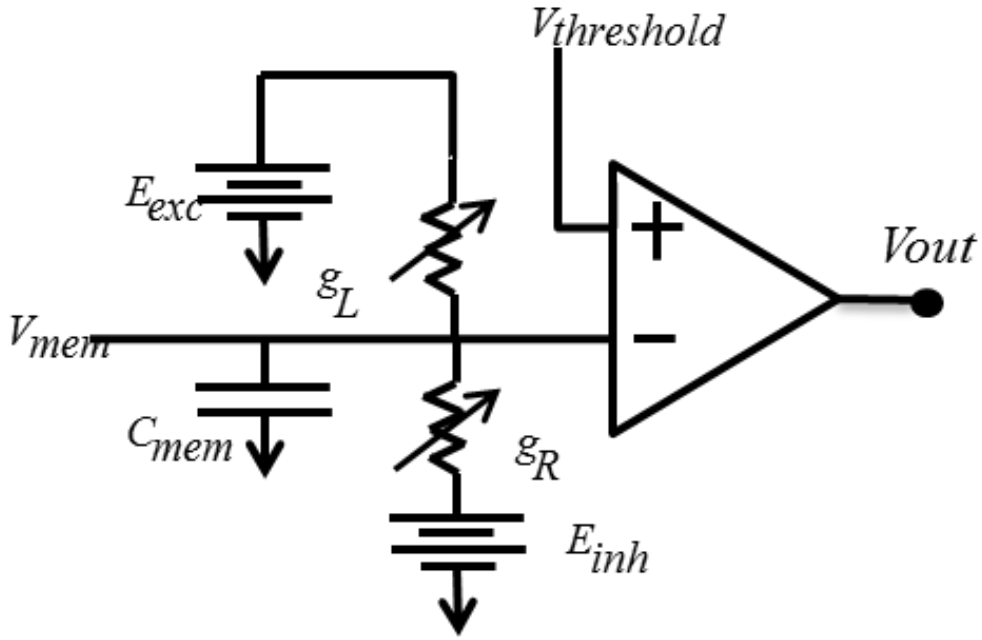

Fig. 58 [98] Schematic of the conductance model of the neuron indicates that the output of the neuron depends upon the ratio of the excitatory and the inhibitory synaptic inputs (represented by E_{exc} and E_{inh}) which are incident on it from both the ears. Thus, the LSO neuron is able to calculate the ILD of sound inputs received at the two ears.

As shown in the schematic of the model (Fig. 58), in the steady state, V_{mem} is a weighted average of conductances scaled by the inputs as shown in equation (23)

$$V_{mem} = \frac{g_R}{g_R + g_L} E_{inh} + \frac{g_L}{g_L + g_R} E_{exc} \qquad (23)$$

Substituting from equations (17)-(22) into (23) shows that the neuronal output (determined by the membrane potential) depends only on ILD and other fixed parameters.

$$V_{mem} = \frac{k_r.10^{\frac{ILD}{20}}}{k_L + k_r.10^{\frac{ILD}{20}}} E_{inh} + \frac{k_L}{k_L + k_r.10^{\frac{ILD}{20}}} E_{exc} \quad (24)$$

Moreover, the intensity of sound received is encoded as a change in the number or the frequency of pulsed inputs received at each ear as has been done in earlier works on the LSO. However, to use this neuron model to represent the LSO neuron, we need to have a synapse circuit which could convert these pulsed inputs to time varying conductances which are proportional to the number or frequency of these pulsed inputs and hence, to the intensity of sounds received at the two ears.

Intensity of sound → number or frequency of pulsed inputs to each ear→ time varying excitatory and inhibitory conductances at the neuron.

So, for this work such a synapse circuit (Fig. 78) was designed. This is a second order synapse circuit which summates several input spikes or spike trains to produce a conductance whose peak is proportional to the number of pulsed inputs and its average is proportional to the frequency of inputs.

In short, the azimuthal direction is encoded in the intensity difference of sounds received at the two ears. In this work, the intensity is represented by the number or frequency of inputs to the synapse circuit. This is converted to a time varying conductance change by the synapse circuit. Two synapse circuits – one excitatory

and the other inhibitory, are connected to each neuron on the LSO column. The excitatory synapse reduces the membrane potential of the neuron and increases its firing rate while the inhibitory synapse increases the membrane potential reducing its firing rate. The conductances integrate to change the membrane potential of the neuron as a weighted average of the inputs. Thus, this implementation more closely resembles that observed biologically in the LSO than that performed using difference computation.

E. Prior implementation

The LSO has been implemented in silicon earlier using difference computation (Horiuchi and Hynna, 2001, Shi & Horiuchi, 2004, 2005, 2007). These two implementations also included demonstration of azimuth tuning of IC neurons. The difference between these two implementations (at the system level) was primarily in the connections between LSO, DNLL and IC. Horiuchi & Cheely, 2003, 2007 also demonstrated the range and the ILD detection by the IC and the LSO neurons and came up with more detailed concepts on encoding of sounds with spike numbers or frequencies, using AER circuits to detect output and communicate between chips. In H. Abdalla, 2009, azimuthal and elevation information was detected together by using spectral resolution at the cochlea and the ILD at the LSO. Further, since output of the biological neurons is proportional to the weighted sum of the inhibitory and the excitatory conductances and not their differences, Horiuchi, et. al., 2009 demonstrated function of the LSO based on the conductance model primarily using ILD to detect the azimuthal direction. However, azimuthal localization using the population response was never

demonstrated. Farthest attempt in this direction has been in Shi & Horiuchi, 2007, where the authors note that a column of LSO neurons responds differently to inhibitory and excitatory inputs solely based on mismatch (not systematic design). In this work, they also demonstrated the processing of inputs by the dorsal nucleus of lateral lemniscus (DNLL) and by inferior colliculus (IC) to generate direction selective encoding by the cells of the IC. But all this was done at a single cell level and not at the population level.

In the present work, we demonstrate the first instance of azimuthal localization of sound based on the population response of the LSO. Moreover, we route the inputs from the two ears to the LSO neuron through two second order synapse circuits whose conductance is proportional to the intensity of inputs. And the intensity of inputs is represented by changing either the number or the frequency of input spikes to the synapse circuit as would be done by the antero ventral cochlear nucleus (AVCN) in biology. The results so obtained were analysed further in software to demonstrate the directional selectivity of IC neurons based on the ILD curves obtained from the neurons in the LSO column on the chip.

F. System design

An LSO chip (Fig. 61) was designed, fabricated and tested to realize the function of the LSO in silicon. On this chip, some test circuits and an array (Fig. 59) of 32 synapse- neuron circuits was designed to mimic the arrangement of synapse-neurons in the LSO. Each neuron in the array was connected to an inhibitory synapse representing the input from the contralateral ear and an excitatory synapse representing input from the ipsilateral ear.

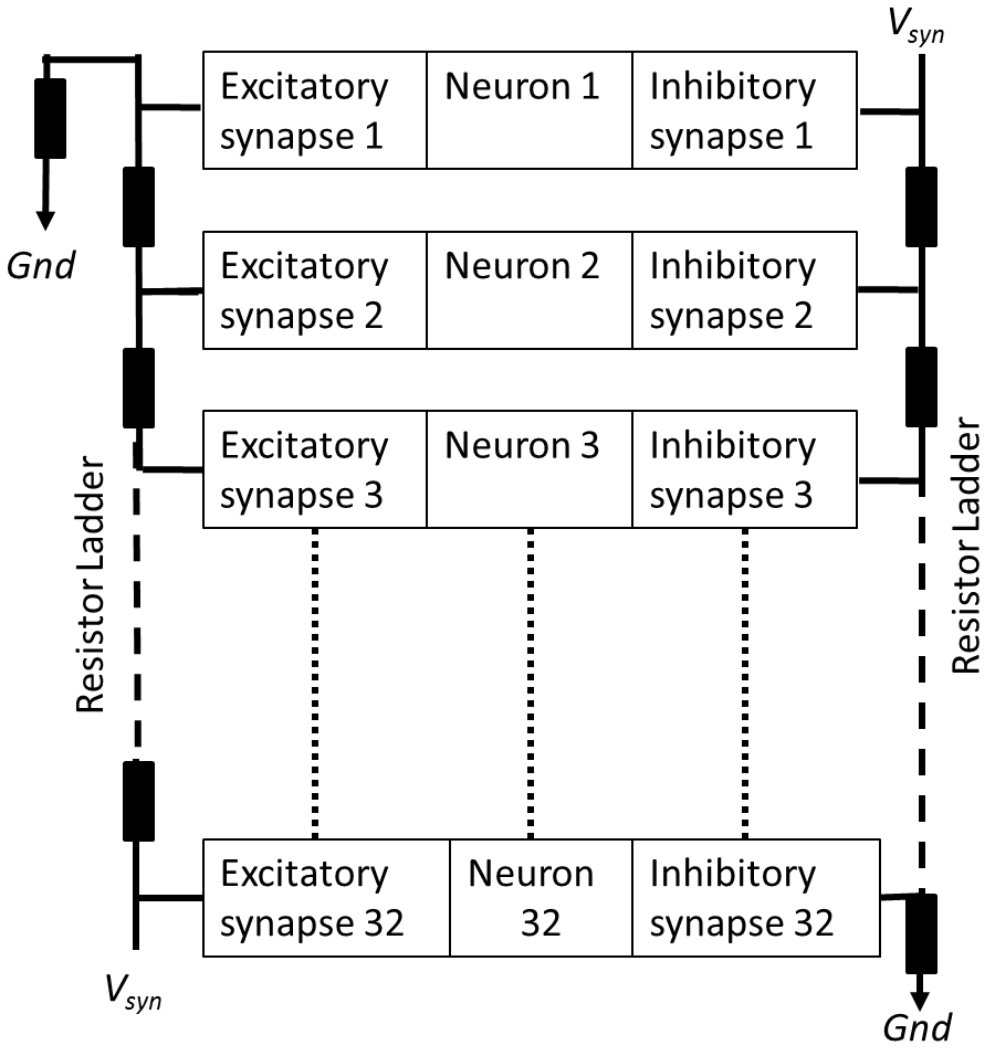

Fig. 59 Schematic of the arrangement of the synapse neuron circuits in the array representing the column of LSO neurons on the LSO chip. This was desgined to implement the population response of the LSO based on the Reed and Blum's model. Here, each synapse circuit is that of a second order synapse (Fig. 78), two of which (excitatory and inhibitory) were used to route external inputs to each conductance neuron (Fig. 60). The strength of excitatory and inhibitory inputs was varied along the length of the LSO column in opposite direction by using two resistor ladders to provide gradation to the parameter V_{syn} which determines the strength of the synapse circuit. This leads to a different ILD ci value for each neuron along the length of the LSO column.

The strength of inputs was varied along the length of the LSO column- the excitatory inputs increased and the inhibitory inputs decreased in strength along the length of the column from top to bottom. This was done using two resistor ladders (one each for excitatory and inhibitory synapses) to vary the strength of parameter V_{syn} to the synapse circuit. The resistor ladders were arranged in opposite directions along the length of the column.

Each synapse circuit was that of the second order synapse (Fig. 78) and each neuron circuit was that of the conductance neuron (Fig. 60). Each neuron circuit was designed based on the conductance model so that response to subsequent inputs will not be affected by those received before it and output will depend on the weighted average of the excitatory and the inhibitory inputs, as seen in biology. The inputs were routed through second order synapses which produce conductance change proportional to the number or the frequency of inputs incident on the ear, i.e., the output current is proportional to the frequency or the number of input pulses applied to the circuit (as shown in Fig.34). The number and frequency of inputs was varied depending on the intensity of the sound received by the ears. The intensity of inputs in turn depends upon the azimuthal direction from which the sound was incident.

G. Circuits

To implement the LSO function in silicon, a standalone test synapse circuit, a test neuron circuit, a test synapse-neuron circuit and an array of 32 synapse-neuron circuits was fabricated on an LSO chip (Fig. 61). The standalone synapse and neuron circuits helped in confirming the function of the synapse and the neuron as

required for implementing the conductance model. The array of synapse-neuron circuits, helped in azimuthal localization of sound based on ILDci using the LSO structural model by Reed and Blum.

The synapse circuit, shown in Fig. 78 produces a time varying conductance (output current) as described earlier (section 4. B. ii) a)). Two of these synapses provide inputs to each conductance neuron (Fig. 58) representing an LSO neuron. The synaptic inputs are exactly similar but are connected to the neuron such that one of them provides excitatory input resembling that provided by the ipsilateral cochlear nucleus and the other provides inhibitory input resembling that provided by the ipsilateral MNTB. Varying the V_{syn} parameter allows for changing the synaptic strength and changing V_{thr}, V_s and V_f allow changing the latency of neuronal spiking outputs.

The synapse circuit has already been introduced in section 4 on The Grid and the place cells: Silicon implementation. Further tests on it will be described in the tests and results part of this section. The circuit for the neuron gets two inputs- excitatory and inhibitory (V_{exc} and V_{inh}) from the two synapses, which are integrated on C_{mem} to V_x. The V_e from the excitatory synapse pulls the V_x down to V_{we} and V_e from the inhibitory synapse pulls the V_x up to Vdd. The resulting V_x is compared to V_{thr} and if it is comparable to V_{thr}, then the neuron fires. A baseline V_{inh} was provided to prevent the neuron from firing in the quiescent state. R_{out} is the spike generated which is the request sent to the AER and the acknowledge (*ack*) is the signal coming back from the AER which resets the neuron and prepares it to fire again. The time for resetting is adjusted by V_{refr}.

i) The Synapse circuit

This has already been introduced and further tests on it will be described in the tests and results part of this section.

ii) The Neuron Circuit

While it has been quite common in the VLSI literature to use current sources for simulating synaptic input to integrate-and-fire neurons, biological synapses are best described as time-varying conductances. And the biological neurons produce an output proportional to the weighted average of the excitatory and the inhibitory inputs. To implement the conductance model of the biological neuron, a current-mode neuron circuit with excitatory and inhibitory conductances was used (Fig. 60). The excitatory conductance was controlled by the input current I'_e. Note that excitatory inputs were provided at two different points in the circuit (defined by V_{exc} on transistors M1 and M5) one of which produces I_e and the other I'_e.[12]

[12] Earlier version of this circuit was developed by me jointly with Prof Horiuchi. I modified it to perform the same function but have a smaller footprint by removing a leak transistor which was dumping leak current on to the V_m as is M6.

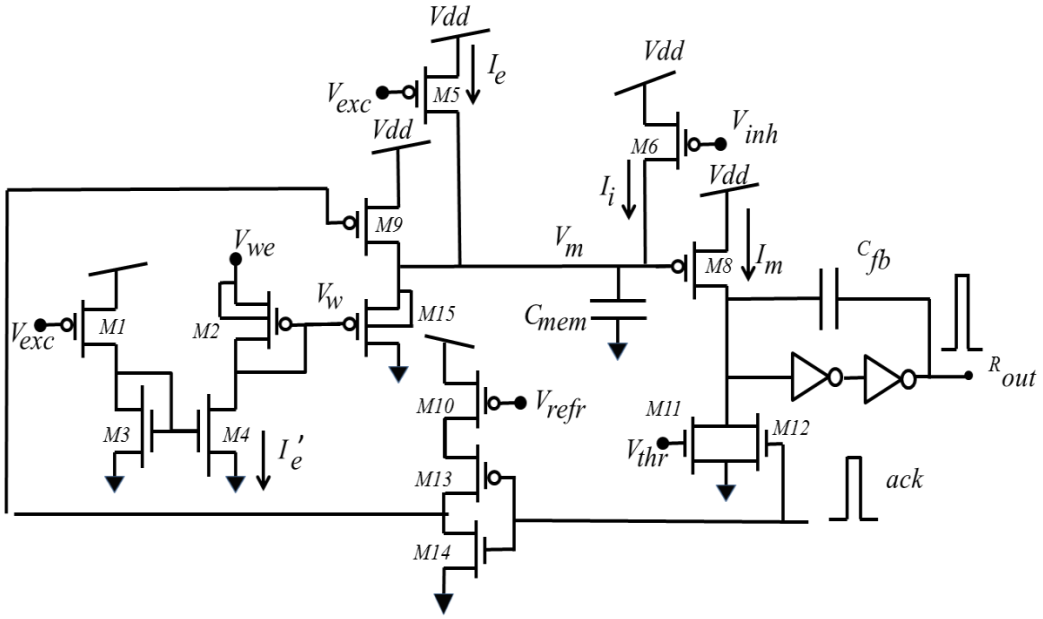

Fig. 60 Circuit schematic of the neuron, whose membrane potential was the weighted average of the excitatory and the inhibitory conductances and was compared to the threshold voltage to determine the neural response. The excitatory and the inhibitory inputs to this were provided from two different synapse circuits shown in Fig. 78. The V_e node of the excitatory synapse was connected to the gates of M1, M5. The V_e node of the inhibitory synapse was connected to the gate of M6. Transistor M6 of the *synapse* circuit was not used in this design and is shown only to illustrate the I_{syn} for other purposes. All the transistor W/L=2.4 µm /2.4 µm and all the capacitors were 0.1 pF. Transistors M2 and M15 had their body terminals connected to their source terminals and were provided with a separate well. Capacitor layout was designed using poly-poly1.

Table 6 Showing the function of various transistors in the neuron 3 circuit

Transistor	Function
M1-M4, M15	To copy and scale the input current received from the excitatory synapse circuit
M5	To copy current from the excitatory synapse
M6	To copy current from the inhibitory synapse
M7	Leak transistor to prevent neuronal firing in the quiescent state
M8	To convert membrane potential V_m to output current
C_{fb} and 2 invertors	To amplify the output spike amplitude and to hold membrane potential at a value for a while.
M9, M12	To reset the neuron.
M13-M14	Buffers to produce a correct logic level pulse at the required point.
M10	To set the refractory period
M11	To set threshold voltage value for the neuron

The inhibitory conductance is controlled by the input current I_i (defined by V_{inh} on M6). A constant baseline leak conductance, I_i (o) (controlled by V_{inh} on M6) is also provided to prevent the neuron from firing in the quiescent state. The inhibitory input is scaled to account for this leak conductance factor. Starting from the drain equations for M15, M2, and M8,

$$I_e + I_i = I_0 e^{\frac{\kappa(V_m - V_w)}{V_T}} \quad (25)$$

$$I_e' = I_0 e^{\frac{\kappa(V_{we} - V_w)}{V_T}} \quad (26)$$

$$I_m = I_0 e^{\frac{\kappa(Vdd - V_m)}{V_T}} \quad (27)$$

The steady state value of the "membrane potential" current (I_m), when the two inputs, V_{exc} and V_{inh} are constant, is described by combining the above to give the following equation,

$$I_m = I_o e^{\frac{\kappa(V_{dd}-V_{we})}{V_T}} \left(\frac{I_e'}{I_e + I_i} \right) \qquad (28)$$

In the case where I'_e is much larger than $I_e + I_i$, I_m becomes large (near the excitatory synaptic reversal potential defined by V_{we}) and when I_i is much larger than I_e, the membrane current will be near zero. The inhibitory input pulls the representation of the membrane potential (I_m) down to zero and the excitatory input pulls I_m towards a maximum level defined by V_{we}. The I_m in steady-state becomes a function of the ratio of the two conductances. When the membrane potential exceeds a threshold level, the neuron generates a logic level pulse. The interface circuits for the neuron to communicate with the AER are shown along with circuits for the control of a refractory period (V_{refr}) in Fig. 58.

H. Tests & Results

The chip (Fig. 61) containing some test synapse and neuron circuits and an array of 32 synapse-neuron circuits was fabricated using 0.5 µm ON semiconductor technology. With no critical sizing issues as part of our design, all the transistors in the circuits were designed to have W/L= 2.4µm/2.4µm and values of all the capacitors were 0.1pF. A test PCB was designed to test the chip.

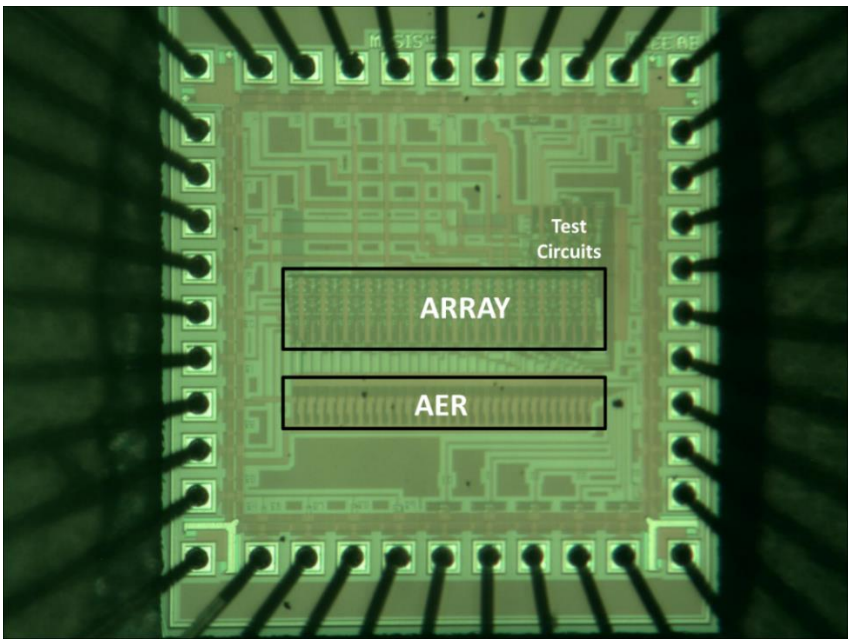

(a)

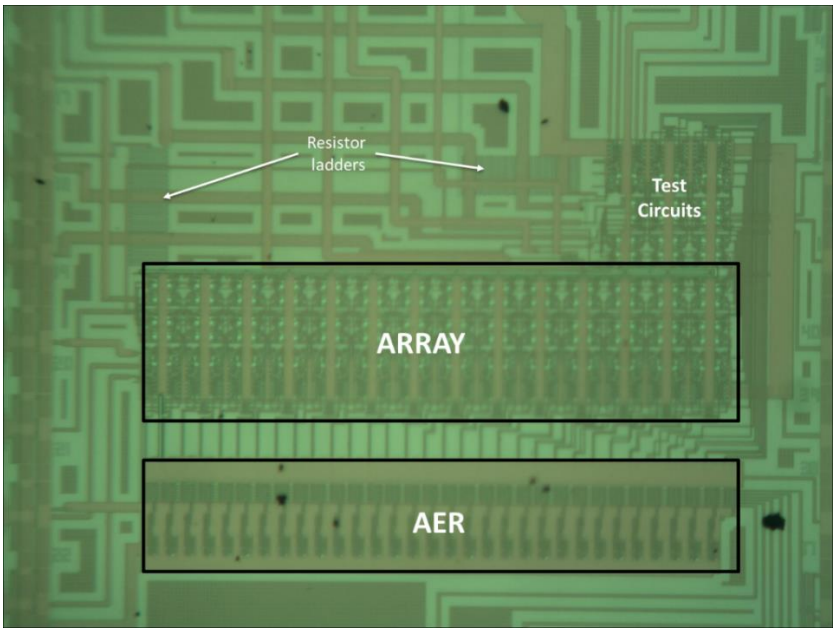

(b)

Fig. 61 (a) Micrograph of the LSO chip showing an array of synapse-neuron circuits and some test circuits. Outputs from the array were neuron numbers which were read using an AER circuit. The resistor ladders were designed in poly. (b) Zoomed in version of the micrograph showing portion of the resistor ladders.

i) The Synapse Circuit

An array of measurements was performed on the circuit in Fig. 78 to demonstrate the basic operation of the circuit to generate the second order function with control over the time constants and the amplitude, to show the linearity of the response to a burst of spike inputs, and to show the smooth output for regular pulse trains. Some of these have already been described in section 4 on The Grid and the place cells: Silicon implementation, the remaining tests will be described here. For all these tests, a single input spike, V_{spk} was 4V, 0.5 μs, $V_{\tau 1}$ was 3.5V, and $V_{\tau 2}$ was 4.5V. The amplitude of V_{spk} was kept at 4V as that of $V_{\tau 1}$ was only 3.5V. Other parameters are mentioned in appropriate sections. In the following sections: the basic second order function shaped response is demonstrated and compared to simulation, the linear response to spike frequency is shown, different synaptic weight tunings are demonstrated, and different postsynaptic spike latencies are demonstrated. Finally, a simple demonstration of the second order synapse in spiking, conductance-model neuron oscillator is shown.

a) Second order function

The goal in this test was to adjust the parameters to obtain an alpha function (a special type of second order function) with a rise time of ~1ms and decay time of greater than 3ms (as observed in many biological synapses). The parameters are shown in Table 11 in the Appendix I under '*synapse output*'. The output current obtained is shown in Fig. 62. The graph shows that the output current converts the narrow input spike (0.5 μs duration applied at time, t=0) into a smooth and broad output current which resembles a second order function. Equation (29) was

simulated in MATLAB with amplitude, *A*=290 pA (with adjustment made for the offset current) and time constant τ = 1ms. This resulted in a pulse with a rise time of ~1ms and a decay time of ~4ms. As noted before, the output current will have a non-zero background current that is a function of the control parameters.

$$I_{syn} = A \cdot \frac{t}{\tau} e^{\frac{-t}{\tau}} \tag{29}$$

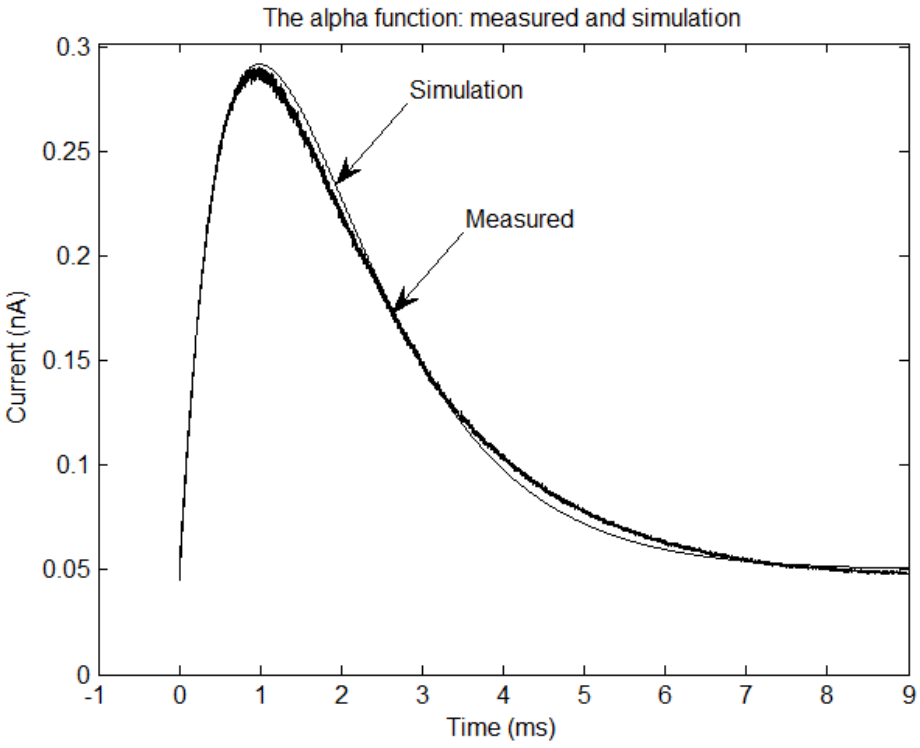

Fig. 62. Synaptic output current following stimulation of the synapse circuit with a digital input spike (4V, 0.5 µs duration): measurements from circuit were compared to simulation results. Note that a short input spike is converted to a long second order function by the synapse circuit and it fits well to a MATLAB simulated alpha function with time constant=1ms.

b) Effect of changing the input spike frequency

To demonstrate the use of the synapse in a mean-rate representation, the input was a continuous train of spikes with a constant inter-spike interval. For this set of measurements, the parameters for the synapse circuit are shown in Table 11 in the Appendix I under '*Regular spiking*'. Results from frequencies of 1, 10, 100, 200, 300, 400, 500, 600, 700, 800, 900, 1000- 40000 Hz (increments of a kHz at each step) are shown in Fig. 63. These show that as the input spike frequency increases, the average output current increases. Up to about 10 kHz, this increase is proportional to the frequency, but above this frequency, the average current is super-linear. The graph shows the mean and the standard deviation from five different average readings that were taken at each frequency. The baseline DC current is visible in this graph. In addition to results from the circuit, Fig. 63 (a) and (b) also include the plot of the expected average current for these frequencies based on MATLAB simulations using equation (8). In simulation, the currents increase in proportion to the number of pulses as was expected from equation (8).

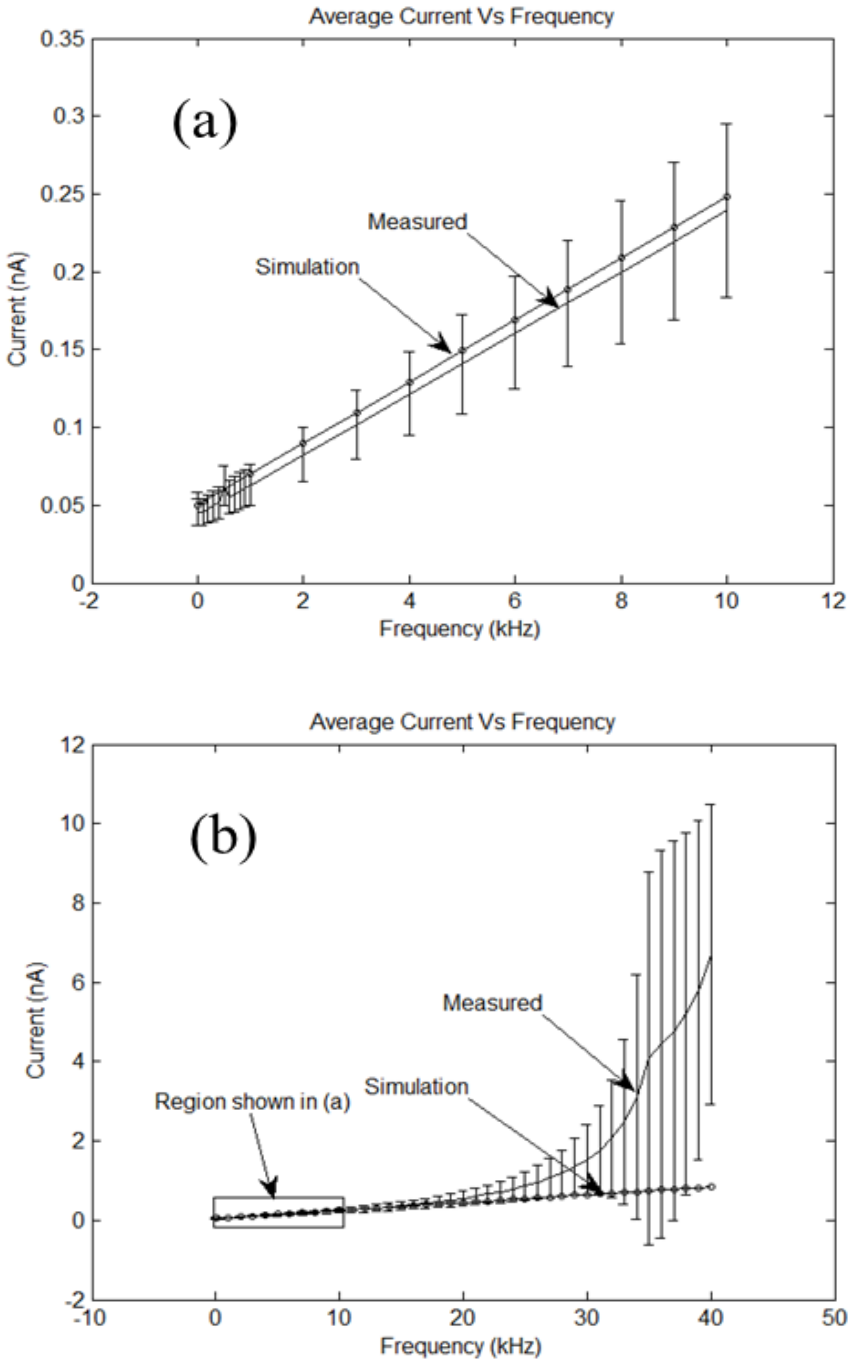

Fig. 63. In this experiment, the second order syanpase circuit on the LSO chip was provided different frequency of input pulses and the corresponding average output current was calculated from the recorded (using oscilloscope) output voltage (V_e). The average current obtained from the circuit with input spikes of different frequencies was plotted in MATLAB. A plot of the average output current shows an increase with the frequency of the input pulses. (a) For frequencies below 10 kHz, the output current is proportional to the frequency of applied input pulses but (b) it is not proportional to input frequencies above 10 kHz.

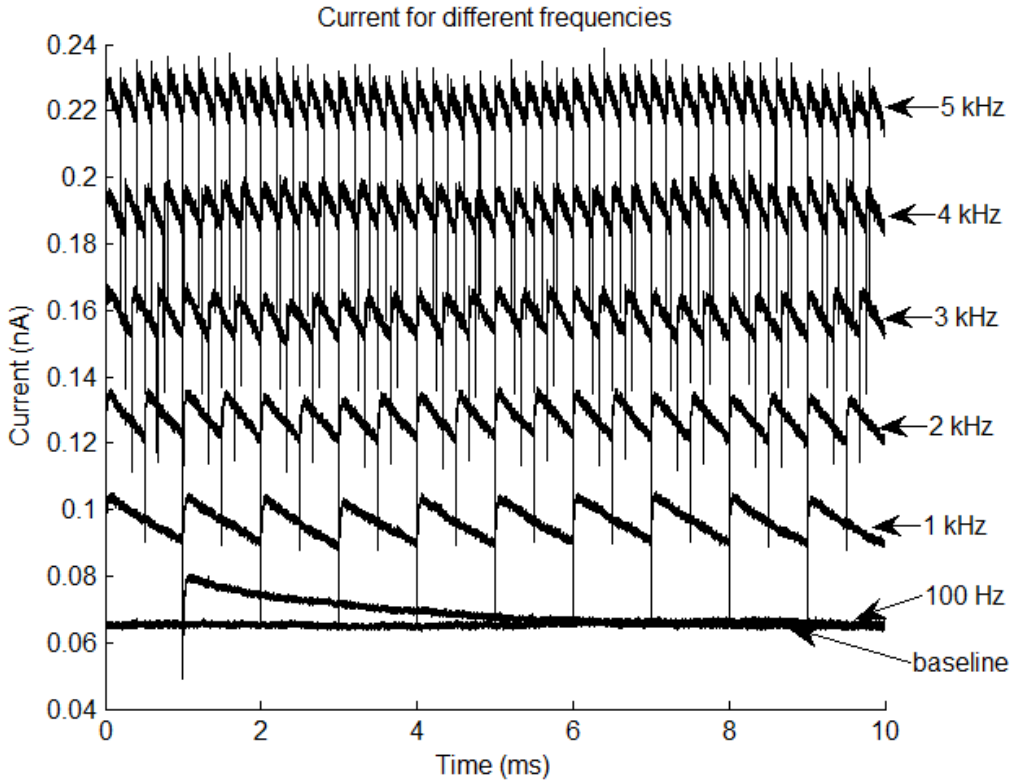

Fig.64. These are measured synaptic currents from the second order synapse circuit on the LSO chip when six different input spike frequencies were applied to the circuit. It can be seen that with each input pulse, almost the same amount of output current is produced as was expected from the analysis of the circuit. The sharp transients are measurement artefacts that occur at the time of input spikes.

It can be seen that the measured current follows the expected results at lower frequencies though with different slope and amplitude; it deviates from the expected as the circuit leaves the subthreshold region of operation. Current traces for some selected frequencies are shown in Fig.64. The linearly increasing average current and the level of current ripple are apparent in these traces.

c) Effect of varying the synaptic strength (V_{syn})

This set of measurements was done to highlight the circuit behaviour under various bias conditions. These results were obtained by changing the synaptic

strength by varying V_{syn} from 2.56V (strongest) to 2.60V to 2.65V (weakest). These voltages were chosen so the circuit operates in the subthreshold region. Other parameters for the experiments with the input burst are provided in

Table 11 in the Appendix I under '*Varying V_{syn} (burst)*' and the parameters used for the experiments with continuous spiking are provided under '*Varying V_{syn} (train)*'. The graphs of Fig.65, Fig.66, and Fig.67 show the response to burst inputs and regular spike trains for different synaptic strengths. In Fig.65, note that while the magnitude varies with changing synaptic strength, the time of the peak does not. Fig.66 shows that when the strength of the synapse is greater (lower V_{syn}), the increment in the output current is larger. Here again, the baseline current of ~40 pA was subtracted from the graphs. Five readings were taken at each set of parameters and the mean and the standard deviation are plotted.

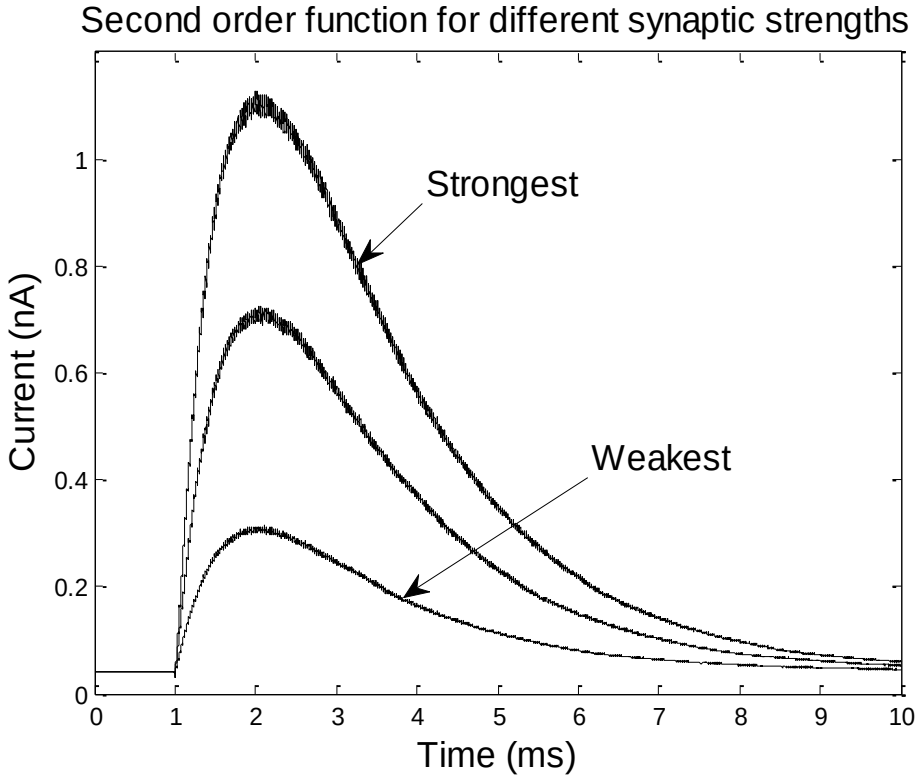

Fig.65. In this experiment, three measurements were made from the second order synapse circuit on the LSO chip at different synaptic strengths. The synaptic strength was varied using different values for the parameter V_{syn}. At each of these values, the synapse circuit was provided 5 input pulses. Shown here are output currents from the circuit during the three measurements. The peak current varies in magnitude with changing synaptic strength but occurs at the same time in the different traces. The strongest means the maximum possible current (V_{syn} =2.56V) and the weakest means the least possible current (V_{syn} =2.65V) while the circuit operates in the sub threshold region.

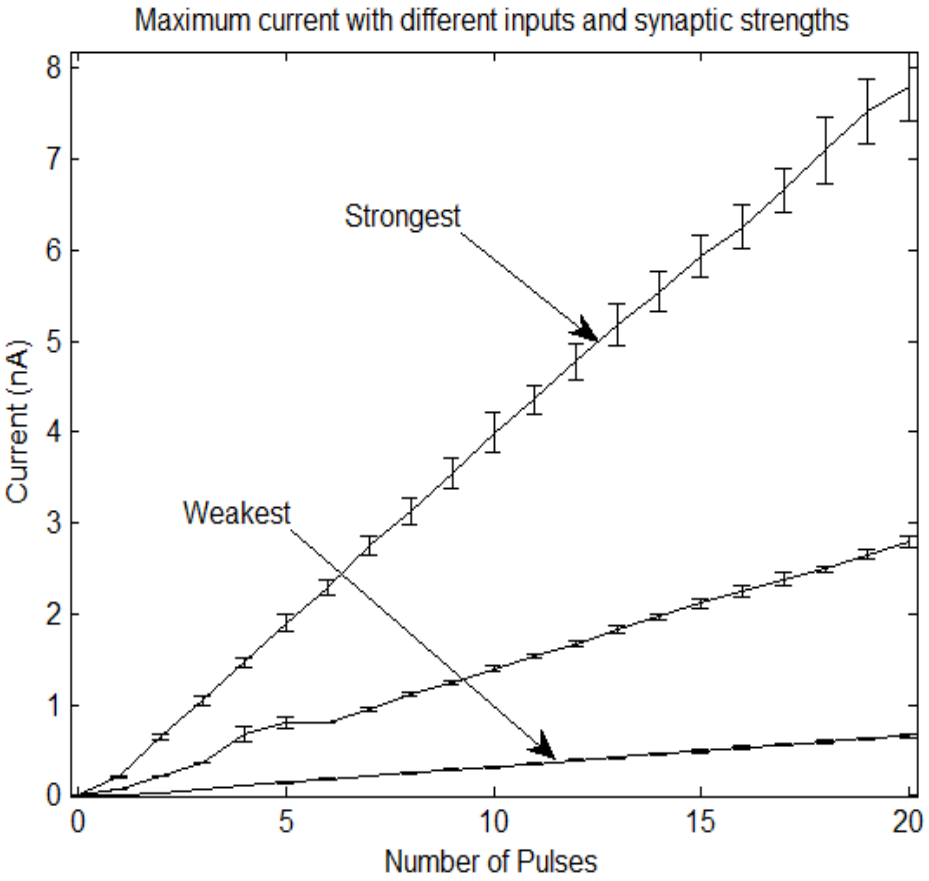

Fig.66. Shown here are the peak output current obtained from chip measurements on the second order synapse circuit and plotted in MATLAB. During these, the synaptic strength was varied by applying different values of the parameter V_{syn} and at each of these values, different number of input pulses (from 1-20) was applied to the synapse circuit and 5 different readings were taken for each of the settings. As seen, the peak output current from the circuit varies in proportion to the number of pulses in the input burst and different synaptic strength changes the slope of the line obtained. (The baseline current of about 10-40 pA was subtracted from all the currents). The labels strongest and the weakest have the same meaning as in Fig. 65.

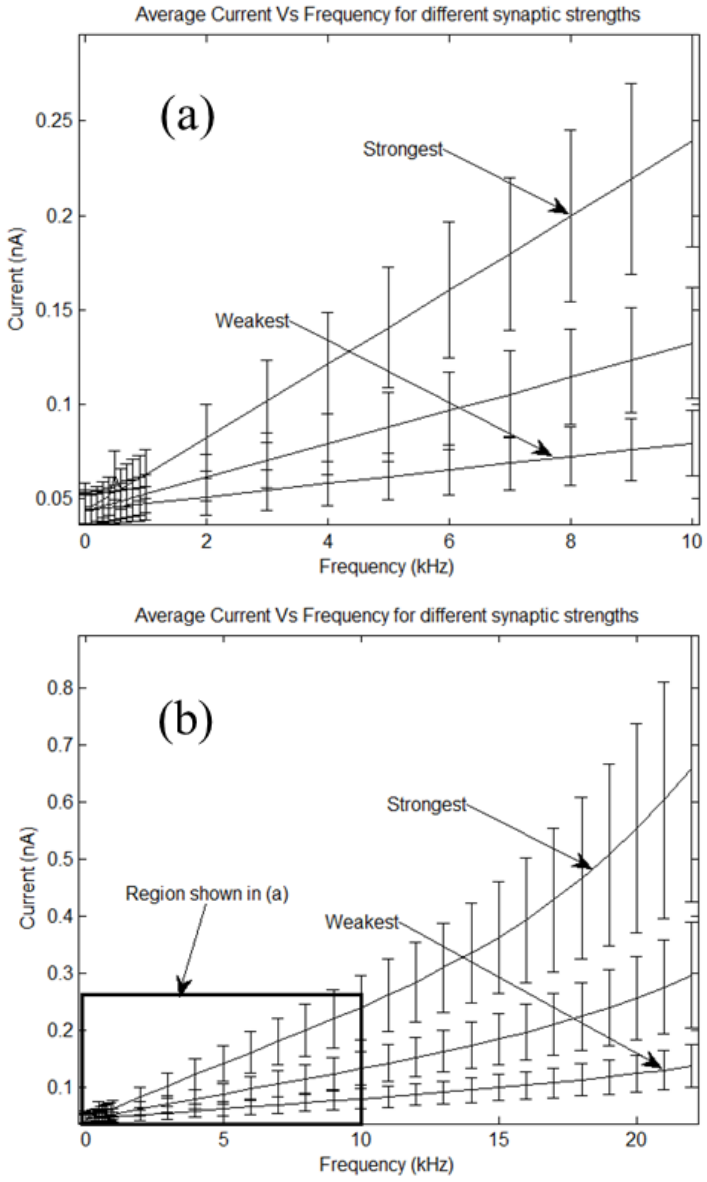

Fig.67. In this experiment, different frequency of input pulses was applied at three different values of parameter V_{syn} to the second order synapse circuit on the LSO chip and the corresponding V_e was measured using an oscilloscope. Five different measurements were performed at each of the 3 voltages and different frequencies. The average output currents were calculated from the measured V_e. Shown here is that the average output currents vary in proportion to the frequency of input spikes and the slope of the line is determined by the synaptic strength setting (V_{syn}). (a) Frequencies up to 10 KHz show a response proportional to input frequency. (b) Beyond these frequencies, the response is not proportional to the frequency of input pulses. This is because the responses to adjacent pulses start overlapping (as the time constant for the synapse circuit was kept at 5ms). 'Strongest' and 'weakest' have the same meaning as above.

The results shown above demonstrate that the peak output current from the synapse circuit increases linearly with the inputs (at least for a few inputs or a few lower frequencies). Moreover, the strength of output can be changed by varying the parameter V_{syn}. Thus, this circuit can be used to implement the synapse circuit for realizing the function of the LSO in silicon which needs changing the synaptic strength.

d) Spike Latency

As an aside, this section higlights some more features of this synapse circuit which have not been directly used in the VLSI implementation of the LSO but could be useful in other computational neuroscience models. This synapse circuit can be used to generate variable temporal delays in a network of neurons to produce different spike timing patterns as used in networks to demonstrate polychronization[13] (Izhikevich, 2006, Wang et. al., 2011, 2012, 2013).

As with any synapse circuit that can produce a current that outlasts the duration of the input pulse, this synapse can be used with a neuron circuit to produce significant postsynaptic spike latencies based on how long it takes to charge the neuron to its threshold for firing. In a conductance-model neuron, when both the excitatory and the inhibitory conductances are present, the neuron operates more like a lowpass filter charging to a steady-state value set by the instantaneous balance of excitation and inhibition. For this reason, the time course of the membrane potential is tightly coupled to the time course of the synaptic

[13] Polychronization is a mechanism by which different memories are stored in the brain using same neurons but using time difference between them.

conductances and the spike must occur *before* the peak in the excitatory conductance.

To demonstrate the postsynaptic latency from a single spike input and to highlight how the choice of threshold level affects latency and temporal jitter, three different rise times of the excitatory synaptic output were used. The three parameter sets used to create them are shown in

Table 12 in Appendix I.

Set 1 (*Producing spike latencies from 0.72 to 2 ms*): The V_{thr} was varied from 0.59 V to 0.61 V for this set of measurements. The parameters were so adjusted that the peak of the output current was at 5 ms.

Set 2 (*Producing spike latencies from 2.72 to 9 ms*): The V_{thr} was varied from 0.58 V to 0.60 V for this set of measurements. The parameters were adjusted so that the peak of the output was at 10 ms.

Set 3 (*Producing spike latencies from 9 to 19.8 ms*): The V_{thr} was varied from 0.52 V to 0.56 V for this set of measurements. The parameters were set to obtain the peak of the output function at 20 ms.

For each of the three output current curves, V_{thr} was varied (in 50 mV steps) and the resulting spike latency was recorded. The results shown in Fig.68 demonstrate latencies from 0.72 ms to about 20 ms. Longer latencies could be produced but are not included in this analysis. The graphs clearly show that the spike latency increases as the threshold is increased and that the latency is bounded by the timing of peak, t_{pk} of the driving output function. Also visible is the trend for the

jitter to increase as the latency approaches the t_{pk} for the output current. This occurs because the output flattens out as it approaches its peak value and the membrane potential approaches the threshold value relatively slowly, allowing noise to have a large influence on the exact time of the spike.

A simple demonstration of the second order synapse circuit used to create delay in a neural circuit is presented here in an oscillator. In this circuit, (Fig.69) two neurons excite each other in turn with a synaptic delay, producing an alternating firing pattern. In Purves et.al. 2012, time dependent conductance changes are proposed to be responsible for regulating the period of this oscillation which is used in this demonstration of the oscillatory system. It should be noted that known biological oscillators utilize different mechanisms to produce oscillatory bursts, such as bursting pacemaker potentials, plateau potentials, post inhibitory rebound, frequency adaptation, and graded transmitter release (Izhikevich, 2006, and Selverston & Moulins, 1985).

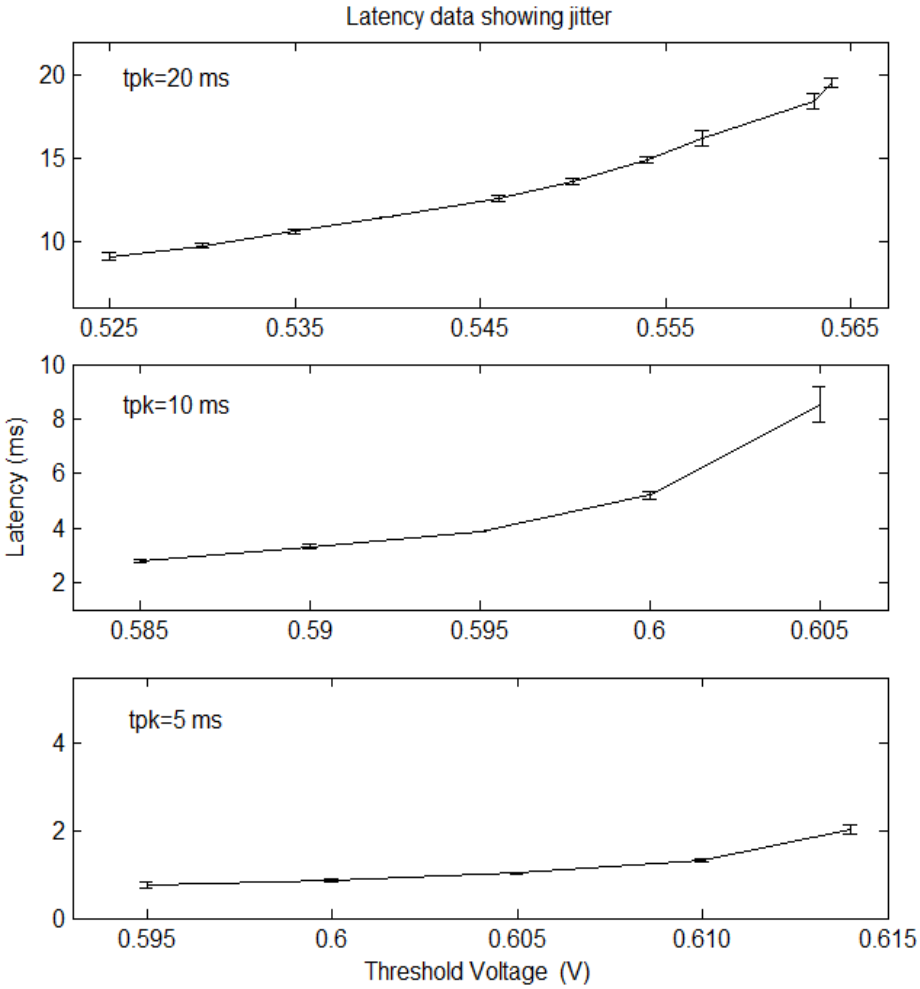

Fig.68. In this experiment, the parameter values applied to the second order synapse circuit were varied to produce the output current with a different time constant indicated by the parameter t_{pk} in these graphs – 5, 10 and 20 ms. Then the V_{thr} parameter on the neuron circuit connected to the synapse was changed from 0.525 to 0.615V and the corresponding time difference between application of an input pulse to the synapse and output from the neuron as neuronal firing was noted (called latency here). The graphs show rising latency and jitter as the threshold voltage increases.

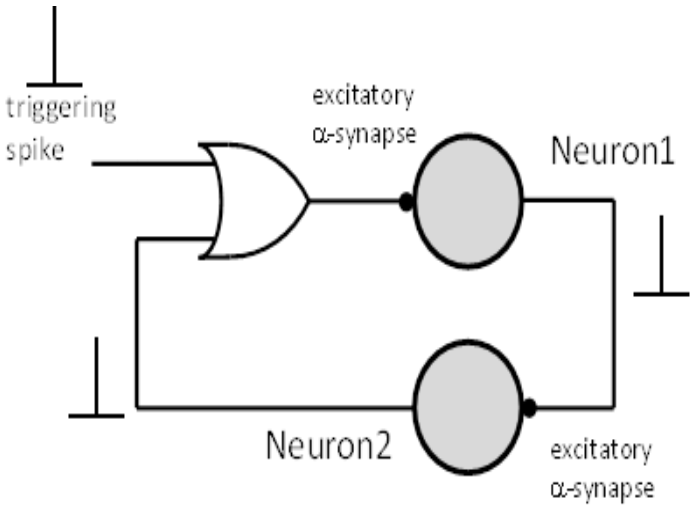

Fig.69. Circuit conenctions for demonstration of the second order synapse and the conductance neuron circuit on the LSO chip as a simple two-neuron oscillator based on the excitatory synaptic delay is shown here. In this experiment, the output from one synapse-neuron circuit was connected to a second synapse-neuron circuit whose output was connected back to provide input to the first one. To trigger the system, an input pulse was routed to the first synapse-neuron circuit through an OR gate once. After the initial trigger, the system was expected to continue triggering the subcircuits in reciprocal manner as happens in biology.

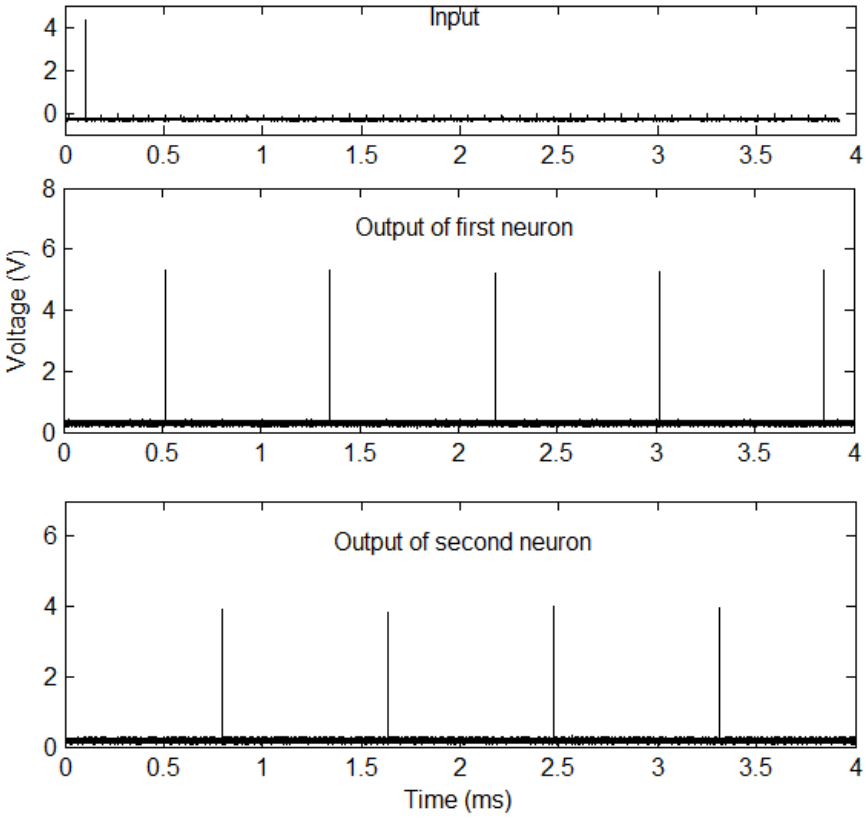

Fig.70. Demonstration of synaptic delay in a two-neuron oscillator. Top panel: An input spike triggers the excitatory synapse onto Neuron1. Middle and Bottom panels: With a delay between spikes, Neuron1 and Neuron2 fire spikes in alternation. This demonstration was performed to see if neuron firing patterns of different frequencies could be obtained using the synapse neuron circuits in an oscillator configuration.

For this demonstration, both synapse parameters were set to: $V_{\tau 1}$ =3.5V, $V_{\tau 2}$ =4.5V, V_s =3.74V, V_f=2.93V, V_{syn}=2.6V, Vdd=5V, V_{we}=4.1V, V_{refr}=4.3V; for neuron1, V_{inh}=0.62V, for neuron2, V_{thr}=0.59V. A triggering input pulse (V_{spk}=4V, duration 0.5 µs) was applied to an excitatory synapse onto Neuron1 (through an OR gate). The output of Neuron1 projected to an excitatory synapse onto Neuron2. The output of Neuron2 projected back to the same excitatory synapse onto Neuron1 completing the circuit. The results are shown in Fig.70. Although this example

was shown at 1 kHz, this network can generate this oscillating pattern with a wide range of frequencies through parameter modifications or through an expansion in the number of neurons (e.g., ring oscillators). This basic architecture of reciprocal connectivity (both excitatory and inhibitory) is found to produce oscillation, resonance, and synchronization in a range of biological circuits.

ii) The Neuron Circuit (Neuron 3)

The output voltage, R_{out} was recorded using Tektronix TDS 5104 Digital Phosphor oscilloscope. Different measurements were performed on the LSO chip- firstly, the standalone neuron circuit, with provision to provide direct voltage inputs was tested for its proper function and its response to varying strengths of excitatory and inhibitory inputs was studied and the resulting ILD curve was plotted. Then, its V_{thr} was varied to observe the effect on ILD curves.

Thereafter, the neuron circuit, inputs to which were routed through the two synapses (excitatory and inhibitory), was tested to determine its ILD curves using different number of bursts and frequencies of inputs; effect of varying V_{syn} (synaptic strength) on the ILD curve; effect of changing threshold on ILD curve of the neuron; changing intensity of both inputs at constant ILD and its effect on the response latency; the effect of changing latency on the ILD curve; and the effect of multiple bursts to check whether there is residual effect from the preceding input. Details are provided in the sections below.

a) Initial measurements

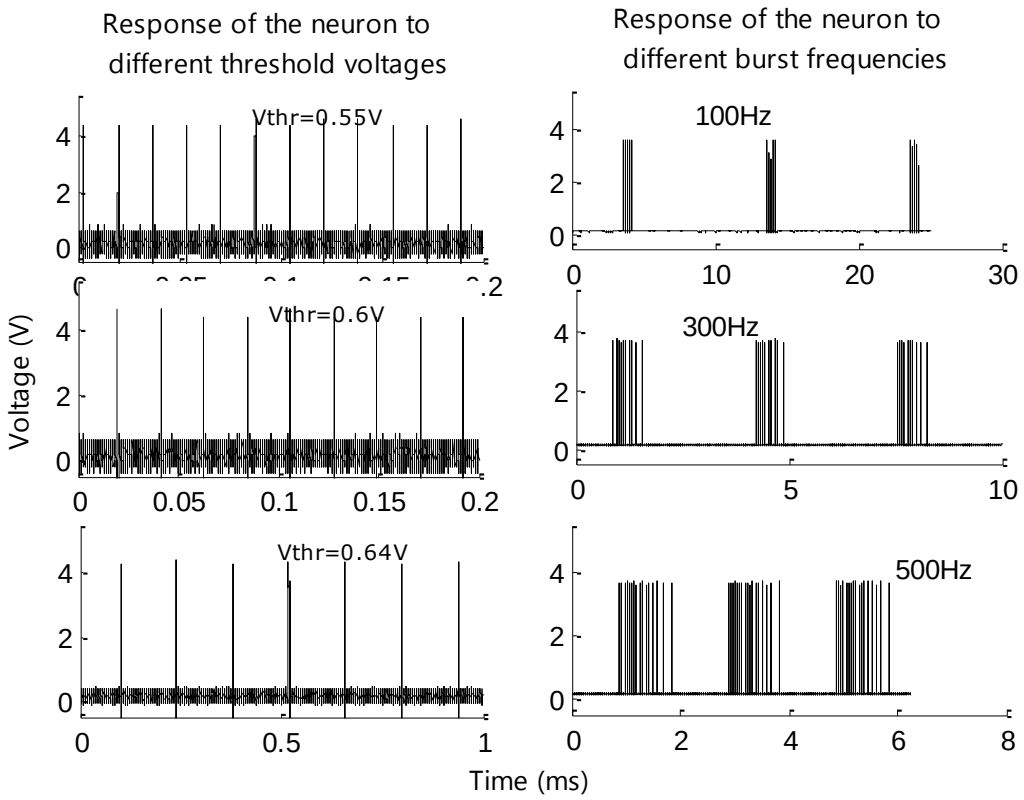

Fig. 71 (left) Spiking outputs from the neuron 3 circuit - as the threshold voltage rises, the inter-spike interval also rises. (right graphs) Show that the neuron response to subsequent bursts is not affected by that to priors. This is an important feature to implement the working of the LSO neurons because this ensures that the output due to latter sounds is not influenced by that due to former so that each one can be localized separately (without interference from those prior to it).

Here, R_{out} was recorded at different values of threshold voltage, V_{thr}=0.55, 0.6, 0.64V using the oscilloscope. Other parameters were set to values shown in Table 13 in row labelled *'Initial measurements'*. The results shown in Fig. 71 (left column) indicate that the neuron is working properly and that the spike frequency is inversely proportional to the threshold voltage.

b) Relation between the firing frequency and the ILD

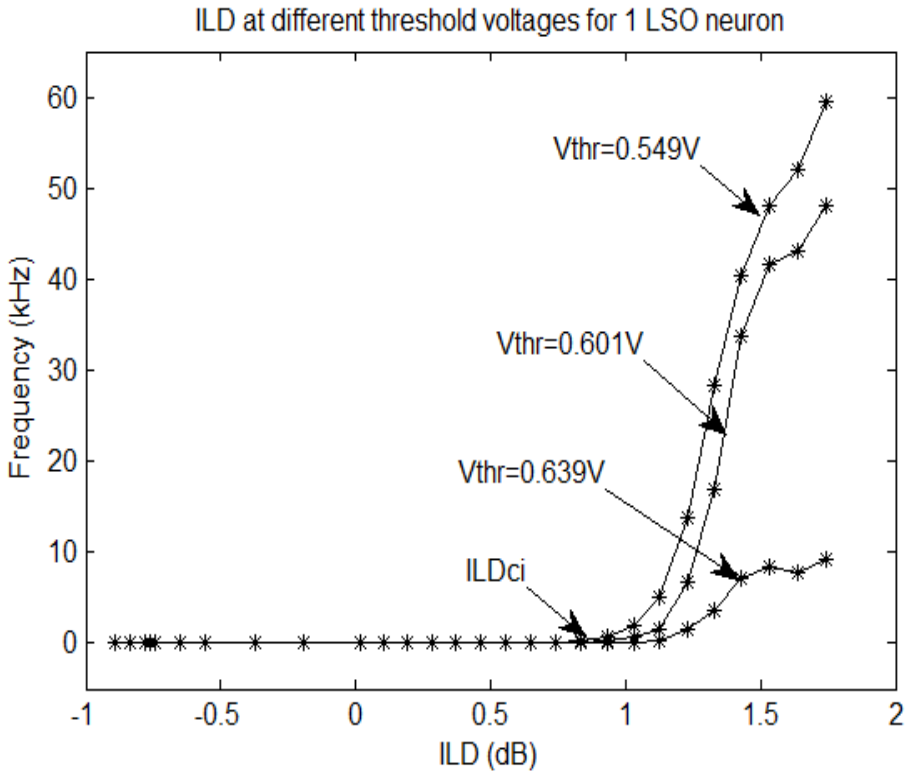

Fig. 72 ILD curve for the standalone neuron when it was provided with varying excitatory and inhibitory inputs at a particular V_{thr}. This graph shows that the ILD curves are similar to those of the biological LSO neuron (Fig. 54) and that as the V_{thr} increases, the response of the neuron decreases even though the shape of the ILD curve and the ILD ci do not change.

In the next set of measurements, the goal was to determine the relation between the firing frequency and the ILD for three different values of threshold voltages. Parameters used are shown in Table 13 in the row labelled *'ILD curves'*. At each of the V_{thr} values, V_{exc} was changed from 5.01V to 4.10V in steps of 5 mV and V_{inh} from 5.01V to 4.50V (over and above the baseline inhibitory input to avoid firing in quiescent state) in steps of 10 or 5 mV and the corresponding firing frequency was recorded using Agilent digital logic analyser. The ILD (in dB) was calculated by multiplying log of ratio of V_{exc} and V_{inh} by 20. The results from test, shown in

Fig. 72, indicate that the response of the neuron circuit to varying ILDs is similar to that observed from the LSO in biology (Fig. 54).

iii) Synapse-Neuron circuit

a) Effect of consecutive bursts on response

Another feature of the biological LSO neuron is that the response to an input does not depend upon that to prior inputs. This was tested here using parameters shown in Table 14 in row labelled '*Consecutive Bursts'*. 3 consecutive bursts were repeated with different time intervals: 10, 3.33, and 2 ms. As shown in Fig. 71 (right), the response of the neuron to subsequent pulses did not change due to those applied before them. This is an important requirement for the azimuthal localization system as we do not want the incoming sounds to interfere with each other.

b) Neuron response to varying ILDs

This experiment shows the response of the neuron to varying ILDs and varying V_{thr}. For these measurements, the parameters used are shown again in Table 14 in the row labelled '*ILD curves'*. For the measurements, different number of input spikes were applied to the excitatory synapse. The results shown in Fig. 73 (a), recorded using a logic analyser, demonstrate that as the V_{thr} rises, the frequency of outputs from the LSO neuron goes down and vice versa while the ILD curve maintains its shape, as observed empirically.

c) Change in latency with varying intensity for a given ILD

As the intensity of inputs increases for a given ILD level, based on empirical observations, we expect no change in the response except for reduction in its

latency. To test this, similar inputs were applied to both synapses and the strength of both side synapses was changed by the same amount (by changing V_{syn}). Parameters used are shown in Table 14 in the row labelled *'Latency'*. Fig. 73(b) shows that as the synaptic strength increases, the latency decreases, indicating that these circuits can correctly mimic the function of the biological LSO.

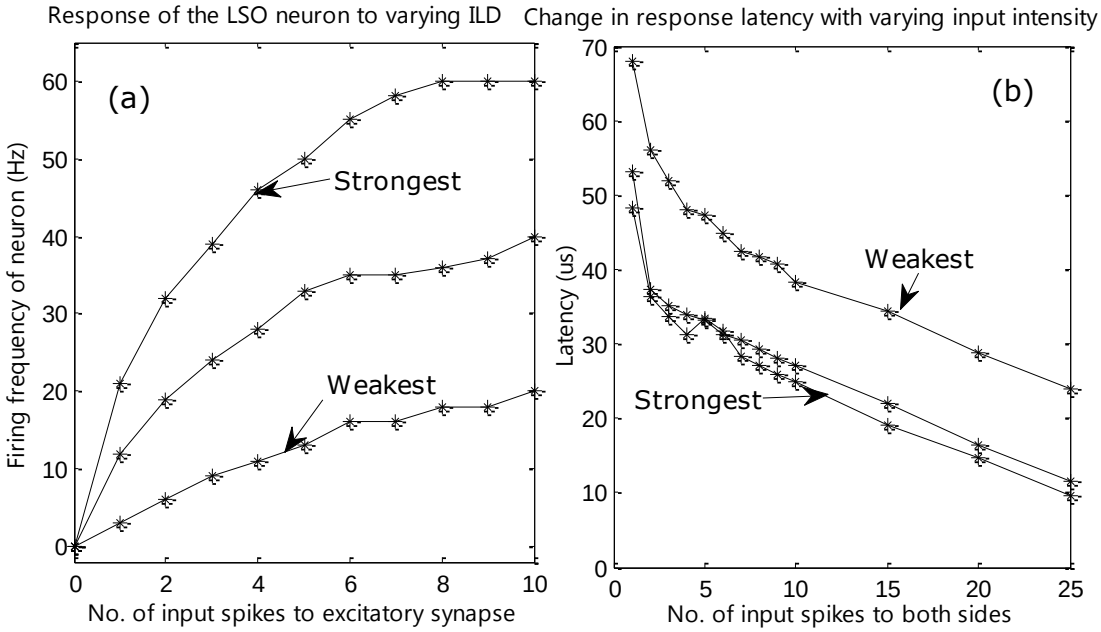

Fig. 73 Shown here are measurement results from the LSO chip when the excitatory synapse was provided different number of inputs at different synaptic strengths. (a) Shows that an increase in neuron threshold voltage causes a decrease in its output for three different synaptic strengths. (b) Different number of input spikes were applied to the synapse circuit at three different synaptic strengths. The results show that as the input strength increases, the response latency decreases for different synaptic strengths. In this implementation of the LSO, we used different number of input pulses to represent intensity of sounds received at the two ears and as seen in biology, we expect the response of the LSO neuron to change with change in ILD and the latency of response (but not its magnitude) to change with change in intensity of input at both ears by an equal amount. This is what is seen here which confirms that our circuits do represent the function performed by the LSO in biology.

The results indicate that we can implement the conductance model of the LSO using the circuit shown and that the synapse circuit can allow scaling of inputs as required for implementing the Reed and Blum's model of the LSO.

iv) Population response of the LSO

Different measurements were performed on an array of 32 synapse-neuron circuits, viz., plotting rasters and calculating the azimuth from ILD ci of 32 different neurons on the LSO chip. The neuronal response was recorded using the 1672 Deep memory logic analyser from Hewlett Packard.

a) Rasters: population response

To test the population response of the LSO and azimuthal localization based on the Reed and Blum's model, initially V_{thr} was changed from 2.015 to 2.8 V in steps of 5 mV each and corresponding neuron firing was plotted as rasters (Fig. 74(a)). Other parameters used for the test were: V_{spk} to the excitatory synapse was a 1kHz, 0.5 µs pulse train, each of 4V magnitude, with no inputs to the inhibitory synapse, V_{refr}=4.3V, V_{bias}=4.15V, V_{syn}=2V, V_s=3.15V, V_f=2.85V, $V_{\tau 1}$ =3.5V, $V_{\tau 2}$=4.5V. As per the chip design, the strength of inputs (value of parameter V_{syn}) changes linearly along the length of the array of the LSO neurons. Thus, we expected the ILD ci of the neurons to vary linearly in that order (thermometer response) and that is what is seen in Fig. 74. However, some of the neurons had similar response to that of their neighbors. Thus, instead of 32, only 22 different ILDci were seen. Thus, the resolution of azimuthal localization is ~8 degrees (180/22).

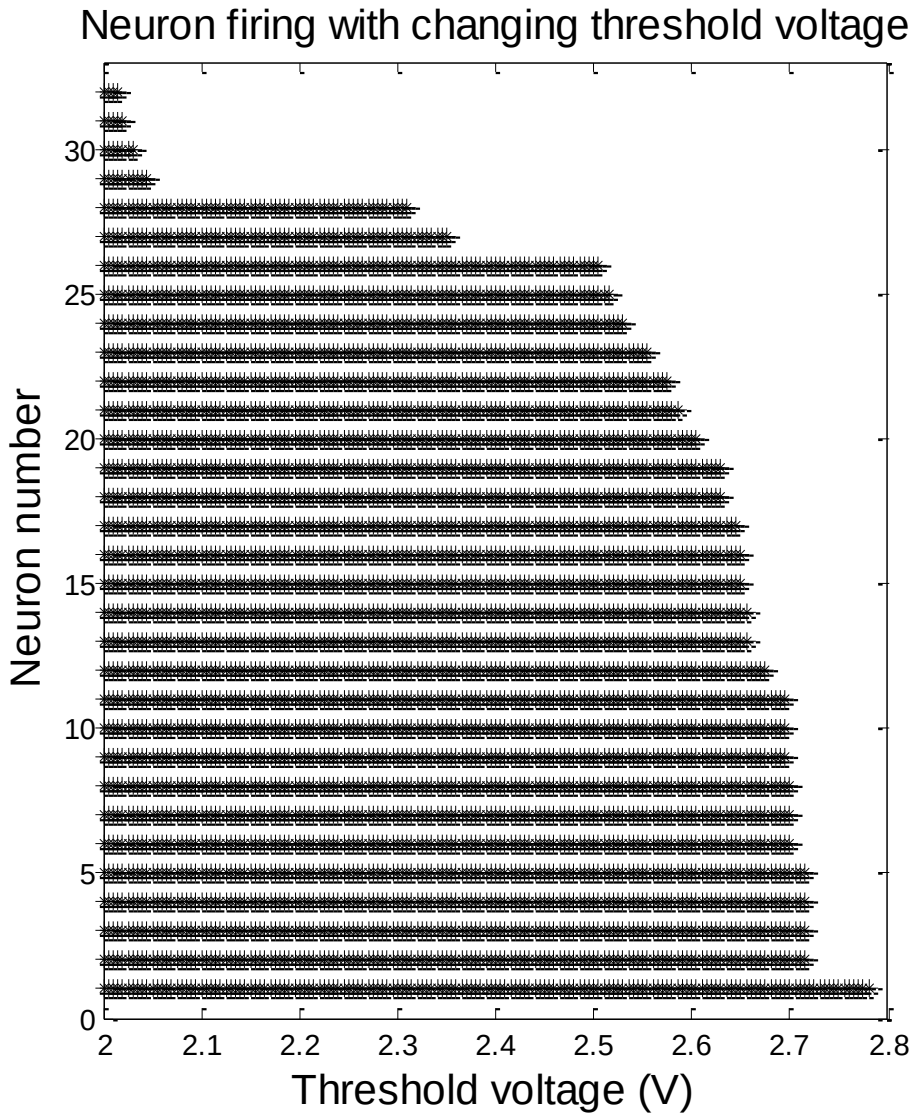

Fig. 74 In this experiment, chip measurements were taken from the array of synapse-neuron circuits while input pulses at 1kHz were applied to the excitatory synapse and threshold voltage of the neuron was varied. The neuron numbers of the neurons which fired at each threshold voltage were recorded using the digital logic analyser and the results plotted in MATLAB. The graph here shows rasters from 32 neurons on the LSO chip. Since the strength of inputs was varied linearly by circuit design, the neuronal response varied along the length of the column as expected from system design and the Reed and Blum's model. These patterns are important as these are used by the LSO to perform azimuthal localization. However, due to small steps on the resistor ladder, some of the neurons have firing patterns similar to that of their neighbors which brings the resolution of the system down to ~8 degrees as compared to ~6 degrees which was expected.

b) Azimuthal localization with the LSO chip

Since the ILD received depends on the azimuthal direction from which the sound is received, we assigned each ILD used in testing the population response to an azimuthal direction. According to the Reed and Blum's model, the ILDci of each neuron along the LSO column is different and, thus, the neuron number that stops firing for an ILD or an azimuthal direction is unique to that direction. Tabulating this mapping from azimuthal direction to ILD to ILDci and the neuron number which stops firing, provides a look up table (Table 7) for the azimuthal localization using the population response of the LSO. As shown in the table row 5, if the neuron number 12 along the column stops firing, then it can be inferred that the sound is coming from 33 degrees along the azimuth as seen from the animal's center. The parameters used for the test were: V_{spk} to the excitatory synapse was changed from 100 Hz to 2200 Hz while that to the inhibitory synapse was kept at 100 Hz. All the pulses were 0.5 µs, 4V magnitude, V_{thr}=2.57V, V_{refr}=4.3V, V_{bias}=4.15V, V_{syn}=2V, V_s=3.15V, V_f=2.85V, $V_{\tau 1}$ =3.5V, $V_{\tau 2}$ =4.5V.

Table 7 Look up table for the neuron number encoding azimuthal direction on the LSO.

S.No.	Neuron number experiencing ILDci	ILD	Direction (degrees)
1	1	100/100	0
2	2, 3, 4, 5	200/100	8
3	6, 7, 8	300/100	16
4	9, 10, 11	400/100	25
5	12	500/100	33
6	13-14	600/100	41
7	15-16	700/100	49
8	17	800/100	57
9	18-19	900/100	66
10	20	1000/100	74
11	21	1100/100	82
12	22	1200/100	90
13	23	1300/100	98
14	24	1400/100	107
15	25	1500/100	115
16	26	1600/100	123
17	27	1700/100	131
18	28	1800/100	139
19	29	1900/100	148
20	30	2000/100	156
21	31	2100/100	164
22	32	2200/100	172

I. Conclusion

This work describes the analog VLSI design, fabrication, measurements and data analysis from a chip implementing the conductance model of the LSO neuron, population response of the LSO and the azimuthal localization based on that. All the above was implemented using synapse and neuron circuit blocks. The synapse circuit is a second-order lowpass filter; which produces a delayed peak current well after the input is gone, enabling the implementation of biological synaptic delay. The linearity of the filter enables the temporal summation of overlapping

responses allowing a single synapse circuit to replace multiple synapse circuits when synchronous inputs are required to produce a larger synaptic response. The rise and fall time of the output current are adjustable from 0.5ms to as long as 50ms. Average current was used as a measure to indicate linear summation of pulses at different frequencies as different frequencies change the average current. In contrast, for summation of different numbers of pulses, the maximum current at the output was compared as this parameter is most indicative of linear summation.

The ability to vary time constants and strengths of inputs by changing the synapse circuit parameters enabled demonstration of the effect of latency on response and implementation of the Reed and Blum's model of population response of the LSO. These inputs were connected to the neuron (conductance model) to drive its membrane potential to bias voltage (V_{we}) or to *Vdd* based on whether the excitatory or the inhibitory inputs were more active. It was demonstrated that the neuron circuit worked as per the conductance model of the LSO as the response to varying ILDs is a monotonic curve which gently saturates at either extremes of ILD as observed in biology.

Another part of this chip was designed to demonstrate the population response of the LSO and the azimuthal localization based on that. As observed, there was variation in ILD ci for neurons in the array on the LSO chip. Processing the ILD ci data from all the neurons showed that it could help in azimuthal localization with a resolution of ~8 degrees.

Future work could include mounting all the five chips on to a robot buggy, providing it with a front end system which could process the incoming sound and

convert it to spikes for the synapse circuits on both sides and a back end data processor which can process the data from the LSO array and calculate the azimuthal angle. This can be used for autonomous robotic spatial navigation. This circuit can not only perform the ILD and the azimuthal echolocation but also general analog computations requiring ratio calculations (based on the equations described in the section on the conductance model of the LSO).

9. OPEN QUESTIONS & FUTURE WORK

In this work, I successfully demonstrate

1. The working of the hippocampal formation in silicon. This can be used for robotic spatial navigation. For instance, if a robot is sent out to an unknown place, it can find its way around by using directional signals from the head direction cells and the map of the environment formed by the place cells. It can update the environmental map as it navigates around in space. Thus, it can learn autonomously from the environment and encode this information in memory. It can also update this information based on new inputs from the environment. In contrast, most of the current robotic systems act based on fixed sensory signals and react to them. They have little or no capacity to update their response if the information changes as they do not maintain and update spatial maps of the environment.
2. The ring circuit developed as part of the system implementation was so compact that it can enable integration of all the circuitry required to implement the hippocampal formation in silicon as done here on a portion of a single tiny chip unit.
3. We also came up with a novel sensori-motor model of the hippocampal place cells which can be used in future silicon implementation of the place cells to provide a closer correspondence with the patterns of place cell firing observed empirically.

4. The population response of the LSO based on the Reed and Blum's model. This can help in azimuthal localization of sound to about 8 degrees resolution. Azimuthal localization of sound is of survival value for animals. The silicon implementation of the system could be useful for robotics when robots need to move around in space based on sound signals or need to detect the direction along the azimuth from which the sound is incident. Future work could also include mounting the LSO chip on to a robot buggy, providing it with a front end system which could process the incoming sound and convert it to spikes for the synapse circuits on both sides and a back end data processor which can process the data from the LSO array and calculate the azimuthal angle.
5. Although the central pattern generator has already been implemented earlier, its implementation in this dissertation work was in a very compact form and hence, can enable area and power saving when used in artificial systems. The central pattern generator, as used from earlier realizations of the same, can be used in robotic motor control.

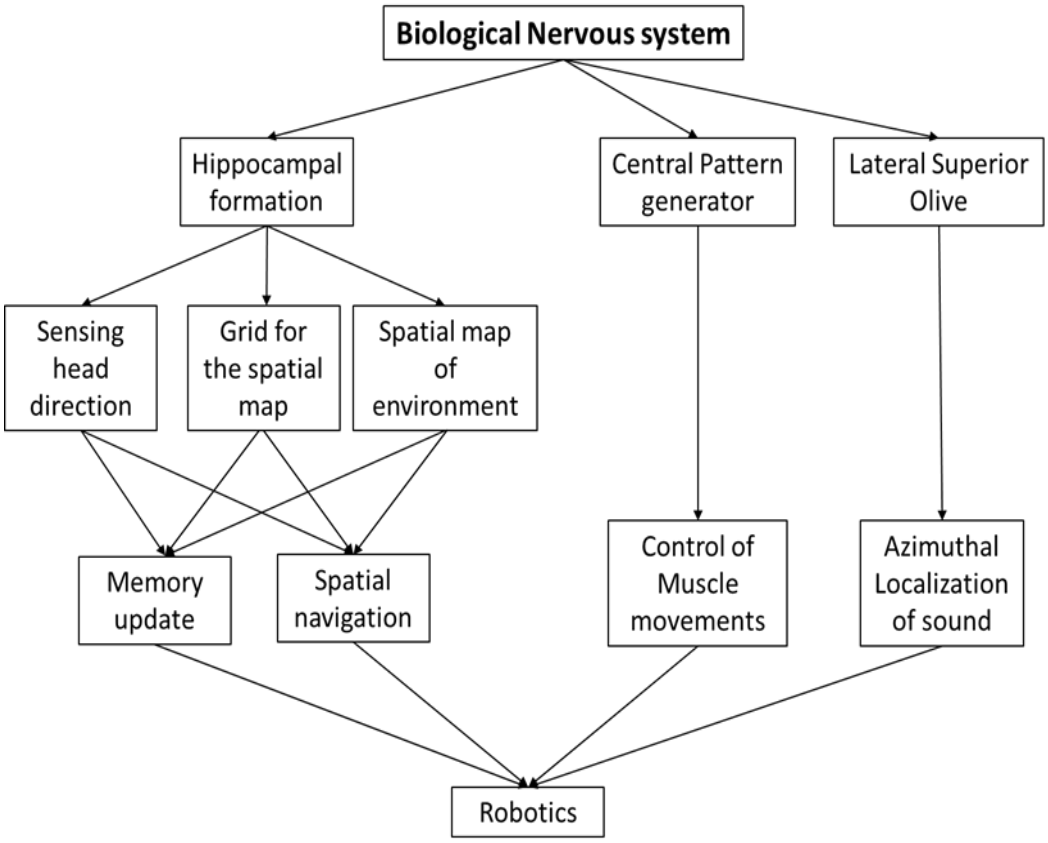

Fig. 75 Showing the potential applications of the various systems, designed in silicon as part of this dissertation work, in robotics. The hippocampal formation can be used for spatial navigation and encoding episodic memories including updating the maps of the environment. Central pattern generator can generate patterns which can be provided as inputs to muscles to control their movement. Electronic LSO can be used for azimuthal localization of incoming sounds which can aid in spatial navigation.

While working on these projects, it was fascinating to understand the myriad computations that our brain can perform. The brain uses similar, simple, but several such units connected in big and at times complex networks to perform its functions.

Currently, most of the work done in the neuromorphic engineering (inspired by the pioneering work of Carver Mead, Hugo Schmitt and Hewitt Crane) is based on implementing different parts of the brain using the available cmos technology.

The basic units of this technology are much bigger and much less power efficient than the smallest units (neurons) of the brain. Hence, the systems built to emulate brain's function in silicon are far less efficient than their inspiration. The other alternative is to build these networks in software. However, this implementation suffers from constraints of performance speed. Thus, looking forward, we need to come up with newer, simpler basic units (like memristors) or more power efficient ones, a lot of which could be implemented on silicon to realize the big brain networks to perform mathematical computations.

Another remarkable thing about the brain is its ability to learn from its interactions with environment and to change its surroundings or to adapt to them continuously. This property needs to be used more widely in circuit design than is being currently used.

10. APPENDIX I

Table 8. Parameters used for tests on the second order synapse: the grid chip

Test	Vsyn (V)	Vf(V)	Vs(V)	Time Constant(ms)
Varying time constants	2.60	2.83	3.74	0.5
	2.63	2.88	3.74	1
	2.56	2.94	3.80	50
Summating spikes	2.63	2.88	3.74	1

Spike inputs were always digital pulses 4V in amplitude and 0.5 μs in duration. In all cases, $V_{\tau 1}$ = 3.5V and $V_{\tau 2}$ = 4.5V except for the simulations where $V_{\tau 1}$ = 4V.

Table 9 Parameters for tests on the standalone neuron circuit (neuron 2): the grid chip

Test	V_{thr} (V)	V_{refr} (V)	V_{we} (V)	V_{lk} (V)	V_{exc} (V)
Initial measurements	0.55, 0.60, 0.64	4.10	4.10	5.01	4.10

Table10 Parameters used for testing the hippocampal formation as a system

Chip	Parameter	Voltage (V)
Stripe cells' ring chip	**V2**	4.15
	V1	3.9
	V_{leak} (ring)	0.40
	V_{bias}	1.46
	cCon	4.17
	V_{lk}(neuron)	0.52
	V_{refr}	0.5
Grid cell chip	**V_{syn}**	2.6
	$V_{\tau 1}$	3.5
	$V_{\tau 2}$	4.5
	V_f	2.88
	V_s	3.79
	V_{we}	4.1
	V_{lk}	4.29
	V_{refr}	4.38
	V_{thr}	0.75
Place cell chip	**V_{bias}**	1.5
	V_{thr}	0.6
	V_{lk}	4.41
	V_{we}	4.05
	V_{refr}	4.26

Table 11. Parameters used for tests on the second order synapse: the LSO chip

Test	V_{syn} (V)	V_f (V)	V_s (V)	Time constant (ms)
Synapse output	2.63	2.88	3.74	1
Synapse output 2	2.58	3.3	3.85	1
Regular spiking	2.56	2.75	3.75	1
Varying Vsyn (burst)	2.56, 2.60, 2.65	2.88	3.74	1
Varying Vsyn (train)	2.565, 2.60, 2.65	2.75	3.75	1

Spike inputs were always digital pulses 4V in amplitude and 0.5 μs in duration. In all cases, $V_{\tau 1}$ = 3.5V and $V_{\tau 2}$ = 4.5V except for the simulations where $V_{\tau 1}$ = 4V.

Table 12. Parameters used for latency experiment: the LSO chip

		Set1	Set2	Set3	ILD curves
Synapse	**Vs**	3.78	3.80	3.84	3.76
	Vf	2.96	2.98	3.00	2.88
	Vsyn	2.59	2.59	2.59	2.57
Neuron	**Vthr**	variable			0.61
	Vdd	4.78	4.72	4.61	5.00
	Vrefr	3.87	3.80	3.71	4.10
	Vwe	3.87	3.80	3.70	4.10

Table 13 Parameters for tests on the standalone neuron circuit: the LSO chip

Test	V_{thr} (V)	V_{refr} (V)	V_{we} (V)	V_{inh} (V)	V_{exc} (V)
ILD curve	0.55, 0.60, 0.64	4.10	4.10	5.01-4.50	5.01-4.10

Table 14 Parameters for tests on the synapse-neuron circuit: the LSO chip

Test	V_{thr} (V)	V_{refr} (V)	V_{we} (V)	V_{syn} (V)	V_f (V)	V_s (V)
ILD curves	0.55 0.60 0.65	4.10	4.10	2.57	2.88	3.76
Latency	0.65	4.10	4.10	2.57, 2.60, 2.65	2.88	3.76
Consecutive bursts	0.65	4.10	4.10	2.57	2.88	3.76

11. APPENDIX II

Verilog code

a) Simulated motion in Open Space

Pseudocode:

1. To simulate animal motion in Open space, we need to provide inputs to the 3 ring circuits on the stripe cell ring chip to correspond to animal motion in space along the preferred firing direction of ring 1 for ¼ m, then along a direction perpendicular to that of ring 1 for 1/2 m.
2. This maps to moving ring 1, 6 places to the right and then moving rings 2 and 3 by 6 positions and then repeating the pattern over and over.
3. Need to provide ring 1 with 6 RS pulses while holding the winning node position on rings 2 and 3 at a place, followed by 6 RS pulses to rings 2 & 3 while the position of winning node in ring 1 is held constant. Need to repeat this pattern over and over.
4. Meanwhile, need to read the corresponding ring numbers from the 3 rings.
5. If the neuron numbers 2, 8, 14 and 20 on all the 3 rings fired at the same time, send an input pulse to the first grid cell, if neuron numbers 2 and 14 fire. Then send an input pulse to the second grid cell and if neuron number 2 on all the rings fire simultaneously, then send an input pulse to grid cell 3.

To implement this, we made a state machine so that the system is initially at state 0 (reset state) and enters state 1 at the press of the push button on the FPGA board.

In state 1, the neuron positions of all the rings are shifted to neuron number 2. Then the system alternates between states 2 and 3. In state 2, 6 RS signals are provided to ring 1 and in state 3, six RS signals are provided to rings 2 & 3 and the pattern is repeated over and over until the press of the push button on the FPGA board causes the state machine to enter the reset state 0.

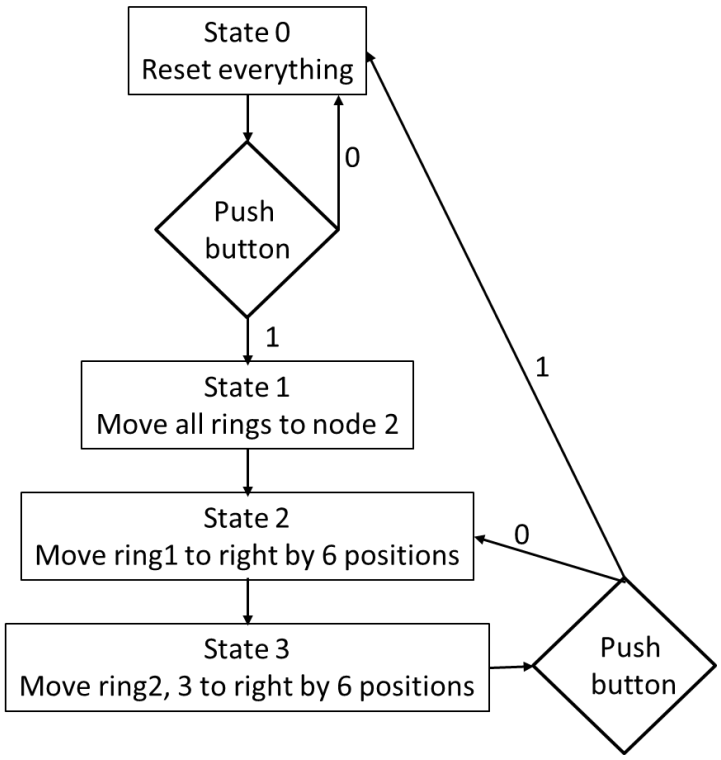

Fig. 76 Showing the FSM designed in verilog to generate input signals to the system of chips implementing the grid and the place cell firing patterns when the animal motion in open space was simulated. In this case, the system, on being started at the press of the push button on the FPGA board, shifts the winning position of all the rings to node number 2 and then provides 6 RS signals to ring 1 or rings 2 & 3 alternately. This pattern of inputs is repeated over and over until the system is forced back to state 0 by pressing the same push button.

```
module openSpace2(
    input clk,
    input [3:0] btn,
```

```
input [4:0] neuronNum1,
input [4:0] neuronNum2,
input [4:0] neuronNum3,
output reg spk,
output reg spk1,
output reg spk2,
output reg [1:0] req1,
output reg [1:0] req2,
output reg [1:0] req3,
output reg [7:0] Led,
output reg [7:0] seg,
output reg [3:0] an
);
        integer count;
        integer state;
        integer count2;
        integer count3;
        integer count4;
        integer count5;
        integer i;
       // Assign initial values to the variables
        initial begin
                i=0;
```

```
        count=0;
        count2=0;
        count3=0;
        count4=0;
        count5=0;
        state=0;
        req1=2'b11;
        req2=2'b11;
        req3=2'b01;
        Led=state;
        seg={1, 1, 0, 0, 0, 0, req1};
        spk=0;
        spk1=1;
        spk2=0;
        an=btn;  end

    always@(posedge clk)
        begin
        count=count+1; // counts the number of clk pulses (clk frequency is
50MHz) needed to provide a debounce function for the push button on the FPGA
board
                if (count>=50000000) begin
                        count=0; // reset count after 1 s
```

```
                    if(btn[0]&&state==0)
// at the push of the button on the FPGA start the FSM and the system
                        state=1;
                    else if(btn[0]&&state==3)
// at the push of the button again, stop the FSM and the system
                        state=0;
                end
// to produce 6 RS pulses to rings 1, and then another 6 to rings 2 & 3, need to alternate at particular intervals between states 2 and 3.
                if((state==1)&&(i>=2000020))begin
                        state=2; i=0; end
                else if((state==2)&&(i>=6000060)) begin
                        state=3; i=0;
                        end
                else if((state==3)&&(i>=6000060)) begin
                        i=0; state=2;   end
                case(state)
                    0: begin
                        req1=2'b11;    req2=2'b11; req3=2'b11; i=0;
//reset count to change states, set the address bit on the decoder to select RS signal.
                    end
                    1:begin
```

```
                    count2=count2+1; i=i+1;
//set the address bit to choose ring 1 RS signal
                    req1[0]=1; req2[0]=1;req3[0]=1;
                    if((count2>1000000)&&(count2<1000010))
                        begin
// send 1 input pulses to all the rings for 10 counts of the clock to shift the node position after reset to node number 2
                        req1[0]=0; req2[0]=0;req3[0]=0; end
                    else if((count2>1000010)) begin
                count2=0; end
            end
                2: begin
// send input pulses to ring 1 for 10 counts of the clock to shift the node position to right as long as the system stays in state 2 (allows application of 6 input pulses)
                    count2=count2+1;i=i+1;
                    req1[0]=1; req2[0]=1;req3[0]=1;
                    if((count2>1000000)&&(count2<1000010))
                        begin
                        req1[0]=0; req2[0]=1;req3[0]=1; end
                    else if((count2>1000010)) begin
                        count2=0; end
                end
                3: begin
```

```
// send input pulses to rings 2 & 3 for 10 counts of the clock to shift the node position to right as long as the system stays in state 2 (allows application of 6 input pulses)
                                        req1[0]=1; i=i+1;
                                        count3=count3+1;
                                        req2[0]=1;req3[0]=1;
                                    if((count3>1000000)&&(count3<1000010))
                                            begin
                                             req1[0]=1; req2[0]=0; req3[0]=0;end
                                             else if((count3>1000010)) begin
                                                    count3=0; end
                                             end
                                endcase
                            end
always@(posedge clk)
begin
// read the neuron numbers on the rings constantly using the FPGA and if desired combination is obtained, send input spikes to one of the three grid cells.
if((neuronNum1==20)&&(neuronNum2==20)&&(neuronNum3==20))begin
            count4=count4+1; spk1=0;
        if(count4>50)begin
                count4=0; spk1=1;      end
 end
```

```
if((neuronNum1==14)&&(neuronNum2==14)&&(neuronNum3==14))begin
count4=count4+1; spk=1; spk1=0;
        if(count4>50)begin
            spk=0; spk1=1; count4=0;end
                end
                else
else if((neuronNum1==8)&&(neuronNum2==8)&&(neuronNum3==8))begin
          count4=count4+1; spk1=0;
           if(count4>50)begin
                count4=0; spk1=1;      end
 end
else if((neuronNum1==2)&&(neuronNum2==2)&&(neuronNum3==2))begin
          count4=count4+1; spk2=1;     spk1=0; spk=1;
          if(count4>50)begin
                spk1=1; spk=0; count4=0; spk2=0; end
 end
else begin
          spk=0; spk1=1; spk2=0; end
Led={0, neuronNum1, state[1], state[0]};
seg={2'b00, req3, req2, req1} ;
an=btn; end
endmodule
```

b) Circle

Pseudocode

To simulate animal motion along a circle of radius 1m, needed to provide inputs to the system as follows.

1. Decided to move the ring positions repeatedly between 12 points on the circle.
2. 6 of these points were taken to be the ones located on the three axis and the rest midway between the three axis.
3. These mapped to neuron numbers [24, 24, 24] on the 3 rings for the 6 points located on the three axis.
4. The rest of the points correspond to neuron numbers [22, 22, 24] or [22, 24, 22] or [24, 22, 22]
5. If the neuron numbers 24 on all the 3 rings fired at the same time, send an input pulse to the first grid cell, if neuron numbers 12 and 24 fire then send an input pulse to the second grid cell and if neuron number 6, 12, 18 or 24 on all the rings fire simultaneously, then send an input pulse to grid cell 3.

To implement this we made a state machine so that the system is initially at state 0 (reset state) and enters state 1 at the press of the push button on the FPGA board. In state 1, the neuron positions of all the rings are shifted to neuron number 24 by applying 1 LS signal to all the rings. Then the system moves from state 2 → 3→…→13 and back to 2 repeatedly unless the push button is pressed to reset the system to state 0. In states 2-13, different signals are provided to the 3 rings and neuron numbers corresponding to the positions are read to send inputs to the 3 grid cells as shown in the state transition table for the FSM (Table 15).

Table 15 Showing the state transition table for the FSM used to implement the movement of the animal along a circle of radius 1m, using the FPGA board.

Current state	Inputs	Next state	Output
0	Push button	1	Reset all the rings to node 1
	No push button	0	
1	-	2	1 LS signal is applied to all the 3 rings to shift the node positions on all the rings to [24, 24, 24]
2	No push button	3	Check node positions and send outputs to all the grid cells if these are at 24 on all the three rings
3	No push button	4	2 LS signals are applied to rings 1 & 2 to shift the node positions on all the rings to [22, 22, 24]
4	No push button	5	Check node positions and send outputs to all the grid cells if these are at 24 on all the three rings
5	No push button	6	2 RS signals are applied to rings 1 & 2 to shift the node positions on all the rings to [24, 24, 24]
6	No push button	7	Check node positions and send outputs to all the grid cells if these are at 24 on all the three rings
7	No push button	8	2 LS signals are applied to rings 2 & 3 to shift the node positions on all the rings to [24, 22, 22]
8	No push button	9	Check node positions and send outputs to all the grid cells if these are at 24 on all the three rings
9	No push button	10	2 RS signals are applied to rings 2 & 3 to shift the node positions on all the rings to [24, 24, 24]
10	No push button	11	Check node positions and send outputs to all the grid cells if these are at 24 on all the three rings
11	No push button	12	2 LS signals are applied to rings 1 & 3 to shift the node positions on all the rings to [22, 24, 22]
12	No push button	13	Check node positions and send outputs to all the grid cells if these are at 24 on all the three rings
13	No push button	2	2 RS signals are applied to rings 1 & 3 to shift the node positions on all the rings to [24, 24, 24]
	push button	0	

```
module testCirc2(
    input clk,
    input [3:0] btn,
    input [4:0] neuronNum1,
    input [4:0] neuronNum2,
    input [4:0] neuronNum3,
```

```
    output reg spk,
    output reg spk1,
    output reg spk2,
    output reg [1:0] bit_Sel,
    output reg [7:0] Led,
    output reg [7:0] seg,
    output reg [3:0] an,
    output reg [1:0] req2,
    output reg [1:0] req3    );
            integer count;
            integer state;
            reg [1:0] req1;
            integer count2;
            integer count3;
            integer count4;
//initialise the variable to their initial values
 initial begin
            count=0;
            count2=0;
            count3=0;
            count4=0;
            state=0;
            req1=2'b01;
```

```
        req2=2'b01;
        req3=2'b01;
        Led=state;
        seg={1, 1, 0, 0, 0, 0, bit_Sel};
        bit_Sel={req1};
        spk=0;
        spk1=1;
        spk2=0;
        an=btn;          end
always@(posedge clk) begin
        count=count+1;
        // debounce circuit
        if (count>=5000000) begin
                count=0;
                if(btn[0]&&state==0)begin
// start the FSM at the push of the button on the FPGA board if the system is in state 0
                        state=1; end
                else if(btn[0]&&state>2)begin
// stop the FSM at the push of the button on the FPGA board  if the system is working
                        state=0; end
                else if(state>=13)
```

```
// move in closed loop until the FSM is stopped
                    state=2;
                else if((0<state)&&(state<13))
// keep moving from state to state one at a time
                    state=state+1; end
                case(state)
                    0:begin
// reset the system so that winning nodes on all the rings are node 1
                    req1=2'b01; req2=2'b01; req3=2'b01; count3=0;
                    end
                    1:begin
// provide 1 LS signal to all the rings to shift the winning node position on all the 3 rings to node 24, such that the resulting neuron positions on all the rings are [24, 24, 24]
                    req1=2'b00; req2=2'b00; req3=2'b00; count3=count3+1;
                    if (count3>5) begin
                        req1=2'b01; req2=2'b01; req3=2'b01; end
                     end
                    3:begin
// provide 2 LS signals to rings 1 &2, such that the resulting neuron positions on all the rings are [22, 22, 24]

                    req1=2'b00; req2=2'b00; req3=2'b01; count3=count3+1;
```

```
if ((count3>13 && count3<500013)|| (count3>500026))
begin
        req1=2'b01;     req2=2'b01;     req3=2'b01;
        count3=count3+1;
        end
end
5:begin
```

// provide 2 RS signals to rings 1 &2, such that the resulting neuron positions on all the rings are [24, 24, 24]

```
req1=2'b10; req2=2'b10; req3=2'b11; count3=count3+1;
if ((count3>13 && count3<500013)|| (count3>500026))
begin
        req1=2'b11;     req2=2'b11;     req3=2'b11;
        count3=count3+1; end
end
7:begin
```

// provide 2 LS signals to rings 2 &3, such that the resulting neuron positions on all the rings are [24, 22, 22]

```
req1=2'b01; req2=2'b00; req3=2'b00; count3=count3+1;
if ((count3>13 && count3<500013)|| (count3>500026))
 begin
        req1=2'b01;     req2=2'b01;     req3=2'b01;
        count3=count3+1; end; end
```

```
                9:begin
// provide 2 RS signals to rings 2 &3, such that the resulting neuron positions on all the rings are [24, 24, 24]
                req1=2'b11; req2=2'b10; req3=2'b10; count3=count3+1;
                if ((count3>13 && count3<500013)|| (count3>500026))
                begin
                        req1=2'b11; req2=2'b11; req3=2'b11;
                        count3=count3+1; end
                end
                11:begin
// provide 2 LS signals to rings 1 &3, such that the resulting neuron positions on all the rings are [22, 24, 22]
                req1=2'b00; req2=2'b01; req3=2'b00; count3=count3+1;
                if ((count3>13 && count3<500013)|| (count3>500026))
                 begin
                req1=2'b01; req2=2'b01; req3=2'b01; count3=count3+1;
                end
                end
                13:begin
// provide 2 RS signals to rings 1 &3, such that the resulting neuron positions on all the rings are [24, 24, 24]
                req1=2'b10; req2=2'b11; req3=2'b10; count3=count3+1;
                if ((count3>13 && count3<500013)|| (count3>500026))
```

```
                    begin
                    req1=2'b11; req2=2'b11; req3=2'b11; count3=count3+1;
                    end
                    end
                endcase
                if((state==2)||(state==6)||(state==10))
// Check the neuron numbers on all the rings and if neuron numbers 24 on all of them fire, then send input pulses to all the grid cells
                begin
                    count3=0;  req1=2'b01; req2=2'b01; req3=2'b01;
        if ((neuronNum1==23)&&(neuronNum2==23) && (neuronNum3==23))
                spk2=1; spk1=0; spk=1; end
        else begin
                spk=0; spk1=1; spk2=0; end
        end
        else if((state==4)||(state==8)||(state==12))
        begin
// Check the neuron numbers on all the rings and if neuron numbers 24 on all of them fire, then send input pulses to all the grid cells
                count3=0;  req1=2'b11; req2=2'b11; req3=2'b11;
        if ((neuronNum1==23)&&(neuronNum2==23) && (neuronNum3==23))
                spk=1;   spk1=0; spk2=1;
        else begin
```

```
                spk=0; spk1=1; spk2=0; end
        end
end
bit_Sel={req1};
an=btn;
end
endmodule
```

c) Straight Line

Pseudocode

For this part, we needed to provide inputs to rings to correspond to animal motion in a straight line along the preferred firing direction of ring 1. This was done by applying a constant RS pulse to ring 1 while winning node positions of rings 2 and 3 were held at node 24.

1. After resetting all the rings to node 1, move all of them to node 24 by applying a LS signal to all of them. Thereafter, need to provide ring 1 with a train of RS pulses while holding the winning node position on rings 2 and 3 at node 24.
2. If the neuron numbers 24 on all the 3 rings fired at the same time, send an input pulse to the first grid cell, if neuron numbers 12 and 24 fire then send an input pulse to the second grid cell and if neuron numbers 6, 12, 18 or 24 on all the rings fire simultaneously, then send an input pulse to grid cell 3.

To implement this we made a state machine so that the system is initially at state 0 (reset state) and enters state 1 at the press of the push button on the FPGA board. In state 1, the neuron positions of all the rings are shifted to neuron number 24 by applying 1 LS signal to all of them. Then the system enters state 2 in which a train of RS signals is provided to ring 1 until the press of the push button on the FPGA board causes the state machine to enter the reset state 0.

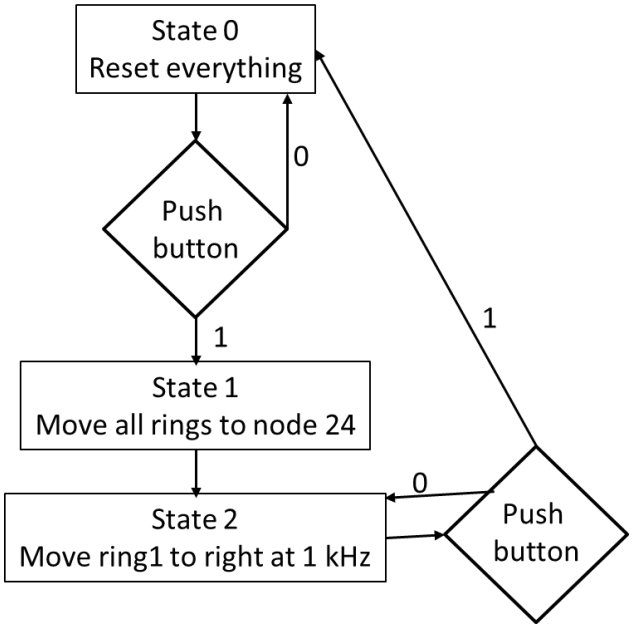

Fig. 77 Showing the FSM designed in verilog to generate input signals to the system of chips implementing the grid and the place cell firing patterns when the animal motion in a straight line along the preferred firing direction of one of the rings was simulated. In this case, the system on being started at the press of the push button on the FPGA board, shifts the winning position of all the rings to node number 24 and then provides a train of RS signals to ring 1. This pattern of inputs continues until the system is forced back to state 0 by pressing the same push button.

```
module test12(

input clk,

    input [3:0] btn,

    input [4:0] neuronNum1,

    input [4:0] neuronNum2,

    input [4:0] neuronNum3,

    output reg spk,

    output reg spk1,

    output reg spk2,
```

```
output reg [1:0] req1,
output reg [1:0] req2,
output reg [1:0] req3,
output reg [7:0] Led,
output reg [7:0] seg,
output reg [3:0] an
);
        integer count;
        integer state;
        integer count2;
        integer count3;
        integer count4;
        integer count5;
        integer i;
       // Assign initial values to the variables
        initial begin
                i=0;
                count=0;
                count2=0;
                count3=0;
                count4=0;
                count5=0;
                state=0;
```

```
req1=2'b11;
req2=2'b11;
req3=2'b01;
Led=state;
seg={1, 1, 0, 0, 0, 0, req1};
spk=0;
spk1=1;
spk2=0;
an=btn;  end

always@(posedge clk)
begin
count=count+1; // counts the number of clk pulses (clk frequency is 50MHz) needed to provide a debounce function for the push button on the FPGA board
if (count>=50000000) begin
count=0; // reset count after 1 s
if(btn[0]&&state==0)
// at the push of the button on the FPGA start the FSM and the system
state=1;
else if(btn[0]&&state==2)
// at the push of the button again, stop the FSM and the system
state=0;
```

```
                    end


case(state)
        0: begin
// set the address bit on the decoder to select LS signal.
        req1=2'b01;     req2=2'b01; req3=2'b01;
        end
        1:begin
//Apply 1 LS signal to all the rings to set the node numbers to 24 on all the rings
        count2=count2+1;
        req1[0]=1; req2[0]=1;req3[0]=1;
        if((count2>1000000)&&(count2<1000010))
         begin
                req1[0]=0; req2[0]=0;req3[0]=0; end
        else if((count2>1000010)) begin
        count2=0; end
         end
        2: begin
// send a train of RS pulses to ring 1
        count2=count2+1;i=i+1;
        req1[0]=1; req2[0]=1;req3[0]=1;
        if((count2>1000000)&&(count2<1000010)) begin
        req1[0]=0; req2[0]=1;req3[0]=1; end
```

```
        else if((count2>1000010)) begin
        count2=0; end
        end
        endcase
        end
always@(posedge clk)
begin
// read the neuron numbers on the rings constantly using the FPGA and if desired
combination is obtained, send input spikes to one of the three grid cells.
if((neuronNum1==18)&&(neuronNum2==18)&&(neuronNum3==18))begin
             count4=count4+1; spk1=0;
         if(count4>50)begin
                  count4=0; spk1=1;     end
 end
if((neuronNum1==12)&&(neuronNum2==12)&&(neuronNum3==12))begin
count4=count4+1; spk=1; spk1=0;
       if(count4>50)begin
            spk=0; spk1=1; count4=0;end
                  end
                  else
else if((neuronNum1==6)&&(neuronNum2==6)&&(neuronNum3==6))begin
        count4=count4+1; spk1=0;
         if(count4>50)begin
```

```
                    count4=0; spk1=1;      end
 end
else if((neuronNum1==24)&&(neuronNum2==24)&&(neuronNum3==24))begin
          count4=count4+1; spk2=1;     spk1=0; spk=1;
          if(count4>50)begin
                    spk1=1; spk=0; count4=0; spk2=0; end
 end
else begin
          spk=0; spk1=1; spk2=0; end
Led={0, neuronNum1, state[1], state[0]};
seg={2'b00, req3, req2, req1} ;
an=btn; end
endmodule
```

12. APPENDIX III

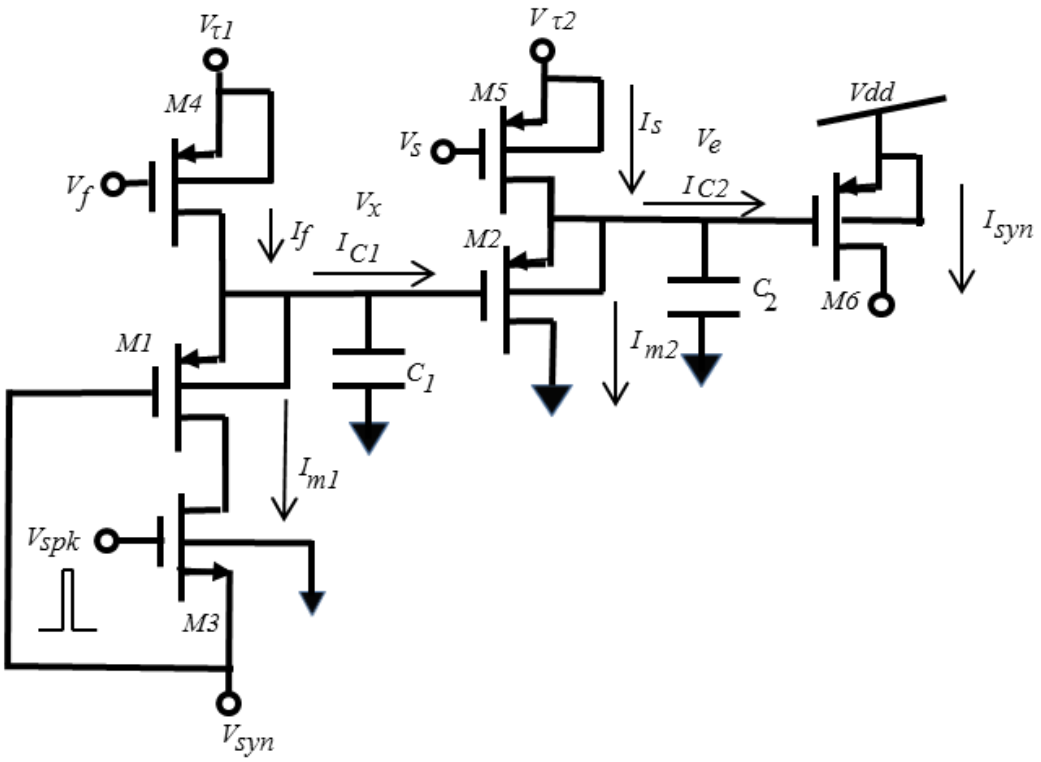

Fig. 78 Circuit of the synapse which converts a short input spike to M3 to a long soft second order function shaped output current. The circuit is designed using a cascade of two first order low pass filters. The first low pass filter (M1, M4, C1) converts the input pulse into an exponential shaped current, I_{m1} whose time constant is determined by the parameter V_f . This is converted into a second order function shaped output current by the second low pass filter (M2, M5, C2). The time constant of this is controlled by the parameter V_S. Output (I_{syn}) from the synapse was connected to the neuron (drain of M1) shown in Fig. 29 such that it acts as an excitatory input to the neuron circuit. The body terminals of all the pfets were tied to their source terminals (separate well for each pfet) and that of the nfet was tied to the ground. The source of M3 is tied to V_{syn} to reduce the charge transfer from parasitic capacitances at the drain of M1 following each input spike. With no critical sizing issues as part of our design, all the transistors were designed to have W/L= 2.4µm/2.4µm and values of all the capacitors were 0.1pF. Capacitors were designed using poly-poly1.

Equations for the second order synapse circuit

To find the DC baseline current, we find the steady state voltages and currents with no inputs applied to the circuit. If no inputs are applied, then M4 pulls V_x all the way up to $V_{\tau 1}$ and entire I_S flows through M2 to ground, then[14]

$$I_{m2} = I_s = I_0 e^{\frac{\kappa(V_e - V_{\tau 1})}{V_T}} \tag{30}$$

$$\frac{V_T}{\kappa}\ln\left(\frac{I_s}{I_0}\right) + V_{\tau 1} = V_e \tag{31}$$

$$I_{syn} = I_0 e^{\frac{\kappa\left(Vdd - \left(\frac{V_T}{\kappa}\ln\left(\frac{I_s}{I_0}\right) + V_{\tau 1}\right)\right)}{V_T}} = I_0 e^{\frac{\kappa\left(Vdd - \frac{V_T}{\kappa}\ln\left(\frac{I_s}{I_0}\right) - V_{\tau 1}\right)}{V_T}}$$

$$= I_0 e^{\frac{\kappa Vdd}{V_T}} \frac{I_0}{I_s} e^{\frac{-\kappa V_{\tau 1}}{V_T}} = \frac{{I_0}^2 e^{\frac{\kappa Vdd}{V_T}} e^{\frac{-\kappa V_{\tau 1}}{V_T}}}{I_s} \tag{32}$$

[14] The second order synapse circuit was developed jointly with Prof T. K. Horiuchi but the circuit equations were reworked jointly with Prof Newcomb as the earlier ones had some errors. Moreover, another modified version of the circuit was developed by me (Fig. 27).

$$I_{syn} = \frac{I_0{}^2 e^{\frac{\kappa Vdd}{V_T}} e^{\frac{-\kappa V_{\tau 1}}{V_T}}}{I_0 e^{\frac{\kappa (V_{\tau 2} - V_s)}{V_T}}} = \frac{I_0 e^{\frac{\kappa Vdd}{V_T}} e^{\frac{-\kappa V_{\tau 1}}{V_T}}}{e^{\frac{\kappa (V_{\tau 2} - V_s)}{V_T}}}$$

$$= I_0 e^{\frac{\kappa Vdd}{V_T}} e^{\frac{-\kappa V_{\tau 1}}{V_T}} e^{\frac{-\kappa (V_{\tau 2} - V_s)}{V_T}} \quad (33)$$

$$I_{syn} = I_0 e^{\frac{\kappa (Vdd - V_{\tau 1} - V_{\tau 2} + V_s)}{V_T}} \quad (34)$$

When an input is applied, however, the V_x does not tend to $V_{\tau 1}$ but depends on the applied input as well. In that case, the output current from the synapse (subthreshold mode of operation), from the transistors M2 and M1 are given by,

$$I_{syn} = I_o e^{\frac{\kappa (Vdd - Ve)}{V_T}} \quad (35)$$

$$I_{m2} = I_o e^{\frac{\kappa (Ve - Vx)}{V_T}} \quad (36)$$

$$I_{m1} = I_o e^{\frac{\kappa (V_x - V_{syn})}{V_T}} \quad (37)$$

The current equations for C_1 and C_2 at node x and e,

$$I_f = I_{m1} + C_1 \frac{dV_x}{dt} \quad (38)$$

$$I_s = I_{m2} + C_2 \frac{dV_e}{dt} \quad (39)$$

Eliminating I_{m1}, I_{m2}, and the time-derivatives of V_x and V_e, (by taking the derivatives of equations (36) and (37) in this section and assuming that the duration of input is very short) it can be shown that the transfer function is

$$I_{syn} = \frac{I_0{}^3 e^{\frac{\kappa V dd}{V_T}} e^{\frac{-\kappa V_{syn}}{V_T}}}{I_{m1} I_{m2}} \tag{40}$$

Now, using the small signal approximation for the exponentials and differentiating equation (37),

$$\frac{dI_{m1}}{dt} = \frac{I_o \kappa}{V_T} \cdot \frac{dV_X}{dt} \tag{41}$$

Now, substituting in equation (38)

$$I_{m1} = I_f - \frac{CV_T}{\kappa I_o} \cdot \frac{dI_{m1}}{dt} \tag{42}$$

Taking Laplace transform

$$I_{m1} = \frac{I_f}{1 + \frac{sCV_T}{\kappa I_o}} \tag{43}$$

Rewriting this in the time domain

$$I_{m1} = I_f . e^{\frac{-t.\kappa.I_O}{C.V_T}} \tag{44}$$

Now, differentiating the small signal approximation for equation (36)

$$\frac{dI_{m2}}{dt} = \frac{I_o \kappa}{V_T} \cdot \left(\frac{dV_e}{dt} - \frac{dV_X}{dt} \right) \tag{45}$$

Substituting the value of *dVx/dt* from equation (38) and that of *dVe/dt* from equation (39) into equation (45) and solving (assume *C1=C2=C*)

$$\frac{CV_T}{\kappa I_o}\frac{dI_{m2}}{dt} + I_{m2} = I_s - I_f + I_{m1} \qquad (46)$$

Taking Laplace transform of equation (46) and rearranging

$$I_{m2} = \frac{I_s - I_f + I_{m1}}{\left(1 + \frac{sCV_T}{\kappa I_o}\right)} \qquad (47)$$

Rewriting (47) in the time domain and substituting the value of I_{m1} from equation (44)

$$I_{m2} = \left(I_f . e^{\frac{-t.\kappa.I_0}{C.V_T}} + I_s - I_f\right) . e^{\frac{-t.\kappa.I_0}{C.V_T}} \qquad (48)$$

Substituting small signal approximation of I_{m1} from equation (44) and I_{m2} from equation (48) into equation (40) (here, t>0)

$$I_{syn} = \frac{I_0{}^3 e^{\frac{\kappa Vdd}{V_T}} e^{\frac{-\kappa V_{syn}}{V_T}}}{I_f . I_s . e^{\frac{-t.\kappa.I_0}{C.V_T}} \left(1 - \frac{I_f}{I_s} . \left[1 - e^{\frac{-t.\kappa.I_0}{C.V_T}}\right]\right)} \qquad (49)$$

13. APPENDIX IV

Matlab code for Bayesian integration of inputs at a place cell

```
clear; clc

%% Load the firing rates obtained from the simulation of the GRIDSmap model in
MATLAB

I1=load('Grid1.txt');
I1=I1(1:150, 10:100);
I2=load('Grid2.txt');
I2=I2(1:150, 10:100);
I3=load('Grid3.txt');
I3=I3(1:150, 10:100);

imagesc(I3)

colorbar
title('Biggest scale grid cell');
figure

imagesc(I2)

colorbar
title('Medium scale grid cell');

figure

imagesc(I1)

colorbar
title('Smallest scale grid cell');

%%     Bayesian integration (multiplication of probabilities)

I=I1.*I2.*I3;
I=I*max(max(I1))/max(max(I));
figure
imagesc(I)
colorbar
title('Place cell formed by Bayesian integration');

%%     Place cell formed by Summation and thresholding

img=(I1+I2+I3)/3;
```

```
s=size(img);
for i=1:s(1)
   for j=1:s(2)
      if(img(i,j)>10)
         imgThresh(i,j)=img(i,j);
      else
         imgThresh(i,j)=0;
      end
   end
end
figure

imagesc(imgThresh)

colorbar
title('Place cell formed by Summation and thresholding');
```

14. APPENDIX V

Arrangement of circuits on the stripe cell ring chip

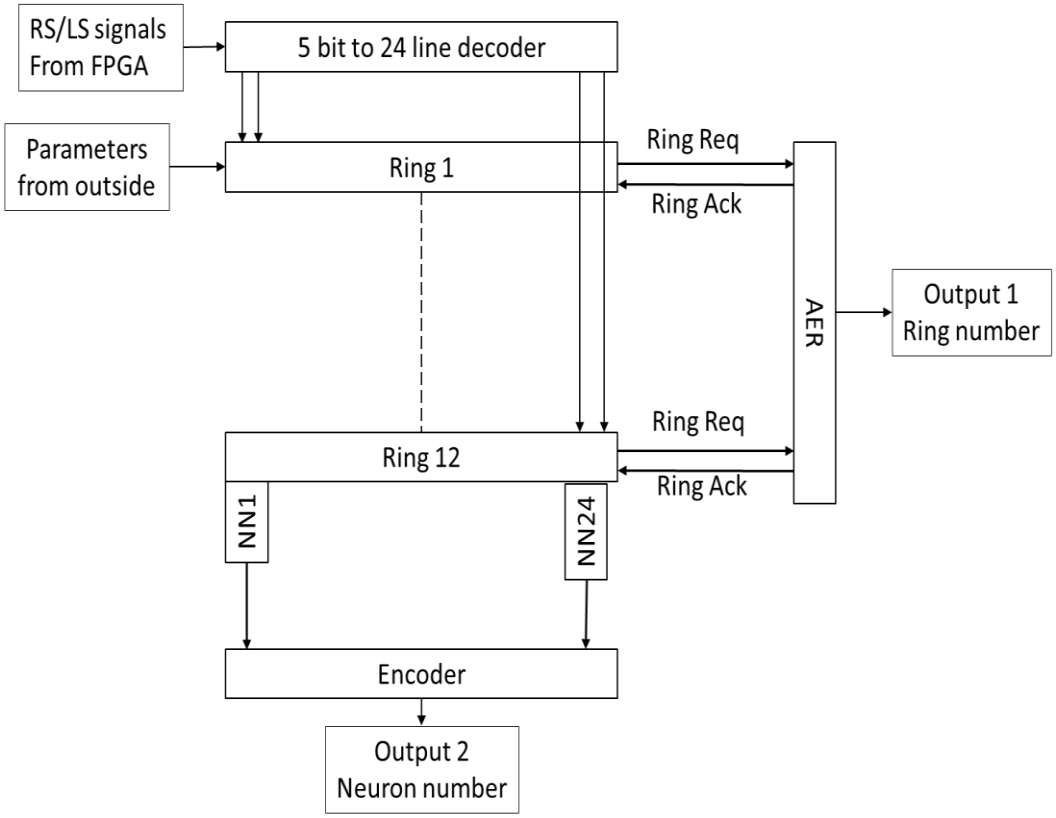

Fig. 79 Schematic of arrangement of circuits on the stripe cell ring chip which was used in silicon implementation of the head direction cell system, the central pattern generator and the grid and the place cell firing patterns. The chip had 12 ring circuits, *RS* and *LS* signals to all of which were routed through an on chip 5 bit to 24 line decoder circuit. The neuron numbers which fired on each ring were read using an encoder circuit and the ring number on which the firing neuron was located was detected using an AER encoder. Thus, inputs to the chip were parameters to set voltages and *RS* or *LS* signals. The outputs were neuron and ring numbers which were read from the encoders using a mixed signal oscilloscope.

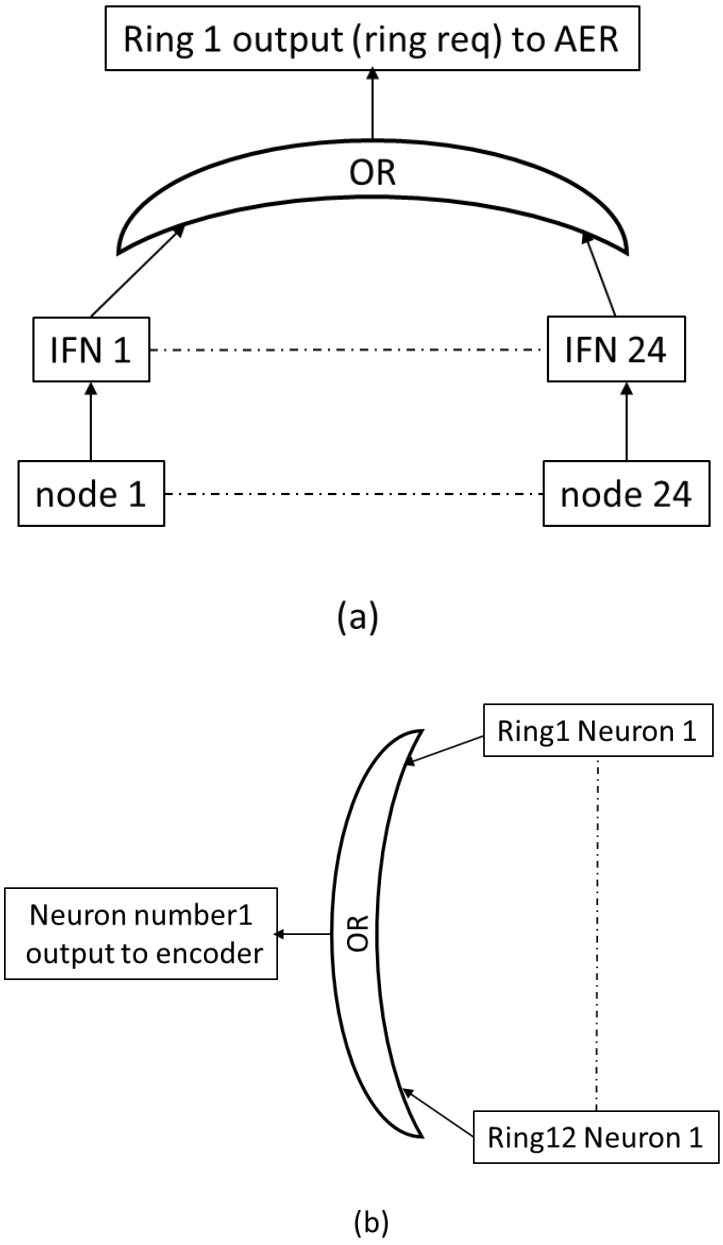

Fig. 80 (a) Schematic of circuit arrangement for processing output from the winning node of each ring through the IFN to the AER. (b) Schematic of circuit arrangement to process output from a neuron from all the rings and send it to the encoder. The OR gate in both cases was formed with pfets whose gates received inputs from the IFN and drains were tied together to send input to the AER whenever one of the neurons fired.

Decoder circuit

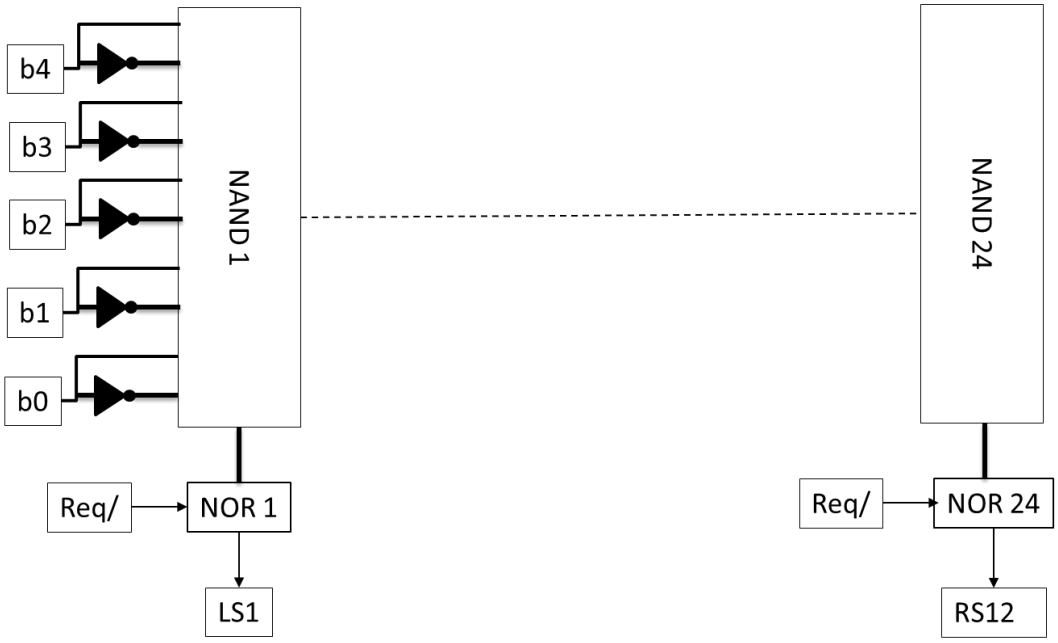

Fig. 81 Schematic of the circuit diagram of the 5 to 24 decoder used in the stripe cell ring chip. Input to the decoder was a 5 bit address and the req/ signal and outputs provided *LS* and *RS* parameters to all the 12 rings (24 in total).

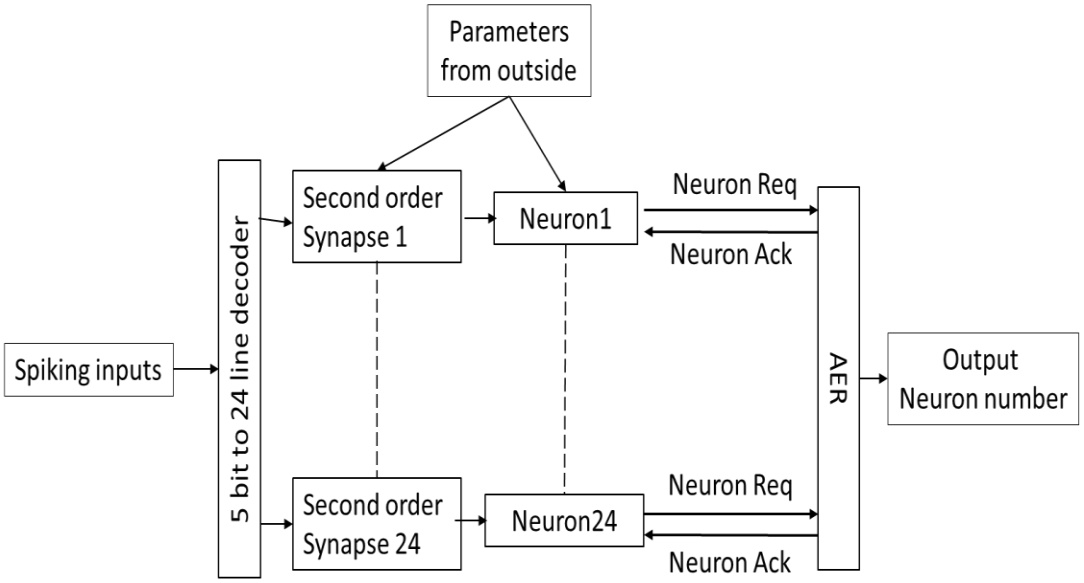

Fig. 82 Schematic of circuit arrangments on the grid chip. The grid chip had an array of 24 synapse-neuron circuits on it, inputs to which were routed through an on-chip decoder and outputs as neuron numbers of the firing neurons were read out using an on chip AER encoder.

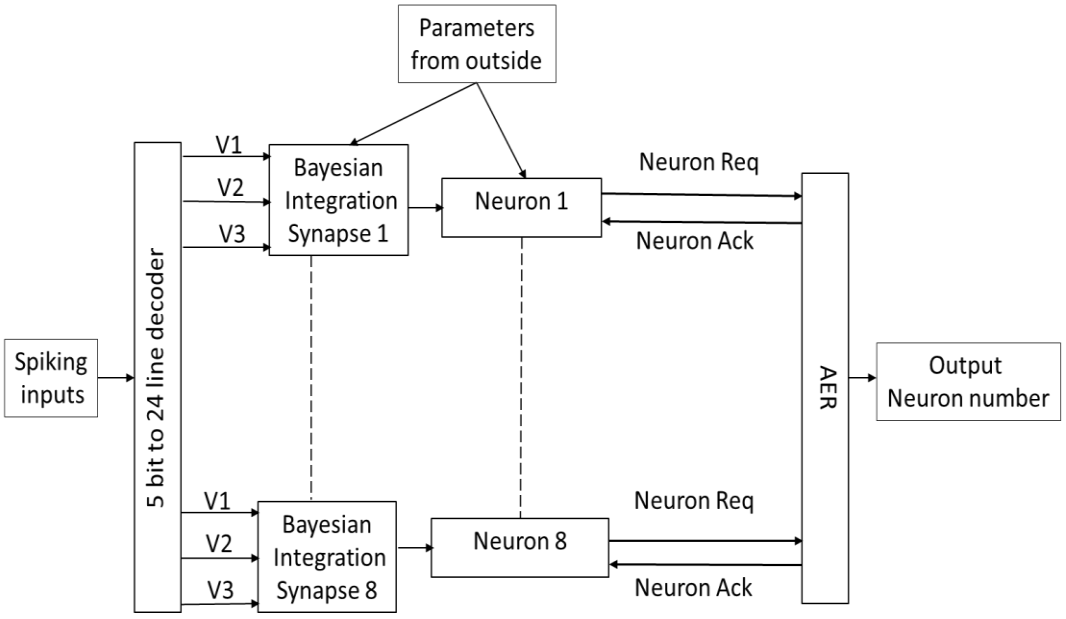

Fig. 83 Schematic of circuit arrangments on the place chip. Each place chip had an array of Bayesian integration synapse and neuron 2 circuits, inputs to which were routed through an on chip decoder circuit. The neuron numbers of the neurons which fired were read using an AER encoder.

15. REFERENCES

Hippocampal formation

[1] L. de Almeida, M. Idiart, J. E. Lisman, 2009, "The input-output transformation of the hippocampal granule cells: from grid to place fields", *J. Neurosci*, 29, 7504-7512.

[2] D. J Amit, 1989, "*Modeling brain function: The world of attractor neural networks*", New York, NY: Cambridge University Press.

[3] P. Arena, L. Fortuna, M. Frasca, L. Patane, 2005, "A CNN based chip for robotic locomotion control", *IEEE Trans. Circuits and Systems-I,* 52(9), 1862-1871.

[4] C. Barry, C. Lever, R. Hayman, T. Hartley, S. Burton, J. O'Keefe, K. Jeffery and N. Burgess, 2006, "The boundary vector cell model of place cell firing and spatial memory", *Rev. Neurosci*.: 17 (1-2): 71-97.

[5] C. Barry, N. Burgess, 2014, "Neural Mechanisms of self-location", *Curr. Biol.*, 24, R330-339.

[6] P. J. Best, L.T. Thompson, 1989, "Persistence, reticence and opportunism of place field activity in hippocampal neurons", *Psychobiology,* 17:230-235.

[7] K. A. Boahen, 1997, "Retinomorphic Vision Systems: Reverse engineering the vertebrate retina", Unpublished Doctoral Dissertation, California Institute of Technology.

[8] K. A. Boahen, 1998, “Communicating Neuronal Ensembles between Neuromorphic Chips”, *Neuromorphic Systems Engineering*, The Springer International Series in Engineering and Computer Science, 447, 229-259.

[9] M. P. Brandon, A. R. Bogaard, C. P. Libby, M. A. Connerney, K. Gupta, M. E. Hasselmo 2011, “Reduction of Theta Rhythm Dissociates Grid Cell Spatial Periodicity from Directional Tuning”, *Science* 332, 595.

[10] M. P. Brandon, J. Koenig, J. K. Luetgeb, S. Leutgeb, 2014, “New and distinct place codes are generated in a new environment during septal inactivation”, *Neuron*, 82, 789-796.

[11] Y. Burak, I. Fiete, 2006, “Do we understand the emergent dynamics of grid cell activity?” *Jour. Neurosci.,* 26(37), 9352-9354.

[12] Y. Burak, I. R. Fiete, 2009, “Accurate path integration in continuous attractor network models of grid cells”, *Comp. Bio.,* 5(2):1-16, e1000291.

[13] N Burgess, J O'Keefe, 2002, “Spatial Models of the Hippocampus,” in *The Handbook of Brain Theory and Neural Networks, 2nd Edition* Ed: Arbib M A, MIT press, Cambridge MA.

[14] N. Burgess, C. Barry, J. O'Keefe, 2007, “ An oscillatory interference model of grid cell firing”, *Hippocampus,* 17, 801-812.

[15] D. Bush, N. Burgess, 2014, “A hybrid oscillatory interference /continuous attractor network model of grid cell firing”, *Jour. Neurosci.,* 34(14), 5065-5079.

[16] D. Bush, C. Barry, N. Burgess, 2014, “What do grid cells contribute to place cell firing?”, *Cell,* 37(3), 136-145.

[17] Cadence PSPICE simulator, SPB_16.3. Available at https://www.ema-eda.com

[18] S. Cheng, L. M. Frank, 2011, "The Structure of networks that produce the transformation from grid cells to place cells", *Neuroscience*, 197, 293-306.

[19] E. Chicca, and G. Indiveri, 2003, "An adaptive silicon synapse", in *Proceedings of the 2003 International Symposium on Circuits and Systems*, Bangkok, Thailand, 1, I-81 - I-84.

[20] M. Colombo, P. Series, 2012, "Bayes in the brain-on Bayesian modelling in Neuroscience", *Brit. J. Phil. Sci.* 63, 697-723.

[21] F. Corradi, D. Zambrano, M. Raglianti, G. Passetti, C. Laschi, G. Indiveri, 2014, "Towards a neuromorphic vestibular system", *IEEE Trans. Circuits and Systems I*, (*in print*)

[22] M. O. Ernst, M. S. Banks, 2002, "Humans integrate visual and haptic information in a statistically optimal fashion", *Nature*, 415 (24), 429-433.

[23] A.S. Etienne, 1992, "Navigation of small mammal by dead reckoning and local cues", *Curr. Dir. Psychol. Sci*., 1, 48-52.

[24] A. S. Etienne, R. Maurer, V. Seguinot, 1996, "Path integration in mammals and its interaction with visual landmarks", *J. Exp. Biol.*, 199, 201-209.

[25] A. Fenton et. al., 2008, "Unmasking the CA1 ensemble place code by exposures to small and large environments: more place cells and multiple, irregularly arranged and expanded place fields in the larger space", *J. Neurosci*., 28, 11250-11262

[26] M. Franzius, R. Vollgraf, L. Wiscott, 2007, "From grids to places", *J. Comput. Neurosci.*, 22, 297-299.

[27] M. C. Fuhs, D. S. Touretsky, 2006, “A spin glass model of path integration in rat medial entorhinal cortex”, *Jour. Neuroci*., 26(16), 4266-4276.

[28] M. S. Goldman, J. Golowasch, E. Marder, L.F. Abbott, 2001, “Global structure, robustness and modulation of neuronal models”, *J. Neurosci*, 21(14), 5229-5238.

[29] J. Golowasch, M. S. Goldman, L.F. Abbott, E. Marder, 2002, “ Failure of averaging in the construction of a conductance based neuron model”, *J. Neurophys*., 87, 1129-1131.

[30] T. Hafting, M. Fyhn, T. Bonnevie, M. B. Moser., E. I. Moser, 2008, “Hippocampus independent phase precession in entorhinal grid cells”, *Nature*, 453, 1248-1252.

[31] T. Hafting, M. Fyhn, S. Molden, M. B. Moser., E. I. Moser, August 2005, “Microstructure of a spatial map in the entorhinal cortex”, *Nature,* 436, 801-806.

[32] T. Hartley, N. Burgess, C. Lever, F. Cacucci, J. O’Keefe, 2000, “Modeling place fields in terms of the cortical inputs to the hippocampus”, *Hippocampus,* 10, 369-379.

[33] T. Hartley, C. Lever, N. Burgess, John O’Keefe, 2014, “Space in the brain: how the hippocampal formation supports spatial cognition”, *Phil. Trans. R. Soc*., B 369: 20120510.

[34] M. Hasselmo, 2012, “*How we remember*”, MIT press Cambridge MA.

[35] M. Hasselmo, M. P. Brandon, 2012, “A model combining oscillations and attractor dynamics for generation of grid cell firing”, *Frontiers in Neural Circuits,* Vol 6, Article 30, pp 1-13.

[36] J. J. Hopfield, 1982, "Neural networks and physical systems with emergent collective computational abilities", *Proceedings of the National Academy of Sciences*, 79, 2554–2558.

[37] T. K. Horiuchi, C. Bansal, and T. M. Massoud, 2009,. "Binaural intensity Comparison in the Echolocating Bat Using Synaptic Conductance", in *IEEE International Symposium on Circuits and Systems*, TWN Taipei.

[38] K. J. Jeffery, J. M. O'Keefe, 1999, "Learned interaction of visual and idiothetic cues in the control of place field orientation", *Exp. Neurol.*, 127, 151-161.

[39] J. O'Keefe, & J. Dostrovsky, 1971, "The hippocampus as a spatial map Preliminary evidence from unit activity in the freely moving rat", *Brain Res*, 34 (1), 171-175.

[40] J. O'Keefe, 1976, "Place units in the hippocampus of the freely moving rat", *Exp. Neurol.* 51, 78-109.

[41] J. O'Keefe, D. Conway, 1976, "Sensory inputs to the hippocampal place units", *Neurosci. Letters*, 3, 103-104.

[42] J. O'Keefe, L. Nadel, 1977, "*The Hippocampus as a cognitive map*", Oxford, Clarendon Press.

[43] J. O'Keefe and D.H. Conway, 1978, "Hippocampal Place Units in the freely moving rat: Why they fire where they fire", *Exp. Brain Res*. 31, 573-590.

[44] J. O'Keefe and N. Burgess, 1996, "Geometric determinants of the place fields of the hippocampal neurons", *Nature*, 381, 425-428.

[45] J. O'Keefe, N. Burgess, 2005, "Dual phase and rate coding in hippocampal place cells: theoretical significance and relationship to entorhinal grid cells", *Hippocampus*, 15, 853-866.

[46] D. C. Knill, A. Pouget, 2004, "The Bayesian Brain: the role of uncertainty in neural coding and computation", *Trends in Neurosci.*, 27(12), 712-719.

[47] J. Koenig, A. N. Linder, J. K. Leutgeb, S. Leutgeb, 2011, "Spatial Periodicity of Grid Cells is not sustained during reduced theta Oscillations", *Science* , 332 (6029), 592-595.

[48] K. P. Kording, D. M. Wolpert, 2004, "Bayesian integration in sensorimotor learning", *Nature*, 427, 244-247.

[49] R. F. Langston, J. A. Ainge, J. J. Couey, C. B. Canto, T. L. Bjerknes, M. P. Witter, E. I. Moser, M. B. Moser, 2010, "Development of the Spatial Representation System in the Rat", *Science*, 328, 1576-1580.

[50] J. Lazzaro, S. Ryckebusch, M. A. Mahowald, C. A. Mead, 1989, " Winner take all networks of O(n) complexity", *Advances in Neural Information Processing Systems*, 1, 703-711, San Mateo, CA. Morgan Kaufmann.

[51] M. A. Lewis, A.H. Cohen, R. E. Cummings, M. Hartmann, 2000, "Toward biomorphic control using custon aVLSI CPG chips", *Proceedings of the 2000 IEEE International conference on Robotics and Automation*, San Francisco, CA, 494-500.

[52] S. C. Liu, J. Kramer, G. Indiveri, T. Delbruck, R. Douglas, 2002, "*Analog VLSI: Circuits and principles*", the MIT press, Cambridge, MA, 168-175.

[53] C. Luo, J. W. Clark, C. C. Canavier, D. A. Baxter, J. H. Byrne, 2004, "Multimodal behaviour in a four neuron ring circuit: mode switching", *IEEE Trans. Biomedical Engineering*, 51(2), 205-218.

[54] W. J. Ma, J. M. Beck, A. Pouget, 2008, "Spiking networks for Bayesian inference and choice", *Curr. Opi. In Neurobio.* 18, 217-222.

[55] P. R. MacNeilage, N. Ganesan, D. E. Angelaki, 2008, "Computational approaches to spatial orientation: from transfer functions to dynamic Bayesian inference", *J. Neurophysiol*, 100, 2981-2996.

[56] T. Madl, S. Franklin, K. Chen, D. Montaldi, R. Trappl, 2014, "Bayesian integration of information in hippocampal place cells", *PLOS one,* 9(3), e89762.

[57] T.M.Massoud, T.K. Horiuchi, 2011, "Online correction of orientation estimates using spatial memory in a neuromorphic head direction system", presented at the *International Symposium on Circuits and Systems (ISCAS),* 2011, 2429-2432.

[58] T.M. Massoud, T.K. Horiuchi, 2011, "A neuromorphic VLSI head direction cell system", *IEEE Trans. Circuits and Systems I,* 58(1), 150-163

[59] T.M. Massoud, T.K. Horiuchi, 2012, "A neuromorphic VLSI grid cell system", *International Symposium for Circuits and Systems (ISCAS),* 2421 - 2424.

[60] MATLAB R2011b. Available at <http://www.mathworks.com> Accessed 01/03/14.

[61] B. L. McNaughton, L. L. Chen, E. J. Markus, 1991,"Dead reckoning, landmark learning, and the sense of direction: a neurophysiological and computational hypothesis", *Journal of Cognitive Neuroscience,* 3, (2), 190-202.

[62] B. L. McNaughton, F. P. Battaglia, O. Jensen, E. I. Moser & M. B. Moser, 2006, “Path integration and the neural basis of the 'cognitive map‘”, *Nature Reviews Neuroscience*, 7, 663-678.

[63] H. Mhatre, A. Gorchetchnikov, and S. Grossberg, 2012, “Grid Cell Hexagonal Patterns Formed by Fast Self-Organized Learning within Entorhinal Cortex”, *Hippocampus,* 22:320–334.

[64] M. L. Mittelstaedt and H. Mittelstaedt, 1980, “Homing by path integration in a mammal”, *Naturwissenschaften*, 67, 566-567.

[65] C. Molter, Y. Yamaguchi, 2008, “Entorhinal theta phase precession sculpts dentate gyrus place fields”, *Hippocampus*, 18, 919-930.

[66] J. D. Monaco, L. F. Abbott, 2011, “Modular realignment of entorhinal grid cell activity as a basis for hippocampal remapping”, *J. Neurosci.*, 31, 9414-9425.

[67] R. U. Muller, J. L. Kubie, 1987, “The effects of changes in the environment on the spatial firing of hippocampal complex-spike cells”, *J. Neurosci.*, 7, 1951-1968.

[68] K. Nakazawa, M. C. Quirk, R. A. Chitwood, M. Watanabe, M. F. Yeckel, L. D. Sun, A. Kato, C. A. Carr, D. Johnson, M. A. Wilson, S. Tonegawa, 2002, “Requirement of hippocampal CA3 NMDA receptors in Associative memory recall”, *Science*, 297, 211-218.

[69] R. Nieuwenhuys et. al. , 1988, “*Human Central Nervous System*”, 3rd edition, Springer Verlag, New York, 334-344.

[70] G. Pfuhl, H. Tjelmeland, R. Biegler, 2011, “Precision and reliability in animal navigation”, *Bull Math Biol.*, 73, 951-977.

[71] B. Poucet, F. Sargolini, E. Y. Song, B. Hangya, S. Fox and R. U. Muller, 2014, "Independence of landmark and self-motion guided navigation: a different role for grid cells", *Phil. Trans. R. Soc. B,* 369, 20130370.

[72] D. Purves, G. J. Augustine, D. Fitzpatrick, W. C. Hall, A. S. LaMantia, and L.E. White, 2012, "*Neuroscience*", 5th edition, Sinauer Associates, Sunderland, MA, USA.

[73] G. J. Quirk, R. U. Muller, J. L. Kubie, 1990, "The firing of hippocampal place cells in dark depends upon the rat's recent experience", *J. Neurosci.*, 10, 2008-2017.

[74] J. B. Ranck, 1984, "Head direction cells in the deep cell layer of dorsal presubiculum in freely moving rats", *Society Neuroscience* Abs.

[75] E. T. Rolls, S. M. Stringer, T. Elliot, 2006, "Entorhinal cortex grid cells can map to hippocampal place cells by competitive learning", *Network*, 17, 447-465

[76] F. Savelli, J. J. Kneirim, 2010, "Hebbian analysis of the transformation of medial entorhinal grid cell inputs to hippocampal place fields", *J. Neurophysiol.*, 103, 3167-3183.

[77] E. Save, L. Nerad, B. Poucet, 2000, "Contribution of multiple sensory information to place field stability in hippocampal place cells", *Hippocampus*, 10(1), 64-72.

[78] W. B. Scoville, B. Milner, 1957, "Loss of recent memory after bilateral hippocampal lesions", *J. Neurol. Neurosurg. Psychiatr.* **296**, 1–22.

[79] R. Z. Shi and T. Horiuchi, 2004, "A summating, exponentially-decaying CMOS synapse for spiking neural systems", *Advances in Neural Information Processing*

Systems, 16, eds. Thrun, S., Saul, L., and Schölkopf, B. MIT Press, Cambridge MA.

[80] B. Si, A. Treves, 2009, "The role of competitive learning in the generation of DG fields from EC inputs", *J. Neurophysiol.* , 103, 3167-3183.

[81] T. Solstad, E. I. Moser, G. T. Einevoll, 2006, "From grid to place cells: A mathematical model", *Hippocampus*, 16, 1026-1031.

[82] S. Still, K. Hepp, R. J. Douglas, 2006, "Neuromorphic walking gait control", *IEEE Trans. Neural Networks*, 17(2), 496-508

[83] J. S. Taube, R. U. Muller, J. B Ranck., Jr., 1990a, "Head direction cells recorded from the postsubiculum in freely moving rats. I. Description and quantitative analysis", *J. Neurosci.*, 10, 420-435.

[84] J. S. Taube, R. U. Muller, J. B Ranck., Jr., 1990b, "Head direction cells recorded from the post-subiculum in freely moving rats. II. Effects of environmental manipulations", *J. Neurosci.*, 10, 436-447.

[85] T. J. Wills, F. Cacucci, N. Burgess, J. O'Keefe1., 2010, "Development of the Hippocampal Cognitive Map in Preweanling Rats", *Science*, 328, 1573-6.

[86] M.P. Witter and H.J. Groenewegen, 1984, "Laminar origin and septotemporal distribution of entorhinal and perirhinal projections to the hippocampus in the cat", *J. Comp. Neurol.*, 224, 371-384.

[87] M.P. Witter, H.J. Groenewegen, F.H. Lopes da Silva and A. H. M. Lohman, 1989, "Functional organisation of the extrinsic and intrinsic circuitry of the parahippocampal region", *Prog. Neurobiol.*, 33, 161-253.

[88] R. S. Zemel, P. Dayan, A. Pouget, 1998, "Probabilistic interpretation of population codes", *Neural Computation,* 10, 403-430.

[89] K. Zhang, 1996, "Representation of spatial orientation by the intrinsic dynamics of the head-direction cell ensemble: A theory", *Journal of Neuroscience* 16, 2112–2126.

[90] T.K. Horiuchi, T. M. Massoud, 2014, "A neuromorphic VLSI model of grid cells in the echolocating bat", *BIOCAS, 2014,* 540-543.

[91] M. B. Zugaro, A. Arleo, A. Berthoz, S. I. Weiner, 2003, "Rapid spatial reorientation and head direction cells", *Jour. Of Neurosci.*, 21, RC 154.

[92] J. S. Taube, 2007, "The head direction signal: Origins and sensory-motor integration", *Annu. Rev. Neurosci.,* 30, 181-207.

Lateral Superior Olive

[93] H.A.N. Abdalla, 2009, "Estimation of elevation and Azimuth in a neuromorphic VLSI bat echolocation system", unpublished, PhD Thesis

[94] M. Cheely, T. K. Horiuchi, 2003, "Analog VLSI Models of Range-Tuned Neurons in the Bat Echolocation System", *EURASIP Journal on Applied Signal Processing*, 7, 649-658.

[95] T. Horiuchi and K. Hynna, 2001, "Spike based VLSI modelling of the ILD system in echolocating bat", *Neural Networks*, 14, 755-762.

[96] T. Horiuchi and K. M. Hynna, 2001, "A VLSI based model of azimuthal echolocation in the big brown bat", *Auton. Robots*, 11(3), 241-247.

[97] T. K. Horiuchi, M. Cheely, 2007, "A systems view of a neuromorphic VLSI echolocation system", *Circuits and Systems, 2007, ISCAS 2007, IEEE International Symposium on,* 605-608.

[98] T. K. Horiuchi, C. Bansal, and T. M. Massoud, 2009, "Binaural intensity Comparison in the Echolocating Bat Using Synaptic Conductance", in *IEEE International Symposium on Circuits and Systems*, TWN Taipei, 2153 - 2156.

[99] E. M. Izhikevich, 2006, "Polychronization: Computation with Spikes", *Neural Computation*, 18, 245-282,

[100] NEURON simulator, Available at http://www.neuron.yale.edu/neuron.

[101] T. J. Park, B. Grothe, G. D. Pollak, and Ursula Koch, 1996, "Neural delays shape selectivity to inter aural intensity differences in the Lateral Superior Olive", *J. Neurosci*., 16(20), 6554-6556.

[102] D. Purves, G. J. Augustine, D. Fitzpatrick, W. C. Hall, A. S. LaMantia, and L.E. White, 2012, "*Neuroscience*", 5th edition, Sinauer Associates, Sunderland, MA, USA.

[103] M. C. Reed, J. J. Blum., 1990, "A model for the computation and encoding of azimuthal information by the lateral superior olive", *J. Acoust. Soc. Am*., 88 (3), 1442-1453.

[104] J. W. H. Schnupp and C. Carr, 2009, "On hearing with more than one ear: lessons from evolution", *Nature Neuroscience*, 12 (6), 692-697.

[105] A. I. Selverston, M. Moulins, 1985, "Oscillatory Neural Networks", in *Annu. Rev. Physiol.*, 47, 29-48

[106] G. M. Shepard, 2004, *"Synaptic Organization of the Brain",* 5th edition, Oxford University Press, USA.

[107] R. Shi and T. Horiuchi, 2004, "A VLSI model of the bat lateral superior olive for azimuthal echolocation", *Circuits and Systems, 2004. ISCAS'04. Proceedings of the 2004 International Symposium on,* 4, IV-900-3.

[108] R. Shi and T. Horiuchi, 2005, "A VLSI model of the bat dorsal nucleus of the lateral leminiscus for azimuthal echolocation", *International Symposium on Circuits and Systems. ISCAS'05*, 5, 4217-4220.

[109] R.Z. Shi and T.K. Horiuchi, 2007, "A neuromorphic VLSI model of bat interaural level difference processing for azimuthal echolocation", *Circuits and Systems I: Regular Papers, IEEE Transactions on,* 54(1), 74-88.

M. Zacksenhouse, D.H. Johnson, J. Williams, C. Tsuchitani, 1998, "Single neuron modelling of LSO unit responses", *J. Neurophysiol*., Vol. 79, pp 3098-3110.